APPLICATION OF BIOMATERIALS AND NANOMATERIALS IN ENVIRONMNETAL REMEDIATION

By

SURESHKUMAR M K
CHEM012008040017

Bhabha Atomic Research Centre, Mumbai

A thesis submitted to the

Board of Studies in Chemical Sciences

in partial fulfillment of requirements

for the Degree of

DOCTOR OF PHILOSOPHY

of

HOMI BHABHA NATIONAL INSTITUTE

August 2015

Homi Bhabha National Institute

Recommendations of the Viva Voce Committee

As members of the Viva Voce Committee, we certify that we have read the dissertation prepared by **SURESHKUMAR M.K** entitled " **Application of Biomaterials and Nanomaterials in Environmental Remediation** " and recommend that it may be accepted as fulfilling the thesis requirement for the award of Degree of Doctor of Philosophy.

Chairman – Prof. C.P. Kaushik **Date:** 16.12.2016

Guide / Convener – Prof . R.M. Tripathi **Date:** 16.12.2016

Examiner – Prof. Dinesh Mohan **Date:** 16.12.2016

Member 1- Prof. G.G Pandit **Date:** 16.12.2016.

Member 2- Prof. Rakesh Verma **Date:** 16.12.2016

Final approval and acceptance of this thesis is contingent upon the candidate's submission of the final copies of the thesis to HBNI.

I/We hereby certify that I/we have read this thesis prepared under my/our direction and recommend that it may be accepted as fulfilling the thesis requirement.

Date: 16.12.2016

Place: TROMBAY

Prof. R.M.Triapthi
Guide

Version approved during the meeting of Standing Committee of Deans held during 29-30 Nov 2013

STATEMENT BY AUTHOR

This dissertation has been submitted in partial fulfillment of requirements for an advanced degree at Homi Bhabha National Institute (HBNI) and is deposited in the Library to be made available to borrowers under rules of the HBNI.

Brief quotations from this dissertation are allowable without special permission, provided that accurate acknowledgement of source is made. Requests for permission for extended quotation from or reproduction of this manuscript in whole or in part may be granted by the Competent Authority of HBNI when in his or her judgment the proposed use of the material is in the interests of scholarship. In all other instances, however, permission must be obtained from the author.

Sureshkumar M K

DECLARATION

I, hereby declare that the investigation presented in the thesis has been carried out by me. The work is original and has not been submitted earlier as a whole or in part for a degree / diploma at this or any other Institution / University.

Sureshkumar M. K

ACKNOWLEDGEMENTS

I take this opportunity to express my heartfelt gratitude and respect to Dr. R.M Tripathi, Professor, HBNI & Head, Health Physics Division, Bhabha Atomic Research Centre, who has always stood with me, cheerfully encouraging, supporting and guiding throughout the course of my research work. It was nothing but impossible to finish this task without the support and patience he has shown to me as a student.

I am indebted to Dr K.S Pradeepkumar, Associate Director HS&E Group, Bhabha Atomic Research Centre for his encouragement during the course of the work. It was a private discussion with him nearly a decade ago turned my attention to the migration of radioactivity, resulting in my study on humic substances, which was the initial seed for this thesis.

I am grateful to the experts of my Doctoral Committee, Dr Y.S Mayya, Dr C.P Koushik, Dr G.G Pandit, Dr Rakesh Verma and Dr S.K Mukerjee for their suggestions, comments and guidance from time to time which immensely helped me in improving the quality of my research work.

I express my gratitude to all my colleagues of radiation hazard control unit, Plutonium Plant for the encouragement and all the major and minor help rendered during my research work. All of them were eagerly waiting for me cross this stage, and their love and support in abundance is the source energy for me, to attempt any task, however difficult it may be.

There is no need of formal words of thanks to my entire family for the invaluable support, but it is not possible, not to recollect the patience so long and the support so continuous from my Mrs and I am sure that she will be more joyous than me to see me completing this task.

Sureshkumar M K

CONTENTS

SYNOPSIS

“Environmental pollution is an incurable disease. It can only be prevented.”

Barry Commoner

Pollution can be defined as the introduction of undesirable substances to the environment. Ever increasing human needs for better quality of life has lead to the pollution of air, soil and water around us, knowingly or unknowingly, sometimes with global implications and much more cases of local disasters. Pollutant chemicals could lead to imbalances in specific ecosystems, health impairment for human and other flora and fauna and undesirable weather and climate variation. Among the various pollutants, pollution due to toxic metal ions is of extreme concern due to their non-biodegradability, possibility of presence of multiple species with different toxicities and easy transferability from source to distance [1]. Metallic pollutants could be generally classified into two categories: heavy metals, which are by convention, a metal or metalloid of environmental concern and radionuclides which are toxic due to their property of emitting radiation, irrespective of their chemical form.

Commonly encountered heavy metals are chromium, cobalt, nickel, copper, zinc, arsenic, selenium, silver, cadmium, antimony, mercury, thallium and lead. Heavy metals are naturally occurring, but become a cause of concern due to various anthropogenic activities which could result in increased mobility and bioavailability in comparison to their naturally existing forms. Mining and concentration, effluents from industries such as tanning and electroplating, vehicular emission and electronic waste are examples of anthropogenic activities leading to heavy metal pollution. In few cases such as that of arsenic, it is an identified health hazard in many parts of the world at the naturally existing concentrations itself. Health effect of heavy metal toxicity range from kidney, neurotic, reproductive and developmental disorders to carcinogenesis of various organs [2]. Radionuclides could be naturally occurring such as ^{238}U and ^{40}K or manmade isotopes such as ^{137}Cs and ^{60}Co. Exposure to artificial radionuclides could possible only from the inadvertent release of such materials to the environment from nuclear or other industrial facilities using radioisotopes. On the other hand, anthropogenic activities could lead to enhanced mobility of naturally occurring radionuclides such as ^{238}U, ^{232}Th etc. resulting in exposure of human via various routes of intake [3]. Carcinogenesis is the common hazard from all radionuclides whereas most heavy radionuclides like uranium possesses both chemical and radiotoxicity.

The prudent strategy to minimise the release of toxic metal ions to the environment is to treat the effluents before its release. In fact achieving *"zero discharge of pollutants"* from industries has become a paradigm among environmental protection professionals [4]. Many matured technologies are in practice such as coagulation/precipitation, membrane technology, solvent extraction, ion exchange and adsorption for the treatment of effluents containing toxic metal ions [5]. Any of these technologies is not absolutely superior to the rest and each of them has some advantages and disadvantages. Along with proven advantages of adsorption process such as low energy requirements and amenability for batch and continuous process, development of new and improved adsorbent materials, keep this technology a viable option and an area of intense research.

In recent years biomaterials received significant interest as good candidates for environmental remediation, for their high abundance, environmentally benign nature and low cost. The kinds of substrates of biological origin that have been investigated for biosorbent preparation include microbial biomass (bacteria, filamentous fungi etc.), seaweeds (microalgae), industrial wastes (fermentation and food wastes, activated sludge etc.), agricultural wastes (fruit/vegetable wastes, rice straw, soybean hulls etc.), natural residues (plant residues, tree barks etc.) and other materials (chitosan, cellulose etc.) [6]. Despite the large quantum of research available on the uses of biomaterials for adsorption applications, continuous efforts are underway to improve the existing materials and identify newer materials for such applications. Modifications are indented either to improve the stability of adsorbent in solution or to improve its efficiency and selectivity by the introduction of target specific functional groups.

Advances in nanotechnology have opened yet another window of opportunity by providing smart material for adsorption applications [7]. Nanomaterials are excellent candidate as adsorbent, due to their high specific surface area and consequent high reactivity. TiO_2, various iron oxides and hydroxides, MgO, ZnO, SnO_2, ZrO_2, CuO, nano-Zero Valent Iron (nZVI), and carbon nanotubes (CNTs) are some of the nanomaterials of interest as adsorbent for metal ions. Among the various nanomaterials studied for sorption application, magnetic nanomaterials are of special interest due to the ease in their solid-liquid separation. Continuous efforts are underway to prepare advanced nanomaterials for adsorption application, such as introduction of specific functional group on surface for improving selectivity and sorption capacity and other surface modifications for improving their stability in working solutions.

For environmental remediation, composite materials made from structurally different biomaterials, and combinations of nanomaterials and biomaterials have also attracted significant interest as adsorbents [8]. One approach in nano-biocomposite preparation is to use biomaterials as a carrier for nanomaterials, without compromising their nano-characteristics and thus their superior adsorption properties. Such composites, because of their macro-size are found to be easily separable from the solution, on completion of the sorption process. In another widely followed procedure, adsorbent biomaterials are used to coat magnetic nanomaterials, resulting in magnetically separable bio-nano composites [9]. Overall, these new approaches have the potential to deliver superior adsorbents for environmental separation than the use of individual components as adsorbents.

In natural environment too, separation mediated by biomaterials and naturally occurring nanomaterials play a very important role in the fate, transport and sequestration of contaminants. Inorganic metal oxide nanoparticles and organic colloids such as humic materials are the two most common environmental components in the nano-size domain that could play an active role in the environmental processes at contaminated sites. Learning from nature, it is proposed that materials in the nano size domain could be used for environmental remediation at contaminated sites. Use of nano-Zero Valent Iron (n-ZVI) as Permeable Reactive Barrier (PRB) for arresting the contaminant transport is one highly studied system for such in-situ applications. Humic materials are also being proposed for remediation of metal contaminated sites and treatment of contaminated water bodies and mine water [10]. However developments of these methods to robust technologies for field application need additional fundamental understanding of interaction of these components with various contaminant metal ions.

In the present thesis modified biomaterials and nanomaterials were studied as sorbents for the removal of heavy metals from contaminated solutions. Two well recognised materials of biological origin were selected for the present studies: a) chitosan, a material known to have excellent binding properties with various metal ions and b) humic acid, which is a complex heterogeneous mixture of different chemical structures having ionisable and chelating functional groups. Additionally, a new composite sorbent is prepared by immobilisation of humic acid on chitosan beads and used for metal ion sorption. Two nanomaterials, bare magnetite and humic acid coated magnetite were prepared and studied for the sorption of metal ions from aqueous solution. Uranium is the principal model contaminant metal ion used in these studies which is supplemented by the use of other toxic metal ions; lead and chromium in certain cases. An attempt is also made to bring to light the intricacies of in-situ remediation using biomaterials. Brown humic acid and gray humic acid from the same source is found to show significant difference in their binding characteristics with uranium, indicating that in-situ remediation proposal should be more complex than as it appears at first sight.

This thesis has been organised into seven chapters and a brief description of each chapter is as follows:

Chapter 1: Introduction

This introductory chapter starts with a general and historical overview of the environmental pollution; a description of various agents causing it and the known impacts of several polluting agents. A brief description of various metal ions and radionuclides often encountered as environmental hazard and their health hazards is given followed by a short description of the currently used technologies for abatement of metal ion pollution. This introduction is followed by a brief review of the current level of knowledge on the application of biomaterials and nanomaterials in pollution abatement. The chapter ends with scope, specificities and motivation for the present work leading to this thesis.

Chapter 2: Experimental techniques

This chapter deals with various experimental methods and modelling techniques used for the present studies. It starts with general description of the preparation, purification and characterisation of the different biomaterials and nanomaterials used as adsorbents. A brief description of the various analytical instruments used for present studies such as UV-Visible absorption spectroscopy, fluorescence spectroscopy, Fourier Transform Infrared Spectroscopy (FTIR), Scanning Electron Microscopy (SEM), BET surface area analysis, X-Ray Photo Electron Spectroscopy (XPS), Atomic Emission Spectroscopy (AES) and X-Ray Diffraction (XRD) analysis are provided in this chapter. Langmuir and Freundlich isotherm models used for analysing the adsorption data as well as the kinetics model such pseudo-first order, pseudo-second order and intra-particle diffusion model used for analysing sorption kinetics are presented. The chapter ends with a brief description of the methods used for deriving the apparent stability constants and aggregation kinetics for the interaction of humic acid components with uranium [11,12].

Chapter 3: Sorption of metal ions on Chitosan Tripolyphosphate (CTPP) beads.

This chapter presents the sorption of metal ions on chitosan tripolyphosphate (CTPP) beads prepared by the ionic cross-linking of chitosan with sodium tripolyphosphate. The synthesized material is characterised using FTIR spectroscopy and the surface morphology is analysed using SEM. Beads at two different cross-linking densities were studied for the sorption of U(VI) and Cr(III) from aqueous solutions. Sorption studies were carried out as a function of various operating parameters such as solution pH, concentration of metal ions and contact time [13, 14]. For both the metal ions, it is observed that pH=5 is optimum for sorption and sorption capacity is higher for the higher cross-linked beads. Adsorption data are analysed using Langmuir and Freundlich isotherm models and the Langmuir model is found to fit the experimental data more closely than the Freundlich model. From Langmuir model the sorption capacity of the sorbent for U(VI) and Cr(III) is found to be 236.9 mg/g and 469.5 mg/g respectively. The adsorption of U(VI) and Cr(III) on CTPP beads were found to be slow, taking ca 72 hours to complete the saturation. Experimental kinetics data were analysed using pseudo-first order, pseudo-second order and intra-particle diffusion model. Both U(VI) and Cr(III) sorption is found to match the pseudo-second order model more closely than pseudo-first order model. Additionally application of intra-particle diffusion model to the U(VI) sorption data showed three distinct regions among which the intermediate time scale showed the best statistical fit for this model. The competition effect of common metal ions on adsorption of Cr(III) were studied using batch sorption experiments and trivalent metal ion Al(III) is found to offer significant competition for the sites on CTPP. Recovery of Cr(III) from the adsorbent, post adsorption is found to be effective with NaCl solutions. The findings in this chapter show that CTPP beads could be used for toxic metal ion removal from contaminated solutions.

Chapter 4: sorption of metal ions on humic acid coated chitosan tripolyphosphate beads.

This chapter presents the preparation of humic acid coated chitosan tripolyphosphate (HA-CTPP) beads and its application for the sorption of metal pollutants, U(VI) and Pb(II) ions [15]. HA-CTPP beads were prepared by coating HA onto wet CTPP beads in aqueous solution. SEM images of the beads showed that the HA-CTPP bead surface is highly porous in comparison to that of CTPP beads. Leaching behaviour of HA from HA-CTPP beads were tested by equilibrating the beads in aqueous medium in the pH range 1-8 for 24 hours. HA release is found to be negligible below pH=3 and less than ten percentage even at the highest pH studied. The stability of the beads is tested at different pHs by measuring the swelling capacity and found that HA-CTPP beads shows three times lower swelling in comparison to CTPP beads. Sorption of U(VI) and Pb(II) on HA-CTPP beads is studied using batch adsorption technique. The sorption data in case of both the metal ions is found to fit the Langmuir model with adsorption capacity 71.4 mg/g and 223.7 mg/g respectively for U(VI) and Pb(II) ions. Adsorption process is found to complete in ~6 hours in case of Pb(II) ions and ~10 hours in case of U(VI) ions. In both cases, sorption kinetics is found to follow the pseudo-second order model. The observed sorption capacity for U(VI) ions on HA-CTPP beads is significantly lower than that on the non-immobilised humic acid reported in literature [15]. In case of Pb(II) ions, the sorption capacity observed was comparable to that of unmodified HA reported in previous studies[16].

Chapter 5: Sorption of uranium on magnetite and humic acid coated magnetite (HA-magnetite) nanoparticles.

Sorption of uranium on magnetite nanoparticles and Humic Acid coated magnetite (HA-magnetite) nanoparticles is described in this chapter. The nanoparticles were prepared by co-precipitation of salts in aqueous media and characterised using FTIR spectroscopy, SEM, XRD and XPS. For bare magnetite and HA-magnetite the optimum pH for adsorption of uranium is found as pH=7 and 5 respectively [17]. With bare magnetite, the adsorption kinetics showed two distinct steps: the initial step which completes in four hours where 95% of the sorption capacity is achieved, followed by a slow step extending to several days. Uranium adsorption on bare magnetite is found to be ionic strength independent. The overall sorption capacity for bare magnetite for uranium was 5 mg/g. XPS analysis of the uranium loaded bare magnetite showed the presence of reduced uranium species on the surface. Though sorption capacity is not encouraging, with actual Ammonium Di-Uranate (ADU) supernatant containing 3.8 mg/L uranium as the test solution, it is observed that magnetite nanoparticles is a suitable adsorbent for treatment of solutions having lower initial metal ion concentrations. In contrast to bare magnetite,

HA-magnetite is found to have different surface morphology, higher specific surface area (99 m^2/g instead of 59m^2/g for bare magnetite) and more sorption capacity (22.4 mg/g) for uranium. For HA-magnetite the sorption data is found to fit the Langmuir isotherm and from XPS spectra of the loaded sorbent, no presence of reduced uranium species were observed on the surface. In contrast to that of bare magnetite, sorption of uranium on HA-magnetite was fast, completing saturation in thirty minutes. Thus these studies indicate that significant differences are possible in the sorption properties of bare and organic coated nanomaterials, which in turn may affect their application in separation process and their impact on natural environment.

Chapter 6: Binding characteristics of U(VI) with Grey and Brown humic acid.

This chapter deal with the differences in the interaction of the two principal components of humic acid, Gray Humic Acid (GHA) and Brown Humic Acid (BHA) with uranium. Commercially available Aldrich humic acid is purified and separated into GHA and BHA using standard methods [18]. Characterisation of fractions shows more alkyl carbon group and less acidic functional group content in GHA than that in BHA. Analysis using conventional fluorescence quenching method results in comparable apparent stability constants for binding of uranium with GHA and BHA. Uranium induced precipitation of GHA and BHA from aqueous solution is studied at pH=4 and despite their comparable stability constant for the complex formation, GHA is observed to get precipitated at lower total concentration of metal ion and with faster kinetics. Fluorescence analysis of the HA-U system over three months period showed that GHA-U system takes more time to reach the equilibrium configuration and is less stable than BHA-U system. Findings from these studies shows that field application of biomaterials such as humic substances at contaminated sites for preventing the contaminant transport, needs elaborate and in-depth analysis.

Chapter 7 Summary and conclusions

This chapter summarise the conclusions from this research and also the future research prospectus on the topic explored under this thesis.

References :

1 Pitchel J *Fundamentals of Site Remediation For Metal and Hydrocarbon-Contaminated Soils* (2nd edn) (2007) Pages 1-26 The Rowman & Littlefield Publishing Group, Inc. Maryland,USA

2 Jarup L , *British medical bulletin* 68(1) (2003) 167-182

3 Guzman E T R, Regil E O, Malagon G P, *J Radioanal. Nucl. Chem. Lett.* 201 (1995) 313-320

4 McCleskey T M, Foreman T M, Hallman E E, Burns C J, Sauer N N, *Environ. Sci. Technol. 36* (19) (2002) 4187

5 Chen J P (2012) *Decontamination of Heavy metals: Processes, Mechanisms, and Applications*, CRC Press, Florida, United States.

6 Fomina M, Gadd G M, *Bioresour. Technol.* 160 (2014) 3-14

7 Trujillo-Reyes J, Peralta-Videa J R, Gardea-Torresdey J L, *J Hazard. Mater.* 280 (2014) 487–503

8 Liu H, Yang F, Zheng Y, Kang J, Qu J, Paul Chen J, *Water Res.* (2 0 11) 145-154

9 Vinh Tran H, Dai Tran L, Ngoc Nguyen T, *Mater. Sci. and Eng. C* 30 (2010) 304–310

10 Wan J, Dong W, Tokunaga T K, *Environ. Sci. Technol* 45 (2011) 2331-2337.

11 Nakashima K, Xing S, Gong Y, Miyajima T, *J Mol. Struct.* 883-884 (2008) 155-159

12 Kloster N, Brigante M, Zanini G, Avena M, *Colloid Surf A: Physicochem. Eng. Aspects* 427

(2013) 76– 82

13 Sureshkumar M K, Das D, Mallia M B, Gupta P C, *J Hazard. Mater.* 184 (2010) 65–72

14 Das D, Sureshkumar M K, Radhakrishnan K, Nuwad J, Pillai C G S *J Radioana.l Nucl. Chem.* 289 (2011) 275–285

15 Sureshkumar M K, Das D, Mary G, Nuwad J, *Sep. Sci. Technol.* 48 (2013) 1132–1139

16 Li L, Wei Z, Li Z, Wang J, Zhou Q, Guo J, *Desal. Water Treat.* 54 (2015) 2541-2545

17 Das D, Sureshkumar M K, Koley S, Mithal N, Pillai, C G S, *J Radioanal. Nucl. Chem.* 285 (2010) 447–454

18 Stevenson F J *Humic Acid; Genesis, Composition, Reactions*, (2nd Edn) (1992) John Wiley and Sons, New York

List of Figures

Figure Caption **Page No.**

List of tables

Chapter 1

Introduction

“Environmental pollution is an incurable disease. It can only be prevented.”

Barry Commoner

1.1 Environmental Pollution

Pollution is defined as “the addition of any substance or form of energy (e.g. heat, sound, radioactivity) to the environment at a rate faster than the environment can accommodate it by dispersion, breakdown, recycling, or storage in some harmless form” [1]. Although pollution is as old as human civilisation (at least since people started using fire thousands of years ago), it had seen the growth of truly global proportions only from 19th century as the result of the *industrial revolution*. Ever increasing human needs and associated technological progress for better quality of life has lead to the pollution of air, soil and water around us, mostly unknowingly, sometimes with global implications and much more cases of local disasters. Pollutants could lead to imbalances in specific ecosystems, health impairment of human and other flora and fauna and undesirable weather and climate variation. But the knowledge base on the effect of pollutants on environmental health was only slowly evolving, since on first time appearance of any new phenomena, much research is required to understand it. For example, killer smog has appeared several times and taken away thousands of life, before air pollution got the attention, it deserves [2]. As the awareness of public and governments on the social and economic cost of pollution build up, world over, efforts are underway to better understand the cause and effect of pollutants, mitigate and reclaim the existing polluted zones and to prevent further pollution by adopting enhanced technology. In order to keep the environment clean and safe, in addition to promoting technological innovations, each country is enacting more and more stringent rules and regulations for matters pertinent to the environment.

Pollution can be due to chemicals or energy such as heat, light or noise. The global history of pollution shows that chemicals are the most common source of pollution than other agents. The matter is further complicated by the fact that new synthetic chemicals, hitherto unknown to nature, are regularly introduced for various applications. The deleterious effects of many of them, on human and environmental health, will appear only over a longer time frame. It is also important that, however efficient the life cycle assessment of a new chemical is, it is impossible to simulate nature to predict how it will process it. Further, the chemicals once released to the environment do not respect the boundaries between air, water and soil anymore than they respect political boundaries. Thus water, soil or air pollution from a chemical agent is interdependent and the only fool proof strategy to keep the nature safe and clean for the future generation is to completely stop the release of toxic chemicals to the environment. In fact achieving *"zero discharge of pollutants"* from industries has become a paradigm among environmental protection professionals [3].

1.2 Chemical pollution

Chemicals causing environmental pollution are generally classified into organic and inorganic pollutants.

1.2.1 Organic pollutants

Organic pollutants include Persistent Organic Pollutants (POPs), high oxygen demanding natural waste, oil spill etc. POPs include large number of chemicals such as certain herbicides and pesticides, pharmaceuticals, industrial organic solvents, and components of personal care products. Health effect of some of them includes cancers, neurological disorders, reproductive dysfunction and birth defects.

1.2.2 Inorganic Pollutants

Inorganic pollution is largely due to heavy metals and radionuclides. Pollution due to toxic metal ions has specific significance due to their non-biodegradability, easy transferability from source to distance and possibility of simultaneous presence of multiple species with differing in toxicity.

i) *Heavy metal pollution*

The term heavy metal was originally used to represent toxic elements *cadmium*, *mercury* and *lead*, owing to the fact that all of them were denser than iron. Over the course of time, this term got into general use to represent group of metals or metalloid having similar toxicity such as *chromium, cobalt, nickel, copper, zinc, arsenic, selenium, silver, antimony* and *thallium.* Among them *zinc, copper* and *nickel* belongs to the essential elements having some biological functions in organism at lower concentration while toxic at higher concentrations. The other group known as non-essential elements have no any known biological function and are toxic at higher concentrations, though some are tolerable up to certain level. The toxicity of metallic pollutants depends on the nature of the metal ions and sometimes on the concentration levels also. Major health effects of toxic heavy metals are kidney, neurotic, reproductive and developmental disorders and carcinogenesis of various organs [4].

Mining industry was always a source of heavy metal pollution. Various other industries such as electroplating, wood processing, leather tanning, pigment manufacture, battery manufacture etc also produce large quantity of effluents containing significant concentrations of heavy metals in mobile form [5]. In few cases such as that of arsenic, it is an identified health hazard in many parts of the glob at the naturally existing concentrations itself [6].

ii) Radionuclide

Radionuclides could be naturally occurring such as ^{238}U and ^{40}K or manmade isotopes such as ^{137}Cs and ^{60}Co. Exposure to artificial radionuclides could possible only from the inadvertent or regulated releases of such materials to the environment from nuclear or other industrial facilities using radioisotopes. Despite the very stringent engineering controls and technology available with the nuclear industry, all phases of nuclear fuel cycle operations such as uranium mining, reactor operation, spent fuel reprocessing and waste management operations are prone to release some activity to the environment. Release potential exists for other industries such as medical, research and development (R&D) establishments and industrial facilities using radioisotopes. On the other hand, anthropogenic activities could lead to enhanced mobility of naturally occurring radionuclides such as ^{238}U, ^{232}Th etc. resulting in exposure to human via various routes of intake [7]. Carcinogenesis is the common hazard from all radionuclides whereas most heavy radionuclides like uranium possesses both chemical and radiotoxicity.

1.3 Present technologies for metal ion removal.

The basic approach used for the prevention of environmental pollution from toxic metals is to treat and recover it from the waste streams, before its release to the environment. This is usually achieved by employing suitable separation technologies such as solvent extraction, precipitation/co-precipitation, ion exchange, membrane separation, adsorption etc in the waste treatment process. A brief description of each of these technologies is as follows [8].

1.3.1 Solvent Extraction

Solvent extraction is the process of removing or extracting one component of interest from one liquid to another liquid which is immiscible with the first. The separation is achieved by the difference in solubility of the component of interest between the two liquids. The liquid containing the solute to be separated (most often an aqueous solution) is mixed with the other liquid called solvent (mostly organic) and shaken together to effect the transfer of solute from one to another. The immiscibility of the solvents helps in the separation of the two liquids, after the extraction of the components. The technology is well proven in the recovery of valuable heavy metal ions such as plutonium and uranium from dissolved spent nuclear fuel, but not in wide spread use for conventional heavy metals due to limitations such as requirements of expensive special solvents, high capital investment, large volume of the secondary waste generation etc.

1.3.2 Precipitation and co-precipitation

In this method the metal ions to be removed is precipitated with the addition of other chemical agents. Precipitation depends on the solubility product K_{sp} of the metal salt involved, pH of the wastewater and concentration of metal ions and relevant anions. Precipitation of a sparingly soluble heavy metal salt from a saturated solution may be represented by the following dynamic equilibrium:

$$MX_{2\ (s)} = M^{2+}\ (aq) + 2X^{-}\ _{(aq)},$$

where the constant $K_{sp} = [M^{2+}]\ [X^{-}]^2$

At equilibrium, the metal ions removal rate in the form of a precipitate equals the dissolution rate from the precipitate. When the product values of the concentration of cations and anions exceed K_{sp}, precipitation occurs. Additionally, heavy metals can co-precipitate with secondary minerals in wastewater. Copper, nickel, zinc, manganese etc. are co-precipitated in iron oxides and cobalt, iron, nickel and zinc are co-precipitated in manganese oxides [9]. Though this method has found some applications in heavy metal removal, large amount of sludge generation is a major drawback.

1.3.3 Ion exchange

In Ion Exchange (IX) process, the target metal ions affecting water purity are concentrated on the resin, while non-toxic ions (usually hydrogen or sodium) are released from the resin to replace them in solution. Ion exchange process is typically intended to be a reversible one, for the purpose of reuse of the resin. As a cost-effective method, ion exchange process usually involves low-cost materials and convenient operations. Ion exchange treatment methods are found to be very effective for removing heavy metals from aqueous solutions, in particular for treating water with low concentration of heavy metals. Major limitations of the technique are non-selectivity of the resin and disposal of the spent resin.

1.3.4 Membrane based separation

Application of semi permeable membrane has gained significant importance in pollutant removal including removal of heavy metals. In this process, one membrane acts as a physical barrier for the contaminant to pass and thus only pure water flows to the other side. Depending on the pore size and type of membrane used, many technologies evolved such as ultrafitraion, nanofiltration, reverse osmosis etc. Membrane based technologies can achieve very high purity for the treated water, but have several limitations such as high energy requirement, membrane fouling etc.

1.3.5 Sorption

Sorption is the process in which a solute is getting concentrated onto a solid from a fluid medium. The solid medium used is called the sorbent and the solute is called sorbate. When the accumulation is restricted to the surface of the solid (*restricted to two dimensional space*) the process is called *adsorption*, and when it involves the bulk of the solid (*three dimensional* *matrix*) it is called *adsorption*. The generic term *sorption* is used to represent adsorption and/or absorption without referring to the actual mechanism involved. Sorption is generally classified into two types based on the forces of interaction between the sorbent and sorbate.

i) **Chemisorption.** In this process, a chemical bond or exchange of electron is taking place between the sorbent moieties responsible for the uptake and the sorbate species. The energy involved in chemisorption is of the order of tens of kcal/mol, corresponding to the formation of chemical bonds. Chemisorption usually shows the saturation character due to limited availability of active groups on the sorbent, but is stable compared to physisorption.

ii) **Physisorption:** In this process no chemical bond formation is taking place, and no exchange of electron between the sorabte and sorbent. The binding between the two is due to less stable interactions like Van der Walls forces. The energy involved is maximum few kcal/mol and multilayer sorption is often encountered.

Though each of these technologies described above have associated advantages and limitations, adsorption on solid surfaces is one of the most prominently used separation process in pollution abatement, mostly due to its relative merits such as low energy requirements, low capital investment, amenability to batch and continuous process and increasing supply of new and efficient materials as sorbents. Previously, the choice of adsorbent material was limited to few proven materials like charcoal, silica gel, zeolites, alumina etc. Due to the advent of biotechnology and nanotechnology in recent decades, research towards using these materials as sorbent has taken the centre stage in the development of technologies for waste remediation.

1.3.5.1 Sorption on Biomaterials:

Materials of biological origin, both living organism and non-living biomaterials were proved to be useful for biosorption process. In search of new opportunities for pollution control and element recovery and recycling, all kinds of microbial, plant and animal biomass and derived products have received investigations in a variety of forms and in relation to variety of substances. Substrates of biological origin that have been investigated for biosorbent preparation include microbial biomass (bacteria, filamentous fungi etc.), seaweeds (microalgae), industrial wastes (fermentation and food wastes, activated sludge etc.), agricultural wastes (fruit/vegetable wastes, rice straw, soybean hulls etc.), natural residues (plant residues, tree barks etc.) and other materials (chitosan, cellulose etc.) [10]. Constant addition is taking place regularly to the pool of biomaterials capable for toxic metal removal. Similarly most of the metals or metalloids in periodic table having some toxicity or economic value have received attention in the bisorption studies. Biosorptive capacity of a biosorbent largely depends on the experimental conditions employed and prehistory and pre-treatment to which the biomaterial is subjected, prior to use. Thus from the vast pool of materials having biosorption properties, it is a challenging task to select the most appropriate sorbent for a specific purpose. However it may not be justifiable to search for new and additional material for remarkable properties, because so many representative materials have already been studied. A preferable bisorbent should be of low cost, easy to replenish, requires little processing or a by-product or waste material from another industry. Basically future research should orient more towards doing product and process modification for using the already proven materials. In fact large quantity of research has gone into modifications of biomaterials for sorption applications. This include modifications to improve the efficiency and selectivity towards pollutants by incorporating new functional groups, improving the physical properties like stability and rigidity by cross-linking and other physic-chemical modifications, making the separation easier by introducing ferric, ferro or super- paramagnetic

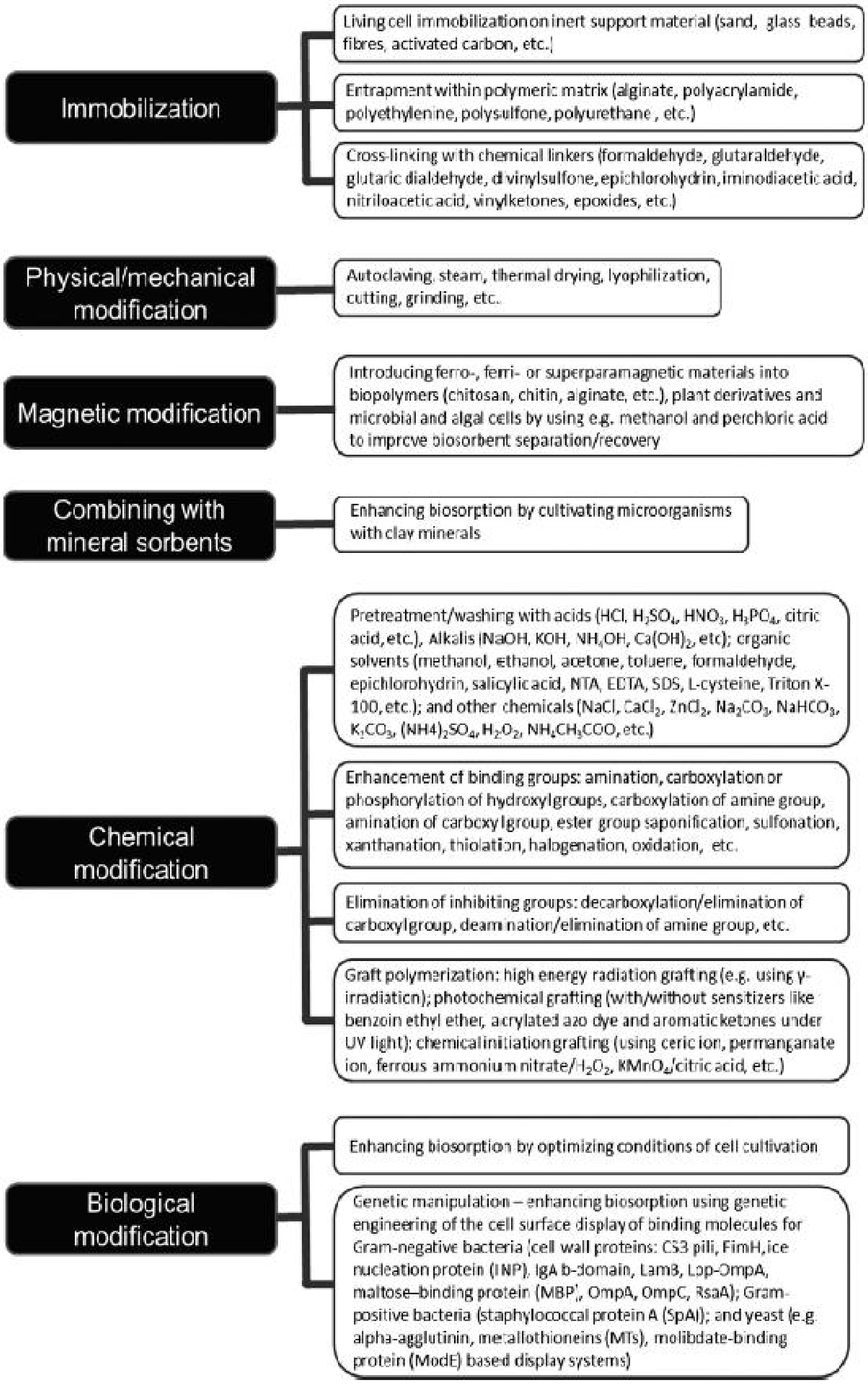

Fig. 1.1 Common modifications applied to biomaterials (***Fomina and Gadd [11]*** **)**

materials into biosorbents etc [11]. A comprehensive list of modifications applied for biomaterials is given in figure 1.1.

The mechanism of biosorption includes adsorption, ion exchange and complexation/coordination with functional groups. A variety of functional groups such as carboxyl, phosphate, hydroxyl, amino, thiol etc are involved in the biosorption process. In addition to the above mentioned mechanism, surface precipitation is also found to act in certain cases. Among the various available sorption sites, the actual mechanism could vary depending on the nature of the metal ion; eg. whether the target is a hard or soft metal ion. This also indicates that multiple mechanisms can simultaneously operate even in the case of a single adsorbent- adsorbate system. Due to these myriad complications, for any selected system, experimental investigations are essential to derive the sorption parameters and sorption characteristics.

1.3.5.2 Sorption on Nanomaterials

Nanomaterial provides unique opportunity as a sorbent for the remediation of pollution due to toxic metal ions. The high surface area and reactivity of nanomaterials are the major attraction for the use of them in pollutant remediation. Nanomaterials used for heavy metal removal includes: a) single metal oxides such as TiO_2, various iron oxides and hydroxides, MgO, ZnO, SnO_2, ZrO_2 and CuO; b) neutral metal nanoparticles such as nano-Zero Valent Iron (n-VI), Cu^0, and Pd^0; c) organic nanoparticles such as carbon nano tubes (CNT) and d) bimetallic nanoparticles such as Carboxy Methyl Cellulose(CMC) stabilised Fe(III)/Ce(IV) and Fe(III)/Cu(II) nanomaterials [11]. Among the various nanomaterials studied for the separation of heavy metals, magnetic nanoparticles are of special interest due to the ease they provide in solid-liquid separation [12,13]. Magnetic nanomaterials for heavy metal removal is so far reported to and limited to iron based magnetic nanoparticles such as Fe_3O_4, Fe_2O_3, γ-Fe_2O_3 and certain bimetallic iron oxides such as $CuFe_2O_4$. One major shortcoming observed in those studies is the instability of these nanoparticles in the solution conditions, limiting their overall efficiency as adsorbents. Various surface engineering methods such as providing polymeric coating to the nanoparticles are under development to enhance their stability in solutions. A list of modifications suggested or applied for modification of nanoparticles is listed in figure 1.2. It should be noted that many of these modifications lead to a third class of adsorbents which could be categorised as composite adsorbents.

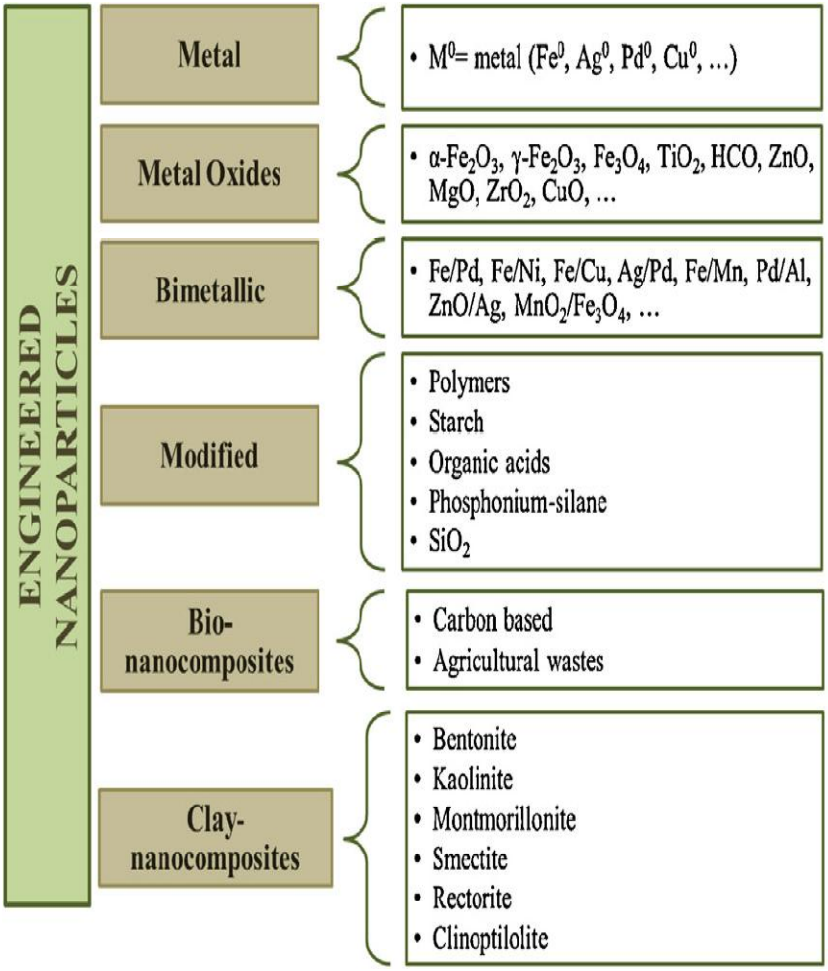

Fig 1.2 Modified nanomaterials used in environmental remediation (*Peralta-Videa et al [12]*)

1.3.5.3 Sorption on composite materials

Along with many advantages of biomaterials and nanomaterials described above, few limitations surfaces in utilising their full potential as sorbents for contaminants. The poor stability of these materials in solution, the difficulty in separation of them from the bulk liquid on completion of the process etc is serious technological bottlenecks. One obvious continuation is the preparation of composites with improved physico-chemical characteristics in comparison to the individual components. Voluminous work has been reported on such approaches [14] which could be classified into: i) composite of chemically distinct biomaterials ii) composite of biomaterial and a natural component such as clay and mineral phases iii) composite of biomaterials and synthetic organic polymers iv) biomaterials coated on nanoparticles such as peptides and proteins on magnetite nanoparticles. In case of nanomaterials, the approach is essentially to use biomaterials and synthetic polymers as a support for the nanoparticles to be used, in order to ease its solid-liquid separation and/or to increase its stability in working solutions [15].

The objective of the composite preparation, most often is to improve the physical properties of adsorbent such as stability and ease of separation. But many studies proved that a synergism could be possible, where the composite shows higher sorption capacity than the individual components. One most sought after groups of composite are that of magnetic nanomaterials coated with biosorbent such as chitosan derivatives [16]. Functionalised biomaterials for high selectivity and efficiency combined with magnetic separation achieved in such processes are very suitable for environmental cleanup operations. Additionally the organic coating on magnetic nanoparticles in-turn improves their stability in aqueous medium. Overall the trend in composite preparation proves that much scope remains in the use of bio-nano composite materials for environmental cleanup operations.

1.4 Strategies for in-situ remediation.

While it is important that future contamination could be minimised by adoption of improved technologies, world over many sites exists, contaminated with pollutant materials due to past incidents, accidents or reckless releases when the rules and regulations were not so stringent as it is today. Biomaterials and nanomaterials have huge potential to be used as in-situ barrier for target pollutants at such sites, thus limiting its environmental foot print to smaller region. The most studied system in this respect is the use of nZVI as the Permeable Reactive Barrier (PRB) for various contaminants including metal ions like Ni, Cu, Zn, Cd, Pb, Cr, Hg, Se, Sb, As, U, Tc, Mo, Pu, U, Am, ^{137}Cs and ^{90}Sr [17]. Many other synthetic and natural minerals and biomaterials also have been studied for such applications. Biomaterials subjected to the test as PRBs against metallic pollutants include bone char, peat moss, chitosan, pecan shells, lignite and coal [18,19]. Humic substances are also identified as a potential agent for the in-situ remediation of contaminants. Wan et al [20] used humic acid based soil amendment for the retardation of uranium in a contaminated site. Bogush et al [21] and Olds et al [22] reported that humic acid could be used for the treatment of acid mine drainage. Decontamination of organic and metallic pollutants from natural waters by crude humic acid blend was reported by Yates and Wandurska [23]. Alexadrova et al [24] demonstrated that the presence of high humic acid concentration results in increased immobilisation and lower bioavailability of radionuclides at South Ural lake. All these studies indicate that humic substances are potential biomaterial for in-situ treatment of contaminated sites. However due to the very complex and yet to be fully revealed structure and properties of humic materials, detailed analysis of humic-pollutant interactions are to be done for development of such technology for field scale applications.

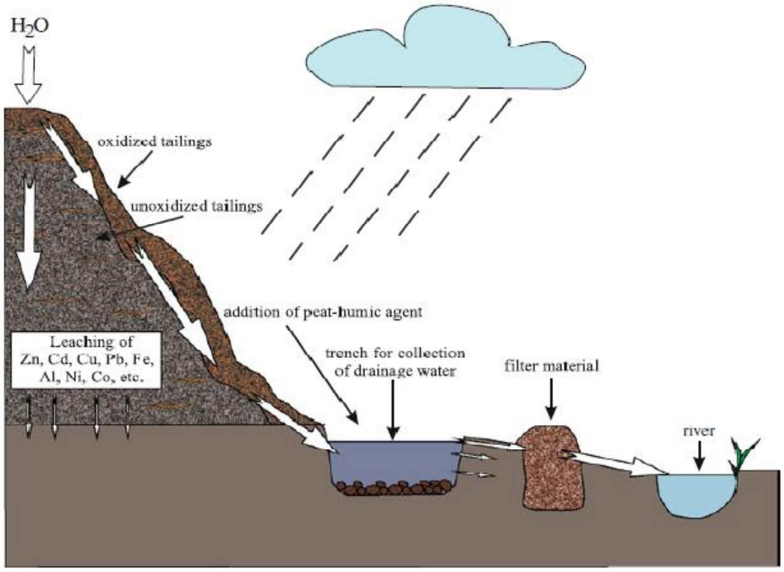

Fig. 1.3 A proposed scheme for application of humic acid at contaminated site (***Bogush and Voronin [22]*****)**

1.5 Objective of the thesis

As described in previous sections, carefully designed physico-chemical modifications of a given sorbent leads to better products. In such attempts, it is important that the modification methods employed should not involve complex multi-step reactions so as to result in overall reduced yield for the final product. Preferably, for modifications, as a better eco-friendly practice, non-toxic chemicals should be used. The present thesis is an effort to study the application of modified biomaterials and nanomaterials as sorbents for selected metal contaminants. Chitosan, humic acid and magnetite nanoparticles were the selected sorbents. Uranium(VI) was the principal model heavy metal employed in the studies though chromium(III) and lead(II) were also employed in some studies. While all substrates selected as sorbents are popular among the environmental chemists, the studies presented here is novel with respect to the selection of targets and/or the modifications procedures applied to these sorbents.

Chitosan, the first biosorbent selected for the studies is made from chitin, the second most abundant biopolymer after cellulose on earth. It is found to have excellent sorption capacity for various heavy metals including radionuclides [25]. Chitosan is the copolymer composed of β-2-amino-2-deoxy-D-glucopyranose units and the residual 2-acetamido-2-deoxy-D-glucopyranose units. The metal uptake by it is primarily attributed to the amine and hydroxyl groups present in the polymer chain, which can interact with various metallic species through ion exchange and/or chelation mechanism. In fact sorption of almost every toxic element in the periodic table might have been studied on chitosan[26]. But chitosan flakes, as originally available, have many disadvantages such as formation of gel like material on use at acidic pH. Stabilising with suitable cross-linking agents is the usual procedure to enhance its stability for practical applications. Earlier modifications of chitosan for sorption of uranium used toxic chemicals such as glutaradehyde, epiclorohydrine or ethylene glycol diglycidyl [27-29]. A cross-linking method based on the non-toxic chemical, sodium tripolyphosphate could be better alternative to prepare a chitosan based uranium sorbent. Additionally the presence of phosphate groups introduced as a result of the cross-linking process could enhance the uranium uptake, due to the excellent affinity of phosphates for uranium. Based on these assumptions, this thesis investigates the utility of chitosan cross-linked with tripolyphosphate as an adsorbent for toxic metal ions.

Natural Organic Matter (NOM) is the most abundant organic carbon form on earth and humic materials are the major component of NOM in aquatic and terrestrial environment [30,31]. They are formed by the decay of dead plants and organism and have the ability to complex with various metal ions principally through interaction with carboxylic and phenolic groups and to a lesser extend through less abundant keto, amino and thiol groups present in them. Due to the strong complexing ability, it is pointed out that they are the most abundant ligands on earth crust for metal ions binding. Though many attempts are reported on the use of humic materials for metal ion removal, serious shortcomings were observed for many of them. In this thesis, a new solid humic sorbent is prepared using simple procedures and their metal ion sorption properties were studied.

Magnetite nanoparticles are easy to prepare and often present in the natural environment. Studying their metal ion sorption characteristics is important; both to use it as an environmental cleanup agent and also to gather better understanding of their role in the natural environment. Due to this technical and fundamental importance, the sorption characteristics of uranium on magnetite is studied as a part of this dissertation. In natural environment, rather than its naked form, magnetite may appear as nanoparticle coated with natural organic materials such as humic acid. It is reported that such modifications could significantly affect their sorption characteristics towards various chemical agents [32]. In order to understand this, humic acid coated magnetic nanoparticles were prepared and studied for the sorption of uranium.

Full fledged use of humic materials for in-situ remediation of metal contaminated sites requires a deeper understanding of the various aspects of their interactions with metal ions, especially due to the fact that humic materials are not well defined chemical entities and is a complex mixture of heterogeneous organic molecules. Some of the complexities observed in the interaction of humic materials with metal ions and various geological media are preferential sorption of low or high molecular weight components on mineral phases, preferential precipitation of high molecular weight components, preferential interaction of metal ions with high or low molecular weight components etc [33-35]. This warrants more elaborate examination of the behaviour of various fractions of humic materials with metals and mineral components. Towards this, a comparative study of the interaction of uranium with Gray Humic Acid (GHA) and Brown Humic Acid (BHA) fractions were carried out as a part of this dissertation.

1.6 Outline of the thesis

The thesis is divided into seven chapters, including this chapter on introduction to the subject. Chapter two describes the various instrumental techniques and experimental procedures adopted for the studies. Chapter 3 to chapter 6 gives the details of the studies carried out for this dissertation. Chapter 3 presents the preparation and characterisation of chitosan tripolyphosphate beads as well as the sorption studies of U(VI) and Cr(III) ions on this sorbent. Chapter 4 presents the preparation of a new sorbent, humic acid coated chitosan tripolyphosphate beads, and their sorption characteristics for U(VI) and Pb(II) ions. Chapter 5 deals with sorption of uranium on bare and humic acid coated magnetic nanopartcles. Chapter 6 devote to the studies carried out on the binding characteristics of gray humic acid and brown humic acid fractions with uranium. The last chapter (chapter 7) summarises the finding of this research.

Chapter 2

Experimental

2.1 Introduction

Applications of some modified biomaterials and nanomaterials in the remediation of heavy metal pollution are bought out in the research pertaining to this thesis. This chapter gives the generic details on the preparation of the adsorbent materials employed, analytical and characterization instrumentation utilised in the studies, modeling of the experimental results, and the approaches used to study the heavy metal humic acid interactions.

2.2 Materials

Humic acid sodium salt (Lot No. 31938-042), chitosan (medium molecular weight), sodium tripolyphosphate and calcium acetate monohydrate were purchased from Sigma Aldrich (USA). Barium chloride and uranyl nitrate hexahydrate (ACS grade) were purchased from E.Merck Germany. AAS standard solutions (1000 mg/l) of Na(I), Ca(II), Mg(II), Al(III), Cr(III) and Fe(III) in 0.5 N nitrate medium were purchased from E.Merck. All other chemical and reagents used in the experiments were of analytical reagent grade purity and obtained from local chemical suppliers.

2.3 Preparation and purification of sorbents and other chemicals.

Modified biomaterial, Chitosan Tripolyphosphate (CTPP) beads are prepared by the in-liquid ionic polymerization of chitosan following a method described by Lee et al [36]. The details of the preparation and characterization are elaborated in chapter 3. Humic Acid coated Chitosan Tripolyphospahte (HA-CTPP) beads were prepared by a single step wet coating of chitosan tripolyphosphate beads in aqueous medium, which is described in details in chapter 4. Bare and humic acid coated magnetite nanoparticles for adsorption studies were prepared by the alkaline hydrolysis of iron(II) and iron(III) salts in absence and presence humic acid sodium salt respectively as described in chapter 5 [37]. Commercial humic acid is purified and separated into two fractions, brown and gray humic acid based on its ionic strength dependant solubility [38]. Details of the separation and purification procedures are provided in chapter 6.

2.4 Analytical methods

2.4.1 UV-Visible absorption spectroscopy

UV-Visible spectroscope is one of the classical analytical instruments used for material characterization and concentration measurement [39]. The principle of absorption spectroscopy is based on the *"Beer-Lambert's Law"*, according to which ' *the decrease in intensity (dI) of a narrow beam of light passing through a solution of small volume of absorbing molecules is proportional to the intensity of the light entering the medium (I), the concentration of absorbers C, and the length of the light path through the element, (dl).*

Mathematically,

$$-dI = ICdl$$

This could be reduced to the normally used expression,

$$\log\frac{I_o}{I} = \varepsilon cl \qquad (2.1)$$

where *Io* is the initial intensity of light, *I* is the intensity of light after passing through the medium, ε is the molar absorbtivity or extinction coefficient of the analyte, *c* is the concentration of the analyte and *l* is the path length of the cell. When a monochromatic radiation is used to excite the analyte molecules, the fractional absorption is a property of the molecules and a scanning of absorption across the wavelength gives the absorption properties of the analyte molecules. Similarly the concentration of molecules in the solution can be obtained from the absorbance measured usually at an appropriate peak wavelength of the analyte. For present studies, absorption spectral scanning and concentration measurements were done using the double beam UV-Visible spectrometer ***UV540 model (Thermo Spectronic, USA).***

2.4.2 Fourier Transform Infra Red (FTIR) spectroscopy

The functional groups on organic and inorganic substances could be identified using the vibrational absorption properties of the material applying the same principal as applied to the UV-visible absorption spectroscopy (usually represented in terms of the transmitted intensity). Infrared spectra in the present studies were carried out using **JASCO 400 FTIR spectrometer**, using KBr pellet method or using NUJOL mull on **JASCO 610** spectrometer.

2.4.3 Molecular Fluorescence Spectroscopy.

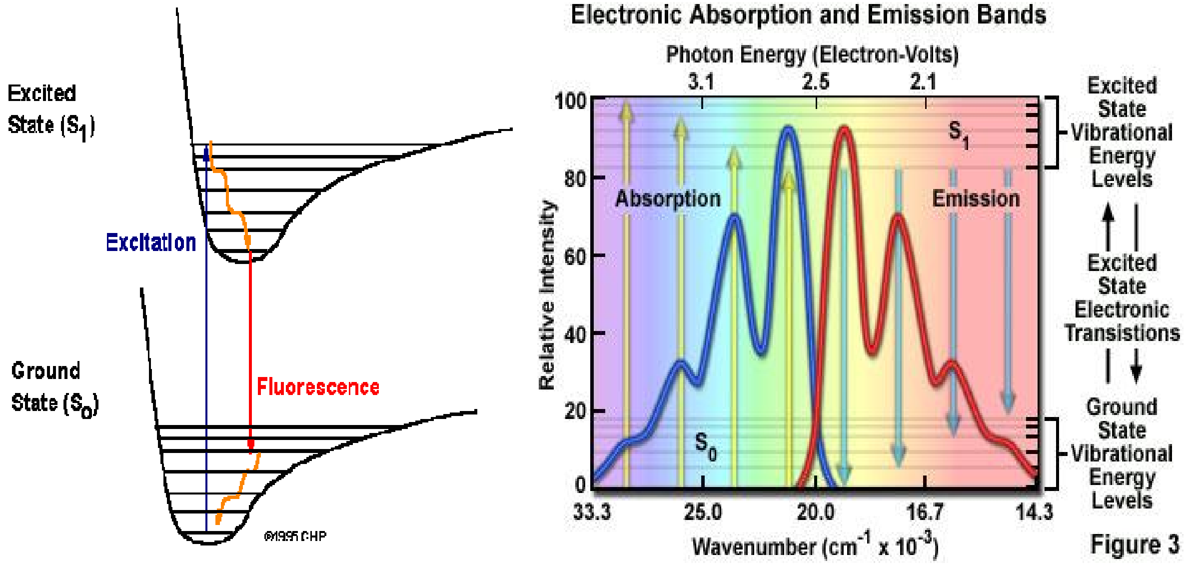

Fig. 2.1 Schematic presentation of the fluorescence transition and fluorescence spectrum.(*image courtesy: elchem.kaist.ac.kr*)

Molecular fluorescence is the phenomenon of emission of light from a substance subsequent to its absorption, usually at wavelength higher than the absorbed wavelength. Similar to absorption spectra, emission spectra also could be used for identification and quantification of analyte samples. This technique is widely used for studying the interactions of metal ions and organic compounds with biomolecules [40]. In the present studies fluorescence measurements were done using **JASCO 4500 fluorescence spectrometer**. This instrument uses a 150 W xenon lamp as the light source for exiting the sample.

2.4.4 Inductively Coupled Plasma Atomic Emission Spectroscopy (ICP-AES).

It is a type of emission spectroscopy that uses the inductively coupled plasma to produce excited atoms and ions that emit electromagnetic radiation at wavelengths characteristic of a particular element [39]. Usually plasma is generated from the argon gas in a plasma torch by the application of radio frequency. Sample is nebulised into this plasma using a peristaltic pump where the various molecules in the sample break up into their respective atoms which then ionize and recombine repeatedly, giving off radiation at the characteristic wavelengths of the elements involved. The intensity of this emission is indicative of the concentration of the element present in the sample. It is a multi-elemental analysis technique with ppb level detection limit. A schematic diagram of the instrumentation is given in figure 2.2. In present studies, ICP-AES

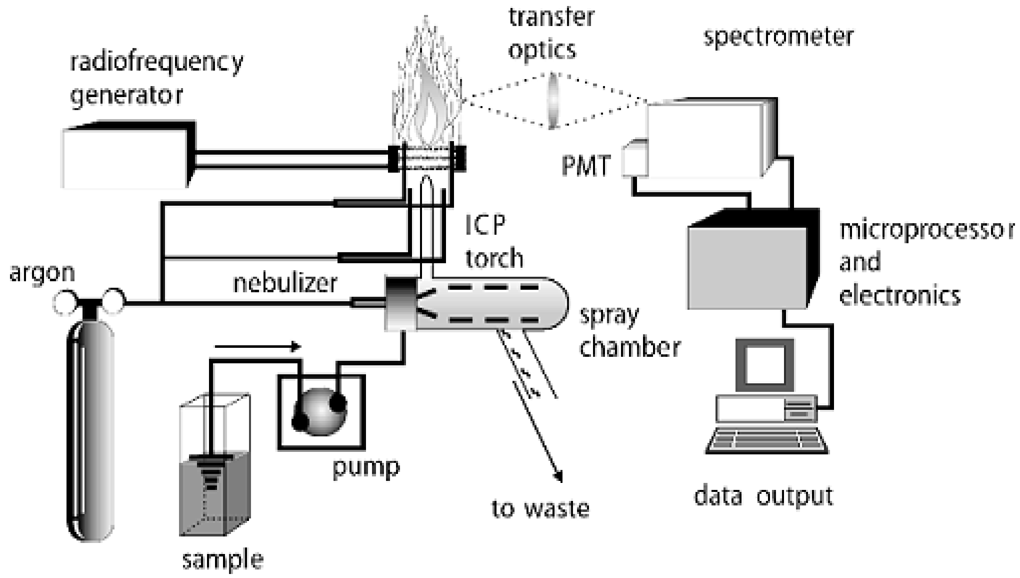

Fig. 2.2 Schematic pesentation of ICP-AES spectroscopy system
(image courtesy:quoteimg.com)

model **JY-238 (Jobin Vyon, France)** was used for the analysis of concentration of Na, Ca, Mg, Pb, Cr, Al and Fe in solutions.

2.4.5 X-ray Diffraction analysis

X Ray Diffraction (XRD) is the most commonly used technique for fingerprint characterization of the crystalline materials, as well as for the determination of their unit cell parameters [41]. The theory of diffraction is based on the Bragg's law:

$$n\lambda = 2d_{hkl}Sin\theta \tag{2.2}$$

where n is an integer, d_{hkl} is the interplanar distance of the crystal lattice which causes the constructive interference, and θ is the angle of incidence of the X-ray beam with the crystal plane. In XRD, the sample is irradiated by a collimated monochromatic X-ray beam generated from a cathode ray tube. While scanning the sample through a range of 2θ angles, diffraction

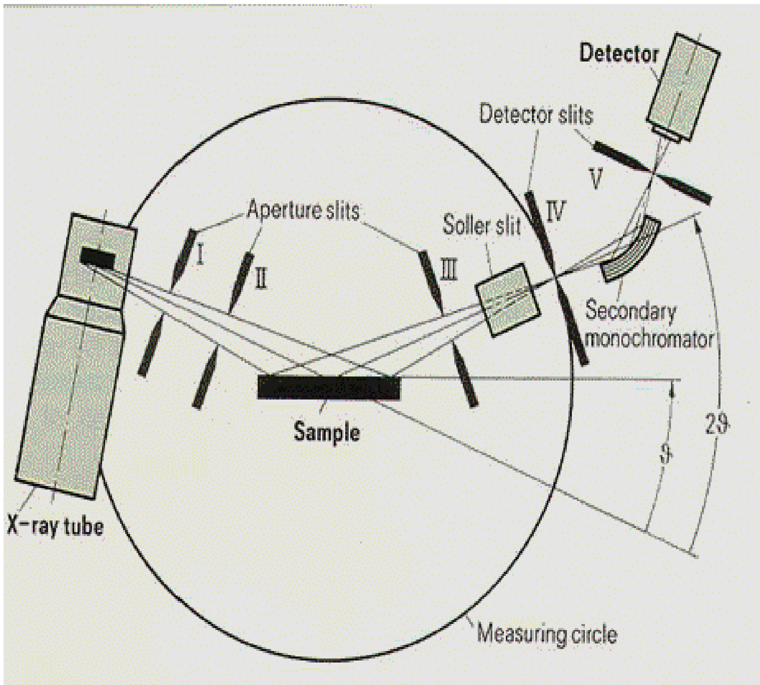

Fig. 2.3 Schematics of the XRD instrumentation (image courtesy: jessdavenport.com)

taking place only for the incident angle for which the Braggs law is satisfied and from the obtained diffraction pattern identification of the sample is possible. A schematic diagram of X-ray diffractometer is given in figure 2.3. XRD was used in the identification of magnetite nanoparticles in the present investigations. Powder XRD of the nanoparticles was recorded with the Cu k_{α} radiations ($\lambda = 1.5405$) using **Philips analytical X-ray machine.** The data were collected at room temperature in the range of 2θ between 20^{o} and 70^{o}.

2.4.6 Scanning Electron Microscope (SEM).

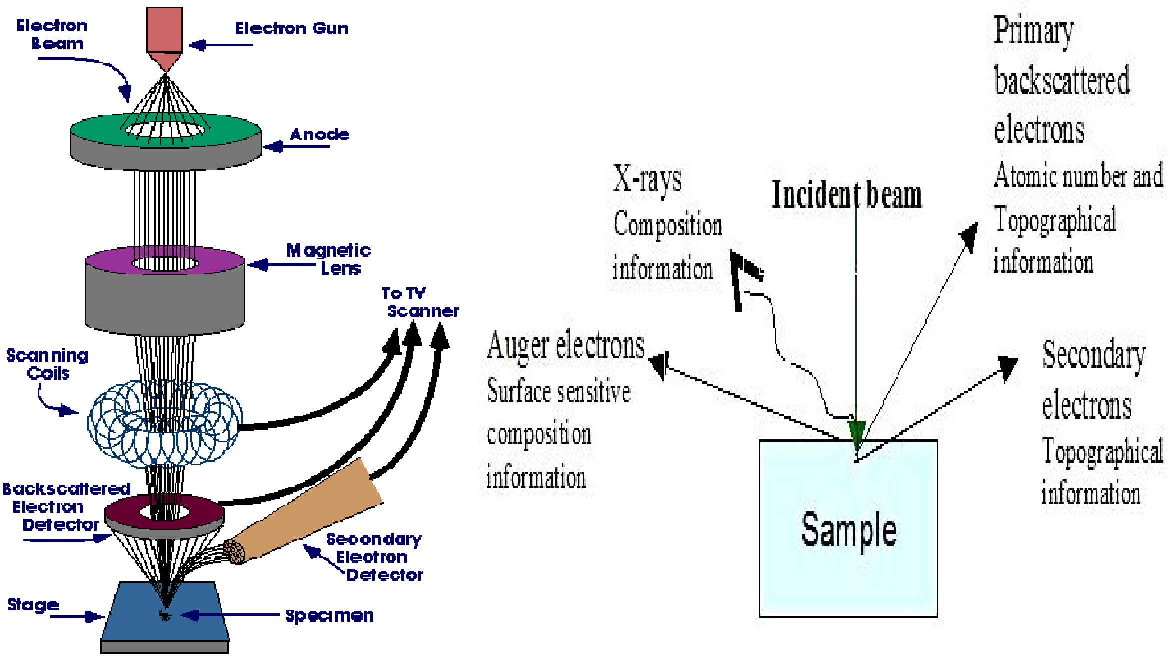

Fig. 2.4 Schematic presentation of the Scanning Electron Microscope and the different particles emitted in the process (image courtesy: purdu.edu)

SEM gives information about topography, morphology, composition and crystallographic details of the arrangement of the atoms in a material. In a typical SEM, an electron beam in the energy range of hundreds of eV to 50 keV is focused on a small area of the sample, under vacuum [39]. As the electrons strike and penetrate the surface, a number of interactions occur, that result in the emission of Secondary Electrons (SEs), Back Scattered Electrons (BSEs), characteristics X-rays, and Auger electrons from the sample. SEs are created near the surface, and are sensitive to the topography of the sample. The BSEs comes from the bulk of the material and carries information about distribution of heavy elements. Auger electrons and characteristic X-rays give information on the chemical composition of the sample. SEM micrographs and EDS for present studies were recorded using **Seron Inc. make AIS 2100** model scanning electron microscope using 20 keV electron beam. For SEM images of powder samples, sample in methanol was placed over a mirror polished Si single crystal and finally a thin gold coating was applied prior to loading the sample. For non-conducting materials such as polymeric beads, gold coating was invariably required for producing the image.

2.4.7 X-ray Photo electron Spectroscopy (XPS)

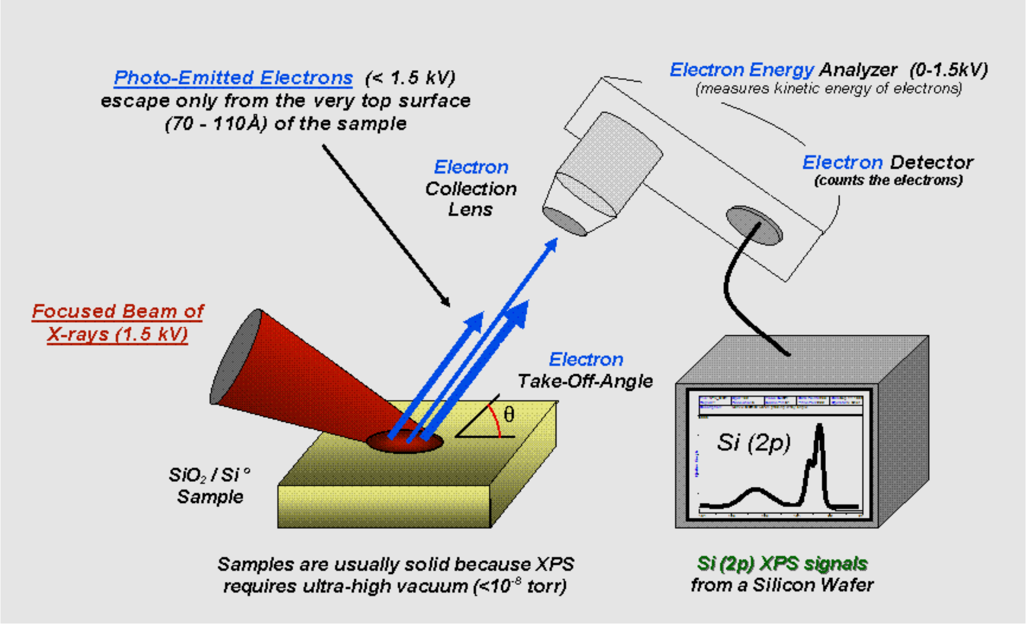

Fig. 2.5 Schematic presentation of XPS instrumentation (image courtesy: en.wikipedia.org)

XPS is a technique used to gather information on the elemental composition and oxidation state of material, usually by irradiating the material by a beam of X-rays, while simultaneously measuring the kinetic energy and number of electrons emitted from the surface [39]. From the kinetic energy of the emitted electron, nature and oxidation state of the element present on the material surface can be identified. A schematic diagram of the XPS set up is given in figure 2.5. For present studies, XPS spectrum of the nanoparticles was recorded using **Perkin Elmer PHI 5400 spectrometer** equipped with a Mg k_{α}* excitation source. In order to take into account the charging effects on the measurement of binding energies, these energies were determined by referencing to the adventitious C1s peak at 284.6 eV.

2.4.8 ZnS(Ag) scintillation detector.

A gross alpha counting system, used for counting alpha activity in samples consists of a detector made of a transparent plate coated with the scintillating ZnS(Ag) crystal particles, a Photo Multiplier Tube (PMT) and a counting set up [42]. Alpha particle incident on the detector surface produces photons which is multiplied by the PMT and counted on the counter. For present studies a PLA make **CS 201 counter** along with **PSP647D alpha probe** was used for the counting of alpha particles emitted by ^{233}U. The detector were calibrated using ^{241}Am standard procured form **Zigert-Egler (Germany)**

2.4.9 Surface area Analyser

Brunauer-Emmett-Teller (BET) surface area of the magnetite nanoparticles was determined by N_2 adsorption- desorption measurement, using the home built surface area analyser in analytical chemistry division. Dynamic, single point BET method based on physical adsorption of nitrogen on the specimen, from a mixture of helium and nitrogen at liquid nitrogen temperature is employed for the measurements.

2.5.10 Zeta potential measurement

Zeta potential of humic acid and magnetic nanoparticles were measured using Malvern Zetasizer **(*Nano ZS model, Malvern Instruments, U K*).** This instrument uses a 4.0 mW He-Ne laser (633 nm) beam to measure the electrophoretic mobility of the particles using dynamic light scattering and obtains the zeta potential by putting this velocity data into Henry's equation

$$U_E = \frac{2\varepsilon z f}{3\eta} \tag{2.3}$$

where U_E, ε, z, η stands for electrophoretic mobility, dielectric constant, zeta potential and viscosity respectively and f is the Henry's function having a value 1.5 under Smoluchowski approximation.

2.6 Sorption Studies

Batch sorption studies were carried out by adding a fixed amount of the sorbent (w) to a fixed volume (V) of the sorbate solution containing known concentration of the contaminant metal ions. Before the equilibration of the mixture, pH of the experimental solutions were adjusted by addition of required amount of acid or alkali. After agitation for known time, a small portion of the aqueous phase was separated and analysed for concentration of the dissolved metal ions, using spectroscopic or radiometry methods. Equilibrium sorption capacity (q_t) at any time t was determined, using equation

$$q_t = \frac{(c_0 - c_t)V}{w} \tag{2.4}$$

where C_o and C_t are the initial and the equilibrium concentrations at time t respectively of the sorbate in solution.

2.6.1 Adsorption isotherms

Various theoretical models have been proposed over the years to describe the sorption process in detail. By analyzing the experimental data, using these models, a thorough understanding about the sorption system under investigation is possible. For present thesis, adsorption experimental data were analysed using the most popular isotherm model, the Langmuir model and the Freundlich model, and at least one of them is found to fit the experimental observations satisfactorily [43] in each of the studied case.

Langmuir Isotherm

The most often used model, Langmuir isotherm is based on assumptions such as: a) the sorbent surface is made of homogeneous binding sites having same energy for sorption, b) sorption on the surface is localized to definite sites and c) each site can accommodate only one molecule, or atom. Langmuir proposed that the rate at which the sorbate molecules comes into contact with the sorbent surface is proportional to the product of the concentration of the sorbate C, and the fraction of the surface remaining uncovered by sorbate. If 'θ' is the fraction of surface sites covered by sorbate molecules and $(1 - \theta)$ is the fraction of surface which is unoccupied, then:

The rate of sorption $\alpha \quad C(1-\theta)$

or rate of sorption = $K_a C(1-\theta)$

rate of desorption $\alpha \quad \theta$

or rate of desorption = $K_d \theta$

At equilibrium:

$$K_a Ce\ (1-\theta) = K_d\theta$$

or

$$\theta = \frac{K_a C_e}{K_d + K_a C_e}$$

or $$\theta = \frac{KC_e}{1 + KC_e} \qquad (2.6)$$

where K is the Langmuir constant K_a/K_d, and C_e is the equilibrium concentration of the sorbate in solution at equilibrium condition.

Freundlich Isotherm

Freundlich isotherm is an empirical equation which assumes heterogeneous sorption sites on the sorbent. The model expect stronger binding sites to occupy first and the binding strength to decrease with increase in the degree of site occupation. For a given concentration of the solute, sorption is directly proportional to the concentration raised to power 1/n. Here, n is a variable having value greater than one. Mathematically Freundlich isotherm can be expressed as:

$$q_e = k_F \times c_e^{1/n} \qquad (2.7)$$

where k_F is the Freundlich constant . A favorable sorption tends to have n between 1 and 10. Larger value of n (smaller value of $1/n$) implies stronger interaction between the sorbate and the sorbent, while $1/n$ equal to 1 indicates linear sorption, leading to identical sorption energies for all the sites.

2.6.2 Adsorption Kinetics

Sorption kinetics describes the time-dependent evolution of the sorption process until equilibrium is reached. The most popular kinetic models used for sorption analysis are 'pseudo-first order' , 'pseudo-second order' and ' intra-particle diffusion model' [44].

Pseudo-first order rate equation

The pseudo- first order rate equation can be represented as

$$\frac{dq_t}{dt} = k_1\ (q_e - q_t)$$

where q_e and q_t are the concentration of solute adsorbed on to the sorbent at equilibrium and at time 't' respectively and k_1 is the first order rate constant. Kinetic parameters are often obtained by applying the integrated form of the equation,

$$\log(q_e - q_t) = \log q_e - \left(\frac{k_1}{2.303}\right)t \tag{2.8}$$

from which, the model constant k_1 can be derived from graphical analysis.

Pseudo- second order equation

The pseudo-second order model is applicable where the overall rate of the reaction is decided by the interaction between the sorbate and sorbent and is represented as:

$$\frac{dq_t}{dt} = k_2\ (q_e - q_t)^2$$

where k_2 is the second order rate constant and can be obtained from the graphical analysis of the integrated expression:

$$\frac{t}{q_t} = \frac{1}{k_2 q_e^2} + \frac{t}{q_e} \tag{2.9}$$

Intra-particle diffusion model.

In many cases, concentration distribution of the solute within the solid sorbent is controlled by the intra-particle diffusion and this could be the rate controlling step in the overall observed kinetics. The Fickian diffusion equation is applicable to explain the sorption process [44], which can be expressed as:

$$q_t = k_{id} \times t^{1/2} \tag{2.10}$$

where, q_t is the adsorption capacity (mg/g) at time t, and k_{id} is the intraparticle diffusion constant (mg/g-h). The plot of q_t as a function of $\sqrt{t}$ gives a straight line, from which the intra-particle diffusion constant, k_{id} can be obtained.

2.7 Determination of apparent stability constants of uranium with HA

Binding constants between humic substances and uranium were derived using the classical fluorescence quenching method following Nakashima et al[45]. In this method no assumptions are made about the number of binding sites per HA molecule or the charge density on the metal ions, whereas the interaction is measured based on the global parameter as the reduction in fluorescence intensity of the humic acid upon its binding with the metal ion. Complex formation of HA with metal ion can be represented as

$$\text{HA} + \text{M} \leftrightarrow \text{HA-M}$$

and the conditional stability constant can be represented as

$$K_b = [HA - M]/[HA][M]$$

where K_b is the conditional stability constant, [HA-M] is the concentration of humic metal complex, [HA] and [M] are the concentration of free humic acid and metal ion at equilibrium.

If the fluorescence intensity of HA in the absence of metal ion is represented as I_o and that in presence of metal ion as I, the binding constant K_b could be related to the ratio of fluorescence intensities by the standard Stern-Volmer equation,

$$\frac{I_0}{I} = 1 + K_b\,[M] \tag{2.12}$$

where [M] is the concentration of the metal ion. A plot of I_o/I against [M] should give a straight line with slope equal to the binding constant K_b .

2.8 Aggregation kinetics of HA

Humic substances aggregate in aqueous media depending on the solution conditions such as pH and ionic strength of the medium and concentration of metal ions [46]. The extend of aggregation of humic acid can be represented as

$$\alpha = (C_o - C)/C_o$$

where α is the degree of aggregation, C_0 is the initial concentration of humic acid and C is the concentration of humic acid in solution at a given instance during the progress of the aggregation. α =0 means zero aggregation and α=1 means complete aggregation.

Aggregation rate can be analysed using the first order rate equation

$$R = \frac{-dC}{dt} = k(C_f - C_0) \tag{2.13}$$

where C is the dissolved HA concentration at an instant t, C_0 and C_f are the initial and final (at the saturation of the aggregation) dissolved HA concentration respectively. Integration of equation (2.13) results in

$$C = C_f + (C_o - C_f)e^{-kt} \tag{2.14}$$

or in terms of α;

$$\alpha = \alpha_f - \alpha_f\, e^{-kt} \tag{2.15}$$

where $\alpha_f = (C_0 - C_f)/C_0$ is the highest degree of aggregation and the aggregation rate constant k can be obtained from the plot of α against t. In the present studies this expressions were used to derive the difference in the aggregation behaviour of GHA and BHA in presence of uranium.

Chapter 3

Studies on sorption of U(VI) and Cr(III) onto Chitosan Tripolyphosphate (CTPP) beads

3.1 Introduction

Chitin is the second most abundant polysaccharide (next only to cellulose) in nature. Chitin is common in biological world and highly abundant in nature principally in shells of crustaceans, terrestrial invertebrates and fungi. Partial deacetylation of chitin by alkaline hydrolysis gives chitosan. The chemical structure of chitin and chitosan is given below.

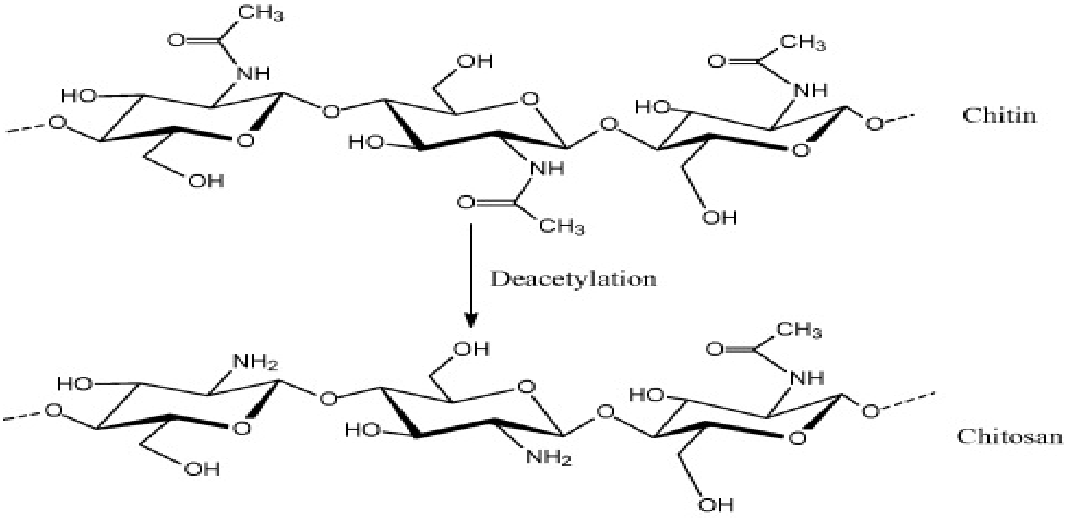

Fig. 3.1: Molecular structure of chitin and chitosan

Chitosan is the copolymer composed of β-2-amino-2-deoxy-D-glucopyranose units and the residual 2-acetamido-2-deoxy-D-glucopyranose units. Chitosan is abundant with amino and hydroxyl groups which could bind metal ions through ion exchange and chelation mechanisms. Due to this and the advantages like non-toxicity and biodegradability, chitosan have been heavily investigated as a medium for the sorption of various heavy metal ions and radionuclides. Nonetheless, the mechanical properties of chitosan is weak and is easily soluble in acidic pH ($pH \leq 5$). Cross-linking with various chemicals is the usual method adopted to improve the physical and engineering properties of this material. Most often, the cross-linking agents used for chitosan modifications are toxic chemicals such as glutaradehyde, epiclorohydrine or ethylene glycol diglycidyl ether.

From the environmental safety point of view, it is preferred to use non-toxic and environmentally benign substances for developing future technologies. Tripolyphosphate (TPP) mediated ionic cross-linking of chitosan is thus a suitable alternative to the use of toxic chemicals for the modification of chitosan. Cross-linking of chitosan by TPP can be achieved by a single step process, where the formation of intra and intermolecular cross-linking leads to solidification of chitosan to chitosan-tripolyphosphate (CTPP) beads [39]. However only few studies are reported on the use of chitosan cross-linked with TPP for sorption of toxic metal ions. Since this cross-linking procedure adds phosphate groups having high affinity for metal ions like uranium to the polymer, a synergism of good physical properties and high sorption capacity can be expected. In the present investigations CTPP beads were prepared by the ionic cross-lining of chitosan and sodium tripolyphosphate and its sorption properties for U(VI) and Cr(III) were investigated using batch adsorption technique. Sorption studies were carried out as a function of contact time, pH and concentration of metal ions. The experimental results were fitted into Langmiur and Freundlich isotherm models. Kinetics of the adsorption process was analyzed using pseudo-first order, pseudo-second order and intra-particle diffusion models. To understand the competition effects, sorption experiments were conducted using binary mixture containing Cr(III) and competing ions. Attempts were also made to identify the binding sites using infrared spectroscopy.

3.2 Materials

Chitosan (medium molecular weight) and sodium trypolyphosphate (STPP), ($Na_5P_3O_{10}$) were purchased from Aldrich chemical company, USA. U(VI) solutions of appropriate concentrations were prepared from $UO_2(NO_3)_2.6H_2O$ (ACS grade) salt purchased from Merck, Germany. Cr(III), Al(III), Fe(III), Ca(II), Mg(II) and Na(I) solutions of appropriate concentrations were prepared by diluting AAS standard solutions in nitrate medium (Merck, Germany) of initial concentration of 1000 mg/l. Higher concentrations of Cr(III) solutions were prepared by dissolving appropriate quantity of $Cr(NO_3)_3.9H_2O$ (Merck, Germany) in nanopure water. 2-(5-Bromo-2-Pyridylazo)5-diethylaminophenol(Br-PADAP), Triethanolamine, (1,2-Cyclohexane Di-amine Tetra Acetic acid (CDTA), NaF and sulphosalicilic acid used for the analysis of uranium concentrations were analytical grade, purchased from Merck, Germany or Sigma-Aldrich, USA. All other chemical used in the experiments were of analytical reagent grade purity. Deionised water used for all experiments was obtained from Milli-Q (Millipore Corporation, USA) water purification system.

3.3 Preparation and characterization of CTPP beads.

CTPP beads were prepared by ionic cross-linking of chitosan solution with sodium tripoliphosphate [39]. Chitosan (10g) was dissolved in 500 ml of dilute acetic acid (1% v/v) to prepare the chitosan solution. The STPP solution was prepared by dissolving 10g of the solid in 100 mL of water. The chitosan solution was pumped into TPP solution using a PVC tip, with an opening of 1mm.The beads were prepared at two different pH for the TPP solution; pH=8.6 (original pH of the STPP solution) and at pH=3.0 by additing 1M HCl, in order to obtain beads with different cross-linking densities[47]. The beads were cured for 12 hours, separated by filtration, washed four times with deionised water and air dried before use in adsorption experiments. Dried beads were spherical and slightly yellowish in colour. The surface morphology of the beads was characterized using SEM. Atomic composition of the surface of the beads before and after sorption of Cr(III) is obtained using Energy Dispersive X-ray Spectroscopy (EDS) analysis.

3.4 U(VI) and Cr(III) concentration measurements.

Concentration of dissolved uranium after the equilibration was determined using the spectrophotometric method using Br-Padap as the complexing agent at pH=7.8 [48]. Triethanolamine buffer (T-buffer) for pH adjustment was prepared by diluting 14 mL of the triethanolamine in 80 mL of deionised water, adjusting the pH to 7.8 by adding con. $HClO_4$ and finally made up to 100mL. Complexing solution for removing the interference of other bivalent cations was prepared by dissolving 3.5g of sulphosalicilic acid, 0.5 g of NaF and 1.25g of CDTA in 40 mL water and adjusting pH to 7.8 by addition of sodium hydroxide pellets and finally made up to 100 mL. For measurement of uranium, 1 mL of complexing solution, 20-100 µL of aliquot of the sample, 1mL T-buffer, 4mL of ethanol and 0.5 mL of Br-Padap were added into the 10 mL volumetric flask and made up to 10 mL using deionised water. The solution was allowed to develop colour for thirty minutes and optical density is measured at 578nm using UV540 double beam spectrophotometer (Thermo Spectronic, USA).

Cr(III) measurements were carried out using ICP AES. The sample aliquot taken from the reaction mixture is diluted to give a concentration less than 2 mg/l and subjected to spectroscopic analysis.

3.5 Batch sorption experiments

For batch equilibration studies, experimental solutions containing measured concentration of metal ions and the adsorbent were adjusted to the required pH and equilibrated in an Erlenmeyer flask at 250 rpm using a horizontal orbital shaker (REMI CIS24 BL model). Temperature during the adsorption experiments were controlled at 25 ± 0.5 ^{o}C. All pH adjustments were carried out with dilute HNO_3/Na_2CO_3, in case of uranium and dilute HNO_3/NaOH in case of Cr(III). Batch adsorption studies were conducted with 50 mL solution containing 50 mg of the adsorbent and different initial concentrations for U(VI) and Cr(III). After fixed time of equilibration, 20-100 µL of the solution was withdrawn from the experimental mixture and concentration of metal ion remaining in the solution was estimated. The amount of metal ion adsorbed onto the CTPP bead at time t, was calculated by:

$$q_t = \frac{(c_0 - c_t)V}{w} \qquad 3.1$$

where q_t (mg/g) is the quantity of metal ion adsorbed on CTPP bead at time t, C_0 is the initial concentration of metal ions used in the experiment, C_t is the concentration of metal ion measured in the liquid phase after equilibration time t ; V is the volume of the solution(L) and w is the mass of the CTPP beads (g). For kinetic investigations, the adsorption experiments were conducted at a stirring speed of 400 rpm, using a magnetic stirrer, in order to minimize the effect bulk and film diffusion on the sorption process [49].

3.6 Competition and desorption experiments for Cr(III) with CTPP beads

Competition experiments were carried out using binary mixtures having Cr(III) as one component and one of the selected cation as the competing ion. Concentration of both the cations were fixed at 100 mg/L. pH of all the experimental mixtures were fixed at 5, except for Al(III) containing mixture, where operational pH = 4 was used due to the hydrolysis of Al(III) at pH above 4. After 72 hours of equilibration, concentrations of the free metal ions remaining in solution were analyzed. For desorption experiments, 400 mg of Cr(III) loaded CTPP beads were prepared under optimum sorption conditions of pH = 5 and equilibration time of 72 h. The Cr(III)-loaded CTPP beads were separated, washed thoroughly with distilled water and air dried.

25 mg of the dried Cr(III) loaded CTPP beads were then equilibrated with 25 mL Ethylene Diamine Tetra Acetic acid (EDTA) or NaCl solutions at three different concentrations i.e. 0.001, 0.01 and 0.1 M. The amount of desorbed Cr(III) ions were determined at specific intervals using ICP-AES. All adsorption and desorption experiments were carried out in duplicates and the average values were taken.

3. 7 Results and discussion

3.7.1 Characterisation of CTPP beads.

Schematic representation of the formation of CTPP beads by the ionic cross-linking of chitosan and sodium tripoliphosphate is presented in figure 3.2. CTPP beads thus prepared were characterized using FTIR spectroscopy. The IR spectra of chitosan powder and the CTPP bead is shown in figure 3.3. The main differences in the IR spectra is the additional peak in the CTPP bead spectrum at 1230 cm^{-1}, which can be assigned to the –P=O stretching vibration indicating the presence of phosphate group in the prepared beads. Peak at 1694 cm^{-1} corresponding to $–NH_2$ group and 1419 cm^{-1} corresponding to –NH deformation vibration of $–NH_2$ groups, present in the original chitosan spectrum is completely disappeared in the spectrum of CTPP bead, with the appearance of a fresh peak at 1541 cm^{-1} which can be assigned to NH_3^+ [50]. The beads are prepared at pH = 3 where the amino group are mostly protonated. From the spectral information it can be concluded that the cross-linking is taking place through the ionic interaction between the negatively charged $–P\text{-}O^-$ moieties of the phosphate group and protonated NH_3^+ moieties of the chitosan molecule.

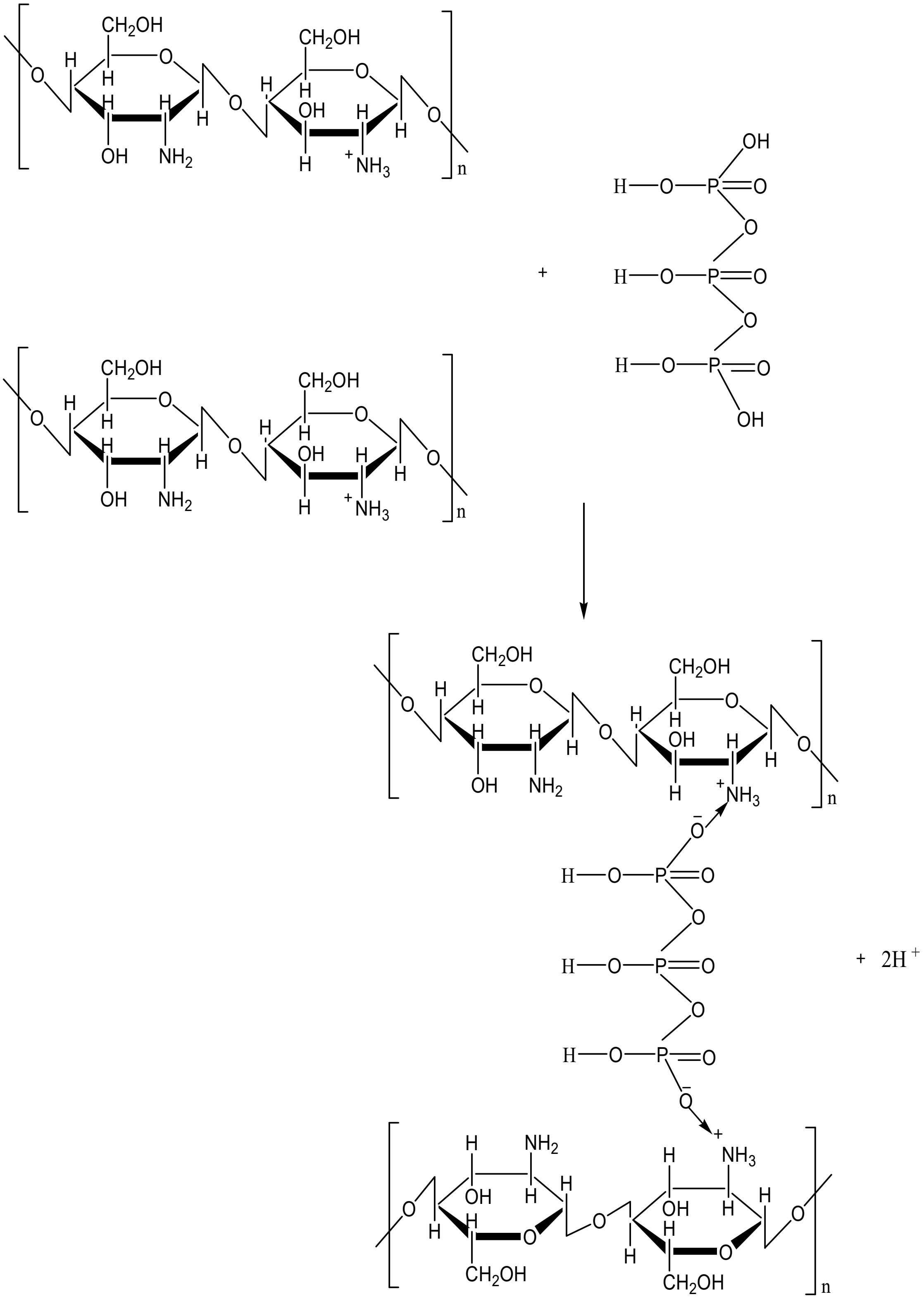

Fig. 3.2 Schematic presentation of formation of CTPP beads by ionic cross-linking

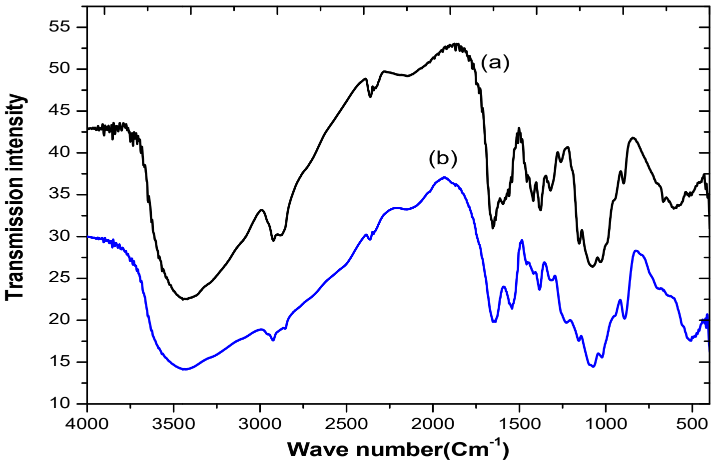

Fig. 3.3 IR spectra of chitosan(a) and chitosan tripolyphosphate beads (b)

SEM image of the beads at two different magnifications were given in figure 3.4. The beads employed in the studies have a diameter of approximately 2mm. SEM image at 10K magnification shows that the surface is porous, which is a desirable characteristic for a substance to be used as an adsorbent.

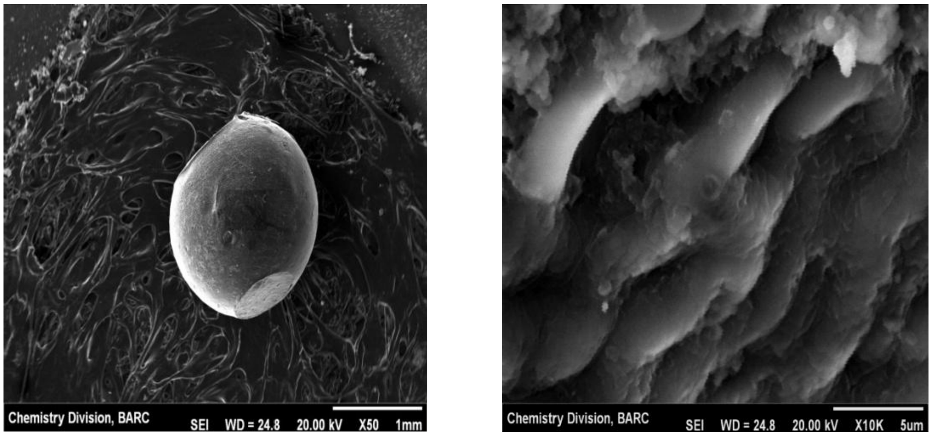

Fig. 3.4 SEM images of CTPP beads at x 50 and x10K magnifications.

3.7.2 Sorption of U(VI) on CTPP beads.

3.7.2.1 Effect of cross-linking and solution pH on uranium sorption.

Chitosan in its native form is brittle, where most of the active functional groups are deeply embedded inside the crystalline phase which leads to reduced adsorption capacity for the adsorbent. Cross-linking of chitosan with various cross-linking agents is found to improve its amorphous character [51]. Figure 3.5 presents the uranium adsorption on lower and higher cross-linked CTPP beads, as a function of the solution pH. Under identical experimental conditions, beads with higher cross-linking show higher adsorption capacity for uranium. The pH dependence also differs significantly with the extend of cross-linking of the CTPP beads. The uranium adsorption capacity of lower cross-linked beads decreased monotonously with pH of the solution. Though for lower cross-linked beads, both amino and phosphate groups may be available for the adsorption of uranium, it is reported that they are more amenable to swelling in acidic solution [47]. In such case, as the pH of the solution increases, due to reduced swelling, more and more active sites may not be reachable by uranium species for adsorption, resulting in

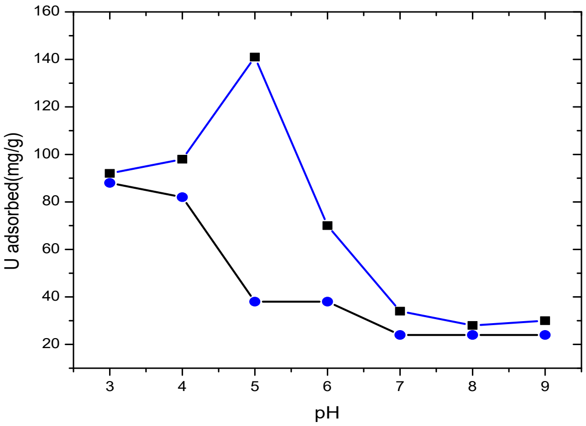

Fig. 3.5 Effect of pH and cross-linking on the sorption of uranium on CTPP beads (-■- higher crosss-linked, -●- lower cross-linked, V= 50 ml, U=200 mg/l, CTPP = 50 mg, T= 25°C)

lower adsorption capacity. On the other hand beads with higher cross-linking showed maximum adsorption at pH = 5. The swelling behavior of higher cross-linked beads is nearly independent of pH and other factors determine the adsorption dependence of uranium on pH of the solution. At lower pH, the amino groups are protonated whereas phosphate groups remain un-dissociated. Thus at lower pH, the positively charged uranyl ion is not favored by the positive or neutral binding groups on the adsorbent, resulting in lower adsorption capacity. At neutral to alkaline pH, uranium is present as anionic hydroxyl-carbonate complexes [52,53], and thus not favorable for adsorption onto the neutral/negatively charged functional groups of CTPP beads, which explain the reduction in adsorption at higher pH. Thus the maximum adsorption capacity observed at pH = 5 for the higher cross-linked CTPP beads is the result of pH dependant speciation of the uranyl ion and the pH dependant dissociation behavior of CTPP functional groups responsible for sorption of uranium. Adsorption peak at pH=5 was earlier reported by Takashi *et al* for the sorption of uranium onto chitin and chitosan phosphates [54]. Due to the higher adsorption capacity, higher cross-linked beads and the optimum pH = 5 were used for further experiments.

3.7.2.2 Effect of contact time on uranium sorption.

To understand the effect of contact time on uranium adsorption onto CTPP beads, experiments were conducted with 100 mL of solution having 400 mg/L uranium and 100 mg of adsorbent. 100 μL of the sample were analysed at various intervals to estimate the concentration of dissolved uranium as a function of equilibration time. Figure 3.6 shows that the process is characterized by a rapid adsorption in the initial four hours of equilibration time, followed by a slow process, reaching equilibrium sorption capacity in 72 hours. The initial fast sorption might be due to the surface adsorption of uranium on the CTPP beads. Uranyl ion is a bulky cation and the diffusion of the bulk ion into the CTPP beads is a slow process leading to the overall slow kinetics for the sorption process. During longer stay of beads in the experimental solution, they become swollen, but no solubility of the beads was observed even after five days of equilibration. Concentration of dissolved uranium measured after 10 days of equilibration was in the same range (within 5%) of the concentration measured after 72 hours of equilibration, showing that for practical purposes 72 hours can be taken as the time required for completing the adsorption equilibrium.

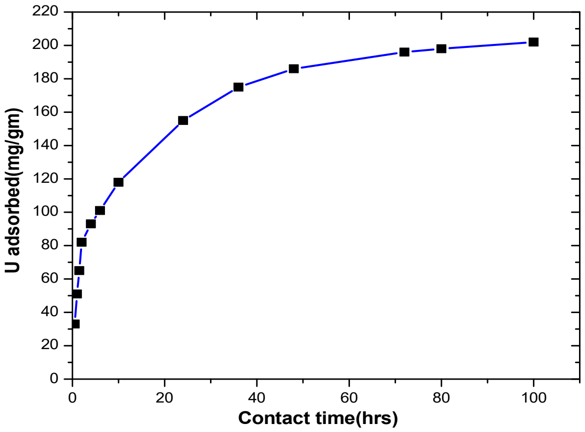

Fig. 3.6 Effect of contact time on the sorption of uranium onto CTPP beads (V = 100 ml, U=400 mg/L, CTPP =100 mg, T=25^{o}C).

3.7.2.3 Adsorption kinetics.

Kinetics data of sorption were analysed using pseudo-first order, pseudo-second order and intra-particle diffusion model as represented by equations 3.2, 3.3 and 3.4 respectively. Here q_e and q_t are the concentration of uranium adsorbed on CTPP at time t and at equilibrium time respectively.

$$\log(q_e - q_t) = \log q_e - \left(\frac{k_1}{2.303}\right)t \tag{3.2}$$

$$\frac{t}{q_t} = \frac{1}{k_2 q_e^2} + \frac{t}{q_e} \tag{3.3}$$

$$q_t = k_{id} \times t^{1/2} \tag{3.7}$$

k_1 , k_2 and k_{id} are the pseudo-first order, pseudo-second order and intra-particle diffusion rate constants. Figure 3.7 gives the pseudo-first order and pseudo-second order plot of the experimental data. The model parameters and the equilibrium concentration obtained by both the models are given in table 3.1. From the results it can be observed that both pseudo-first order and pseudo-second order models are matching with the experimental kinetics data. From the better correlation coefficient and the fact that the equilibrium concentration obtained by the pseudo-second order plot (209 mg/g) is more close to the experimental value than that obtained from the pseudo-first order plot (141.5 mg/g), it can be concluded that pseudo-second order model is more relevant to explain the kinetics of adsorption of uranium on CTPP beads. Application of intra-

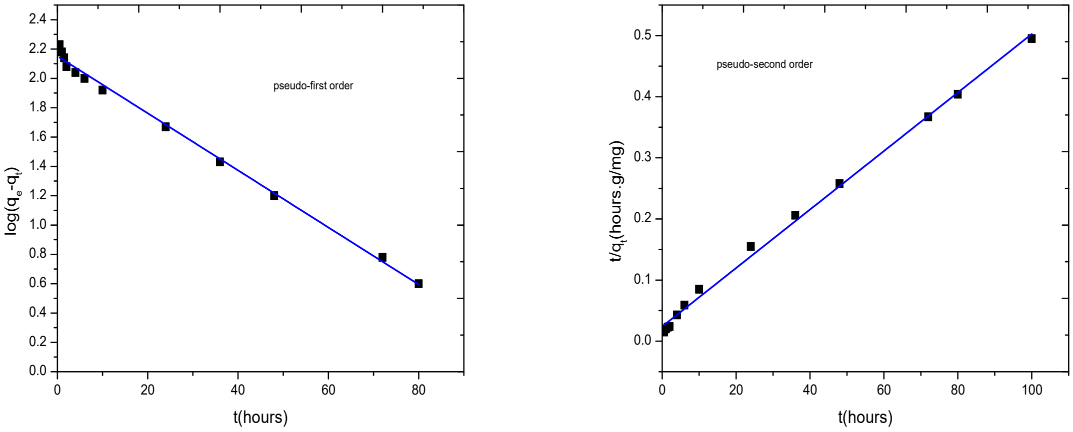

Fig. 3.7 Pseudo- first order and pseudo-second order model plot for the sorption of uranium onto CTPP beads .

particle diffusion model to the experimental data (figure 3.8) shows three regions with independent slopes (all with $r^2 \geq 0.97$). Thus it is clearly evident that intra-particle diffusion is not applicable to the entire time scale of the sorption process. The initial region, which corresponds to the fast adsorption, could be due to the surface adsorption on the dried beads where intra-particle diffusion has no significant contribution. Similarly the third region might be corresponding to the chemical equilibration of uranium in the swollen CTPP beads. Among the three regions, the one corresponds to the intermediate time scales has the best statistical fit as per the intra-particle diffusion model. Thus it can be assumed that uranium diffusion inside the beads have significant influence in controlling the kinetics of uranium sorption onto CTPP beads . However it should be noted that this straight line does not pass through the origin which means intra-particle diffusion is not the sole rate determining factor controlling the adsorption of uranium onto CTPP beads. Similar three stage kinetics was earlier reported for the sorption of humic acid on cross linked chitosan beads [55].

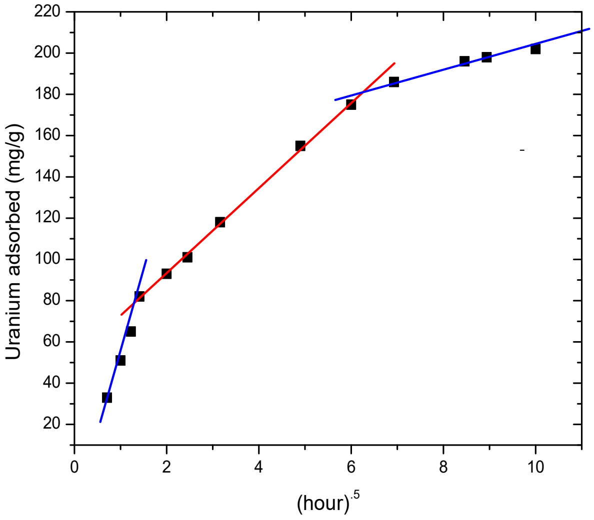

Fig 3.8 Intra-particle diffusion model plot for the sorption of uranium onto CTPP beads.

Table 3.1: Kinetic model parameters for the sorption of uranium onto CTPP beads

Kinetic model	Value
Pseudo-first order	
k_1 (hour^{-1})	4.5×10^{-2}
q_e (mg.g^{-1})	141.6
R^2	0.995
Pseudo-second order	
k_2 (g-mg^{-1}hour^{-1})	9.4×10^{-4}
q_e (mg.g^{-1})	209.2
R^2	0.997
Intra-particle diffusion model	
k_{id} (mg.g^{-1}.hour^{-1})	19.6
R^2	0.993

3.7.2.4 Effect of initial uranium concentration.

For investigating the effect of initial uranium concentration on the adsorption of uranium onto CTPP beads, experiments were conducted with 50 mL solutions having initial uranium concentration varying from 100mg/L to 2000 mg/L and a fixed mass of 50 mg of adsorbent. The results are presented in figure 3.9. As expected, the adsorption capacity increased with increase in initial metal ion concentration. With more uranium present in solution, larger fraction of the active sites is involved in the adsorption process. At higher uranium concentrations adsorption capacity reached a plateau indicating saturation of the available binding sites on the adsorbent. The steep slope at initial uranium concentrations is a desirable feature of the sorption system and the results indicates that a CTPP bead is an efficient adsorbent for uranium.

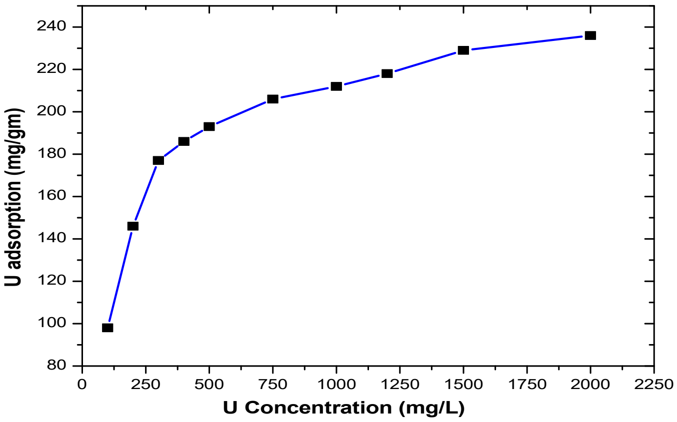

Fig. 3.9 Effect of initial uranium concentration on the sorption of uranium onto CTPP beads (V= 50 ml, CTPP = 50 mg, pH=5, T= 25°C)

3.7.2.5 Sorption isotherm.

Langmiur and Freundlich isotherm models were applied to anlayse the sorption data as per equations 3.8 and 3.9 respectively ,

$$q_e = \frac{bQc_e}{1+bc_e} \tag{3.8}$$

$$q_e = k_F \times c_e^{1/n} \tag{3.9}$$

where q_e is the amount of metal ion adsorbed at equilibrium(mg/g), c_e is the equilibrium metal ion concentration remaining in solution, Q (mg/g) is the amount of metal ion adsorbed at complete monolayer coverage, and *b*(mL/mg) is the Langmiur constant, and k_F and n are Freundlich constants related to adsorption capacity and adsorption intensity respectively. Figure 3.10 shows the linear plot for the experimental sorption data on application of the models.

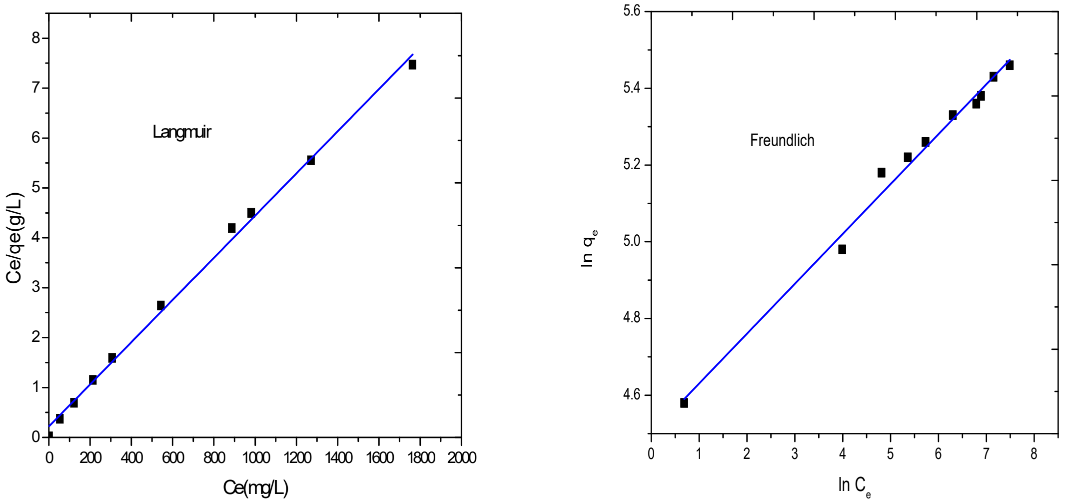

Fig 3.10 Langmuir and Freundlich Isotherm fit of the sorption data of uranium onto CTPP beads

The model parameters obtained by applying both Langmuir and Freundlich model to the experimental data are given in table 3.2. From the better correlation coefficient and the fact that the equilibrium adsorption capacity (Q) obtained from Langmuir model (236.9 mg/g) is close to the experimentally observed saturation capacity, it can be concluded that the monolayer

Table 3.2 Isotherm Constants of the sorption of U(VI) on CTPP beads.

Isotherm model	Value
Langmuir	
Q (mg/g)	236.9
b (L/mg)	0.019
R^2	0.997
Freundlich	
k_F (mg/g)	89.9
n	7.65
R^2	0.991

Langmuir adsorption isotherm is more suitable to explain the adsorption of uranium onto CTPP beads.

The favorability of the CTPP beads as an adsorption medium for uranium can be obtained from the Langmiur adsorption constant b; which is related to the separation factor R_L defined as:

$$R_L = \frac{1}{1 + bc_0} \tag{3.10}$$

where c_0 is the initial metal ion concentration. $0 \langle R_L \langle 1$ indicates that the adsorbent is a favorable medium for the adsorption of the given metal. Table 3.3 presents the calculated R_L values at five different initial uranium concentrations. For all the tested uranium concentrations, it is found that $0 \langle R_L \langle 1$, which proves that CTPP bead is a favorable adsorbent medium for uranium. The same conclusion can be arrived from the Freundlich constant 'n' in which case a value of n between 1 and 10 indicates the acceptance of the medium as the suitable adsorbent.

Table 3.3 Calculated R_L values at different initial concentrations of uranium

Initial U concentration(C_o) (mg/L)	Separation factor (R_L)
10	0.840
50	0.512
100	0.256
500	0.095
1000	0.050

3.7.3 Sorption of Cr(III) on CTPP beads

3.7.3.1 Effect of pH on Cr(III) sorption on CTPP beads.

Studies on the effect of pH on sorption was restricted to pH = 3-5 due to significant solubility of the beads at pH<3, and precipitation of Cr(III) as $Cr(OH)_3$ for pH above pH=5, which could lead to inaccurate interpretation of the obtained results. Figure 3.11 shows the amount of Cr(III) adsorption as a function of initial solution pH. From the graph it can be seen that, with increase in pH, amount of Cr(III) adsorbed also increases. Speciation data of Cr(III) shows that below pH=6, chromium exists as positively charged species [56]. At higher pH, more sorption sites on CTPP are deprotonated an thus resulting in higher uptake. Moreover under identical

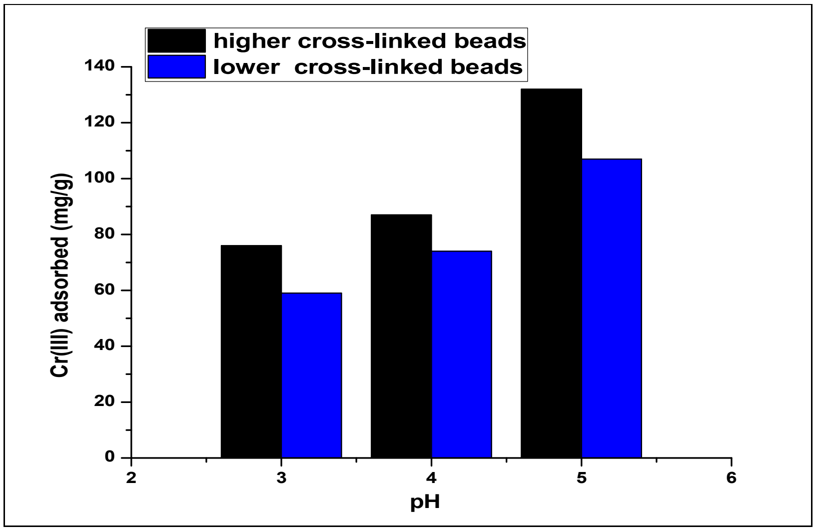

Fig. 3.11 Effect of pH on the sorption of Cr(III) onto CTPP beads (V= 50 ml, Cr(III) = 200 mg/L, CTPP= 50 mg, T=25^{o}C)

Exper imental conditions, beads with higher cross-linking showed higher adsorption capacity for chromium. As a result of cross-linking with TPP, phosphate groups are getting introduced in to the matrix whereas the original amino groups of chitosan are getting consumed for ionic cross-linking. Thus higher uptake for higher cross-linked beads indicates that phosphate groups are the principal sites of binding. Due to the higher adsorption capacity, beads with higher cross-linking and the optimum pH = 5 were selected for further experiments.

3.7.3.2 Effect of contact time on sorption of Cr(III) on CTPP beads.

Figure 3.12 shows the effect of contact time on the sorption of Cr(III) on CTPP beads. The process is characterized by a rapid adsorption in the initial 4 hours of equilibration time, followed by a slow process, leading to equilibrium adsorption in around three days. The initial fast sorption might be due to the surface adsorption of Cr(III) on the CTPP beads. During longer stay of the beads in the experimental solution, they become swollen, and chromium ions are slowly diffused into the bulk of the beads, gradually increasing the sorption capacity. Kinetics of Cr(III) sorption on CTPP is found to be slow, similar to that observed for U(VI) and this is again due to large size of the beads used in the present investigations.

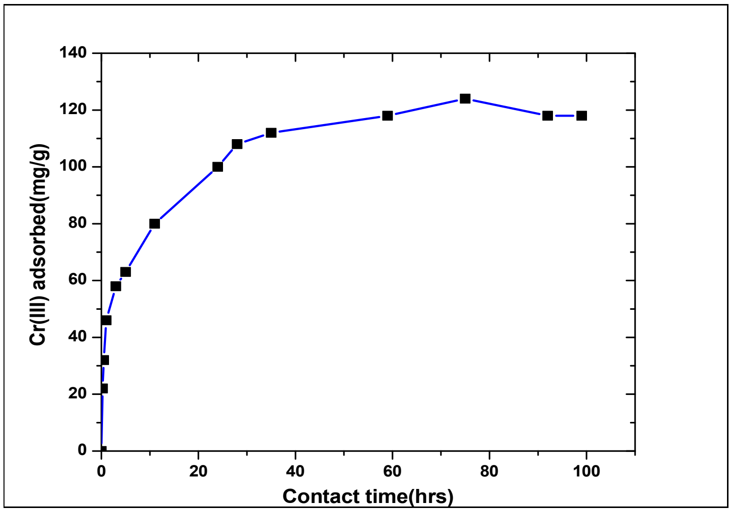

Fig . 3.12 Effect of contact time on the sorption of Cr(III) onto CTPP beads (V= 100 mL, Cr(III) – 200 mg/L, CTPP = 100 mg, pH=5, T= 25^{o}C)

3.7.3.3 Adsorption kinetics

Both pseudo-first order and pseudo-second order kinetics were applied to analyze the experimentally observed kinetic data (figure 3.13). The model parameters and the equilibrium concentration obtained by both the models are given in table 3.4. From the results it can be observed that both pseudo-first and pseudo-second order models are matching with the experimental kinetics data. From the better correlation coefficient and the fact that the equilibrium concentration obtained by the pseudo-second order plot (126.1 mg/g) is more close to the experimental value (124.0 mg/g) than that from the pseudo-first order plot (81.1 mg/g), it can be concluded that pseudo-second order model is more applicable for the adsorption of chromium on CTPP beads.

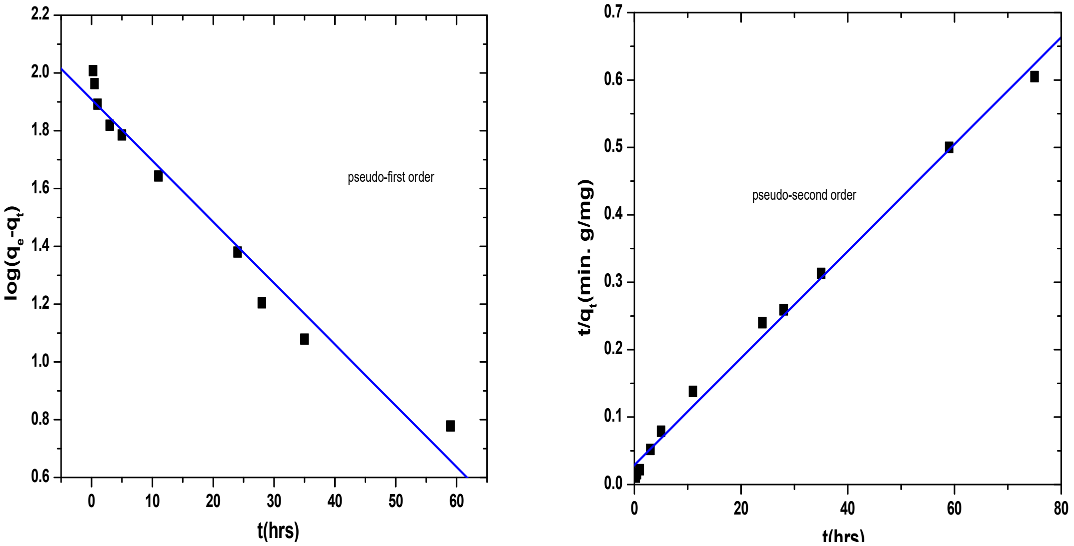

Fig 3.13 Pseudo first order and Pseudo second order kinetics plots for the sorption of Cr(III) on to CTPP beads.

Table 3.4: Kinetic parameters for the sorption of Cr(III) on to CTPP beads.

Kinetic model						Experimentally observed adsorption capacity (mg/g)
Pseudo-first order			Pseudo-second order			
k_1 (hour^{-1})	q_e (mg.g^{-1})	R^2	k_2 (g.mg^{-1}hour^{-1})	q_e (mg.g^{-1})	R^2	
0.049	81.1	0.967	21.8×10^{-4}	126.1	0.995	124.0

3. 7.3.4 Effect of initial chromium concentration on adsorption:

To investigate the effect of initial chromium ion concentration on adsorption, experiments were conducted with 50 mL solutions having initial chromium concentration varying from 10 to 5,000 mg/L and a fixed mass of 50 mg of adsorbent. Figure 3.13 shows the amount of Cr(III) adsorbed onto CTPP beads (mg/g) as a function of initial concentration of Cr(III) ions in solution. As expected, with increase in Cr(III) ion concentration, the adsorption capacity increased and reached a plateau at still higher concentrations. This is the typical behavior of saturated adsorption in which the sorption capacity is limited by the availability of active sites on the

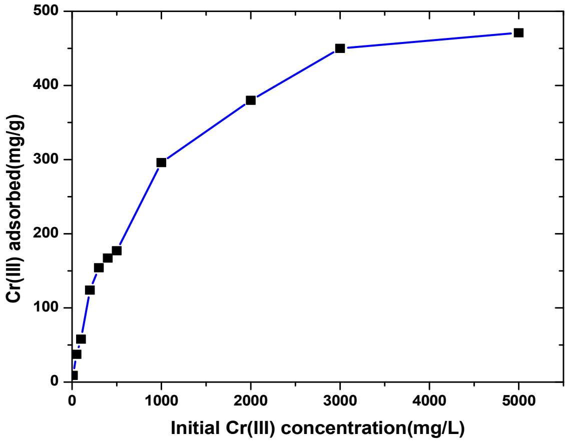

Fig 3.14 Effect of concentration on the sorption of Cr(III) onto CTPP beads (V = 50 ml, CTPP =50 mg, pH=5 , T=25°C)

adsorbent. The steep slope at initial Cr(III) concentrations is a desirable feature for the sorption system and the results indicate that CTPP bead is an efficient sorbent for Cr(III).

3.7.3.5 Sorption isotherm.

Both Langmiur and Freundlich isotherm were applied to the sorption data and found to fit well for the proposed models (figure 3.15). The calculated model parameters are presented in table 3.5. From the results it can be seen that, the experimental data is best fitted with the Langmuir model and the maximum adsorption capacity (469.5 mg/g) obtained from Langmuir plot is very close to the experimentally observed saturation sorption capacity (471.0 mg/g).

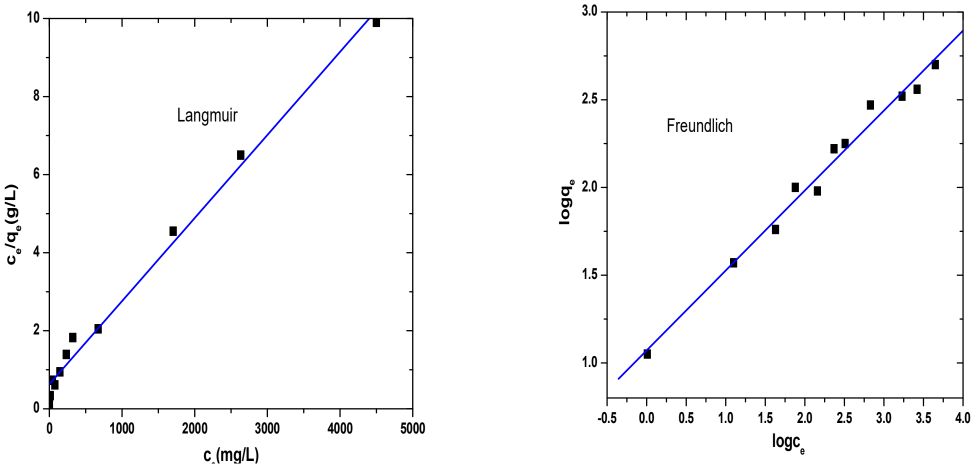

Fig 3.15: Langmuir and Freudlich plot for the sorption of Cr(III) onto CTPP beads.

Table 3.5 Model parameters for the sorption of Cr(III) onto CTPP beads.

Langmuir model	
Q(mg/g)	469.5
b(L/mg)	3.4×10^{-3}
R^2	0.9898
Freundlich model	
K_F(mg/g)	12.8
n	2.19
R^2	0.9720

R_L values calculated at selected initial Cr(III) concentrations are given in table 3.7. The values are in the range of $0 < R_L < 1$, which indicates that the adsorption of chromium (III) on CTPP is favorable process. The same conclusion can be arrived from the Freundlich constant ‘n’ in which case a value of n between 1 and 10 indicates the acceptance of the medium as the suitable adsorbent.

Table 3.6 R_L values for the sorption of Cr(III) onto CTPP beads.

Initial Cr(III) Concentration(C_o) (mg/L)	Separation factor (R_L)
10.0	0.967
50.0	0.856
200.0	0.597
500.0	0.372
2000.0	0.129
3000.0	0.090
5000.0	0.056

3.7.3.6 Observation of Cr on CTPP surface by EDS analysis.

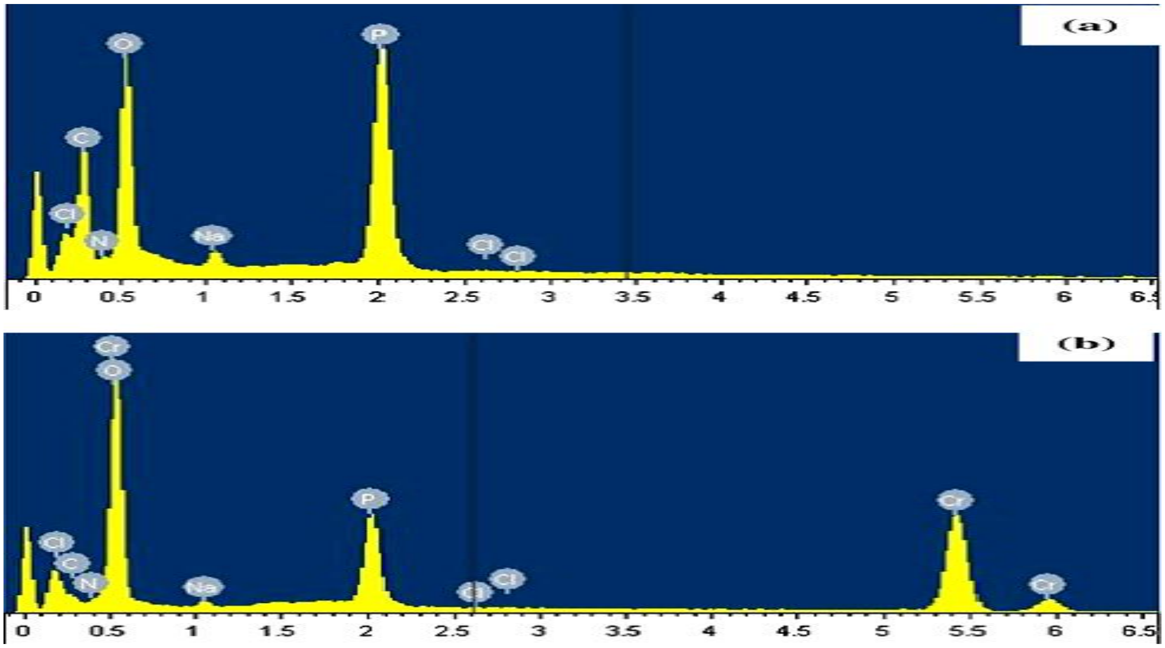

Fig 3.16 EDS spectra of CTPP beads taken before and after sorption of the Cr(III) ions.

Though concentration measurement shows the uptake of Cr(III) on CTPP beads, additionally EDS spectra of the CTPP beads were taken before and after sorption Cr(III). Figure 3.16(a) and 3.16(b) shows the EDS spectra and the clear peaks corresponding to chromium visible in the latter, confirms that the metal is getting adsorbed onto the sorbent.

3.7.3.7 Competition of metal ions in binary mixture

Table 3.8 shows the competitive effect of few selected metal ions on the adsorption of Cr(III) onto CTPP beads. Among the cations studied in competition experiments, Na(I), Mg(II) and Ca(II) have no significant sorption onto CTPP beads and thus does not affect the sorption of Cr(III). Interestingly in Fe(III)/Cr(III) binary system, CTPP beads showed almost equal sorption capacity towards both the metal ions. However adsorption of Fe(III) didn’t affect the sorption Cr(III) presumably due to the fact that these metal ions are going to different adsorbing sites of the adsorbent. In presence of Al(III), sorption capacity for Cr(III) is significantly reduced. Al(III) is a small cation, which effectively compete for the same adsorbing sites on the CTPP beads. Results of competition experiments shows that CTPP beads are effective in removing Cr(III) even in presence of other common ions.

Table 3.7 Effects of competing cations on the sorption of Cr(III) onto CTPP beads.

Binary mixture	Metal ions	Initial concentration (mg/l)	Final concentration (mg/l)	Adsorption capacity (mg/g)
Al(III)-Cr(III)	Al(III)	100	61.2	38.8
	Cr(III)	100	81.2	18.8
Fe(III)-Cr(III)	Fe(III)	100	42.7	57.3
	Cr(III)	100	39.7	60.3
Ca(II)-Cr(III)	Ca(II)	100	89.5	10.5
	Cr(III)	100	43.1	56.9
Mg(II)-Cr(III)	Mg(II)	100	100.2	-
	Cr(III)	100	53.4	46.6
Na(I)-Cr(III)	Na(I)	100	99.3	-
	Cr(III)	100	47.7	52.3

3.7.3.8 Desorption study for Cr(III) ions

Desorption of the loaded adsorbents is essential for the recovery of the metal ions and reuse of the adsorbent. Among the two desorption agents used, NaCl is found to be better than EDTA at all the three concentration studied (table 3.9). For NaCl itself, desorption is found to be more efficient at higher concentrations. It is also observed that at higher NaCl concentration, the swelling of the beads are more compared to lower NaCl concentration. Better desorption at higher NaCl concentrations could be attributed to the easy diffusion of the metal ions from the bulk of the beads into the desorbing medium due to its higher swelling. Incidentally it should be noted that the desorption is completed around 72 h, a time scale similar to that required for reaching the adsorption equilibrium, indicating that both desorption and adsorption are slow process probably due to the larger size of the beads used in these investigations.

Table 3.8 : Results of the desorption experiments of Cr(III) from loaded CTPP beads

Desorption time (hrs.)	Percentage recovery (%)					
	0.001 M EDTA	0.01 M EDTA	0.1 M EDTA	0.001 M NaCl	0.01 M NaCl	0.1 M NaCl
5	1.2	1.6	2.9	1.2	1.4	2.8
14	1.5	2.0	4.9	2.4	3.3	3.9
24	2.4	3.2	6.0	8.4	21.1	32.2
48	4.4	5.0	8.2	20.4	52.0	81.7
72	6.3	7.4	12.5	31.8	97.3	98.7

3.7.4 Identification of metal ion binding sites on CTPP beads

Two potential binding sites in CTPP beads available for adsorption of metal ions is presented in figure 3.17. Highly cross-linked beads used for the adsorption studies were prepared at pH = 3, where most of the amine groups are protonated. Ionic cross-linking with tripolyphosphate might have consumed most of these amino groups, thus not available for binding of metal ions. Thus the principal functional groups responsible for metal uptake by CTPP beads might be the phosphate group. In order to identify the functional groups responsible for the sorption of

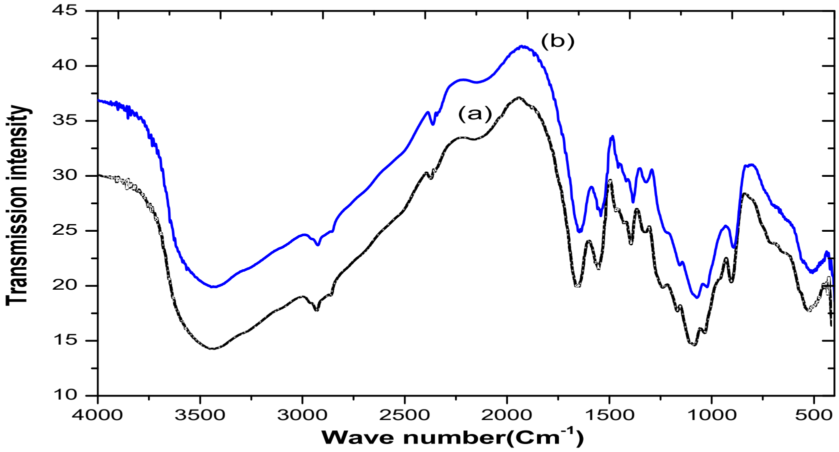

Fig. 3.17 FTIR spectra of CTPP beads before (a) and after (b) sorption.

uranium onto CTPP beads, FTIR spectra of the CTPP beads were recorded after the adsorption of uranium. Figure 3.18 presents the FTIR spectra of the CTPP beads before and after adsorption of uranium. Significant decrease in the peak at 1230 cm^{-1} corresponding to –P=O stretching vibration in the spectrum after adsorption of uranium indicates that phosphate groups are affected due to the adsorption process. Though the peak at 1319 cm^{-1} corresponding to –C-N stretching vibration is slightly shifted, no significant change is observed in the peak position of any other major peaks corresponding to either nitrogen or oxygen functional groups[50]. Thus, from the spectral characterization of the beads, it is evident that phosphate groups are the major contributor for the adsorption of uranium (binding site I), though it does not preclude some involvement of the amino groups (binding site II) in the adsorption process. The fact that both for both U(VI) and Cr(III), higher cross-linked beads having larger phosphate content, shows higher sorption capacity also points towards the major role of phosphate group in the sorption process.

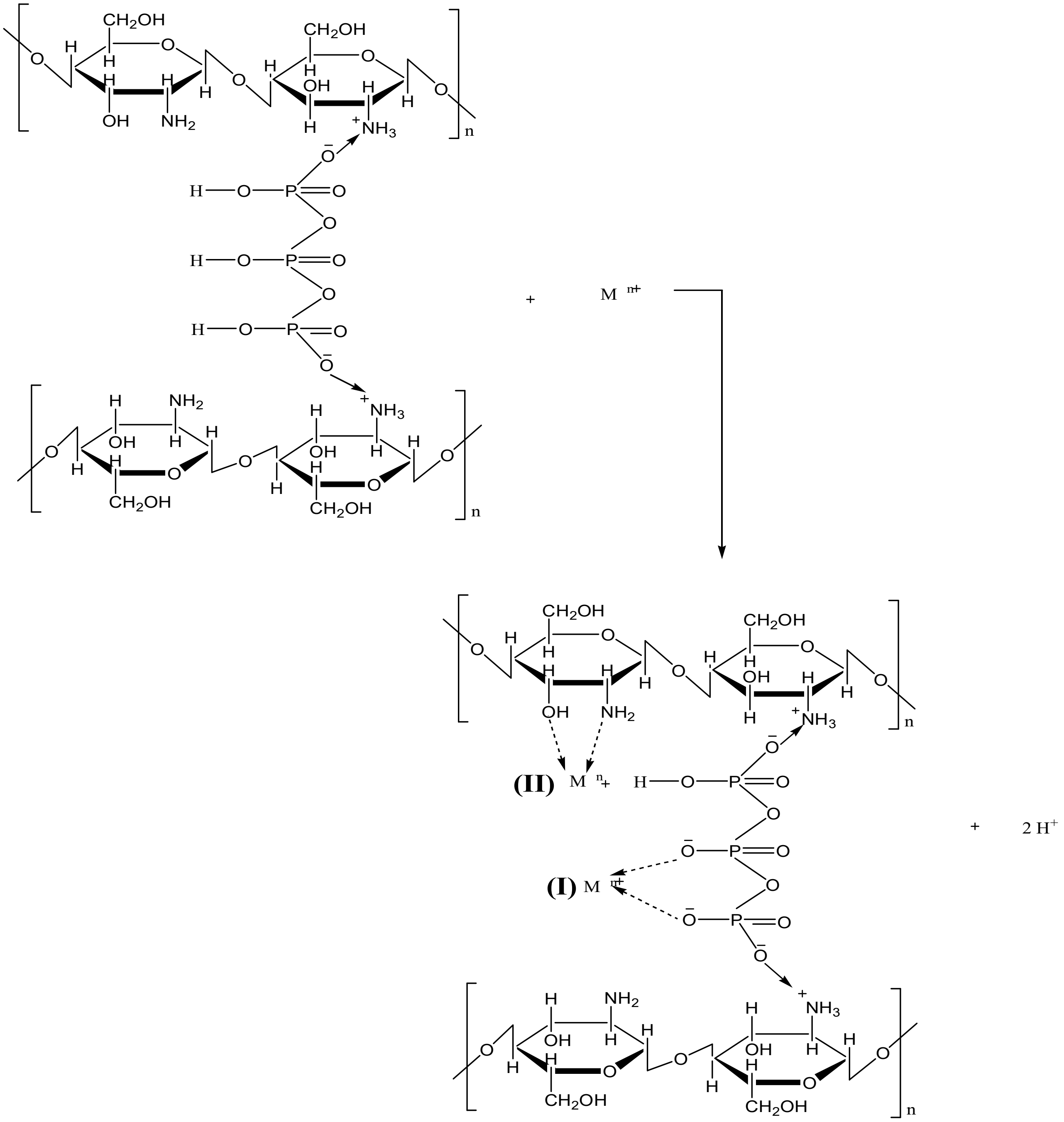

Fig. 3.18 Proposed sites for metal ions sorption on CTPP beads.

3. 8 Conclusions

The research presented in this chapter on the sorption of U(VI) and Cr(III) ions onto CTPP beads shows that this adsorbent is a suitable medium for the sorption of metal ions from aqueous solution. For the macro-sized beads used in the present studies, the sorption kinetics is observed to be slow completing in around 72 hours. Pseudo-second order kinetic model could satisfactorily explain the sorption kinetics for both the metal ions. Application of intra-particle diffusion model to the kinetics data for U(VI) sorption showed that at intermediate time scale, intra-particle diffusion is the rate controlling process. Langmuir adsorption isotherm is found to fit the experimental data showing sorption capacity of 469.5 mg/g and 236.9 mg/g respectively for Cr(III) and U(VI). Ions of similar charge and size could hamper the sorption of target pollutants such as the interference from Al(III) in case sorption of Cr(III). Thus CTPP sorbent is not highly selective, but the sorption of trivalent target like Cr(III) is found to be not affected by t ions such as Na(I), Ca(II) and Mg(II). This proves that the sorbent is an effective decontaminant for toxic elements even in presence of many common metal ions. Added phosphate moieties are found to be the principal sorption sites on the sorbent. Metal recovery subsequent to the sorption is possible using NaCl solution.

Chapter 4

Sorption of metal ions on Humic Acid coated Chitosan Tripolyphosphate (HA-CTPP) beads

4.1 Introduction

Humic materials formed by the degradation of biomaterials are one of the biggest pool of carbon on earth [57]. Its role in speciation, bioavailability, transport and sequestration of various organic and inorganic pollutants in aquatic and terrestrial environment is well understood [58]. The ability of humic materials to complex with metal ions is primarily attributed to the abundant –COOH and –OH groups present in these macromolecules. A hypothetical model of humic molecule is presented in figure 4.1. The artifact that humic materials can strongly bind heavy metals and radionuclide have been the subject of many investigations, with the aim of developing suitable technology utilizing these materials for treatment of contaminated water [59]. Humic acid (HA) which is operationally defined as the fraction of the humic materials which is water soluble above pH > 2 is the prime candidate in these investigations, principally due to the high abundance of this fraction relative to others. In addition to its pristine form, humic acid in several physico-chemical modifications such as insoluble solid [60], immobilized on silica [61] and as a composite with various polymers [62] have been tested for removal of various metals. Few attempts were also reported on the use of HA as a polymeric macromolecule

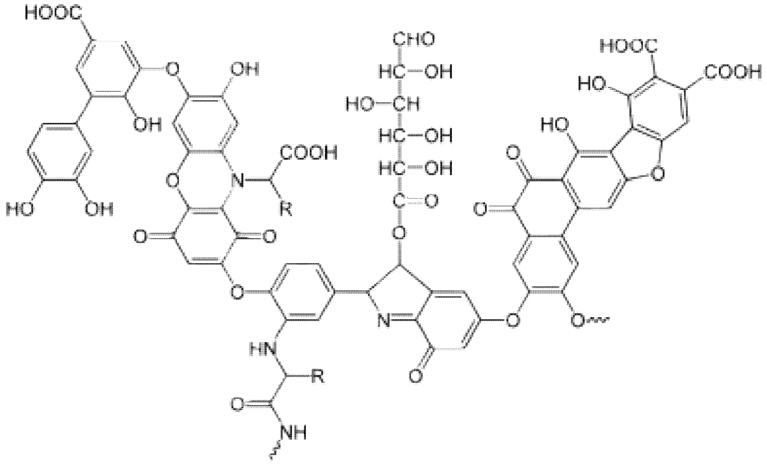

Fig. 4.1: Model of humic molecule (Stevenson *[30]*)

in the separation of metal ions using polyelectrolyte flocculation [63] and polymer enhanced ultra-filtration [64]. Membrane fouling could be a serious bottle-neck in the scaling up of HA based ultra-filtration process [65], whereas the immobilization of HA onto various supports needs multi-step chemical treatment, often resulting in overall poor loading of HA onto the immobilizing medium [66]. It is also reported that insoluble humic acid (IHA) obtained by heat treatment have significantly lower sorption capacity than pristine HA due to thermal decomposition of its metal binding functional groups during the heat treatment[67]. Hence it is desirable to develop new immobilization technique for HA on different substrates, without significantly undermining its inherent sorption capacity.

Herein HA immobilization onto chitosan beads were achieved by dipping wet chitosan beads in HA solution at alkaline pH. The newly prepared sorbent is tested for its sorption properties for U(VI) and Pb(II) ions as model contaminant metal ions. In this context, it should be noted that few attempts have been reported on the use of HA from various origin for the removal of U(VI) and Pb(II) from aqueous solution, but with some notable drawbacks with respect to solid/liquid separation and sorption capacity. Use of HA gel [68] and IHA powder [69] as an adsorbent for Pb(II) required extensive separation of the adsorbent, once the equilibrium is reached. Though Seki et al. [70] studied the adsorption of Pb(II) onto HA immobilized on calcium alginate beads, the sorption kinetics was found to be significantly slow for practical application. Wie et al have studied the sorption of uranium onto soil derived humic acid[71], but solubility of HA at pH higher than 2.5 is found to be a serious limitation in using unmodified humic acid for the sorption applications. The study of Li et al [72] showed excellent sorption capacity for U(VI) on HA but no mention was made on the stability of the sorbent under various experimental conditions. This prompted to look for new and simple method for immobilization of HA for sorbent preparation. In comparison to the earlier published studies, the immobilization procedure reported here is simple and efficient for preparation of a stable solid HA based sorbent for toxic metal ion removal.

4.2 Materials and methods.

4.2.1 Materials

Chitosan (medium molecular weight), sodium trypolyphosphate (STPP), ($Na_5P_3O_{10}$) and humic acid (technical grade) were purchased from Aldrich chemical company, USA. $UO_2.(NO_3)_2.6H_2O$ was procured form E.Merck Germany. $Pb(NO_3)_2$ (AAS standard) as 1000 mg/l solution in 0.5 M HNO_3 was procured from Merck (India) Limited. All other chemical used in the experiments were of analytical reagent grade. Deionized water used for all experiments was obtained from Milli-Q (Millipore Corporation, USA) water purification system.

4.2.2 Preparation of CTPP beads

Wet chitosan beads were prepared at the original pH of the trypolyphosphate solution (pH=8.6) by ionic cross-linking of chitosan and STPP as presented in Chapter 3. The beads were cured for 12 hours, separated by filtration, washed four times with deionized water and used for the preparation of HA coated CTPP beads.

4.2.3 Preparation of H A-CTPP beads.

Efficiency of coating of HA onto mineral and organic surfaces could significantly vary with pH of the solution in which the coating is carried out. In order to identify the suitable pH for efficient coating, preliminary batch experiments were conducted with 100 ml of solution containing 1g of humic acid each and 10 g of wet CTPP beads. pH=3 to 11 were employed in these experiments. After eight hours of equilibration, concentration of free humic acid in solution is measured using absorbance spectroscopy. HA coated CTPP beads for absorbance studies were prepared by placing 100 g of wet CTPP beads in 500 mL of humic acid solution containing 5 g of humic acid at pH=10. The beads were stirred in HA solution for 12 hours, filtered and washed five times in distilled water, before drying at 50^{o}C in air oven. Concentration of the unused humic acid in the solution was estimated using absorbance spectroscopy. From the total weight of the dried HA-CTPP beads and the total HA consumed in the preparation process, it is estimated that the composition of HA in the final dried beads is 43% (w/w).

4.3 Characterization of HA-CTPP beads.

Characterisation of the beads were carried out by SEM and FTIR spectroscopy. Swelling studies of the CTPP and HA-CTPP beads were carried out by equilibrating the beads at selected pH in deionized water for 24 hours. After equilibration the beads were separated, excess water was removed using tissue paper and the final weight is obtained. Swelling capacity of the beads was calculated using the expression:

$$SP = \left[\frac{W_f - W_i}{W_i}\right] \times 100 \tag{4.1}$$

where W_f is the weight of the beads after equilibration with water for 24 hours and W_i is the original weight of the dried beads.

In-order to estimate the stability of HA-CTPP beads in aqueous solution, 100 mg of dried HA-CTPP beads were equilibrated in 100 mL of water after adjusting the initial pH in the range of 1-8 using dilute NaOH or HCl. After 24 hours of equilibration, HA released from the beads to the aqueous medium were measured by absorption measurement at 400 nm.

4.4 Sorption of Metal ions on CTPP and HA-CTPP beads.

Sorption studies with Pb(II) ions were carried out in 100 mL Erlenmeyer flask at 250 rpm using a horizontal orbital shaker. In case of U(VI), experiments were conducted using 10 mL solution in 15 mL polypropylene (Laxbro) vials. Required quantity of sorbent and solution containing metal ions was added and the pH is adjusted using dilute HNO_3/NaOH in case of Pb(II) and HNO_3/ Na_2CO_3 in case of U(VI). Uranium concentrations measurement was carried out using ^{233}U tracer. For this, required quantity of ^{233}U was added to each experimental solutions, before the adjustment of pH and addition of sorbent, so as to get an initial count rate of ~8000 cpm/ml for the reaction mixture. Temperature during the adsorption experiments were controlled at 25 ± 0.5 ^{o}C. After fixed time of equilibration, concentration of the dissolved metal ions were measured by using ICP-AES in case of Pb(II) ions and ZnS(Ag) scintillation counter in case of U(VI) ions. The amount of metal ions sorbed onto the bead at time t, was calculated using the expression:

$$q_t = \frac{(c_0 - c_t)}{w}V \tag{4.1}$$

where, q_t (mg/g) is the quantity of metal ions adsorbed onto the bead at time t (hrs), C_0 (mg/l)and C_t (mg/l) are the initial concentration and equilibrium concentration at time 't' of the metal ion, '*V*' is the volume of the solution(L) and '*w*' is the mass of the dried beads (g) used in the experiment. Kinetic experiments for both the metal ions were conducted with 100 ml solution in borosilicate glass apparatus and at a shaking speed of 400 rpm.

4.5 Results and discussions.

4.5.1 Effect of pH on HA loading onto CTPP beads.

Humic acid sorption onto chitosan derivatives was found to be a highly dependent on the pH of the solution used for the sorption process. Previous studies on sorption of humic substances on chitosan based sorbents shows that the sorption capacity decreases above pH=3- 4 [73-75]. Deprotonation of the amino groups on chitosan and ionization of acidic groups on HA were cited as the reasons for lower sorption at higher pH. The result obtained for the sorption of HA on CTPP beads obtained in this study is different from those previous reports. Figure 4.2 shows that the HA loading onto CTPP beads increase up to pH=4 and remains almost constant thereafter for higher pH. The different result obtained here could be ascribed to two reasons. Earlier attempts were to remove HA from water at environmental concentrations and thus used significantly lower initial HA concentrations in equilibrium studies. At those lower HA concentrations, HA may be present in a different three dimensional structure than that of high HA concentrations used in the present case, which lead to the significant difference in loading onto the adsorbent [76]. Alternatively this difference also could be due to the inherent difference in the sorption property of the adsorbent itself. Interestingly, it should be noted that very high sorption capacity for HA (377mg/g) was reported using another ionic cross-linked chitosan derivative, chitosan-H_2SO_4 beads [77]. At alkaline pH used in the present preparation, due to the ionization of its carboxylic and phenolic functional groups, HA is expected to be present as negatively charged species. Similarly the phosphate group is also expected to be ionized whereas

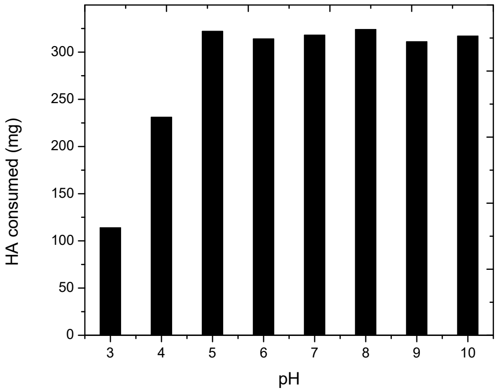

Fig 4.2 Variation in the loading of HA onto CTPP as a function of solution pH (V= 100 ml, CTPP (wet) = 10 g, HA= 1g).

the original amino groups of chitosan in CTPP are expected to be neutral. Since both adsorbent and adsorbate carries a net negative charge, HA coating onto CTPP beads cannot be assigned to ionic bond formation. Most probably other mechanism such as van der Waals interaction and other electrostatic forces such as hydrogen bonding may be responsible for the deposition of HA onto CTPP beads.

4.5.2 Formation of HA-CTPP beads

Digital photograph of CTPP and HA-CTPP beads are presented in figure 4.2. Both CTPP and HA-CTPP beads were nearly spherical in shape with average size of 500 μM. Dried CTPP beads were hard and slightly yellowish in color. Dark color of HA-CTPP beads in comparison to yellowish-white CTPP beads clearly indicates the incorporation of HA onto CTPP beads.

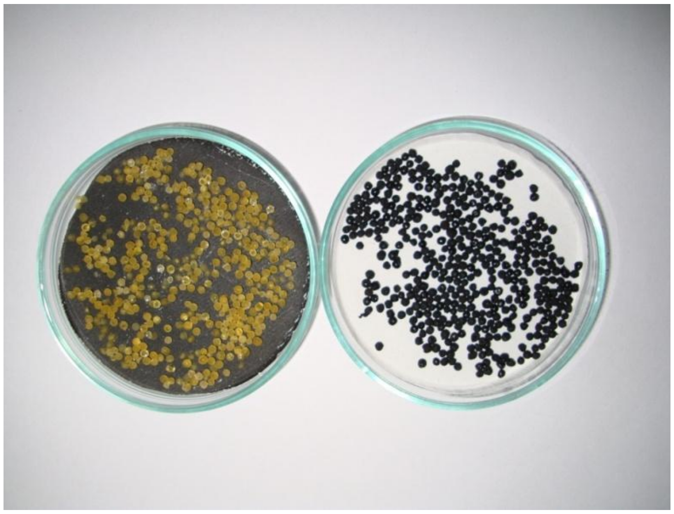

Fig. 4.3 Digital photograph of CTPP and HA-CTPP beads

A visual observation of the HA-CTPP beads, after smooth cutting, showed dark color penetrating into the beads indicating that HA is not just surface adsorbed alone, but diffuse into the bulk of the CTPP beads. Similar diffusion of HA into the bulk of calcium alginate beads were earlier reported by Pandey et al [78] using fluorescence intensity measurements.

4.5.3 SEM images of the CTPP and HA-CTPP beads

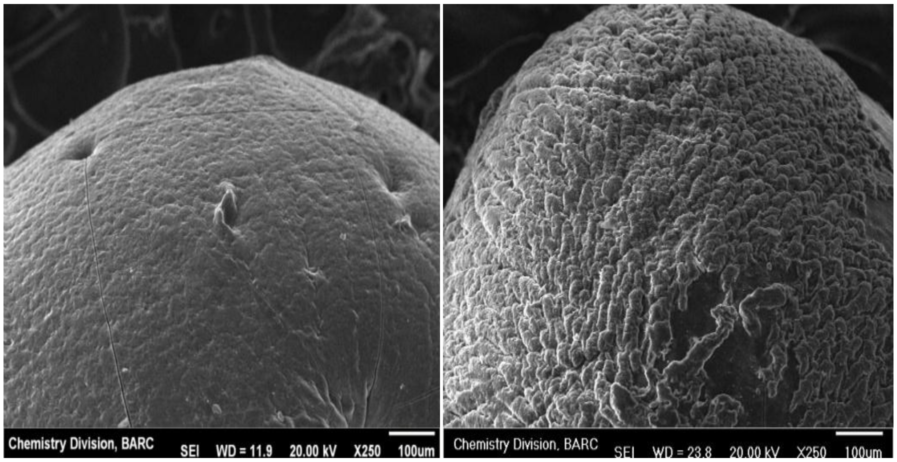

(a) CTPP (b)HA-CTPP

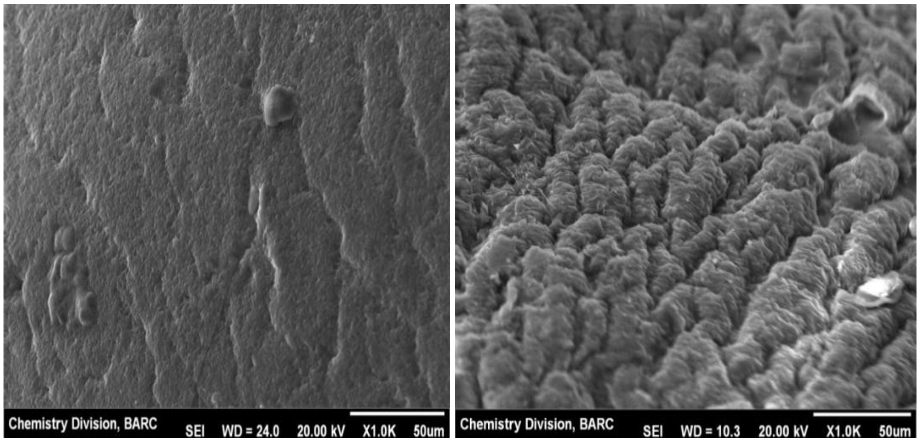

(c) CTPP (d) HA-CTPP

Fig 4.4 SEM images of CTPP (a & c) and HA-CTPP (b & d) beads

SEM images of the beads are presented in figure. 4.3. The CTPP bead surface is seen to be relatively smooth (figure 4.3 a), in comparison to that of HA-CTPP bead (figure 4.3 b). At higher resolution, it is clearly evident that surface of HA coated bead (figure 4.3d) is relatively highly porous in comparison to that of bare CTPP beads (figure 4.3 c).

4.5.4 FTIR spectra of CTPP and HA-CTPP beads

Though the incorporation of HA into the CTPP beads was visually observable, further characterization of the beads were done using FTIR spectroscopy. Spectra of CTPP and HA-CTPP beads are shown in figure 4.4. The peaks at 1461.8 cm^{-1} which can be assigned to the phenolic groups of the original HA is present in HA-CTPP beads also, showing clear indication of the incorporation of HA onto HA-CTPP beads. No peaks around 1720 cm^{-1} corresponding to C=O stretching of the –COOH groups, typically observed in the spectrum of HA samples, were visible in the spectrum of HA-CTPP specimen, and probably this characteristic peak might have been masked by the broad shoulder observed in the wavelength range 1640 cm^{-1} – 1840 cm^{-1}. Comparison of the two spectra shows that there is a shift in the position of individual peaks and/or appearance of new peaks due to the incorporation of HA onto CTPP beads. But the

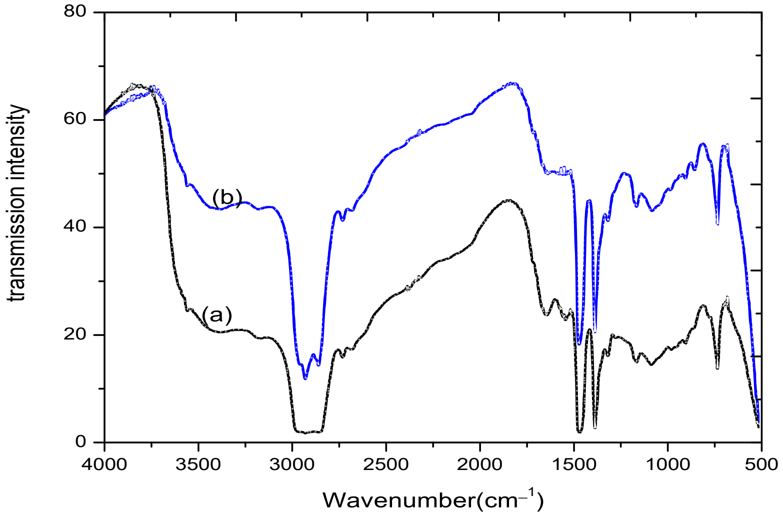

Fig 4.5 FTIR spectra of CTPP(a) and HA-CTPP(b) beads

differences are not strong enough to assign a specific type of chemical bonding between HA and chitosan molecules

4.5 .5 Swelling capacities of CTPP and HA-CTPP beads

Swelling percentage of the two beads as a function of pH is present in figure 4.5. At any given pH, HA-CTPP beads have less swelling compared to CTPP beads. This is due to the complimentary pH dependant solubility properties of humic acid and chitosan. At lower pH, HA is sparingly soluble and thus acts as a protective layer whereas at higher pH, CTPP itself have less solubility. Less swelling of HA-CTPP beads in aqueous solution indicates that the beads can be equilibrated for extended period of time and thus practically more suitable for the adsorption purposes than CTPP beads.

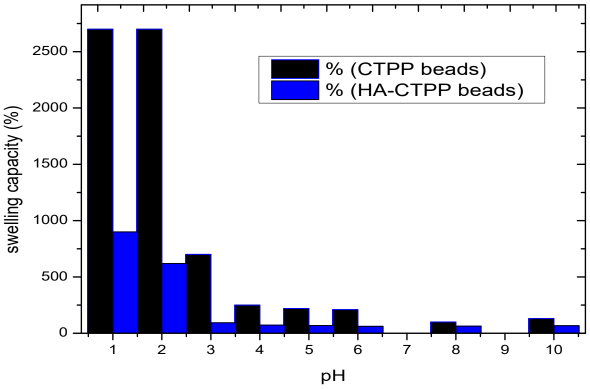

Fig. 4.6: Swelling capacity of CTPP and HA-CTPP beads (24 h equilibration)

4.5.6 Stability of HA-CTPP beads

For practical application of the beads, the stability of the beads in solution is very important. Stability of the HA coating in aqueous medium as a function of pH of the equilibrating medium is presented in figure 4.6. If total HA was eluted out of the beads the final HA concentration expected in the mixture is 430 mg/L. In experiments with pH < 3, concentration of HA in the final solution was below the detection limit. The dissolution of HA from HA-CTPP beads is found to increase with increase in pH. However, at pH=8 (the highest pH studied) too, the leaching of HA in 24 hours is found to be less than 10%, indicating that the beads can be utilized for the adsorption applications. Despite the absence of specific chemical bond formation, the stability of the beads is surprising and most likely due to conformational reasons. Difficulties in re-dissolution of air dried humic acid has been reported earlier [79] and is ascribed to the irreversible conformational changes taking place upon drying of HA.

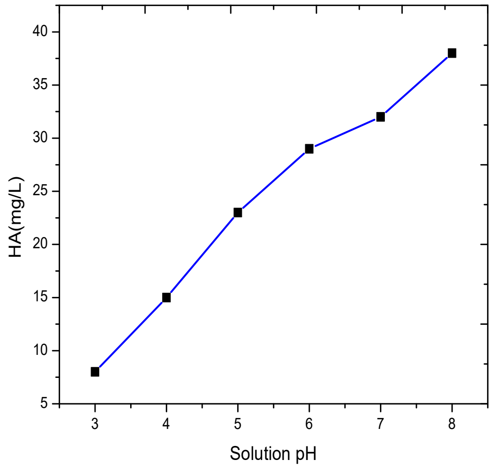

Fig. 4.7 Stability of HA-CTPP beads (V=100 ml, HA-CTPP =100 mg, 24 h equilibration)

4.6 Sorption studies

4.6.1 Sorption of U(VI) on HA-CTPP beads

4.6.1.1 Effect of pH on the sorption of U(VI) on HA- CTPP beads.

Effect of pH on the sorption of U(VI) on HA-CTPP beads were studied in the pH range pH=1-8. Figure 4.8 shows the effect of solution pH on the sorption capacity. Sorption capacity is observed to be maximum at pH=5. At lower pH, the acidic groups on HA are not ionized which prevents the uptake of positively charged UO_2^{2+}. With increasing pH, more sorbent sites are getting ionized resulting in increased uptake. Above pH=5, uranium itself is present as anionic complexes [52,53] which results in reduction of uptake by the sorbent. Further experiments, for elucidating the sorption characteristics were conducted at the optimum solution pH=5.

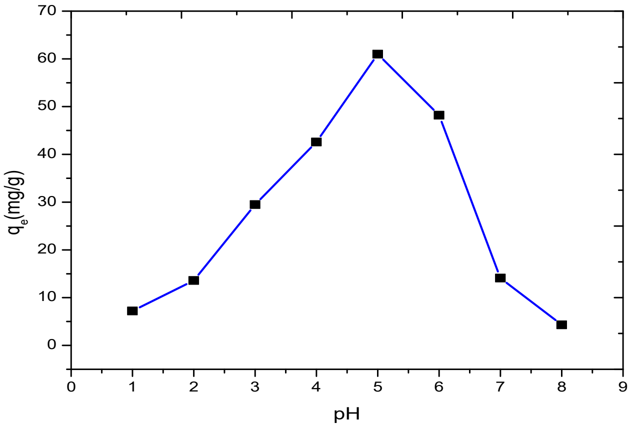

Fig. 4.8 Effect of pH on the sorption of U(VI) onto HA-CTPP beads (V=10 ml, U(VI) = 400 mg/l, HA-CTPP = 50 mg, T= 25°C)

4.6. 1.2 Effect of contact time on the sorption of U(VI) on HA-CTPP beads.

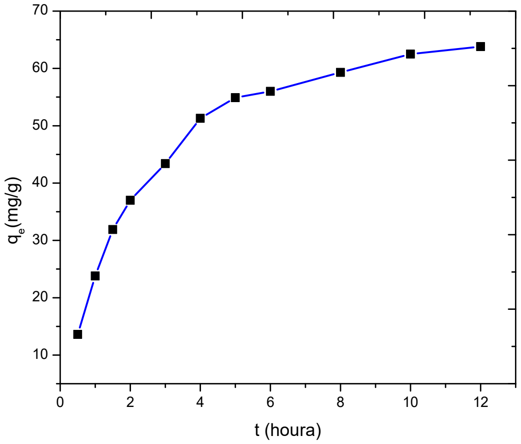

Fig 4.9 Effect of contact time on the sorption of uranium on humic acid coated CTPP beads (V= 100 ml, HA-CTPP= 50 mg, U(VI)= 400 ppm, pH=5, T=25 °C).

Effect of contact time on the sorption of U(VI) on HA-CTPP beads is presented in figure 4.9. From the figure it can be seen that it takes around ~10 hours to reach the equilibrium sorption capacity. This sorption kinetics is faster than that of CTPP beads, but significantly slower in comparison to that reported for solid HA [72]. It is seen that HA is present not on the surface alone and it takes longer time for such sites in the interior of the bead to be saturated by the metal ion, resulting in overall slow kinetics for sorption process.

4.6. 1.3 Adsorption kinetics

Both pseudo-first order and pseudo-second order kinetic models were applied to the experimental data of sorption of U(VI) on to HA-CTPP beads. Figure 4.10 represents the model plots for the kinetic data. The model parameters are present in table 4.1. From the results, it can be seen that though both the models are applicable, pseudo-second order model is more appropriate to describe the results, indicating that chemisorption is the underlying mechanism and site availability is the limiting factor controlling the sorption kinetics.

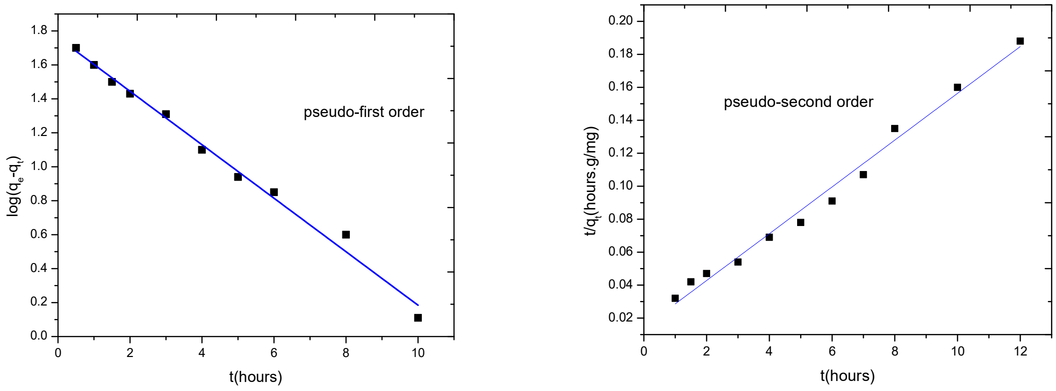

Fig. 4.10 Pseudo-first order and Pseudo-second order kinetic model fits of sorption of uranium onto HA-CTPP beads.

Table 4.1: Kinetic parameters for the sorption of U(VI) on HA-CTPP beads

Pseudo-first order		**Pseudo-second order**	
k_1	q_e	k_2	q_e
0.363	57.53	0.6×10^{-2}	75.35

4.6.1.4 Effect of concentration and Langmuir isotherm

Effect of initial U(VI) concentration on the sorption of U(VI) onto HA-CTPP beads were studied using uranium solutions with initial concentrations ranging from 10mg/l to 100 mg/l. The result is presented in figure 4.11(a). The adsorption data was analysed using Langmuir and Freundlich isotherm models. The latter is found fit the experimental data well ($r^2 = 0.979$) giving a sorption capacity of 71.4 mg/g, whereas Freundlich model gave only very poor fit. Previous studies reported a sorption capacity of 190 mg/g for uranium for humic acid extracted from five meter depth soil [71]. HA-CTPP contains only 43% HA (wt/wt). Even if discounted for this, the sorption capacity is lower than that for pristine HA reported in literature. Thus it could be

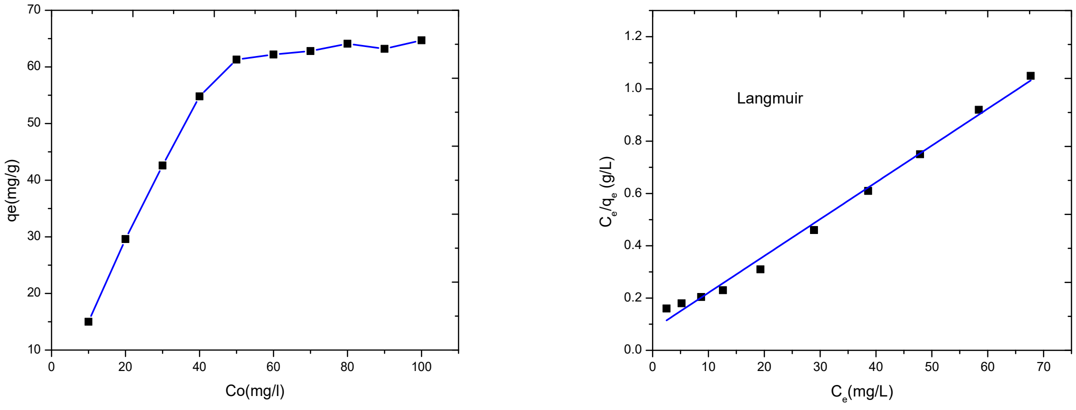

Fig. 4.11 Effect of concentration and Langmuir isotherm plot for the sorption of U(VI) onto HA-CTPP beads (V =100 ml, HA-CTPP= 50 mg, pH=5, T=25^{o}C).

concluded that in case of U(VI), the sorption capacity is significantly deteriorate by the immobilization process.

4.6.2 Sorption of Pb(II) ions on HA-CTPP beads

4.6.2.1 Effect of pH on the sorption of Pb(II) ions onto HA-CTPP beads

Adsorption of Pb(II) ions onto CTPP and HA-CTPP beads were investigated as a function of the solution pH using initial metal ion concentration as 200 mg /L and at fixed pHs in the range pH=1 to 5. No experiments were conducted for pH higher than five, due to the potential for precipitation of Pb(II) ions from solution [80]. The experimental results (figure 4.13) shows that at any given pH, HA-CTPP beads have significantly higher sorption capacity than CTPP beads, which could be assigned to the additional sorption sites provided by the HA. Dependence of sorption on pH was different for CTPP and HA-CTPP beads. For CTPP beads, the sorption capacity increased with increase in pH. For Pb(II) ions sorption onto CTPP beads, similar pH dependence was earlier reported by Ngah and Fatinathan [82]. The lower sorption capacity at low pH could be due to protonated amino and/or phosphate groups on the adsorbent repelling the positively charged metal ions. In contrast, the sorption capacity of HA-CTPP beads shows a maximum at pH=3 and thereafter reduced once again. Previous works on metal ion sorption onto HA derivatives reported continuous increase in sorption capacity with increase in pH, which is ascribed to increased ionization of HA at higher pH [81]. One would expect the same behavior in the present case too, where it is evident that HA is primarily responsible for the metal uptake. For both chitosan and HA, the adsorption is found to increase with increase in pH [82] and thus the reduction in Pb(II) adsorption for the HA-CTPP beads at higher pH's cannot be assigned to the electrostatic interactions between the metal ions and adsorbent. One possible explanation is

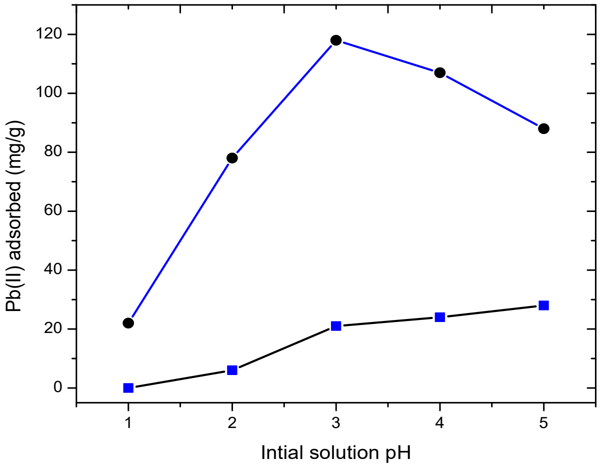

Fig. 4.12 Effect of pH on the sorption of Pb(II) ions onto CTPP (■) and HA-CTPP (●) beads (HA-CTPP = 100 mg, Pb(II) = 200 mg/l, V=100 ml, T= 25°C)

that, due to the reduced swelling of the beads at higher pH, many of the active functional groups of HA are not available for sorption of the metal ions. Cross section of the wet HA-CTPP beads showed that HA is diffused in to the bulk of the beads also, which could be inaccessible for the bulky Pb(II) ions at higher pH. Higher sorption capacity of HA-CTPP beads in comparison to CTPP beads at all pH showed that the former is a better adsorbent for sorption of Pb(II) ions from aqueous media and thus further investigations were limited to HA-CTPP beads .

4.6.2.2 Kinetics of Pb(II) ions onto CH-TPP beads.

To understand the effect of contact time on Pb(II) adsorption onto HA-CTPP beads, experiments were conducted with 100 mL solution having 200 mg/L of Pb(II) ions and 100 mg of adsorbent. 100 μL of the sample were sampled at various intervals to estimate the concentration of dissolved Pb(II) as a function of equilibration time. Figure 7(a) shows that the adsorption process is rapid, reaching the equilibrium in ~ 6 hours. The equilibration time for adsorption of Pb(II) onto HA-CTPP beads are higher than that reported for sorption of Pb(II) onto CTPP beads [82] and HA immobilized on rectorite [83], possibly due to large size of macro sized beads used in the present investigation. Pseudo-first order, pseudo-second order and intra-particle diffusion models were applied to analyze the experimentally observed kinetic data. Among the three tested models, pseudo-second order model is found to fit the experimental data than other kinetic

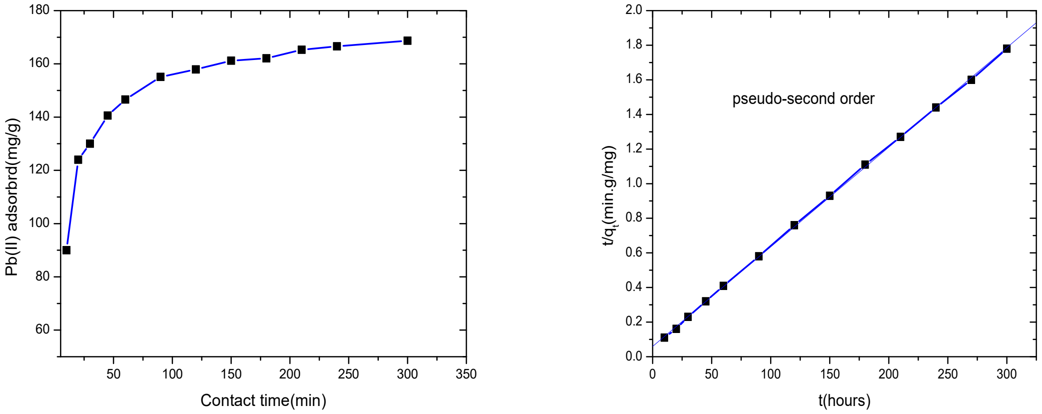

Fig. 4.13: Effect of contact time and pseudo- second order plot of the kinetics data for the sorption of Pb(II) ions onto HA-CTPPP beads (V=100 ml, HA-CTPP =100 mg, Pb(II)= 200 mg, T=25^{o}C)

models (figure 4.13b). The model showed high correlation coefficient (r^2 =0.999) and give equilibrium sorption capacity (173.9 mg/g) close to that of the experimentally observed sorption capacity (168.8 mg/g).

4.6.2.3 Effect of Pb(II) ion concentration and adsorption isotherm.

For investigating the effect of Pb(II) ions concentration on the sorption of Pb(II) onto HA-CTPP beads, experiments were conducted with 100 mL solutions having initial Pb(II) concentration varying from 50 mg/L to 800 mg/L and a fixed mass of 100 mg of adsorbent. Optimum pH=3 were employed for the isotherm experiments. Figure 4.14 (a) shows the amount of Pb(II) ions adsorbed at equilibrium verses the initial concentrations. The adsorption curve shows the typical behavior of saturated adsorption, where the entire sorption sites are consumed at higher metal ion concentration and adsorption capacity reaches the limiting value. The steep slope at initial stage in the adsorption curve is a desirable feature of the sorption system and the results indicates that HA-CTPP bead is an efficient adsorbent for Pb(II), even at lower concentration of metal ions. Adsorption data were further analyzed using Langmiur and Freundlich isotherm models. The model parameters obtained by applying both Langmuir and Freundlich model to the experimental data are given in table 4.2. From better correlation coefficient ($r^2 = 0.998$) and the fact that the equilibrium adsorption capacity (Q) obtained from Langmiur model (223 mg/g) is close to the experimentally observed saturation capacity (215 mg/g), it can be concluded that the monolayer Langmuir adsorption isotherm is more suitable to explain the sorption of Pb(II) ions onto HA-CTPP beads.

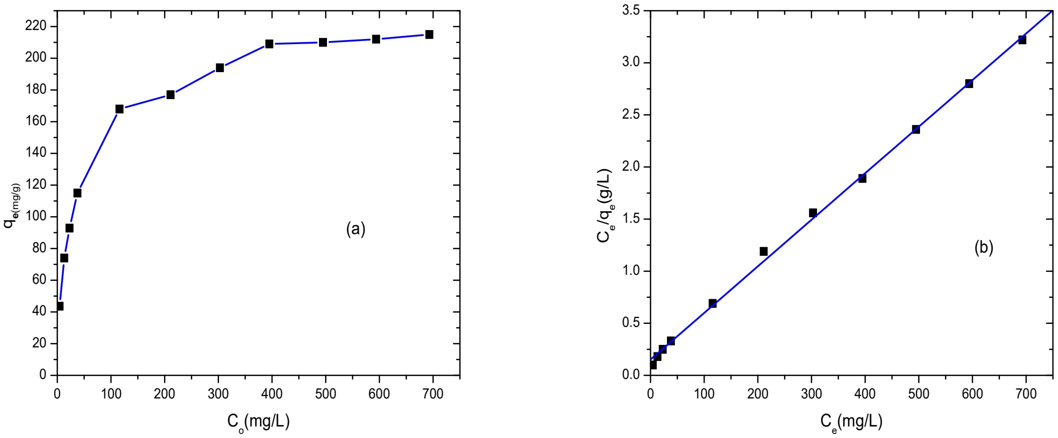

Fig. 4.14 Effect of initial concentration and the Langmuir isotherm plot for the sorption of Pb(II) ions onto HA-CTPP beads (HA-CTPP= 100 mg, Pb(II) ions = 200 mg/l, V= 100 ml, T= 25 °C).

Table 4.2 Model parameters for the sorption of Pb(II) ions onto HA-CTPP beads

Langmiur	
Q (mg/g)	223.7
b (L/mg)	0.029
R^2	0.998
Freundlich	
k_F (mg/g)	40.4
n	3.72
R^2	0.963

4.6.2.4 Characterization of Pb(II) loaded HA-CTPP beads.

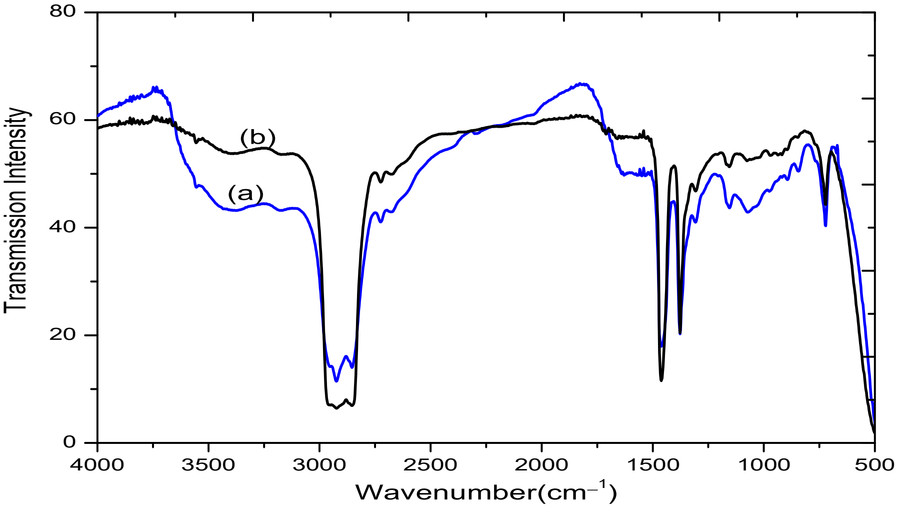

Fig. 4.15: FTIR spectra of bare (a) and Pb(II) ions loaded HA-CTPP (b) beads.

FTIR spectra of the bare and Pb(II) ions loaded HA-CTPP beads is present in figure 4.15 Comparison of the two spectra shows that no additional peaks are present in the spectra of Pb(II) ions loaded material, while broad difference can be observed between the two spectra. This indicates that chemical forces are involved in the sorption process, though specific functional groups responsible for the uptake cannot be identified using this technique. Comparison of EDS spectra of the bare (spectrum1) and Pb(II) ions loaded HA-CTPP beads (spectrum 2), presented in figure 4.16, shows the presence of lead on the latter surface and is a direct evidence for the uptake of Pb(II) ions by HA-CTPP beads.

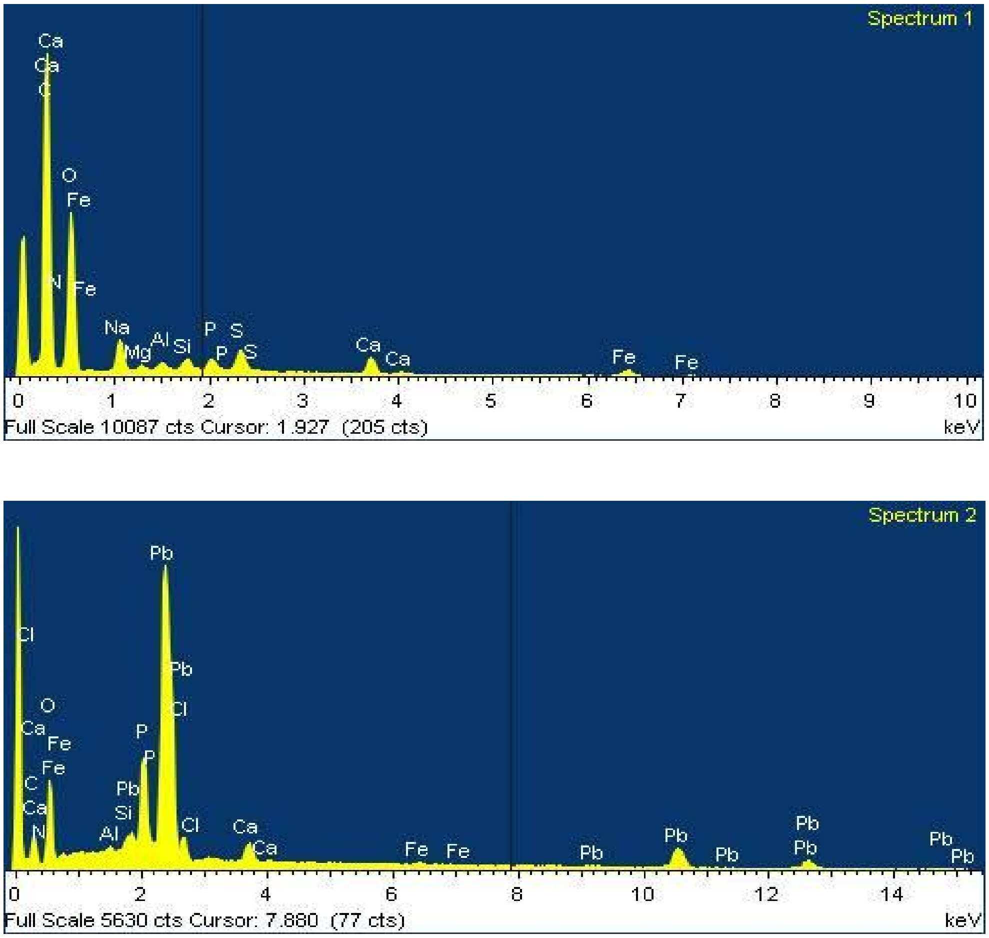

Fig. 4.16: EDS spectra of HA-CTPP beads before after sorption of Pb(II) ions

4.6.2.5 Comparison sorption capacity of HA based sorbents for Pb(II) ions.

Reported sorption capacities for humic acid based adsorbents for Pb(II) ions from aqueous media is presented in table 4.3. Adsorption capacity of HA-CTPP beads reported here is significantly higher than most other solid or insoluble HA reported in literature. In comparison to HA gel, HA-CTPP beads shows slightly lower sorption capacity. As shown previously in figure 4.12, at pH=3, bare CTPP beads shows nearly 20 percent of the adsorption capacity of HA-CTPP beads. This indicates that the sorption of Pb(II) ions onto HA-CTPP beads can be largely assigned to HA present in the HA-CTPP beads. Taking into account the fact that only less than fifty percentage of HA is present in HA-CTPP beads, it can be concluded that the metal uptake capacity of HA in HA-CTPP beads is comparable to that of HA gel reported by Coles and Young [70]. After completion of equilibrium, solid-liquid separation can be easily achieved by the use of macro-sized HA-CTPP beads instead of HA-gel and HA powder and thus is a significant advantage in designing HA based industrial separation process.

Table 4.3 Reported sorption capacity for Pb(II) ions by various HA based sorbents

Adsorbent material	Isotherm model applied	pH	Adsorption capacity (mg/g)	Reference
SiO_2-HA	**E**	7	34.65	84
HA-Rectorite composite	**L**	5.3	34.96	83
HA gel	**L**	1-4	353.6	85
HA gel	**E**	4	455.5	86
IHA	**L**	4	33.2	68
HA-gel	**E**	5	382.7	69
HA-gel/solid HA	**E**	1.5-5.4	220-262	87
HA-CTPP beads	**L**	3	223	present work

(**E**- Experimental; **L** – Langmuir isotherm model)

4. 9 Conclusions:

A new adsorbent, humic acid coated chitosan tripolyphosphate (HA-CTPP) beads was prepared by loading HA onto wet CTPP beads in aqueous alkaline medium. This method gives high loading of HA onto CTPP in comparison to previous reports of HA sorption onto modified chitosan derivatives. The HA content of the resultant adsorbent was 43% HA (wt/wt). HA-CTPP beads were more stable than CTPP at all pH and showed significantly low swelling capacity than CTPP beads. Potential of HA leaching from the solid is found to be limited; < 10% even at pH=8 for twenty four hours equilibration. The new sorbent is studied for its sorption characteristics towards the toxic metal ions U(VI) and Pb(II). pH=5 and 3 were found to be the optimum solution conditions for the sorption of U(VI) and Pb(II) respectively onto HA-CTPP beads. The kinetics of sorption is found to depend on the nature of metal ions; U(VI) sorption saturating in ~10 hours while Pb(II) in ~6 hours of equilibration. In both cases the kinetics could be fitted into the pseudo-second order kinetic model. The new immobilization process resulted in reduction of sorption capacity of HA for U(VI). But for Pb(II) ions, the sorption capacity is found to be comparable with that of other HA based sorbents. Langmuir isotherm model is found to fit the experimental sorption data resulting in sorption capacity of 71.4 mg/g and 223.7 mg/g respectively for U(VI) and Pb(II). In nutshell, the study presented in this chapter proves that the new solid humic acid based sorbent reported here can be utilized as a medium for the removal of toxic metal ions from contaminated water.

Chapter 5

Sorption of uranium on magnetite and Humic Acid coated magnetite (HA-magnetite) nanoparticles

5.1 Introduction

Nanomaterials has found applications in wide areas of technology such as medicine, sensing, electronics and environmental remediation [88,89]. Nanomaterials have properties, sometimes far different from their bulk counterparts due to the high surface area and surface reactivity. This lead to the proposal, that they could be used as highly efficient adsorbents for the toxic materials including heavy metals [90-92]. Among the various nanomaterials used for toxic metal sorption, magnetic nanoparticles such as iron oxides are of special relevance due the ease of solid-liquid separation it offers, in contrast to other non-magnetic nanomaterials [93,94]. Apart from this technical use, since iron oxide nanoaprticles are ubiquitous in the environment, from a fundamental perspective also it is important to understand the interaction of them with various metal ions. For example it is known that iron oxides play a major role in the sorption and red-ox behavior of various contaminant metal ions in the environment [95-97]. Due to this significance, herein a study is carried out on the sorption of uranium on magnetite nanoparticles. The selection of magnetite nanoparticle as sorbent was based on two compelling reasons: a) among the various iron bearing nanoparticles reported for metal ion sorption, magnetite is the foremost choice in most cases and b) in environment, they could form as a corrosion product of steel and as a metabolic product of bacterial respiration [98,99]. It should be noted that many studies have been reported previously on the sorption of uranium on magnetite and on their red-ox behavior [100-105]. However most of them were dealing with anoxic conditions relevant to deep geological disposal, necessitating further studies on this system, for both to develop it as a useful separation medium and to better understand the environmental process involving magnetite and uranium. In addition to bare magnetite, in this thesis, humic acid coated magnetite is also subjected to uranium sorption studies, due to its relative merits as an adsorbent reported in the literature [106,107], and the fact that natural organic matter coated magnetite may be more probable in natural environment than naked one. It has been found that the sorption properties of metal ions on humic acid coated magnetite are different from that of bare magnetite [108-110], though no studies pertaining to uranium is yet reported. Thus this study is an attempt to understand the sorption behavior of uranium on laboratory prepared bare and humic acid coated magnetite nanoparticles.

5.2 Adsorbent preparation and characterization.

5.2.1 Preparation of adsorbent.

Preparation of magnetite nanoparticle was carried out using an aqueous precipitation method following Fuliu et al. [108]. 6.1g $FeCl_3 \cdot 6H_2O$ and 4.2 g $FeSO_4 \cdot 7H_2O$ were dissolved in 100 ml water and heated to 90 °C. Then 100 mL of ammonia solution (30%) was added followed by 100 ml aqueous solution containing 1g of humic acid sodium salt. A black precipitate was formed and the stirring continued for 30 minute at 90 °C. The precipitate was cooled, filtered, and washed several times with nanopure water till no colour of HA is present in the washings. Finally the adsorbent is dried in air oven at 60 °C. Bare magnetite nanoparticle is prepared by utilizing similar procedure, but in absence of humic acid.

5.2.2 Characterization of the adsorbent.

Characterization of the product was carried out by FTIR spectroscopy, Powder X-ray diffraction analysis (XRD), X-ray photoelectron spectroscopy (XPS), zeta potential measurements and BET surface area analysis. The amount of humic acid present on HA-magnetite was determined using Euro-glass TOC analyser.

5.3 Batch equilibration studies.

Batch equilibration experiments were conducted in 15 mL polypropylene (*Laxbro* make) screw capped vials. pH of the U(VI) solution were adjusted using dilute Na_2CO_3/HNO_3 before the addition of the nanoparticles. In all experiments ^{233}U spike were added to get an initial count rate of ~ 6000 cpm/ml of the solution. Equilibration was carried out in a temperature controlled incubating shaker at 25°C with agitation speed of 250 rpm. After equilibration, nanoparticles were separated using a handheld magnet and the adsorbent free liquid was counted for alpha activity, to estimate the dissolved uranium concentration. Counting is done using 2 ml samples in stainless steel planchets, after firing on Bunsen burner. Amount of adsorbed uranium was estimated from the difference between the initial and final count rate of the sample. For experiments with Ammonium Di-Uranate (ADU) supernatant sample, 10 mL of the original sample was spiked with ^{233}U, equilibrated for two days and centrifuged (10000g, 10min) before using in the sorption experiments. Original pH of the ADU supernatant was 8.1 and no further adjustments were done before the sorption experiments.

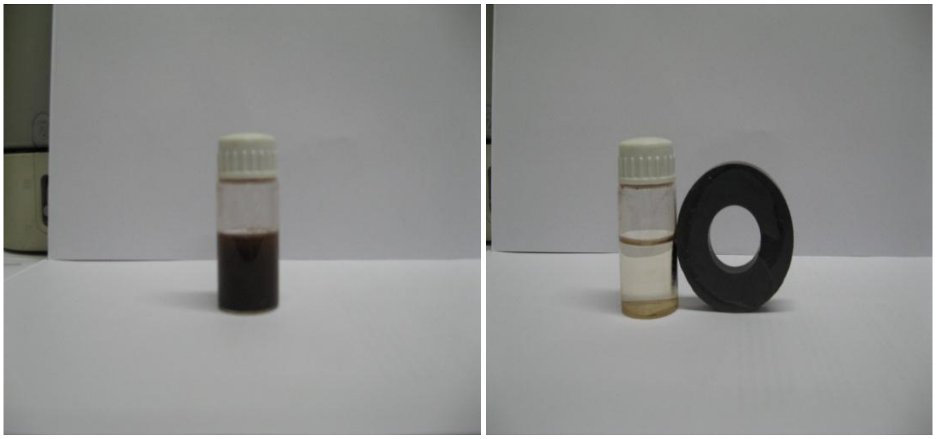

Fig 5.1 Solid-liquid separation using an external magnet

5.4 Results and Discussion

5.4.1 Characterization of nanoparticles

The FTIR spectra of magnetite, HA and HA-magnetite are presented in figure 5.2. The incorporation of HA on magnetite can be seen from the presence of peaks at at 1737 cm^{-1} (corresponding to CO stretching of carboxylic or ketones), 1387 cm^{-1} (corresponding to phenolic O-H or aliphatic C-H) and 2925 and 2851 cm^{-1} (corresponding to aliphatic C-H starching) [30]. Additionally it can be seen that the carboxylic peak of HA is shifted from 1708 cm^{-1} to 1737 cm^{-1} indicating chemical interaction with magnetite and HA.

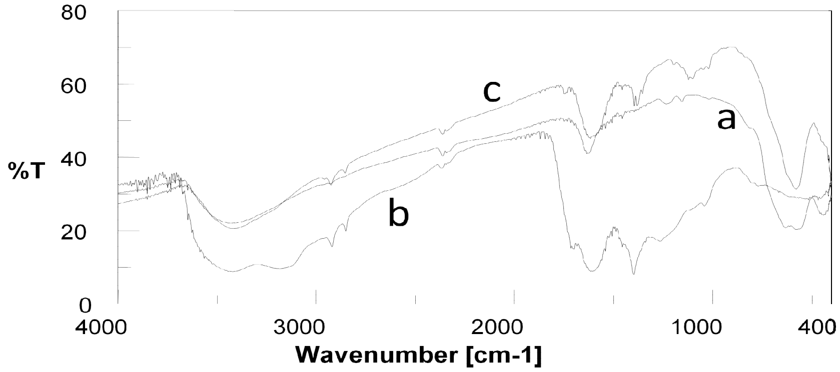

Fig. 5.2 FTIR spectra of bare magnetite (a), humic acid (b) and HA-coated magnetite (c).

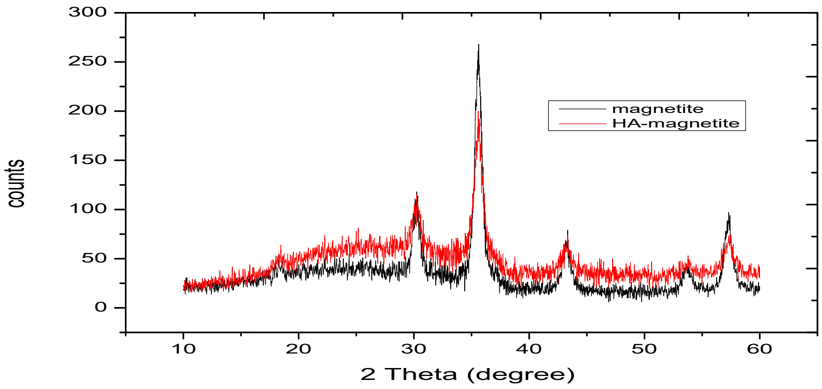

Fig 5.3 XRD of bare and HA coated magnetite.

Figure 5.3 shows the XRD pattern of synthesized products and fit very well with those expected for magnetite [111]. No peaks confirming to other mineral phase were found in the recorded spectrum. HA-magnetite also presented the same peaks as in bare magnetite, showing that the presence of HA is not affecting its crystalline structure of magnetite. But all peaks were broader than that of bare magnetite due to the presence of amorphous humic acid coating over the nanoparticle. Magnetite and another iron oxide, maghemite (γ-Fe_2O_3) have similar XRD pattern and thus XPS were used to confirm that the product is magnetite and not the fully oxidized maghemite. Figure 5.4(a) shows the full range (0 – 1000 eV) XPS spectrum of the synthesized

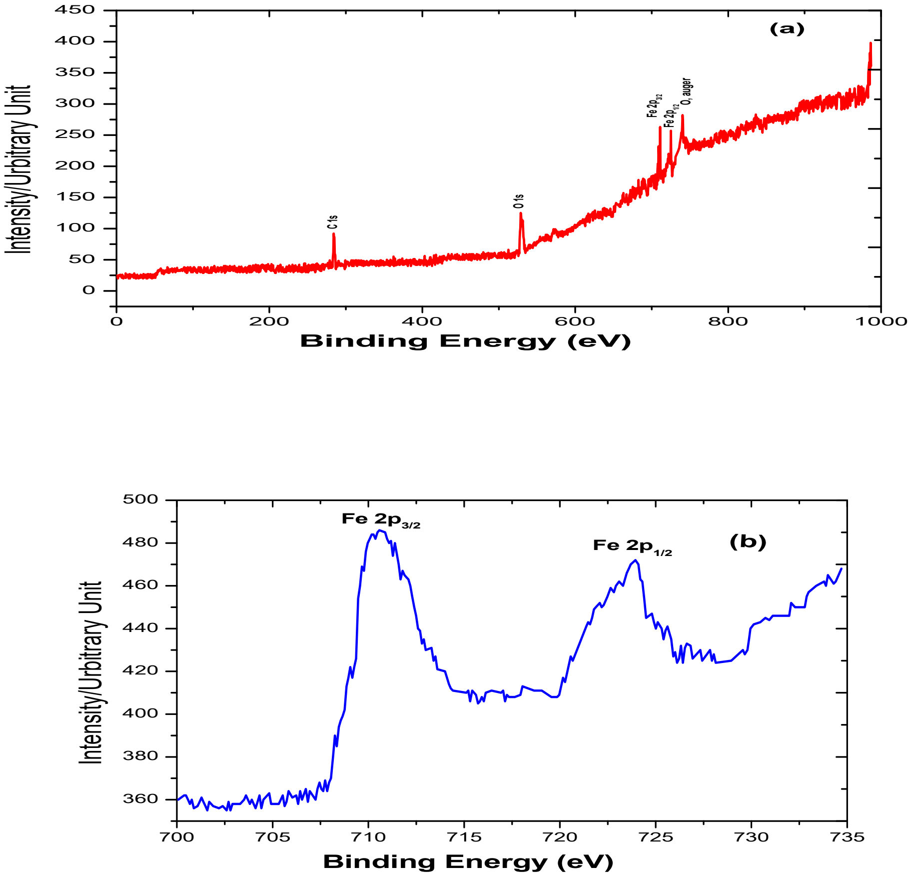

Fig 5.4 XPS spectra (a) and deconvoluted Fe2p peak (b) of bare magnetite.

nanoparticle. The peaks at 284.6 eV, 530.1 eV, and 739.9 eV correspond to C1s, O1s and O-Auger binding energies. The Fe2p peak was deconvoluted into individual peaks corresponding to Fe $2p_{3/2}$, Fe $2p_{1/2}$ components using Gaussian peak fitting algorithm. The two peaks at 710.6 eV and 723.9 eV corresponds to Fe $2p_{3/2}$ and Fe$2p_{1/2}$ respectively and matching well with the previously reported values [112] (figure 5.4b). From the deconvolution of Fe $2p_{3/2}$ peak into Fe(II) and Fe(III) components, Fe(II)/Fe(III) ratio in the synthesized sample was estimated as 0.58.

Zeta potential of the magnetite and humic acid coated magnetite nanoparticls were measured in the pH range 1-10. The result is presented in figure. 5.5. Charge reversal in case of HA-magnetite occurs around pH=2.5, whereas for magnetite it is at pH=6.8. Studies on the dissociation behavior of carboxylic groups on Aldrich HA by various researchers found that that

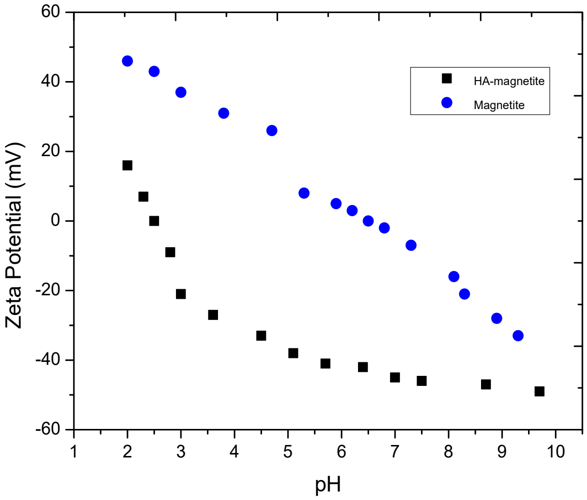

Fig. 5.5 Zeta potential of bare and HA coated magnetite as a function of pH.

the dissociation begins just above pH=2 [113] and this is the reason for the net negative charge on HA-magnetite at lower pH in comparison to naked magnetite. For the latter, the negative charge formation on surface is only due to the ionization of surface hydroxyl groups. BET surface area analysis shows that HA–magnetite surface area (99 m^2/g) is significantly larger than

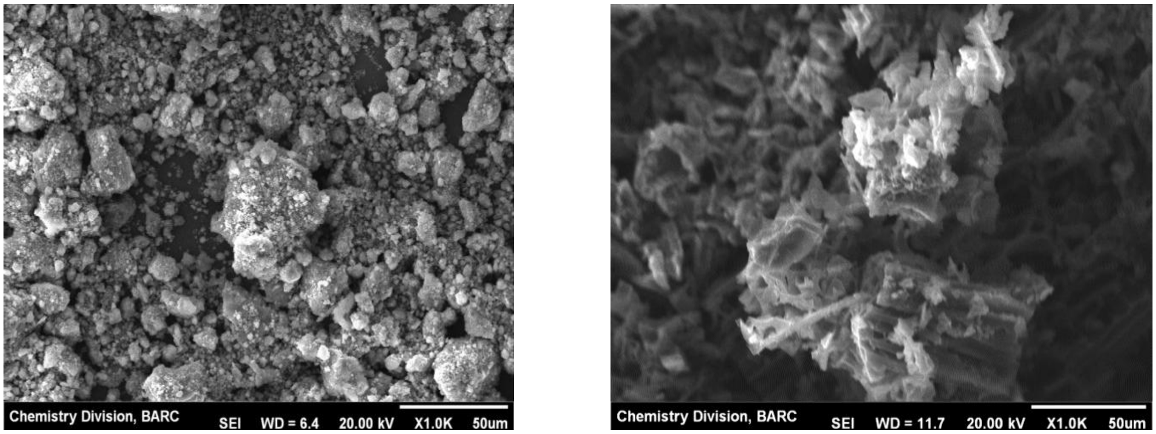

Fig 5.6 SEM image of magnetite nanoparticle and HA-magnetite nanoparticle

that of bare magnetite (59 m^2/g). SEM images of magnetite and HA-magnetite is shown in figure 5.6 . Though extensive aggregation is observed in both cases, HA-magnetite is found to be more porous than bare magnetite which could be the reason for the large surface area observed for the latter. By indirect means, less aggregation of HA-magnetite in comparison to bare magnetite was reported earlier by Fuliu et al [108]. In present case, different surface morphology is observed for bare magnetite and HA-magnetite nanoparticles.

5.4.2 Sorption of uranium on magnetite nanoparticles.

5.4.2.1 Effect of pH and ionic strength on uranium sorption onto magnetite nanoparticles

To find out the optimum pH for the sorption of uranium on magnetite, experiments were conducted by varying the pH from 4-9 while keeping all other experimental parameters constant. The result (figure 5.7a) indicates that the sorption is maximum at around pH = 7 and decreases both in acidic and alkaline medium. Speciation calculations of U(VI) in presence of carbonate [52,53] indicate that in neutral to alkaline medium, uranium is present in the anionic form by complexation with carbonate and hydroxyl anions and present as positively charged species at lower pHs. Below the isoelectric point (pH= 6.8) magnetite surface is positively charged and the surface charge is higher at lower pH. Thus at acidic pH, due to the positive charge on the magnetite surface and metal ion, sorption is unfavorable. Similarly above pH=6.9, the surface of the nanoparticle becomes increasingly negatively charged and uranium is also present as anionic species, leading to the decrease in sorption percentage. To understand the effect of electrolyte on the sorption of uranium on magnetite nanoparticles, experiments were conducted by varying the ionic strength from 0.01 to 0.2 mol/l by addition of $NaClO_4$. From the result (figure 5.7b) it can be inferred that ionic strength has only limited effect on the sorption process. From the apparent independence of sorption on the electrolyte concentration it might be inferred that weak electrostatic effects govern the sorption process. The maximum sorption capacity at the experimental pH corresponding to the isoelectric point of the nanoparticle also confirms that factors other than electrostatic interaction contribute to the sorption process.

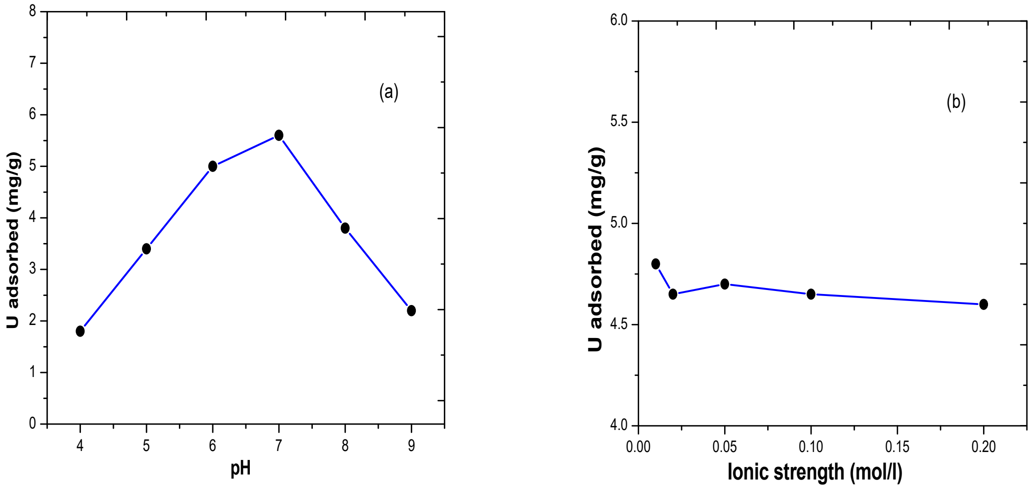

Fig. 5.7 Effect of pH (a) and ionic strength (b) on the sorption of uranium on magnetite nanoparticle (equilibration time = 6h, T=25 °C)

5.4.2.2 Effect of contact time on sorption of uranium on magnetite nanoparticles

Figure 5.8 presents the sorption of uranium on magnetite nanoparticles as a function of contact time. From the figure it can be seen that the sorption process has two distinctive phases, initial fast process completing in approximately four hours followed by a slow uptake extending to several days. Similar two stage kinetics for uranium sorption on magnetite were reported earlier for anoxic conditions, where the initial fast process is attributed to the adsorption of U(VI) ions on surface and the slow process is due to the slow reduction of uranium from solution, due to the favorable Eh-pH combination prevailing in the solution [100]. However in their study it was observed that Fe(II) mediated solution phase reduction of U(VI) is not favorable at pH=7 and even at acidic pH this reaction follows a very slow kinetics. Thus the fast adsorption cannot be assigned to the adsorption of pre-reduced uranium species. However presence of reduced U(IV) on the magnetite after uranium sorption, obtained from the XPS data, indicates that reduction is indeed involved in the process. Due to the absence of temporal data on the speciation of

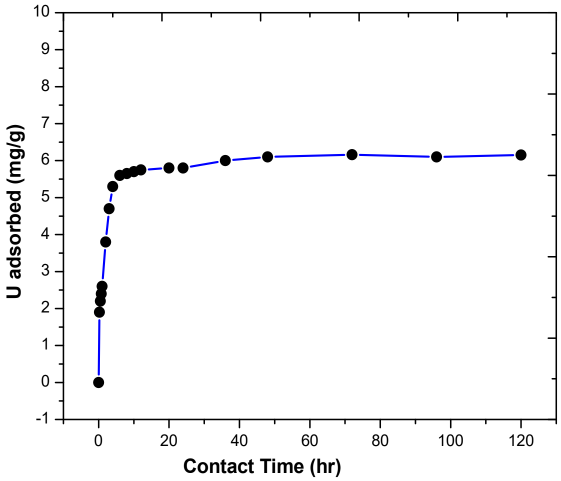

Fig 5.8 Effect of contact time on the sorption of uranium on magnetite nanoparticles (volume 10 ml, adsorbent= 10 mg, U(VI)= 30 mg/L, pH=7).

adsorbed uranium, it cannot be concluded weather the reduction is triggered by the sorption process itself or it is a slow process involving the already adsorbed U(VI) on the amphoteric groups on magnetite. Comparing this results with that of the earlier investigators [114], it can be concluded that U(VI) adsorption on magnetite is accompanied by reduction of a fraction of the U(VI) to U(IV).

5.4.2.3 Effect of initial uranium concentration on the sorption

To find out the effect of initial uranium concentration on the sorption process, experiments were conducted by varying the concentration of uranium from 2 mg/l to 50 mg/l. Figure 5.9 presents the amount of sorbed uranium on the magnetite nanoparticles after six hours of equilibration. In order to account for the loss of uranium by processes other than sorption, parallel experiments were conducted without magnetite nanoparticles. In all cases, the loss is found to be insignificant (< 5%). Thus the removal of uranium in presence of magnetite can be assigned to the interaction between magnetite surface and uranium species present in solution. Saturation sorption capacity for uranium on magnetite is found to be approximately 5 mg/g. The sorption capacity reported

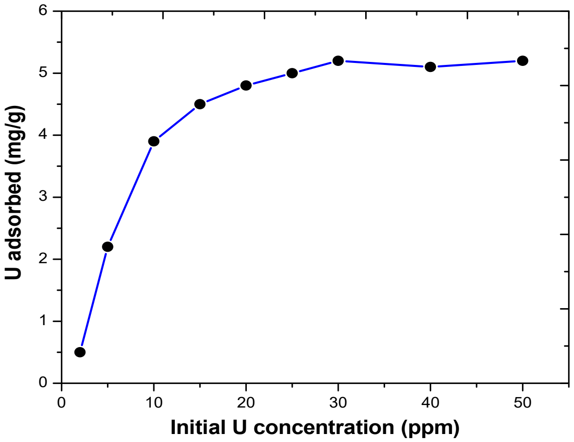

Fig. 5.9 Effect of initial metal ion concentration on the sorption of uranium on to magnetite nanoparticles (V=10 ml, adsorbent = 10 mg, pH=7, equilibration time= 6 h).

here is higher than the value reported by Missana et al [100]. It should be noted that the physico-chemical properties of nanoparticles vary with the method of preparation. Average Fe(II)/Fe(III) ratio (0.45) of the nanocrystals used by Missana et al for uranium sorption is significantly lower than that of the magnetite used in the present work and the higher content of Fe(II) in the present sample may be responsible for the higher uptake of uranium in the present case.

5.4.4.4 Speciation of uranium on magnetite surface.

Hexavalent uranium has a complex red-ox behavior in presence of other minerals. Since Fe(II) coordinated surface functional groups is known to be very effective reductant [101], spectroscopic investigation of the mineral surface is very important for understanding the kind of reaction taking place on the surface. Uranium loaded nanoparticle was subjected to XPS analysis in order to gain information on the oxidation state of iron and uranium. Figure 5.10a shows the full range (0 to 1000 eV) XPS spectrum of the nanomaterial after uranium loading.

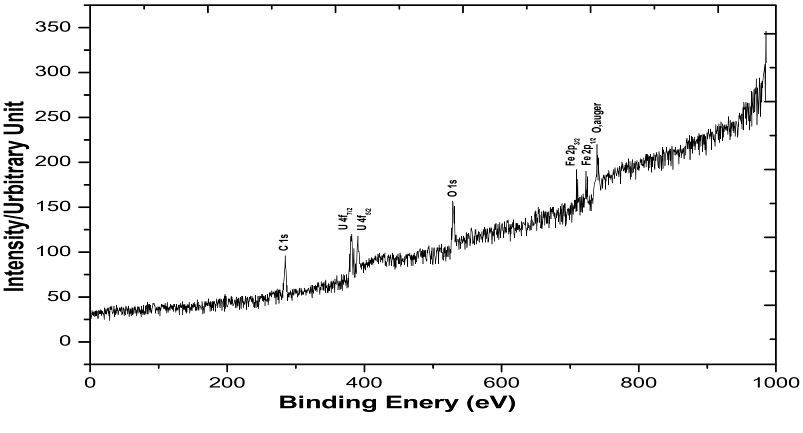

Fig. 5.10: XPS spectra of the uranium loaded magnetite nanoparticles

The peaks centered at 284.6 eV, 530.1 eV and 739.9 eV denote the characteristic C1s, O1s and O-Auger peaks respectively. The peaks at 380.9 and 391.6 eV visible in figure 5.11 corresponds to U $4f_{7/2}$ and $4f_{5/2}$ respectively. By studying a series of uranium minerals, Schindler et al reported that the $4f_{7/2}$ peak for pure U(VI) oxidation state is appearing in the range 381.1-382.6 eV [115]. Also according to Allen et al 380.9 eV for $U4f_{7/2}$ corresponds to the mineral $UO_{2.2}$ [116]. Thus it is clearly evident that, in the present experiments, some of the uranium species sorbed onto the nanomaterial is present in reduced oxidation state. Various reports on the interaction of U (VI) with magnetite gives contradicting results from no reduction to complete reduction [117,118]. Using a series of iron oxides with varying Fe(II)/Fe(III) ratios and different contact times, Huber et al has reported that solid phase Fe(II) could indeed lead to the reduction of U(VI) to lower oxidation states [119]. Deconvolution of the iron peaks in the XPS spectrum showed that the Fe(II)/Fe(III) ratio in the final product is 0.48, indicating that part of the Fe(II) present initially undergone oxidation as a result of sorption of uranium.

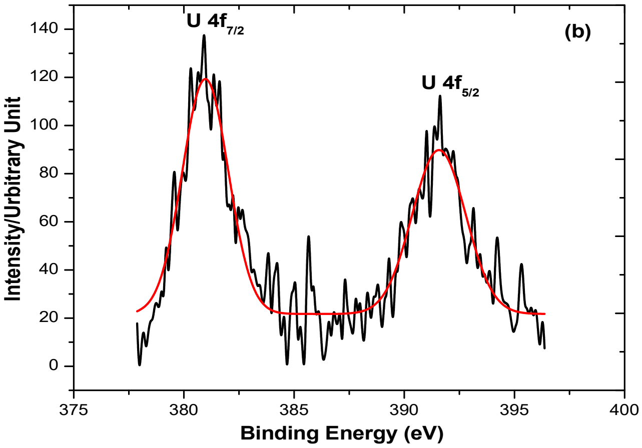

Fig 5.11: 4f peaks of uranium obtained from the uranium loaded magnetite nanoparticles

5.4.3 Sorption of uranium at low Concentration: An experiment with ADU supernatant.

In order to assess the utility of the process in real world situations, experiments were conducted with ADU supernatant collected from the industrial process. Composition of the effluent is given in table 5.1. Results of the sorption experiments (figure 5.12) indicate that magnetite nanoparticles are effective in decreasing the uranium concentration in the effluent. In presence of high concentration of the electrolyte also, sorption is found to reach the equilibrium within ~ 6 hours. A maximum of 42% decrease from the initial concentration of 3.8 mg/l is observed during six hours of contact and thereafter further sorption was insignificant on prolonged equilibration up to four days. The result indicates that iron oxide nanoparticles can be used as a partial remediation strategy for removal of uranium from the contaminated solutions with low concentrations of uranium.

Table 5.1 Composition of ADU supernatant used in the sorption experiments

pH	U (mg/l)	Mg(mg/l)	Ca(mg/l)	Fe(mg/l)	Si(mg/l)	NO_3^-(mol/l)
8.1	3.80	0.93	5.80	0.55	0.05	0.82

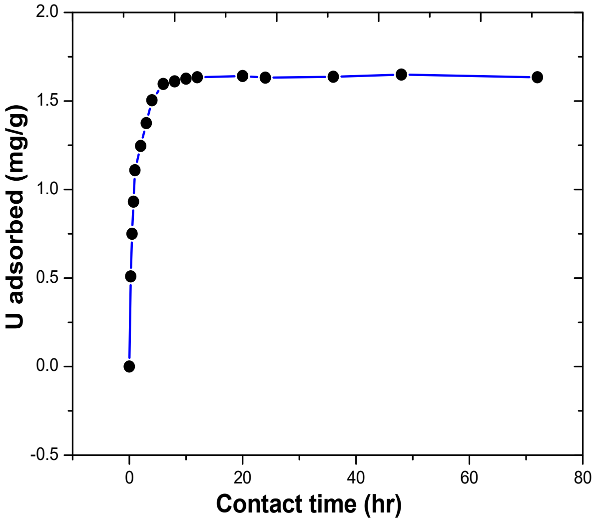

Fig. 5.12 Sorption of uranium on magnetite from ADU supernatant solution (V=10 ml, adsorbent= 10 mg, pH=8.1)

5.4.4 Sorption of uranium on HA-magnetite

5.4.4.1: Effect of pH and ionic strength of the medium on the sorption of uranium on HA-magnetite.

Effect of pH on the sorption of U(VI) on HA-magnetite was studied with a solution containing 100 mg/l uranium solution. The result is presented in figure 5.13. The pH dependence of uranium sorption on HA-magnetite is significantly different from that of magnetite shown in figure 5.7a. Sorption capacity is found to increase up to pH=5 and then decreases. This behavior could be correlated with the dissociation characteristics of HA and the ionic speciation of uranium in solution. Below pH=5, the predominant species of hexavalent uranium is UO_2^{2+} whereas mixed carbonato-hydroxyl complexes of uranyl ions forms at higher pH. The ionization of acidic groups on HA is continuously progressing with pH of the solution. This explains the initial increase in sorption with pH. Above pH=5, uranium is present as neutral or anionic with less affinity to interact with the negatively charged HA-magnetite surface, resulting in drastic reduction in the sorption capacity above pH=5. Similar strong pH dependence for sorption of

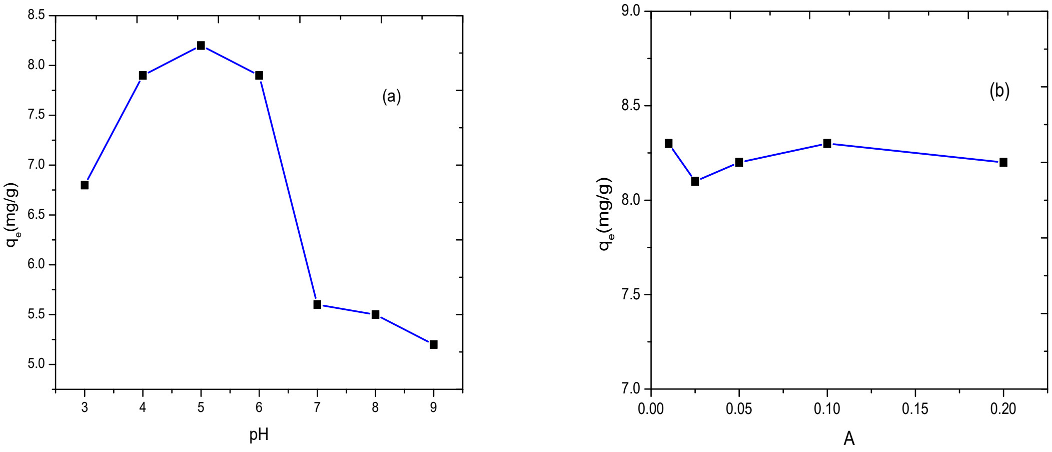

Fig. 5.13 Effect of pH (a) and ionic strength (b) on the sorption of uranium on HA-magnetite (equilibration time = 2 hours, T=25°C)

Pb(II), Cu(II) and Eu(III) on HA-magnetite were reported earlier by other researchers [97]. In each case it could possible to relate the absorption maximum with the aqueous speciation of metal ions. Similar to the results for bare magnetite, uranium sorption on HA-magnetite nanoparticles is also found to be ionic strength independent (figure 5. 13b). This shows that mechanism other than ion exchange is operating in the sorption of uranium onto HA-magnetite nanoparticles.

5.4.4.2 Effect of contact time on the sorption of uranium on HA-magnetite.

Effect of contact time on the sorption of uranium on HA-magnetite was studied using 200 mg/l uranium solution at pH=5. It could be seen that the equilibrium is attained in around 60 minutes. This is slow compared to the kinetics of sorption reported for Cu(II), Hg(I), Pb(II), Cd(II) and Eu(III) ions on HA-magnetite, but found to be faster than that kinetics for uranium sorption on to single components ie bare magnetite and solid humic acid [54, 94]. The slow kinetics of U(VI) in comparison to other metal ions could be due to the bulky nature of uranyl ions, which results in slow site to site exchange, required for the saturated sorption. The experimental data were

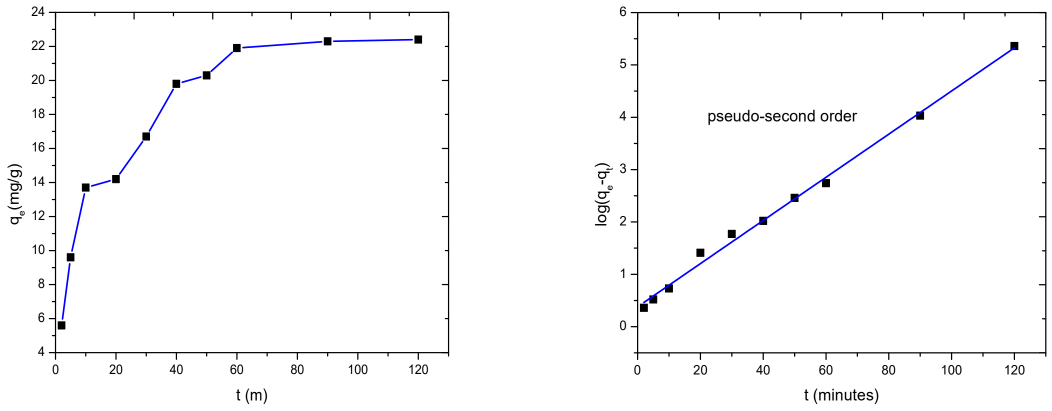

Fig 5.14 Effect of contact time (a) and pseudo-second order plot (b) of the sorption of uranium on HA-magnetite (V=10 ml, HA-magnetite= 50 mg, U(VI)=200 mg/l, pH=5, T=25^{o}C).

analysed using pseudo-first order and pseudo-second order kinetic models. The experimental data found to fit well (r^2=0.995) with pseudo- second order model, resulting in an equilibrium adsorption capacity of 24.39 mg/g at 100 mg/l initial concentration.

5.4.4.3 Effect of initial uranium concentration on the sorption of uranium on HA-magnetite.

Effect of uranium concentration on the sorption of U(VI) on HA-magnetite is studied by varying the concentration of the metal ions form 1 mg/L to 200 mg/l. The result is presented in figure 5.15a. With increasing metal ions concentration, the sorption capacity increases. The data was tried to fit using Langmiur and Freundlich isotherm models, but the former only found to fit the experimental observations. From the model fit the sorption capacity is derived as 25.64 mg/g. This is four times higher than that observed for bare magnetite (5 mg/g). It should be noted that the sorption capacity normalized to surface area is only twice that of magnetite. But the results prove that the humic acid modification in fact improves the sorption uranium on magnetite.

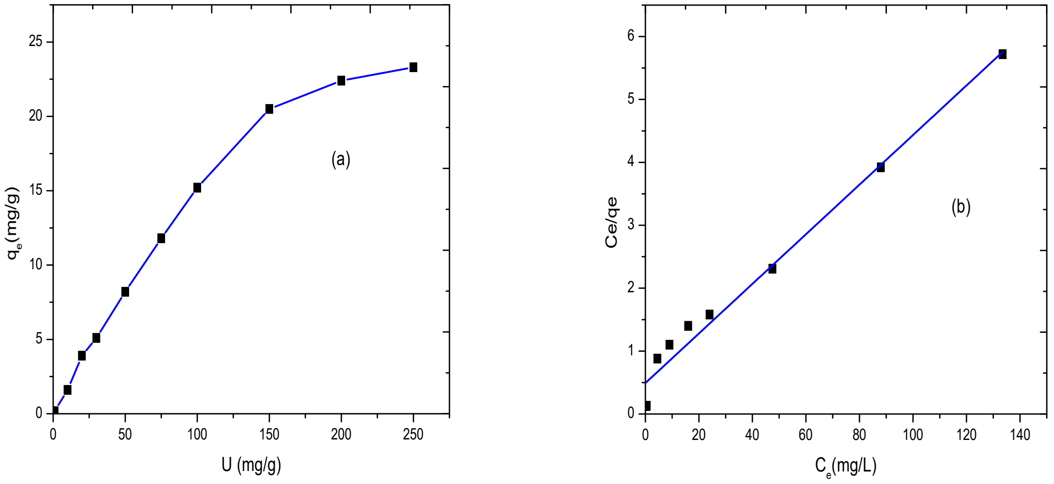

Fig 5.15 Effect of initial uranium concentration (a) and Langmuir isotherm (b) of the sorption of uranium on HA-magnetite (b) (V=10 ml, HA-magnetite=50 mg, pH=5, T=25 °C)

5.4.4.4 XPS spectra of uranium adsorbed HA-Magnetite

An XPS spectrum of the uranium loaded HA-magnetite is shown in figure 5.16. Binding energy observed for U4$f_{7/2}$ at 380.5 eV shows that only U(VI) is visible on the surface of the loaded HA-magnetite. This is contrary to the observation seen for uranium sorbed on to bare magnetite, where reduced uranium species were also observed. One possible reason could be that the sorbed uranium is principally bound to the HA functional groups present on the surface of the nanoparticle. Carbonate complexed U(VI) is reported to have minimum interaction with magnetite surface [120] and complexation with humic acid functional groups also could yield similar results. On the other hand, highly efficient coupled reduction-complexation is found to occur with Cr(VI) on HA coated magnetite[107]. Thus detailed studies in future are required to understand the red-ox behavior of uranium on HA coated magnetite nanoparticles.

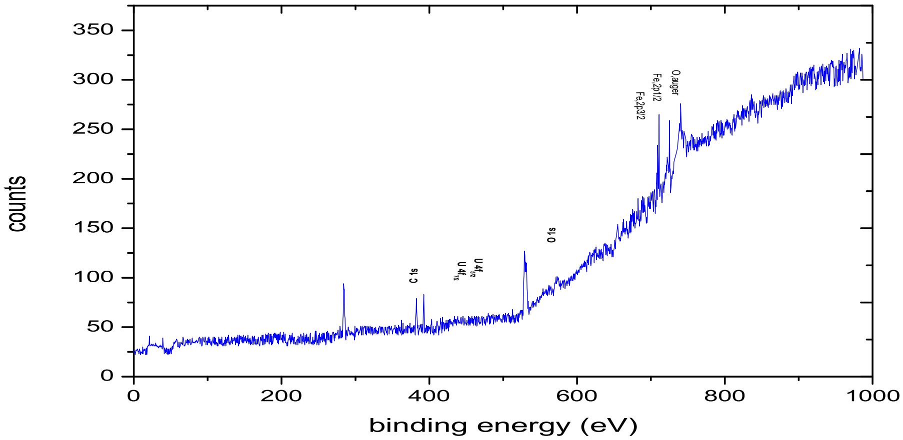

Fig. 5.16 XPS spectra of uranium loaded HA-magnetite nanoparticles.

5.5 Conclusions.

In this chapter, the result of the sorption of U(VI) onto magnetite and HA coated magnetite (HA-magnetite) nanoparticles is presented. HA-magnetite is found to have higher specific surface area, lower isoelectric point and different surface morphology than that of bare magnetite nanoparticles, prepared under identical conditions. U(VI) sorption studies showed difference in the sorption behavior for these two sorbents. Magnetite showed an optimum pH= 7 for sorption with sorption capacity of 5 mg/g. The same was 25.6 mg/g for HA-magnetite at the optimum pH=5. Kinetics of U(VI) sorption on magnetite have two distinct steps, one completing in four hours with sorption of 95% of the sorption capacity followed by a slow sorption extending to two days. Sorption on HA-magnetite is found to be fast reaching saturation within sixty minutes, following a pseudo-second order kinetic model. From XPS analysis it is observed that the sorption of U(VI) onto bare magnetite is accompanied by partial reduction of U(VI) to U(IV), whereas no reduced species are observed in case of HA-magnetite. The results presented here show that organic coating on nanomaterials could significantly alter their contaminant sorption properties and consequently their role in the environmental processes.

Chapter 6

Studies on the binding characteristics of Gray humic Acid (GHA) and Brown Humic Acid (BHA) with U(VI)

6.1 Introduction

Humic substances are ubiquitous in the environment and known to play very important role in the transport and sequestration of environmental pollutants such as heavy metals, radionuclides and hydrophobic organic molecules [121]. Humic substances are characterised with non-stoichiometric compositions, complex and heterogeneous structure and polydisperse molecular weights. Metal uptake by humic substances is principally through interaction with carboxylic and phenolic groups and to a lesser extends through less abundant keto, amino and thiol groups present in them [122]. They are also capable to sequester organic pollutants through hydrophobic domains formed under suitable solution conditions [123]. Though humic substances have many common features, depending on their origin, significant difference are often observed among its content, physico-chemical properties and metal binding characteristics [124-126]. Most of the initial research on humus-metal interaction was focused on studying the complex formation of various metal ions with humic materials, in order to predict the fate, transport and bioavailability of various metal ions. However in recent years this highly abundant environmental component is identified as a potential agent for environmental remediation of contaminated sites [59]. Wan et al [21] used humic acid for soil amendment for the retardation of uranium transport in a contaminated site. Bogush et al [22] and Olds et al [23] reported that humic acid could be used for the treatment of acid mine drainage. From laboratory column studies, Yoshida and Suzuki [127] observed that at higher ionic strength, humic acid could retard the transport of Eu(III) in quartz sand column. Saar and Weber [128] reported that formation of insoluble humic acid-Pb(II) complex is possible in certain organic rich environments. Decontamination of organic and metallic pollutants from natural waters by crude humic acid blend was reported by Yates and Wandurzka [24]. Aleksandrova et al [25] demonstrated that the presence of high organic matter concentration results in increased immobilisation and lower bioavailability of radionuclides at South Ural lake. Many of these results are from field investigations and indicate the high potential for the use of humic materials for in-situ remediation of contaminated sites. It should be noted that these proposed environmental applications of humic substances essentially banks upon specific properties of humic substances such as ability to form insoluble complexes with metal ions, formation of insoluble hydrophobic domains at suitable solution conditions and formation of organic coated mineral phases, which could in turn acts as a sink for the pollutants. Since humic substances are operationally defined fractions of natural organic matter, for effective use for in-situ-remediation in real field, more micro-level information on the interaction of different sub-fractions of humic materials with pollutants are essential.

Humic substances are generally classified into humic acid, fulvic acid and humin depending on their pH dependant water solubility. Each fraction among itself is not a well defined chemical entity, but a complex mixture of different macromolecules. Thus the interaction of various environmental pollutants with any such fraction needs further analysis, for a thorough understanding of their role in the remediation process. Among the three major fractions of humic materials, humin is water insoluble and thus is not normally produced on industrial scale where as the isolation of fulvic acid fraction is cumbersome. Thus humic acid is the most common fraction used in environmental remediation application, though commercial products almost invariably contain other fractions as impurities. Humic acid itself could be fractionated into two fractions: the Gray Humic Acid (GHA), insoluble in water at high ionic strength and neutral pH; and the Brown Humic Acid (BHA), water soluble irrespective of the ionic strength of the medium. Limited studies exist, comparing the interaction of metal ions with GHA and BHA of same origin, though it is understood that their different aggregation behaviour could be related to their structural features [116,117]. Herein, the interaction of uranyl ion with purified GHA and BHA from commercially available Aldrich humic acid is studied. Complex formation is studied using conventional fluorescence quenching method, whereas the partitioning of metal ions within the aggregate and the solution were studied using ^{233}U tracer. Differences were observed in the interaction of uranium with GHA and BHA, with respect to the aggregation kinetics, metal partitioning to the precipitate and long term stability of uranium bound to these separated fractions.

6.2 Materials and methods

6.2.1 Chemicals and purification procedure

Commercially available Aldrich humic acid was used as the source material. The product required extensive pre-treatment and purification before use. The commercial product available as its sodium salt was dissolved in 0.1 M NaOH and centrifuged to remove clay and other insoluble impurities. The clear solution was precipitated by addition of 1.0 M HCl and the precipitated humic acid is separated by centrifugation. The procedure was repeated several times till the non-dissolved impurities and fulvic acid were completely removed. The purified humic acid thus obtained is subjected to dialysis using 5 kD dialysis membrane (*Spectrum USA*) till free of chloride ions and then passed through Dowex 50 X8 cation exchange resin for conversion to hydrogen form. Purified humic acid is further fractionated into GHA and BHA by suspending in 6M KCl solution at pH=7 for twenty four hours [38]. GHA got precipitated and separated using centrifugation. The supernatant consist of BHA. Both fractions were subjected to purification

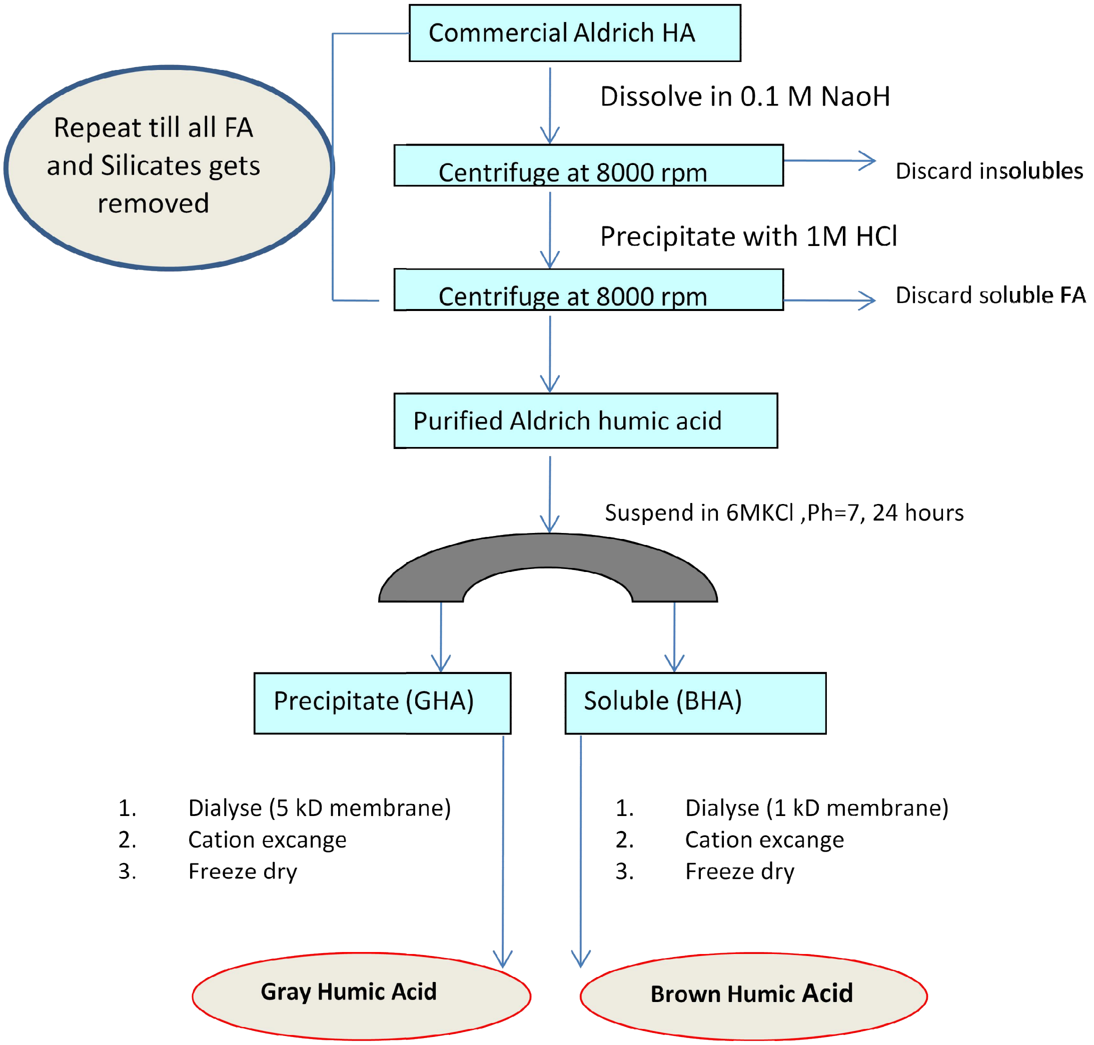

Fig. 6.1 Scheme employed for the fractionation of Aldrich Humic Acid to GHA and BHA

by dialysis; for GHA 5 kD membrane were used whereas for BHA, to prevent the loss of material, 1 kD membrane were used. Finally the solution was passed through ion-exchange column (Dowex 50 X 8) for conversion to hydrogen form and freeze dried. The purification scheme employed in the present work is represented schematically in figure 6.1. Uranyl nitrate hexahydrate (ACS grade, E.Merk, Germany) were used as the source for uranium. ^{233}U produced from neutron irradiation of ^{232}Th and separated by the THOREX process was used as the tracer for quantification of uranium[131]. Before use, the tracer isotope was subjected to one more purification process using Dowex 50 X 4 cation exchange resin. All other reagents used in the experiments were of analytical reagent grade.

6.2.2 Material characterisation and instrumentation.

A sample from the purified humic acid is analysed for the presence of metallic impurities using ICP-AES (JY 238 Ultratrace, Jobyn Vyon France) after destruction of the organic materials using digestion with HCl/HNO_3 mixture. Absorption measurements were carried out using double beam UV-Visible absorption spectrometer (UV 540, Thermo-spectronic USA). FTIR spectra of the samples were recorded on JASCO 400 FTIR spectrometer using KBr pellet method. Carboxylic acidity and total acidity of the humic acid fractions were estimated using the Barita method and calcium acetate precipitation method respectively [30]. Fluorescence measurements were done on JASCO 6500 fluorescence spectrometer using 325 nm excitation wavelengths and using 5 nm band width for both excitation and emission monochromators.

6.2.3 Evaluation of stability constant for U(VI) with GHA and BHA.

Binding constants between humic substances and uranium were derived using the classical fluorescence quenching method following Nakashima et al [45]. Fluorescence measurements were done with 20 ppm HA solution and uranium concentration varying in the range 1-10 mg/L. Application of low concentration of humic acid is essential to avoid the self absorption of humic acid fluorescence during measurements [132]. Fluorescence spectra were recorded using 325 nm as the excitation wavelength and emission wavelength in the range 350 to 600 nm. Fluorescence spectrum were measured after twenty minutes of equilibration of the solution. Complex formation of HA with metal ion can be represented as

$$\mathrm{HA + M \leftrightarrow HA\text{-}M}$$

and the conditional stability constant (K_b) between the humic acid and the metal ion can be represented as

$$K_b = [HA - M]/[HA][M] \tag{1}$$

where [HA-M] is the concentration of humic metal complex, [HA] and [M] are the concentration of free humic acid and metal ion at equilibrium. If the fluorescence intensity of HA in absence of metal ion is I_o and that in presence of metal ion is I, the binding constant K_b could be related to the ratio of fluorescence intensities by the standard Stern-Volmer equation,

$$\frac{I_0}{I} = 1 + K_b\,[M] \tag{2}$$

where [M] is the concentration of the metal ion. A plot of I_o/I against [M] should give a straight line with slope equal to the binding constant K_b.

6.2.4 Characterisation of humic acid precipitation in presence of uranium.

The stability of humic acid solution in presence of metal ions were tested using 100 mg/l HA solution at pH=4. The selected pH was not only relevant for the real terrestrial system, but also ensures that uranium is present mostly as UO_2^{2+} species [53]. Precipitation experiments were carried out in the absence of any other species except for the small quantity of HCl/NaOH added for adjusting the pH of the solution. 10 ml solution consisting of predetermined concentration of uranium in 15 ml polypropylene vials were equilibrated in an orbital shaker at 200 rpm for 24 hours and the precipitate and soluble HA were separated using centrifuge at 10000 rpm. ^{233}U tracer was added at the beginning of the experiment to get a count rate around 8000 cpm/ml in order to facilitate the measurement of uranium by radiometry. Concentration of HA in the supernatant were estimated using absorbance measurement at 500 nm. For deriving the information on the partitioning of uranium between the precipitate and the supernatant, ^{233}U in the supernatant were esti mated using ZnS(Ag) alpha scintillation counter. Quantification of the uranium precipitated with HA is obtained from the difference in count rate of uranium in the initial solution and that in the supernatant.

Experiments for determining the kinetics of aggregation were carried out using 100 mL of solution in borosilicate vessel at two specific metal ion concentrations for both the humic acid fractions. Solution were withdrawn at specific intervals from the reaction vessel and centrifuged at 10000 rpm. Concentration of HA in the supernatant were estimated using absorbance measurement. The methodology reported by Kloster et al [46] was used for the data treatment. The extend of aggregation of humic acid can be represented as

$$\alpha = (C_o - C)/c_o \tag{3}$$

where α is the degree of aggregation, C_0 is the initial concentration of humic acid and *C* is the concentration of humic acid in solution at any given instance during the progress of the aggregation. α=*0* means zero aggregation and α=1 means complete aggregation. Degree of aggregation at any time could be represented using the expression

$$\alpha = \alpha_f - \alpha_f \, e^{-kt} \tag{4}$$

where $\alpha_f = (C_0 - C_f\ )/C_0$ is the highest degree of aggregation. Aggregation rate constant *k* is obtained by fitting α, α_f and t into equation (4) using the *solver function* of *Microsoft Excel.*

6.2.5 Long term stability of uranium binding to GHA and BHA.

Solution containing 20 mg/l GHA or BHA and different concentration of uranium were prepared at pH=4 and fluorescence of the solutions was measured at different time intervals spanning up to three months. In between the measurements, solutions were stored in dark in amber coloured bottles, in order to prevent the photolysis of the sample during storage.

6.3 Results and Discussions.

6.3.1 Characterisation of humic acid fractions

Concentration of common metal ions present in the purified humic acid is provided in table 6.1

Table 6.1 Residual metal ions impurities (mg/g) in the purified Aldrich humic acid

element	Ca	Mg	Fe	Al	Cu
concentration (mg/g)	1.47±.48	0.41±.10	2.24±.50	0.53±.30	0.03±.01

From the result it can be inferred that no significant concentration of multivalent metal ions are present in the purified product so that it will interfere with the present investigations. Density of the acidic functional groups in BHA and GHA are present in table 6.2. Carboxilic, phenolic and total acidity of BHA is found to be higher than that of GHA. Earlier researchers also reported that, for specimens of same origin, BHA is having higher density of oxygen containing functional groups than that in GHA [133]. IR spectra of GHA and BHA (figure 6.2) show the presence of similar functional groups in both the fractions. Broad band at 3420 cm^{-1} is assigned to the hydrogen bonded –OH groups. The relative intensity of 2918 cm^{-1} band corresponding to the aliphatic C-H stretching and 1455 cm^{-1} band of deformation of $–CH_2$ or $–CH_3$ groups were more prominent in GHA than that in BHA. Conversely the 1610 cm^{-1} band corresponding to

Table 6.2 Density of acidic functional groups present in GHA and BHA fractions

	Acidity (meq/g)		
	Carboxylic	Phenolic	Total
GHA	1.18	0.56	1.84
BHA	2.41	1.23	3.64

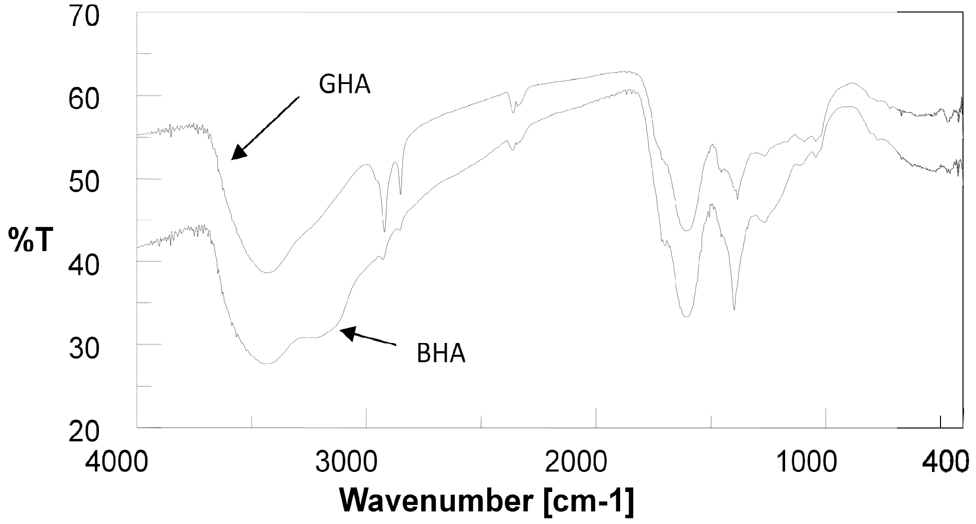

Fig. 6.2 FTIR spectra of GHA and BHA

conjugated C=C or hydrogen bonded –C=O groups and 1714 cm^{-1} corresponding to –C=O stretching of the –COOH groups were more prominent in BHA than GHA. Overall from the IR spectral analysis it can be concluded that GHA is of more aliphatic characteristics and have less carboxylic acid density than BHA. Fluorescence emission spectra obtained at 325 nm excitation (figure 6.3) shows that emission peaks are red shifted in BHA with respect to that of GHA. Also fluorescence yield of BHA is relatively higher than that for GHA for any given wavelength. Both these indications show that BHA is more conjugated or aromatic than GHA, corroborating the finding from IR spectral analysis.

6.3.2 Fluorescence quenching behaviour of GHA and BHA.

Apparent stability constants of GHA and BHA with uranium were estimated using the classical fluorescence quenching experiments. Figure 3 shows the fluorescence spectra of GHA and BHA with increasing concentration of uranium. Both humic acid fractions showed decreasing fluorescence intensity on addition of uranium. For the quantitative evaluation of the interaction constant, quenching of the fluorescence spectra were analysed using Stern-Volmer method. Figure 6.4 shows the Stern-Volmer plots for the quenching of fluorescence of GHA and BHA,

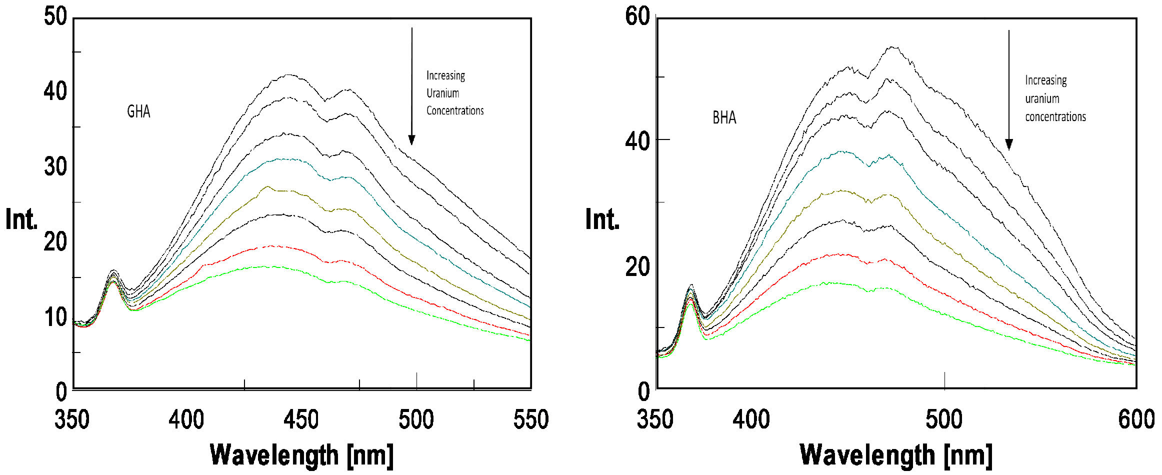

Fig. 6.3 Fluorescence quenching profile of GHA and BHA in presence of uranium (HA= 20 ppm, U(VI)= 0,1,2.3, 4,5,7, 10 ppm)

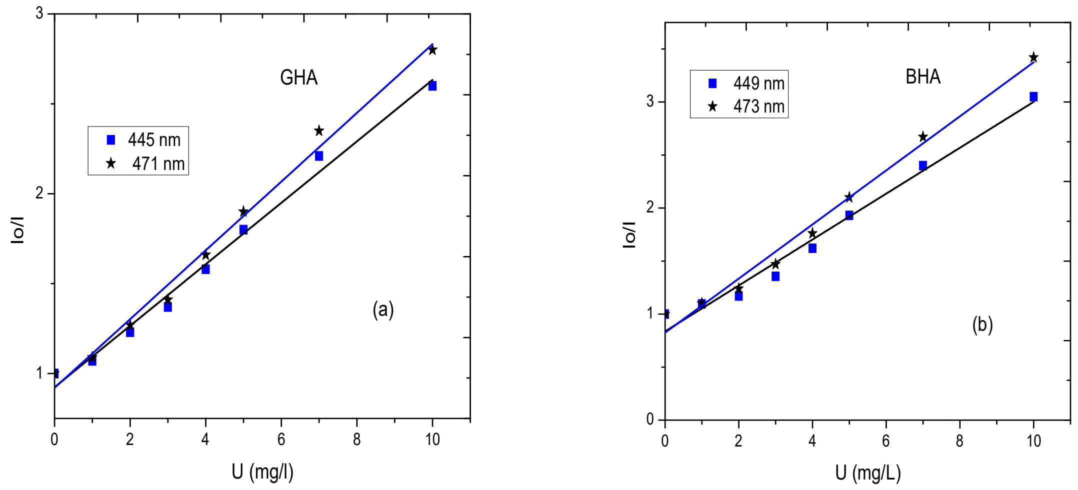

Fig. 6.4 Stern –Volmer plot for the fluorescence quenching of GHA and BHA

respectively on addition of uranium. The data gives a good linear fit showing that the model assumed is applicable in the present experimental scenario. From the derived apparent stability constants (table 6.3) it is evident that though BHA shows slightly higher stability constant than BHA, the difference is not significant in comparison to the difference in stability constants among humic acid from various sources [57]. Most of the functional groups responsible for metal ion interactions could be similar in both the fractions, resulting in comparable stability constants.

Table 1 Conditional stability constants for binding of uranium with GHA and BHA

	Measured stability constants K_b(/mMol)	
	K_{b1}	K_{b2}
GHA	42.1(445 nm)	47.1(471 nm)
BHA	51.4 (447 nm)	61.4 (473 nm)

6.3.3 Precipitation and aggregation behaviour of GHA and BHA in presence of uranium.

Coagulation and precipitation of humic acid from aqueous solution is found to depend on various factors such as pH and ionic strength of the medium and presence of multivalent metal ions and the concentration of humic acid [133-135]. Metal ions bearing multiple charges play dual role in the aggregation process. Neutralisation of negatively charged functional groups in humic acid molecules and facilitating cation mediated intermolecular bridging. In order to understand the effect of electrolyte and metal ion concentration on humic acid, zeta potential of purified non-fractionated Aldrich humic acid at three different ionic strengths were measured as a function of uranyl ion concentrations (figure 6.5). The dashed line shows the uranyl ion concentration at which the HA precipitation is visible within 24 hours on preparation of the sample. As the ionic strength increases, the requirement of uranium for the onset of precipitation decrease drastically, as the case generally observed for any polyelectrolyte. It could be seen that at the highest concentrations of uranium also (where precipitation is complete) humic acid zeta potential is still negative. Similar observation was reported by other researchers also [46] and indicates that

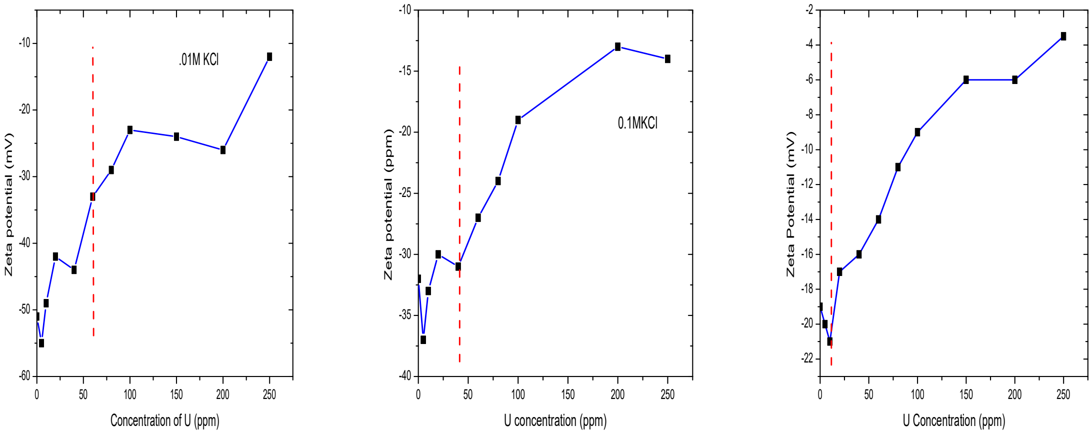

Fig. 6.5 Zeta potential of humic acid solution as a function of initial U(VI) concentration (HA=100 mg/l).

charge neutralisation is not the single reason for precipitation of the humic materials in presence of metal ions. In order to understand whether differences exists in the coagulation behaviour of GHA and BHA, coagulation experiments were conducted at pH=4 at different uranium ion concentrations. To clearly attribute the coagulation behaviour to the humic acid-uranium interaction, no other supporting electrolyte were added to the solution except small quantity of NaOH or HCl added for adjusting the pH of the solution. In fact the original pH of the solutions were close to four and little adjustment were only required in each case. Figure 6.6 presents the extent of precipitation of HA as a function of the initial uranium concentration. It can be seen that precipitation of GHA begins at lower uranium concentration than that of BHA. Similarly precipitation of GHA complete with an initial uranium concentration of 0.34 meq/l, whereas BHA requires significantly higher initial concentration (0.67 meq/l), for completing the

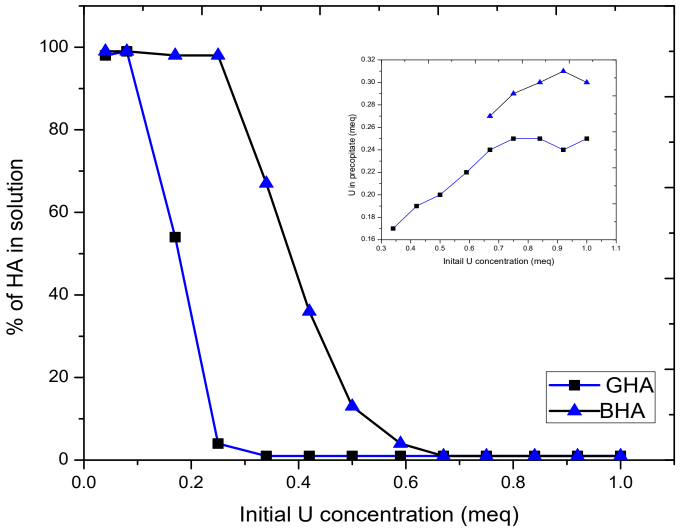

Fig. 6.6 Precipitation of GHA and BHA in presence of U(VI) ions; inset shows the concentration of uranium trapped in the precipitate (HA=100 mg/l, equilibration time = 24 hours).

precipitation. Another notable difference is the concentration range of uranyl ion within which the flocculation begins and complete precipitation of humic acid is achieved. The range is narrow for GHA in comparison to that for BHA. Formation of hydrophobic phase during complexation of metal ions is attributed to neutralisation of charge on humic acid moieties, metal ion induced bridging and reduction of electrical double layer on the colloids at higher ionic strengths [133,134]. As the densities of ionisable groups are lower in GHA in comparison to BHA, early saturation is expected in GHA leading to completion of precipitation at lower uranium concentrations. But even at complete precipitation also zeta potential is still negative [46] indicates that other additional factors are also involved in the precipitation process. More aliphatic characteristics of GHA as revealed from the IR spectra could be one probable reason for the early formation of hydrophobic domains from its aqueous solutions.

The inclusion of metal ion into the precipitate is another indication of the nature of interaction with the metal ions and HA. The inset in figure 6.6 shows the quantity of metal ion associated with humic precipitate in experiments were the initial uranium concentrations were above the threshold concentration for complete precipitation of HA. If charge neutralisation is the only mechanisms involved, then the quantity of uranium associated with the precipitate should be a constant on complete precipitation, since the total binding sites on HA is limited. For both GHA and BHA, an increase in precipitated quantity of uranium is observed with increase in initial uranium concentration. But the increase was more predominant for GHA than BHA. It could also be noted that GHA contains nearly half the acidic functional group than that of BHA. Thus the additional scavenging of metal ions in the precipitate is associated with other phenomena such as surface precipitation and entrapment in humic precipitates. The probability for entrapment is more possible with GHA due to its macromolecular characteristics than BHA. This finding is similar to the results reported by Baigorri et al [38]. By studying GHA and BHA fractions of humic acid from different sources, they reported that the concentration of transition elements associated with GHA is invariably higher than that with BHA from the same source.

Aggregation kinetics experiments were conducted using 100 ml of HA solution containing 100 mg/l of humic acid, and at stirring speed of 250 rpm using a magnetic stirrer. Experiments were done at two different uranium concentrations, one at concentration below the threshold for complete precipitation of HA, and another at above that for the threshold. Figure 6.7 shows that aggregation kinetics of humic acids in presence of uranium at pH=4. Table 6.5 presents the kinetics constant derived from these experiments. For the cases of partial and complete

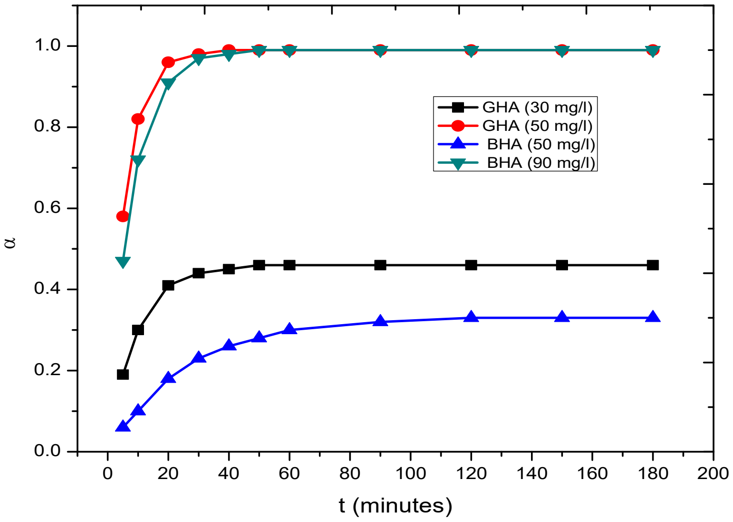

Fig. 6.7 Aggregation kinetics of GHA and BHA in presence of U(VI)

precipitation, GHA shows higher aggregation kinetics than that of BHA. Further at the same initial concentration of 50 mg/l of uranium, GHA aggregation rate is observed to be four times that of BHA. The results of the kinetic experiments also show that GHA is more prone to cation induced aggregation than BHA of same origin.

Table 6.4 : Kinetics constant for the aggregation of GHA and BHA in presence of uranium

	Initial U (mg/l)	α_f	K (min^{-1})
GHA	30	0.46	0.11
	50	0.99	0.17
BHA	50	0.33	0.04
	90	0.99	0.13

6.3.4 Long term behaviour of U-GHA and U-BHA systems.

As GHA and BHA having nearly same observed stability constant, an attempt was made to see whether the long term stability of the uranium bound with these two fractions are the same or not. When exciting the HA-U mixture containing higher concentrations of uranium, characteristic fluorescence peak of uranium is visible. Tracking this on longer time scale gives indication, whether differences exist between the binding of GHA and BHA with uranium over longer time frame. Figure 8a and 8b shows the fluorescence emission spectra of GHA-U

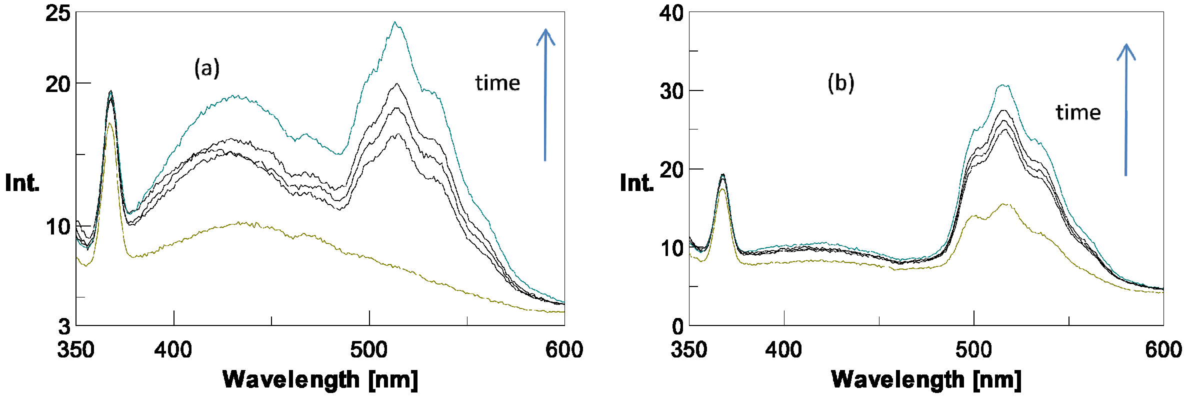

Fig. 6.8 Fluorescence emission spectra of U(VI) –GHA on 0, 14th, 32th, 54th and 80th day delayed (GHA= 20 mg/l, a-U(VI)= 7mg/l, b- U=20 mg/L)

recorded over a period up to three months. At both experimental uranium concentrations, uranium fluorescence is found to increase with time. This indicate the formation of free uranium from the HA-U adduct over the measurement period. Similar experiments done on BHA (Figure 6.9a and 6.9b) also show the enhancement of uranium fluorescence with time. But in sharp contrast to GHA-U system, within one month itself, the BHA-U system is observed to reach the equilibrium configuration and no further release of uranium is observed over the extended period of measurement. One important conclusion from these results is that a fraction of humic acid bound metal ion could become free over a period of time and also that the extent of release depends on the nature of the humic material.

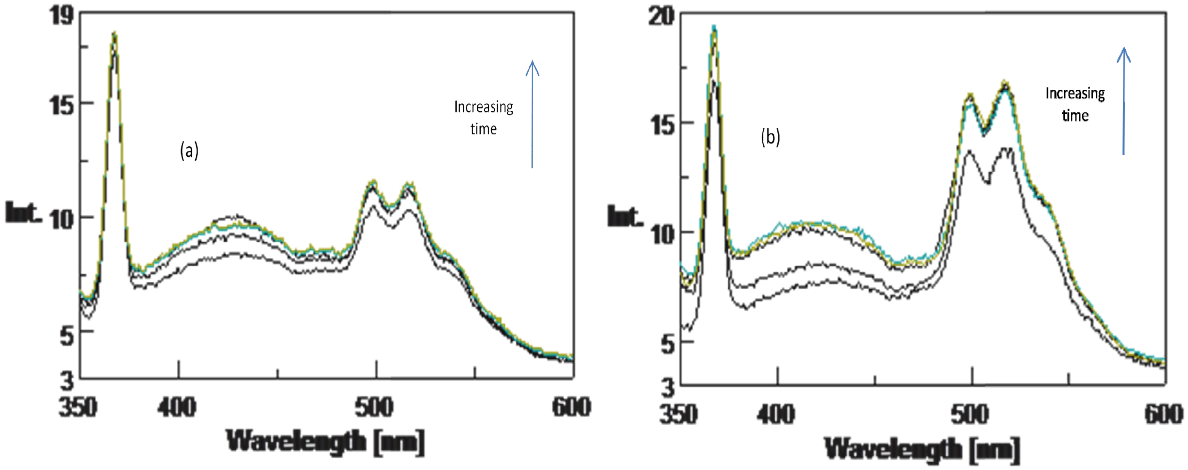

Fig. 6.9 Fluorescence emission spectra of U(VI) –BHA on 0, 14th, 32th, 46th and 80th day delayed (GHA= 20 mg/l, a-U(VI)= 10mg/l, b- U=30 mg/L)

Time-dependent reorganisation of humic acid-metal complex was reported by other investigators also [138-140]. By using pyrene as a fluorescence probe, Wandruzka et al [138] has reported that with time, metal ions moves to more stable binding sites in humic acid. Lippold et al [139] observed that humic acid-alumnium complex is becoming more and more inert on aging and attributed this phenomenon to structural reorganisation, resulting in transfer of the metal ions to more stable binding sites. But in case of Fe(III), it was observed that temporal release of iron from HA-Fe system is due to the depolymerisation of the initially attached polynuclear iron species[140]. At pH=4 used in the present experiments, uranium could not be present as polynuclear species and the slow and time-dependent release could be due to some other phenonmena.

The slow reappearance of uranium fluorescence from the HA-U system could occur due to any of the possible mechanism as represented in figure 6.8. It should be due to the direct decomposition of HA-U complex as described in scheme (1). An enhancement of the fluorescence intensity at all wavelengths indicates that at least partially, decomposition of the

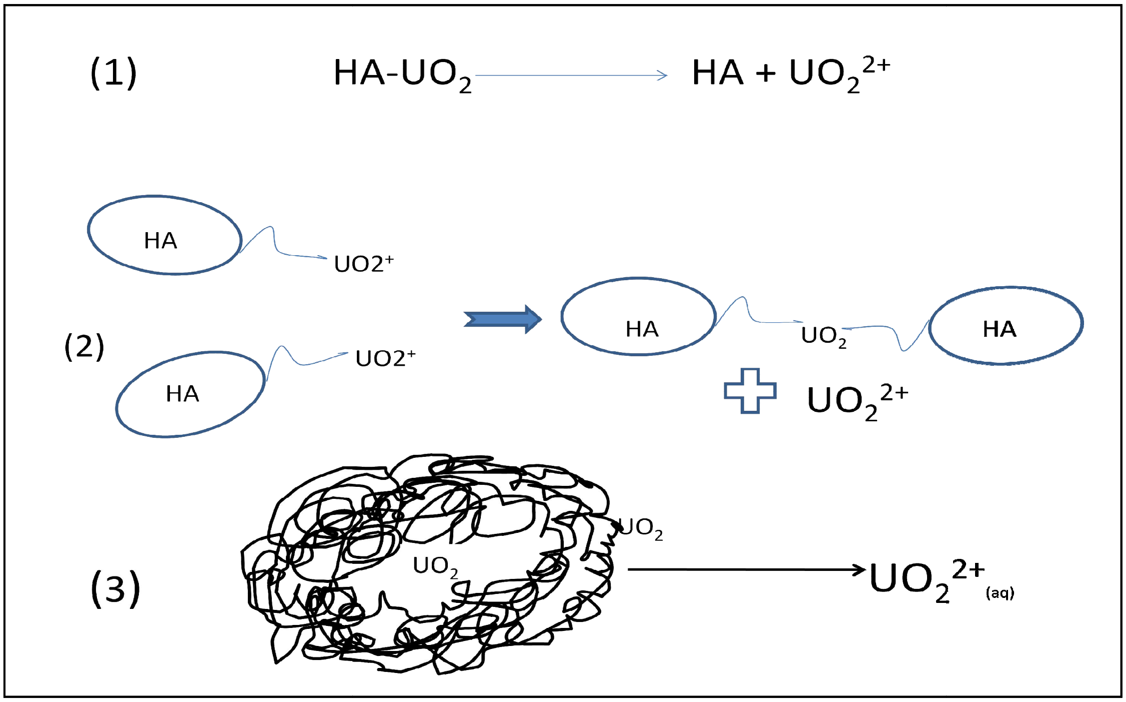

Fig. 6.10 Suggested mechanisms for release of uranium from bound state

complex is one contributing factor for the release of uranium over a period of time. However, the measured apparent stability constant for uranium binding with GHA and BHA are not far apart to explain the wide difference observed between the dissociation behaviour of these two components. Another possibility (scheme 2) is the conversion of some monodentate uranium complex to bidentate, resulting in release of free uranium ions. A third possibility is depicted in scheme 3, in which the uranium ions, which is initially either adsorbed to the surface or physically entrapped in the humic acid cage, get into free form as a result of the reorganisation of the three dimensional humic acid structure. GHA is more prone to such reorganisation than BHA due to its relatively complex three dimensional structure. Experimentally observed higher availability of metal ions with GHA than BHA, also indicates that such physical entrapment is more probable with GHA [13]. Though additional research is required to decipher the exact mechanism of release of the metal ion from the HA-M adduct, it is clear that humic acid consisting of more GHA like components are less preferable for remediation of metal ion contaminants, due to the relative instability of the GHA-M complex.

6.4. Conclusion

Comparative study of the interaction of uranium with GHA and BHA from same origin shows that metal uptake and long term stability of humic acid-metal complex depends on other factors in addition to the availability of metal chelating functional groups. Among the two components studied, GHA is found to aggregate faster in presence of metal ions than BHA. On storage, a part of the initially bound uranium is found to get released to the solution. Though metal ion release is observed from both the fractions, metal ions bound to GHA are found to be more prone to dissociation than that bound to the BHA fraction. The present results indicate that GHA fraction is less preferable as a sink or sorbent for the toxic metal ions than BHA for in-situ remediation application. The results obtained here shows that more elaborate and in-depth studies on humic substances- metal ion interactions are essential to develop environmental remediation technologies based on humic substances.

Chapter 7

Conclusions and future research prospective

This chapter highlights the results obtained from the studies carried out for this thesis on the application of modified biomaterials and nanomaterials in mitigating the environmental pollution due to heavy metals. Chemically modified chitosan, humic acid, magnetite nanoparticles and their combinations were the substrates used in the studies. U(VI) was the principal contaminant metal ions used as the model pollutant which was supplemented by Cr(III) and Pb(II) ions in certain cases.

Chitosan tripoliphosphate (CTPP) beads prepared by ionic cross-linking of chitosan with sodium tripoliphosphate is found to have stability in aqueous medium at pH=3 or above for sorption applications. Application of Langmiur model to the absorption data for U(VI) and Cr(III) on to CTPP beads resulted in sorption capacity of 236.9 mg/g and 469.5 mg/g respectively. In both cases, Freundlich model is also found to fit the sorption data. Due to the higher size of the beads employed (~2 mm size) the sorption/ desorption process is found to be slow completing in approximately seventy two hours. The kinetic data for both the metal ions were found to fit the pseudo-first order and pseudo-second order model. Additionally, intermediate time scale for the sorption of U(VI) is found to fit the intra-particle diffusion model. Competition experiments showed that presence of Na(I), Ca(II) and Mg(II) have no effect on the sorption of Cr(III) on CTPP, whereas Al(III) could partially block the sorption of Cr(III). Fe(III) co-adsorb onto CTPP beads along with Cr(III) without affecting the sorption of the latter. Desorption of Cr(III) from loaded CTPP beads is possible with the use of NaCl solution. Higher cross-linked CTPP beads showed more sorption capacity indicating that the newly introduced phosphate groups are the major contributors for the sorption of metal ions. Overall these results indicate that CTPP based sorbents could be used in the remediation of heavy metal pollution.

A new Humic Acid (HA) based adsorbent with 43% (wt/wt) loading of HA was prepared by coating HA onto wet CTPP beads in aqueous solution under alkaline pH. The new adsorbent is found to be more stable than bare CTPP beads in the pH range 1-10. The coated humic acid was stable against dissolution with leaching rate less than 10% at pH=8 for twenty four hours of equilibration. SEM analysis showed that the HA-CTPP bead surface is more porous than the surface of bare CTPP beads. The new adsorbent is tested for the sorption of pollutant metal ions U(VI) and Pb(II) ions from aqueous solution. The sorption of both the metal ions is found to be pH dependant, with optimum condition as pH=5 for U(VI) and pH=3 for Pb(II) ions. The new adsorbent showed a sorption capacity of 71.4 mg/g for U(VI) and 223.7 mg/g for Pb(II) ions. The uranium sorption capacity of humic acid is reduced due to the immobilization process, but is not affected in case Pb(II) ions. Sorption of Pb(II) ions took six hours for saturation while it is ten hours in case of U(VI) ions. For both the metal ions the sorption kinetics follows a pseudo-second order kinetics model, indicating the involvement of chemical forces in the sorption process. The result obtained from these studies proves that the present immobilization method is a viable process for the preparation of a HA based solid biosorbent for heavy metal sorption.

Magnetite and humic acid coated magnetite nanoparticles (HA-magnetite) were prepared and the sorption of U(VI) onto both the substrates were studied to understand their utility in separation and their role in the natural environment. HA-magnetite have larger specific surface area (99 m^2/g) than bare magnetite (59m^2/g) and their surface morphologies were observed to be different. Zeta potential of HA-magnetite was measured as 2.5, lower than that of bare magnetite as 6.8. Optimum pH for the sorption of U(VI) onto bare magnetite nanoparticles is found to be pH=7 with sorption capacity ~5 mg/g. Sorption kinetics have two distinct stages one completing in around four hours, covering 90% of the saturated sorption capacity, followed by a slow process extending to few days. Sorption is found to be independent of the ionic strength of the medium. Test with real industrial effluent of low initial U(VI) concentration (3.8 mg/l) and high salt content resulted in sorption of 42% of the initial amount within six hours of equilibration. XPS analysis of the uranium and iron oxidation state before and after sorption of the U(VI) showed that a fraction of the uranium present on the magnetite surface is present in the reduced state. In contrast to bare magnetite, HA- magnetite showed higher sorption capacity of 25.64 mg/g, with the optimum pH for the sorption as pH=5. The kinetics were faster than that for the bare magnetite completing, in less than sixty minutes and is found to follow the pseudo-second order kinetic model. Surface area normalized sorption capacity of HA-magnetite is found to be twice of that of bare magnetite. XPS examination of uaranium loaded HA-magnetite has not showed presence of reduced uranium species on the surface. From these results it is concluded that significant difference in the heavy metal sorption characteristics of nanoparticles is possible as a result of their surface coating with humic acid. These difference in sorption behavior have significant bearing on the long term transport and fate of contaminant metal ions in the environment.

Commercially Available Aldrich humic acid was purified and separated into two fractions: Gray Humic Acid (GHA) and Brown Humic Acid (BHA), depending on their ionic strength dependant solubility. Their binding properties with uranium were studied using fluorescence spectroscopy method. From spectroscopic characterization, GHA is found to be more aliphatic and contains less concentration of acidic functional groups than BHA. Apparent stability constants for the binding of U(VI) with GHA and BHA were more or less similar. GHA is found to be more prone to aggregation in presence of U(VI) ions than BHA and the aggregation kinetics is also faster for GHA than BHA under identical experimental conditions. Uranium is found to get sequestered into the HA-metal precipitate, and the sequestration was more predominant with GHA than BHA. On long term storage, HA-Uranium complex is found to undergo dissociation or rearrangement. The rearrangements or dissociation were more predominant and of longer duration for GHA-U system than for BHA-U system. The result obtained in these studies shows that, depending on the structural characteristics of HA fractions, wide difference in their interaction with metal ions could be possible, which could in-turn affect the final performance of a humic substances based in-situ environmental remediation process.

Scope for future work

CTPP beads are found to be good sorbent for the sorption of U(VI) and Cr(III). However the presently used beads of ~2 mm diameter leads to slower kinetics than that is suitable for column application or batch process with high throughput. Studies should be conducted as a function of bead dimensions to optimize the parameters for practical applications. CTPP beads, having good sorption properties for metal ions may find application in decorporation of toxic metal ions, especially from GI track and studies in this direction could be carried out. Contrary to many earlier research results, in this study, high loading of HA on to a chitosan derivative (CTPP) is observed and over a wide range of solution pH. HA removal from water itself is a major problem worldwide and thus CTPP could be investigated as a sorbent for the removal of humic acid. Magnetite and HA-magnetite is found to differ in their sorption characteristics towards U(VI). Sorption characteristics of HA-magnetite for metal ions could be further investigated as a function of organic loading and by application of additive models. Difference observed in the interaction of U(VI) with GHA and BHA indicates that additional studies should be conducted to understand subtle differences of interaction of metal ions with various fractions of humic acids.

Annexure 1

Publications in refereed Journals

Published

1. Adsorption of uranium from aqueous solution using chitosan-tripolyphosphate (CTPP) beads; **M.K. Sureshkumar**, D. Das, M.B. Mallia, P.C. Gupta; *Journal of Hazardous Materials* 184 (**2010**) 65–72
2. Adsorption of Pb(II) ions using humic acid coated chitosan-tripolyphosphate (HA-CTPP) beads; **M.K Sureshkumar**, D. Das, G. Mary, J. Nuwad, *Separation Science and Technology* 48 **(2013)** 1132-1139
3. Adsorptive removal of Cr(III) from aqueous solution using tripolyphosphate cross-linked chitosan beads D. Das, **M. K. Sureshkumar,** K. Radhakrishnan, J. Nuwad, C. G. S. Pillai *J Radioanalytical and Nuclear Chemistry* 289 **(2011)** 275–285

Communicated

A comparative study on the interaction of Gray Humic Acid (GHA) and Brown Humic Acid (BHA) with U(VI) ; **M. K Sureshkumar**, R M Tripathi (communicated to *J Radioanalytical and Nuclear Chemistry*)

Manuscript under preparation

Sorption of uranium on humic acid coated magnetite nanoparticles **M.K Sureshkumar**, S. Susheela, R M Tripathi (to be communicated to *Journal of Environmental Radioactivity*)

Other publications

Sorption of uranium on magnetite nanoparticles; D. Das, **M. K. Sureshkumar,** Siddhartha Koley, Nidhi Mittal, C G S Pillai *J Radioanalytical and Nuclear Chemistry* 285 (**2010**) 285:447–454

References:

[1] *Encyclopedia Britanica*; www.britanica.com/topic/pollution

[2] Bell M L, Davis D L, Flether T (2004) *Environ Health Perspect* 112:6-8

[3] McCleskey T M, Foreman T M, Hallman E E, Burns C J, Sauer N N (2001) *Environ Sc. Technol* 35*:* 547–551

[4] Duruibe J O, Ogwuegbu M O C, Egwurugwu J N (2007) *Int J Phys Sci* 2:112-118

[5] Sorme L, Lagerkvist R (2002) *The Sci Total Environ* 298:131-145

[6] Radloff K A, Zheng Y, Michael H A, Stute M, Bostick B C, Mihajlov I, Bounds M, Huq M R, Choudhary I, Rahman M W, Schlosser P, Ahmed K M, van Green A (2011) *Nature Geosci* 4:793-798

[7] Banning A, Demmel T, Rude T R, Wrobel M (2013) *Environ Sci Technol* 47:13941–13948

[8] Kurniawan T A, Chan G Y S, Lo W H, Babel S (2006) *Chem Eng J* 118:83–98

[9] Sundstrom D W, Klei H E (1979) *Wastewater Treatment*, Prentice Hall, Englewood Cliffs, NJ, pp. 327-330.

[10] Vegilo F, Beolchini F(1997) *Hydromettallurgy* 44:301-316

[11] Fomina M, Gadd G M (2014) *Bioresour Technol* 160: 3–14

[12] Peralta-Videa J R, Zhao L, Lopez-Moreno M L, de la Rosa G, Hong J, Gardea-Torresdey J L (2011) *J Hazard Mater* 186:1–15

[13] Samuel C N, Tang I M C Lo (2013) *Water Res* 47:2613 – 2632

[14] Gómez-Pastora J, Bringas E, Ortiz I (2014) *Chem Eng J* 256:187–204

[15] Mudhoo A, Garg V K, Wang S (2012) *Environ Chem Lett* 10:109-117

[16] Singh S, Barick K C, Bahadur D (2011) *J Hazrd Mater* 192:1539– 1547

[17] Lu X, Hu Q, Fang Z, Zhang X, Zhang B (2009) *Langmuir* 25:3-8

[18] Fu F, Dionysiou D D, Liu H (2014*)* *J Hazard Mater* 267:194– 205

[19] Obiri-Nyarko F, Grajales-Mesa S J, Malina G (2014) *Chemosphere* 111:243–259

[20] Kamari A, Pulford I D, Hargreaves J S J (2011) *Colloids and Surf B: Biointerfaces* 82: 71–80

[21] Wan J, Dong W, Tokunaga T K (2011) *Environ Sci Technol* 45:2331-2337

[22] Bogush A A, Voronin V G (2011) *Mine Water Environ* 30:185-190

[23] Olds WE, Daniel C, Tsang W, Weber P (2013) *Water Air Soil Pollut* 224:1521-1533

[24] Yates E M, Von Wandruszka R (1999) *Environ Sci Technol* 33: 2076-2080

[25] Aleksandrova O N, Schulz M, Matthies M (2010) *Water Air Soil Pollut* 206:203–214

[26] Wan Ngah W S, Teong L C. , Hanafiah M A K M (2011) *Carbohydr Polyms* 83:1446–1456

[27] Wang J , Chen C (2014) *Bioresour Technol* 160:129–141

[28] Atia A A (2005) *Hydrometallurgy* 80:13–22

[29] Wang G, Liu J, Wang X, Xie X, Deng N (2009*) J. Hazard Mater* 168:1053-1082

[30] Stevenson F J, *Humic Substances Genesys, Composition and Reactions* (1994) John Wiley and Sons , New York.

[31] Allard B, Boren H, Grimvall A (Eds) (1991) *Humic Substances in aquatic and Terrestrial Environment* Springer-Verlag

[32] Yang K, Lin D, Xing B (2009) *Langmuir* 25:3571-3576

[33] Schmitt P, Kettrup A, Freitag D, Garrison A W (1996) *Fresenius J Anal Chem* 354: 915-920

[34] Reiller P, Amekraz B , Moulin C (2006) *Environ Sci Technol* 40:2235-2241

[35] Riedel T, Biester H (2012) *Environ Sci Technol* 46:4419-4426

[36] Lee S T, Mi F L, Shen Y J, Shyu S S, *Polymer* (2001) 42:1879-1892

[37] Liu J F, Zhao Z S, Jiang G B (2008) *Environ Sci Technol* 42:6949–6954

[38] Baigorri R, Fuentes M, Gonzalez-Gaitano G, Garcia-Mina M (2007) *J Phys Chem B* 111:10577-10582

[39] Skoog D A, Holler F J, Nieman T A (1992) *Principles of Instrumental Analysis(5th Edition)* Saundes Colllege Publishing, Orlando, Florida.

[40] Lakowicz J R(2006) *Principles of Fluorescence Spectroscopy* (3rd Edn) Springer Science+Business Media, LLC, New York.

[41] B. D. Cullity (1959) *Elements of X-ray Diffraction*, Addison-Wesley Publishing Comp. Inc., USA.

[42] Knoll G F (2010) *Radiation Detection and Measurement* John Wiley and sons, New York,USA.

[43] Crittenden B, Thomas W J (1998), *Adsorption technology and Design*, Reed Educational and Professional Publishing Ltd, UK.

[44] Ngah W S W, Hanafiah M A K, Yong S S (2008) *Colloids Surf B; Biointerfaces* 65:18-24

[45] Nakashima K, Xing S, Gong Y, Miyajima T(2008) *J Mol Struct* 883-884:155-159

[46] Kloster N, Brigante M, Zanini G, Avena M (2013) *Colloids Surf A: Physicochem Eng Aspects* 427:76– 82

[47] Mi F L, Shyu S S , Lee S T, Wong T B (1995) *J Polym Sci B* 37 (1995)1551-1564

[48] Suresh A, Patre D K, Srinivasan T G, Vasudeva Rao P R (2002) *Spectrochim Acta A* 58:34-347

[49] Guibal E, Milot C, Tobin J M (1998) *Ind Eng Chem Res* 34:1554-1463

[50] Ngah W S W, Fatinathan S (2010) *J Environ Manag* 91:958-969

[51] Guibal E (2004) *Sep Purif Technol* 387:43–74.

[52] Maya L (1982) *Inorg Chem* 21:2595-2598

[53] Wanner H, Forest I (Eds) (2004) *Chemical Thermodynamics of Uranium* OECD Nuclear Energy Agency, OECD Publications, Paris, France

[54] Takashi S, Takao H, Akira N (1981) *Agric Biol Chem* 45:2191-2195

[55] Ngah W S W, Hanafiah M A K M, Yong S S (2008) *Coll. Surf. B; Biointerfaces* 65:18-24

[56] Fahim N F, Barsoum B N, Eid A E, Khalil M S (2006) *J Hazard Mater* 136:303-309

[57] Tipping E (2004) *Cation binding to humic substabses;* Cambridge University press, U K

[58] Ghabbour E, Davies G (Eds) (2004) *Humic Substances, Natures Most Versatile Materials* Taylor and Francis Inc, New York

[59] Perminova I V, Hatfield K, Hertkorn N (ed) (2005) *Use of Humic Substances to Remediate Polluted Environments: From Theory to Practice*. Springer, Dordrecht

[60] Celebi O, Kilikli A, Erten H N (2009) *J Hazard Mater* 168(2-3):695-703

[61] Klavins M, Eglıte L (2002) *Colloids Surf A: Physicochem Eng Aspects* 203:47-54

[62] Zhang Y, Li Q, Sun L, Tang R, Zhai J (2010) *J Hazard Mater* 175:404-409

[63] Hankins N P, Lub N, Hilal N (2006) *Sep Pur Technol* 51:48-56

[64] Baek K, Yang J W (2005) *Sep Sci Technol* 40(1-3): 699-708

[65] Yuan W, Zydney A L (2000) *Environ Sci Technl.* 34:5043-5048

[66] Koopal L K, Yang Y, Minnaard A J, Theunissen P L M, Van Riemsdijk W H (1998) *Colloids Surf A: Physicochem Eng Aspects* 141:385-395

[67] Seki H, Suziki A (1995) *J Colloid Interface Sci* 171:490-494

[68] Havelcova M, Mizeraa J, Sykorova I, Pekar M. (2009) *J Hazard. Mater* 161:559-564

[69] Baker H, Khalili F (2004) *Anal Chim Acta* 516:179-186

[70] Seki H, Suziki A, Kashiki I (1990) *J Colloid Interface Sci* 134:59-65

[71] Wei M, Liao J, Liu N, Zhang D, Kang H, Yang Y, Yang Y, Jin J (2007) *Nucl Sci Tech* 18:287-293

[72] Li L,Wei Z, Li Z, Wang J, Zhou Q, Guo J (2015) *Desal Water Treat* 54:2541-2545

[73] Bai R, Zhang X (2003) *J Colloid Interface Sci* 263:30-38

[74] Sun, X F, Wang S G, Liu X W, Gong W X, Bao N, Ma Y (2008) *Colloids Surf A: Physicochem Eng Aspects* 324(1-3):28-34

[75] Zhao L, Luo F, Wasikiewicz J M, Mitomo H, Nagasawa N, Yagi T,Tamada M, Yoshii F (2008) *Biores Technol* 99:1911–1917

[76] Weshaw R L (1993) *Environ Sci Technol* 27:814-816

[77] Ngah W S, Fatinathan S, Yosop N A (2011) *Desalination* 272:293-300

[78] Pandey A K, Pandey S D, Misra V, Santha Devi (2003) *J Hazard Mater B* 98:177-181

[79] Klucakova M, Pekar M (2008) *Colloids Surf A: Physicochem Eng Aspects* 318:106-110

[80] Apak R, Hizal J, Ustaer C (1999) *J Colloid Interface Sci* 211:185-192

[81] Paulenova A, Rajec P, Kandrac J, Saskoiova G, Tothova E, Bartos P, Svec V, Gora R (2000) *J Radioanal Nucl Chem* 246:617-622

[82] Wan Ngah W S, Fatinathan S (2010) *J Environ Sci* 22:338–346

[83] Tanga Y, Yub F, Chen F, Chen C (2011) *Adv Mater Res* 233-235:1972-1980

[84] Stathi P, Deligiannakis Y (2010) *J Colloid Interface Sci* 351:239-247

[85] Cezıkov J, Kozler J, Madronova L, Novak J, Janos P (2001) *React Funct Polym* 47:111-118

[86] Coles C A, Yong R N (2006) *Eng Geol* 85:26-32

[87] Martyniuk M, Wieckowska J (2003) *Fuel Process Technol* 84:23-31

[88] Yan W, Lien H L, Koel B E, Zhang W X (2013) *Environ Sci: Processes Impacts* 15: 63-68

[89] Zhang L, Fang M (2010) *Nano Today* 5**:**128-142

[90] Qu X, Alvarez Pedro J J, Li Q (2013) *Water Res* 47:3931-3946

[91] Englates K E (2011) *Characterization, Sorption and Exhaustion of metal oxide nanoparticles as metal adsorbents.* PhD Thesis submitted to University of Texas at SA

[92] Hua M, Zhang S, Pan B, Zhang W, Zhang Q (2012) *J Hazard Mater* 211/ 212: 317–331

[93] Xu P, Zeng G M, Lian Huang D L, Feng C L, Hu S, Zhao M H , Lai C, Wei Z, Huang C, Xie G X, Liu Z F (2012) *Sci Total Environ* 424:1-10

[94] Singh S, Barick K C, Bahadur D (2011) *J Hazard Mater* 192:1539 -1547

[95] Ilton E S , Boily J F, Buck E C, Skomurski F N, Rosso K M, Cahill C L, Bargar J R, Felmy A R (2010) *Environ Sci Technol* 44:170–176

[96] Xu Y, Zhao D (2007) *Water Res* 41:2101 – 2108

[97] Dien Li, Kaplan D I (2012*)* *J Hazard Mater* 243:1–18

[98] Katsoyiannis I A, Althoff H W, Bartel H, Jekel M (2006) *Water Res* 40: 3646 – 3652

[99] Duffó G S, Farina S B, Schulz F M (2013) *J Nucl Mater* 438:116–125

[100] Missana T, Gutierrez M G, Fernndez V (2003) *Geochim Cosmochim Acta* 67:2543–2550

[101] Scott T B, Allen G C, Heard P J, Randell M G (2005) *Geochim Cosmochim Acta* 69:5639-5646

[102] Singer D M, Chatman S M, Ilton E S, Rosso K M, Banfield J F, Waychunas G A (2012) *Environ Sci Technol* 46:3811−3820

[103] Singer D M, Chatman S M, Ilton E S, Rosso K M, Banfield J F, Waychunas G A (2012) *Environ Sci Technol* 46:3821−3830

[104] Sagert N H, Ho C H, Miller N H (1989*) J colloid Interface Sci* 130:283-287

[105] Missana T, Maffiotte C, García-Gutiérrez M (2003) *J Colloid Interface Sci* 261:154–160

[106] Penga L, Qin P, Lei M, Zenga Q, Song H, Yang J, Shao J, Liao B, Gu J (2012) *J Hazar Mater* 209/ 210:193– 198

[107] Jiang W, Cai Q, Xu W, Yang M, Cai Y, Dionysiou D D, O'Shea K E (2014) *Environ Sci Technol* 48:8078–8085

[108] Fuliu G, Z Hao Z S , Jiang G B (2008) *Environ Sci Technol* 42:6949–6954

[109] Yang S, Zong P, Ren X, Wang Q, Wang X (2012) *ACS Appl Mater Interfaces* 4: 6891−6900

[110] Tang W W, Zeng G M, Gong J L, Liang J, Xu P, Zhang C, Huang B B (2014) *Sci Total Environ* 468/468:1014–1027

[111] Niu H, Zhang D, Zhang S, Zhang X, Meng Z, Cai Y (2011) *J Hazard Mater* 190:559–565

[112] Descostes M, Mercier F, Thromat N, Beaucaire C, Soger M G (2000) *Appl surf Sci* 165:288-302

[113] Laszak I, Choppin G R (2001) *Radiochim Acta* 89:653–659

[114] Armani F. E, Cases I, de Pablo J, Duro L, Grive M, Bruno J (1999) TR99-21: *Experimental and modeling study of the interaction between U(VI) and magnetite*; Swedish Nuclear Fuel and Waste Management Co., Stockholm, Sweden

[115] Schindler M, Hawthorne F C, Freund M S, Burns P C (2009) *Geochim Cosmochim Acta* 73: 2471–2487.

[116] Allen G C, Tucker P M, Tyler J W (1982*) J Phys Chem* 86:224-228

[117] Singer D M,Chatman S M, Ilton E S, Rosso K M, Banfield J F, Waychunas G A (2012*) Environ Sci Technol* 46:3811−3820

[118] Dodge C J, Francis A J, Gillow J B, Halada G P, Eng C, Clayton C R (2002) *Environ Sci Technol* 36:3504–3511

[119] Huber F, Schild D, Vitova T, Rothe J, Kirsch R,Schafer T (2012) *Geochim Cosmochim Acta* 96:154–173

[120] Crane R.A , Dickinson M, Popescu I C, Scott T B (2002) *Water Res* 45:2931-2942

[122] Senesi N, Xing B, Huang P M (Eds) (2009) *Biophysico-chemical process involving Natural Non-living Organic matter in environmental systems.* John Wiley and Sons, NJ

[122] Ghabbour E A, Davies G (Eds) (2001) *Humic Substances Structures models and Functions* Royal Society of Chemistry, London.

[123] Von Wanduszka R (2000) *Geochem Tras* 1:10-15

[124] Tanaka T (2012) *Thermochim Acta* 532:60-64

[125] Chin Y P, Alken G, O'Loughlin E (1994) *Environ Sci Techno.* 28:1853-1858

[126] L M Yates III (1998) *From Pseudomicelle to Chelate: Fundumental and Practical Applications of Humic Substances Associations* ; PhD Thesis submitted to University of Idaho

[127] Yoshida T, Suzuki M (2006) *J Radioanal Nucl Chem* 270:363–368

[128] Saar R A, Weber J H (1980) *Environ Sci Technol* 14:877-880

[129] Palmer N E, von Wandruszka R (2001) *Fresenius J Anal Chem* 371:951–954

[130] Young C, von Wandruszka R(2001) *Geochem Trans* 2:16-20

[131] Mehta D J, Sharma R C, Ramanujam A, Haridasan T K, Sawant P D, Rathinam M (2003) *Radiat Prot Dosimetry* 105:65-68

[132] KubistaM, Sjoback R, Erickson S, Albinsson B (1994) *Analys*t 119: 417-422

[133] Biagorri R, Fuentes M, Gonza´lez-Gaitano G, Ma Garcı´a-Mina, Almendros G, Gonzalez-Vila F J (2009) *J Agric Food Chem* 57: 3266–3272

[134] Wall N A, Choppin G R (2003) *App Geochem*18:1573-1582

[135] Schmitt P, Kettrup A, Freitag D, Garrison A W (1996) *Fresenius J Anal Chem* 354: 915-920

[136] Alvarez-Puebla, Garrido J J (2005) *Chemosphere* 59:659-667

[137] Riedel T, Biester H, Dittmar T (2012) *Environ Sci Technol* 46: 4419-4426

[138] Engebreston R R , Von Wandruszka R (1998) *Environ Sci Technol* 32:488-493

[139] Lippold H, Eidner S, Kumke M, Lippmann-Pipke J (2012) *App Geochem* 27:250-256

[140] Lippold H, Evans N D M, Warwick P, Kupsch H (2007) *Chemosphere* 67: 1050–1056

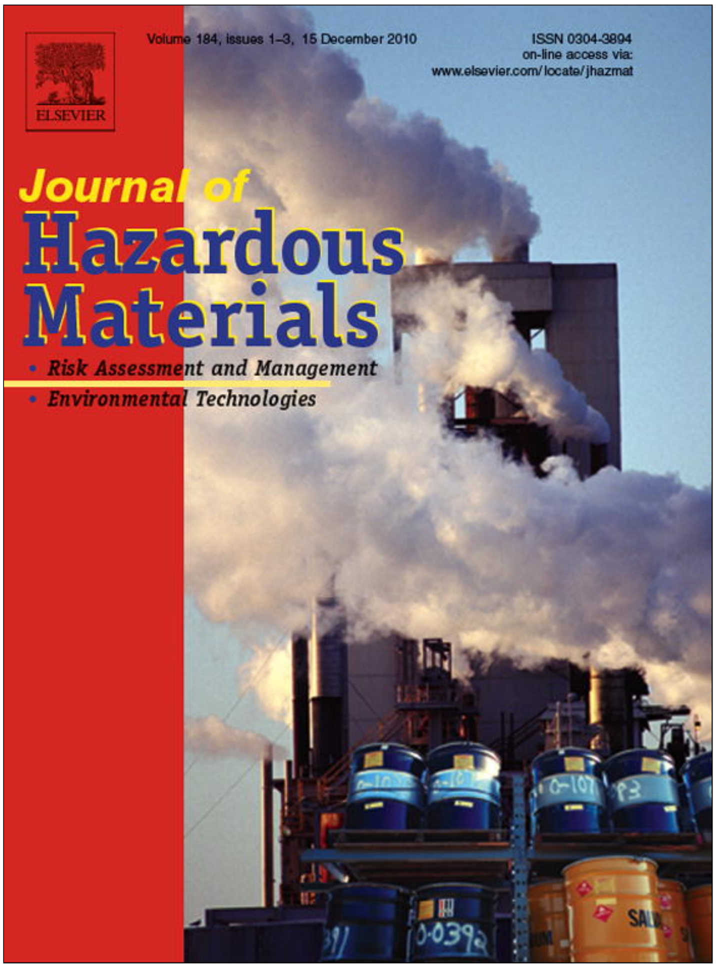
Volume 184, issues 1–3, 15 December 2010
ISSN 0304-3894
on-line access via:
www.elsevier.com/locate/jhazmat
ELSEVIER
Journal of
Hazardous
Materials
• Risk Assessment and Management
• Environmental Technologies

Journal of Hazardous Materials 184 (2010) 65–72

Contents lists available at ScienceDirect

Journal of Hazardous Materials

journal homepage: www.elsevier.com/locate/jhazmat

Adsorption of uranium from aqueous solution using chitosan-tripolyphosphate (CTPP) beads

M.K. Sureshkumar[a,*], D. Das[b], M.B. Mallia[c], P.C. Gupta[a]

[a] *Radiation Safety System Division, Bhabha Atomic Research Centre, Trombay, Mumbai 400085, India*
[b] *Fuel Reprocessing Division, Bhabha Atomic Research Centre, Trombay, Mumbai 400085, India*
[c] *Radiopharmaceutical Division, Bhabha Atomic Research Centre, Trombay, Mumbai 400085, India*

ARTICLE INFO

Article history:
Received 15 March 2010
Received in revised form 21 July 2010
Accepted 30 July 2010
Available online 7 August 2010

Keywords:
Chitosan
Tripolyphosphate
Uranium
Adsorption
Kinetics

ABSTRACT

Chitosan-tripolyphosphate (CTPP) beads were prepared using in-liquid curing method and used for the adsorption of uranium from aqueous solution. Beads were prepared at two different cross-linking densities by adjusting the pH of the tripolyphosphate solution. The synthesized beads were characterized using FTIR spectroscopy before and after adsorption of uranium. Beads having higher cross-linking are found to have better adsorption capacity for uranium. Factors that influence the uranium adsorption onto CTPP beads such as solution pH, contact time and initial uranium concentration were studied in detail. The experimental results were fitted into Langmuir and Freundlich adsorption isotherms. From Langmuir adsorption model the adsorption capacity of CTPP beads for uranium is estimated as 236.9 mg/g. Pseudo-first order, pseudo-second order and intraparticle diffusion model were applied to the observed kinetics data and the results shows that the pseudo-second order model is more suitable to explain the kinetics of adsorption of uranium on CTPP beads. FTIR spectroscopic characterization of the beads showed that the phosphate groups may be more responsible for the adsorption of uranium on CTPP beads.

1. Introduction

Chemical and radiotoxicity of uranium is well documented [1]. Based on the radiological risks by the radiation of uranium isotopes and chemical risks from heavy metals, the health effects of uranium can be divided into carcinogenic and non-carcinogenic effects. Nephritis is the primarily chemically induced effect of uranium in humans, whereas USEPA has classified uranium as a confirmed human carcinogen and suggested that zero tolerance is the only safe acceptable limit [2]. They prescribed that maximum contaminant level goal (MCLG) for uranium as zero in 1991. In addition, the EPA finalized a realistic regulation level of 30 μg/L as the maximum contaminant level. Though stringent environmental regulation exists against the release of uranium contaminated solution into the environment, effluents from nuclear and many other conventional industries are found to have significant quantity of uranium present in it [3]. Therefore it is desirable to develop efficient and economically viable methods for the treatment of water contaminated with uranium. Different methods have been used for cleaning solutions contaminated with uranium such as co-precipitation, ion exchange, membrane based separation and sorption on various surfaces [4–7]. In acidic solutions, uranium exists as U(VI), whereas in neutral or basic pH conditions, it normally exist as neutral or anionic species by complex formation with anionic ligands such as OH^- or $CO_3{}^{2-}$ [8]. Thus in neutral pH ranges, processes such as ion exchange is less effective for the removal of uranium from aqueous medium whereas membrane separation suffers many practical difficulties such as membrane fouling, which requires frequent maintenance. Thus sorption on various media is getting increasing interest as a suitable remediation process for the treatment of uranium contaminated solutions [9]. In past several decades, environmental friendly and potentially inexpensive biosorbents have attracted significant interest as suitable materials for the development of new environmental remediation technologies [10,11]. Chitin is the most abundant biopolymer after cellulose, and its partially deacetylated form, chitosan is found to have excellent sorption capacity for various heavy metals including radionuclides [12–17]. Chitosan is the copolymer composed of β-2-amino-2-deoxy-D-glucopyranose units and the residual 2-acetamido-2-deoxy-D-glucopyranose units and the metal uptake by it is primarily attributed to the amine and hydroxyl groups present in the polymer chain, which can interact with various metallic species through ion exchange and/or chelation mechanism. Two types of modifications are commonly adopted for the preparation of chitosan based sorbents. Cross-linking to improve its solubility and engineering properties and grafting of functional groups for enhancing the adsorption capacity and/or selectivity. Various reports have been published on the use of modified and

---

[*] Corresponding author. Tel.: +91 22 25591247, fax: +91 22 25505151.
E-mail address: smk@barc.gov.in (M.K. Sureshkumar).

0304-3894/$ – see front matter © 2010 Elsevier B.V. All rights reserved.
doi:10.1016/j.jhazmat.2010.07.119

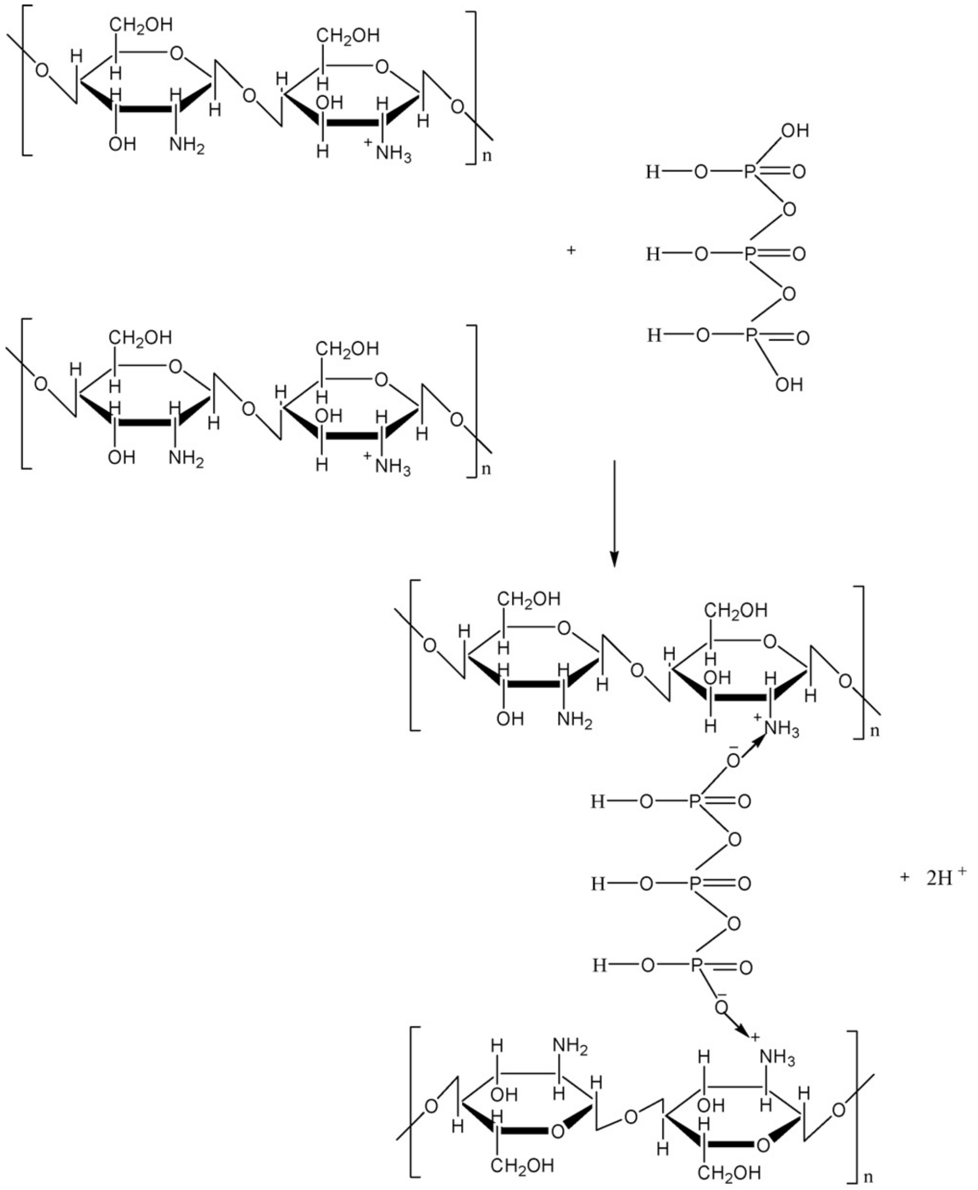

Fig. 1. Schematic representation of cross-linking of chitosan with sodium tripolyphosphate.

unmodified chitosan derivatives for analytical preconcentration [18–20] and sorption of uranium from aqueous solution [21–25]. However all these previous reports, dealing with sorption of uranium on chitosan derivatives; cross-linking agents used where toxic chemicals such as glutaraldehyde (GLA), epiclorohydrine (ECH) or ethylene glycol diglycidyl ether (EGDE).

From the environmental safety point of view, it is preferred to use non-toxic and environmentally benign substances for developing future technologies. Tripolyphosphate (TPP) mediated ionic cross-linking of chitosan is thus a suitable alternative to the use of toxic chemicals for the modification of chitosan. Cross-linking of chitosan by TPP can be achieved by a single-step process, where the formation of intra- and intermolecular cross-linking leads to solidification of chitosan into chitosan-tripolyphosphate (CTPP) beads [26]. Recently Ngah and Fatinathan [27] has reported the adsorption of Pb(II) and Cu(II) on CTPP beads from single and binary metal systems. Since phosphate groups are also known to have good affinity for uranium, CTPP beads may be a good adsorbent for uranium from aqueous solution. In the present work, we studied the adsorption of uranium onto CTPP beads. CTPP beads of two different cross-linking densities were prepared and the sorption of uranium is studied as a function of contact time, pH and concentration of uranium. The experimental results were fitted into Langmuir and Freundlich isotherm models. Kinetics of the adsorption process was analysed using pseudo-first order, pseudo-second order and intraparticle diffusion models. To understand the mechanism of adsorption of uranium onto CTPP beads, the beads were characterized using Fourier transform infrared (FTIR) spectroscopy before and after adsorption of uranium.

2. Experimental

2.1. Materials

Chitosan (medium molecular weight) and sodium tripolyphosphate (STPP) ($Na_5P_3O_{10}$) were purchased from Aldrich Chemical Company, USA. $UO_2(NO_3)_2{\cdot}6H_2O$ (ACS grade) was purchased from Merck, Germany. 2-(5-Bromo-2-Pyridylazo)5-diethylaminophenol (Br-PADAP), triethanolamine, CDTA, NaF and sulphosalicylic acid used for analysis uranium were analytical grade and were purchased from Merck, Germany or Sigma–Aldrich, USA. 2000 mg/l U(VI) standard solution was prepared by dissolving appropriate quantity of $UO_2(NO_3)_2{\cdot}6H_2O$ in deionised water. All other chemicals used in the experiments were of analytical grade. Deionised water used for all experiments was obtained from Milli-Q (Millipore Corporation, USA) water purification system.

2.2. Preparation and characterization of CTPP beads

CTPP beads were prepared using the method described by Lee et al. [26]. Chitosan (10 g) was dissolved in 500 ml of dilute acetic acid (1%, v/v) to prepare the chitosan solution. The STPP solution was prepared by dissolving 10 g of the solid in 100 mL of water. The chitosan solution was added/poured into the TPP solution drop wise using a PVC tip, with an opening of 1 mm. The beads were prepared at two different pH for the TPP solution; pH = 8.6 (original pH of the STPP solution) and pH = 3.0 adjusted by adding 1 M HCl, in order to obtain beads with different cross-linking densities [28]. The formation of cross-linked CTPP beads by the interaction between phosphate groups of tripolyphosphate and amino group of chitosan is schematically represented in Fig. 1. The beads were cured for 12 h, separated by filtration, washed four times with deionised water and air dried before use in adsorption experiments. Dried beads were spherical and slightly yellowish in colour. FTIR spectra of the powdered beads before and after adsorption of uranium were recorded as KBr pellets using JASCO 6200 model FTIR spectrophotometer.

2.3. Uranium measurement by Br-PADAP method

Concentration of dissolved uranium after the equilibration was determined using the spectrophotometric method using Br-PADAP as the complexing agent at pH = 7.8 [29,30]. Triethanolamine buffer (TEA-buffer) for pH adjustment was prepared by diluting 14 mL of the triethanolamine in 80 mL of deionised water, adjusting the pH to 7.8 by adding concentrated $HClO_4$ and finally made up to 100 mL. Complexing solution for removing the interference of other bivalent cations was prepared by dissolving 3.5 g of sulphosalicylic acid, 0.5 g of NaF and 1.25 g of CDTA in 40 mL water and adjusting pH to 7.8 by the addition of sodium hydroxide pellets and finally made up to 100 mL. For the measurement of uranium, 1 mL of complexing solution, 20–100 μL of aliquot of the sample, 1 mL TEA-buffer, 4 mL of ethanol and 0.5 mL of Br-PADAP were added into the 10 mL volumetric flask and made up to 10 mL using deionised water. The solution was allowed to develop colour for 30 min and optical density is measured at 578 nm using UV540 double beam spectrophotometer (Thermo Spectronic, USA).

2.4. Sorption of uranium on CTPP bead

For batch equilibration studies, experimental solutions containing measured concentration of uranium and the adsorbent were adjusted to the required pH and equilibrated in 100 mL Erlenmeyer flask at 250 rpm using a horizontal orbital shaker. Temperature during the adsorption experiments were controlled at 25 ± 0.5 °C. All pH adjustments were carried out with 1 M HNO_3/Na_2CO_3. After fixed time of equilibration, 20–100 μL of the solution was withdrawn from the experimental mixture and uranium concentration was estimated using the spectrophotometric method as described in Section 2.3. The amount of uranium adsorbed onto the CTPP bead at time t, was calculated by:

$$q_t = \frac{(c_0 - c_t)}{w} V \tag{1}$$

where q_t (mg/g) is the quantity of uranium adsorbed on CTPP bead at time t (h), c_0 is the initial concentration (mg/L) of uranium used in the experiment, c_t is the measured concentration (mg/L) of uranium presented in the liquid phase after equilibration time t; V is the volume of the solution (L); w is the mass of the CTPP beads (g). For kinetic investigations, the adsorption experiments were conducted at a stirring speed of 400 rpm, using a magnetic stirrer, in order to minimize the effect bulk and film diffusion on sorption process [31].

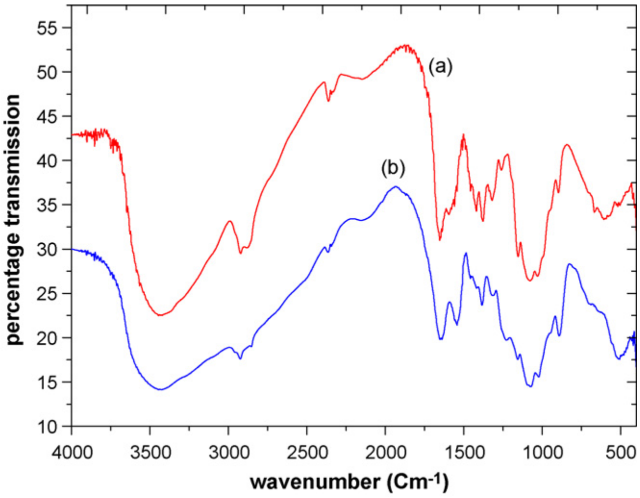

Fig. 2. FTIR spectra of (a) chitosan and (b) CTPP beads cross-linked at pH = 3.

3. Results and discussion

3.1. Characterization of CTPP beads

CTPP beads prepared were characterized using FTIR spectroscopy. The IR spectra of chitosan powder and the CTPP bead is provided in Fig. 2. The main differences in the IR spectra is the additional peak in the CTPP bead spectrum at 1230 cm^{-1}, which can be assigned to the –P=O stretching vibration indicating the presence of phosphate group in the prepared beads. Peak at 1694 cm^{-1} corresponding to $-NH_2$ group and 1419 cm^{-1} corresponding to –NH deformation vibration of $-NH_2$ groups, present in the original chitosan spectrum is completely disappeared in the spectrum of CTPP bead, with appearance of a fresh peak at 1541 cm^{-1} which can be assigned to NH_3^+ [26,27]. The beads are prepared at pH = 3 where the amino group are mostly protonated. From the spectral information it can be concluded that the cross-linking is taking place through the ionic interaction between the negatively charged $-P-O^-$ moieties of the phosphate group and protonated NH_3^+ moieties of the chitosan molecule.

3.2. Effect of cross-linking and solution pH on uranium sorption

Chitosan is brittle, where most of the active functional groups are deeply embedded inside the crystalline phase which leads to reduced adsorption capacity for the adsorbent. Cross-linking of chitosan with various cross-linking agents is found to improve its amorphous character. In order to investigate the effect of cross-linking and solution pH on the uranium sorption process, two sets of experiments were conducted, one using higher cross-linked beads and the other with lower cross-linked beads. Equilibration studies were carried out with 50 ml of 200 ppm U (VI) solution containing 50 mg of the adsorbent in each case and varying the initial pH of the solution from 3 to 9. Fig. 3 presents the uranium adsorption on lower and higher cross-linked beads, as a function of the solution pH. Under identical experimental conditions, beads with higher cross-linking showed higher adsorption capacity for uranium. The pH dependence also differs significantly with the extent of cross-linking of the CTPP beads. The uranium adsorp-

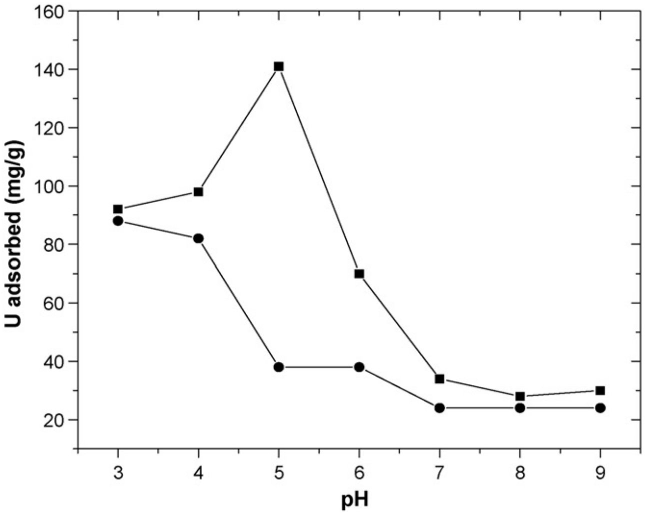

Fig. 3. Effect of pH on the adsorption of uranium on CTPP beads: lower cross-linked beads (●) and higher cross-linked beads (■) (volume = 50 ml, *U* = 200 mg/L, CTPP = 50 mg and *T* = 25 °C).

tion capacity of lower cross-linked beads decreased monotonously with pH of the solution. Though for lower cross-linked beads, both amino and phosphate groups may be available for the adsorption of uranium, it is reported that they are more amenable to swelling in acidic solution [26]. In such case, as the pH of the solution increases, due to reduced swelling, more and more active sites may not be reachable by uranium species for adsorption, resulting in lower adsorption capacity. On the other hand beads with higher cross-linking showed maximum adsorption at pH = 5. The swelling behavior of higher cross-linked beads is nearly independent of pH and other factors determine the adsorption dependence of uranium on pH of the solution. At lower pH, the amino groups are protonated whereas phosphate groups remain undissociated. Thus at lower pH, the positively charged uranyl ion is not favored by the positive or neutral binding groups on the adsorbent, resulting in lower adsorption capacity. At neutral to alkaline pH, uranium is present as anionic hydroxyl-carbonate complexes such as, $UO_2CO_3OH^-$, $(UO_2)_2(CO_3)(OH)_3{}^-$, $(UO_2)_{11}(CO_3)_6(OH)_{12}{}^{2-}$, etc. [32], and thus not favorable for adsorption onto the neutral/negatively charged functional groups of CTPP beads, which explain the reduction in adsorption at higher pH. Thus the maximum adsorption capacity observed at pH = 5 for the higher cross-linked CTPP beads is the result of pH-dependent speciation of the uranyl ion and the pH-dependent dissociation behavior of CTPP functional groups responsible for uranium adsorption. Due to the higher adsorption capacity, beads with higher cross-linking and the optimum pH = 5 were used for further experiments.

3.3. *Effect of contact time on uranium sorption*

To understand the effect of contact time on uranium adsorption onto CTPP beads, experiments were conducted with 100 mL of solution having 400 mg/L uranium and 100 mg of adsorbent. 100 μL of the sample were analysed at various intervals to estimate the concentration of dissolved uranium as a function of equilibration time. Fig. 4 shows that the process is characterized by a rapid adsorption in the initial 4 h of equilibration time, followed by a slow process, leading to equilibrium adsorption in around 3 days. The initial fast sorption might be due to the surface adsorption of uranium on the CTPP beads. Uranyl ion is a bulky cation and the diffusion of the bulk ion into the CTPP beads is a slow process leading to the overall slow kinetics of the adsorption process. During longer stay of the beads in the experimental solution, they become swollen, but no solubility of the beads was observed even after 5 days of equilibration. Concentration of dissolved uranium measured after 10 days of equilibration was in the same range (within 5%) of the concentration measured after 72 h of equilibration, showing that for practical purposes 72 h can be taken as the time required for completing the adsorption equilibrium.

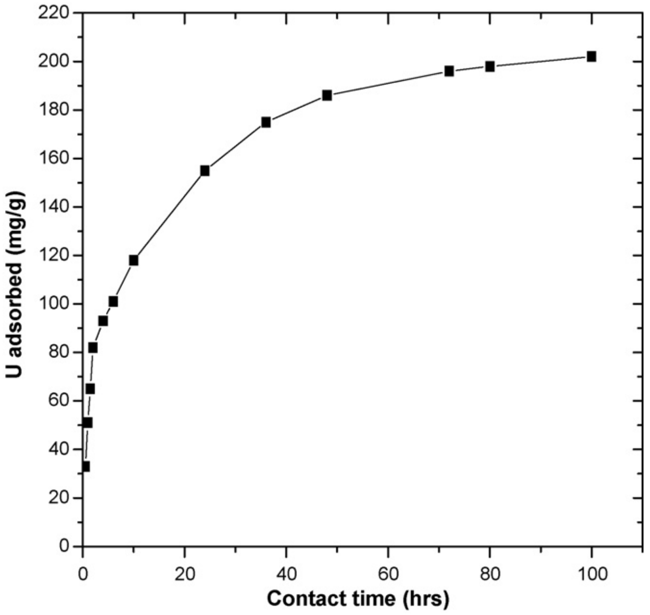

Fig. 4. Effect of contact time on the adsorption of uranium on CTPP beads (volume = 100 ml, *U* = 400 mg/L, CTPP = 100 mg, pH = 5 and *T* = 25 °C).

3.4. *Effect of initial uranium concentration*

The relation between the adsorbed amount and the equilibrium concentration in the aqueous phase is very important in optimizing the sorption process and understanding the sorption behavior. For investigating the effect of initial uranium concentration on the adsorption of uranium onto CTPP beads, experiments were con-

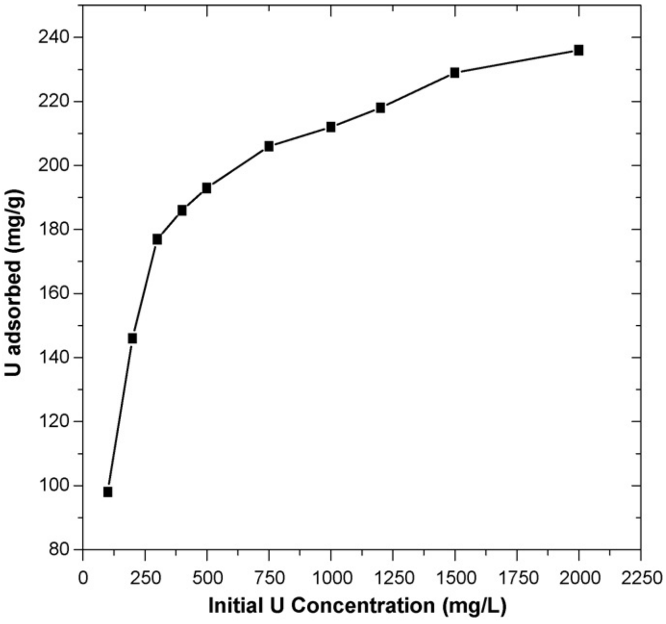

Fig. 5. Effect of initial uranium concentration on adsorption on CTPP beads (volume = 50 ml, CTPP = 50 mg, pH = 5, and *T* = 25 °C).

Table 1
Model constants and correlation coefficients for adsorption of uranium by CTPP beads.

Isotherm model						Experimentally observed saturation capacity (mg/g)
Langmuir			Freundlich			
Q (mg/g)	b (mL/mg)	R^2	k_F (mg/g)	n	R^2	
236.9	0.019	0.997	89.9	7.65	0.991	239.9

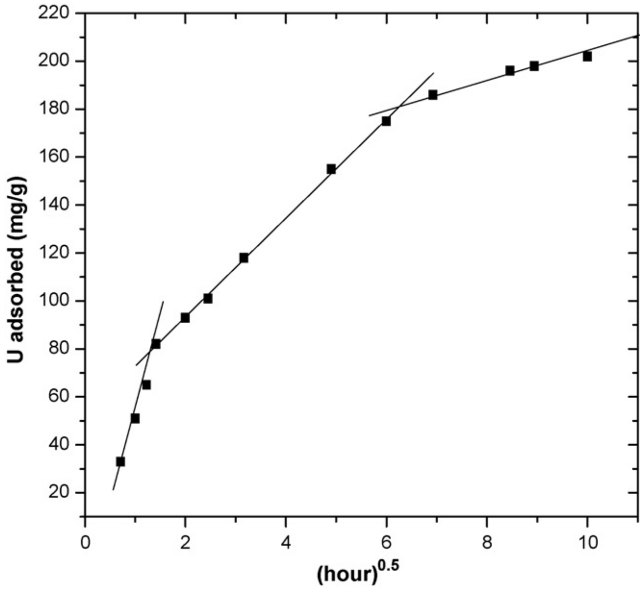

Fig. 6. Intraparticle diffusion kinetics of the adsorption of uranium on CTPP beads.

ducted with 50 mL solutions having initial uranium concentration varying from 100 mg/L to 2000 mg/L and a fixed mass of 50 mg of adsorbent. Fig. 5 shows the amount of adsorbed uranium after equilibrium versus the initial uranium concentrations. As expected the adsorption capacity increased with the initial metal concentration. With more uranium present in solution, larger fraction of the active sites is involved in the adsorption process. At higher uranium concentrations adsorption capacity reached a plateau indicating saturation of the available binding sites on the adsorbent. The steep slope at initial uranium concentrations is a desirable feature of the sorption system and the results indicates that a CTPP bead is an efficient adsorbent for uranium.

3.5. Sorption isotherm

Adsorption isotherm is fundamental in understanding the distribution of the adsorbate on adsorbent surface once the equilibrium is established [33]. The simplest adsorption model is Langmuir isotherm in which it is assumed that the adsorbate form a monolayer on the adsorbent surface and the adsorption energy decreases as the distance from the surface increase, making multilayer adsorption process less favorable. The linear form of the Langmuir isotherm can be expressed as:

Table 2
R_L values for uranium adsorption obtained form Langmuir equation.

Initial U concentration (c_0) (mg/L)	Separation factor (R_L)
10	0.840
50	0.512
100	0.256
500	0.095
1000	0.050

$$\frac{c_e}{q_e} = \frac{1}{Qb} + \frac{c_e}{Q} \tag{2}$$

where q_e is the amount of metal ion adsorbed at equilibrium (mg/g), c_e is the equilibrium metal ion concentration remaining in solution, Q (mg/g) is the amount of metal ion adsorbed at complete monolayer coverage, and b is the Langmuir constant related to the affinity of the binding site (mL/mg).The monolayer adsorption capacity, Q and the Langmuir constant b can be obtained from the linear plot of c_e/q_e against c_e. Other commonly used adsorption model is the Freundlich isotherm which is an empirical model used to explain the adsorption on heterogeneous surfaces. The Freundlich isotherm can be expressed as:

$$\ln\ q_e = \ln k_F + \frac{1}{n} \ln c_e \tag{3}$$

where k_F (mg/g) and n are Freundlich constants related to adsorption capacity and adsorption intensity respectively, and can be obtained from the linear plot of $\ln q_e$ against $\ln c_e$. The model parameters obtained by applying both Langmuir and Freundlich model to the experimental data are given in Table 1. From the better correlation coefficient and the fact that the equilibrium adsorption capacity (Q) obtained from Langmuir model (236.9 mg/g) is close to the experimentally observed saturation capacity (239.9 mg/g), it can be concluded that the monolayer Langmuir adsorption isotherm is more suitable to explain the adsorption of uranium onto CTPP beads.

The favorability of the CTPP beads as an adsorption medium for uranium can be obtained from the Langmuir adsorption constant b; which is related to the separation factor R_L defined as:

$$R_L = \frac{1}{1 + bc_0} \tag{4}$$

where c_0 is the initial metal ion concentration. $0 < R_L < 1$ indicates that the adsorbent is a favorable medium for the adsorption of the given metal. Table 2 presents the calculated R_L values at five different initial uranium concentrations. For all the tested uranium concentrations, $0 < R_L < 1$ which proves that CTPP bead is a favorable adsorbent for uranium. The same conclusion can be arrived

Table 3
Kinetics parameters of uranium adsorption by CTPP beads.

Kinetic model								Experimentally observed adsorption capacity (mg/g)
Pseudo-first order			Pseudo-second order			Intraparticle diffusion model		
k_1 (h^{-1})	q_e (mg g^{-1})	R^2	k_2 (g mg^{-1} h^{-1})	q_e (mg g^{-1})	R^2	k_{id} (mg g^{-1} h^{-1})	R^2	
0.045	141.6	0.995	9.4×10^{-4}	209.2	0.997	19.6	0.993	202.4

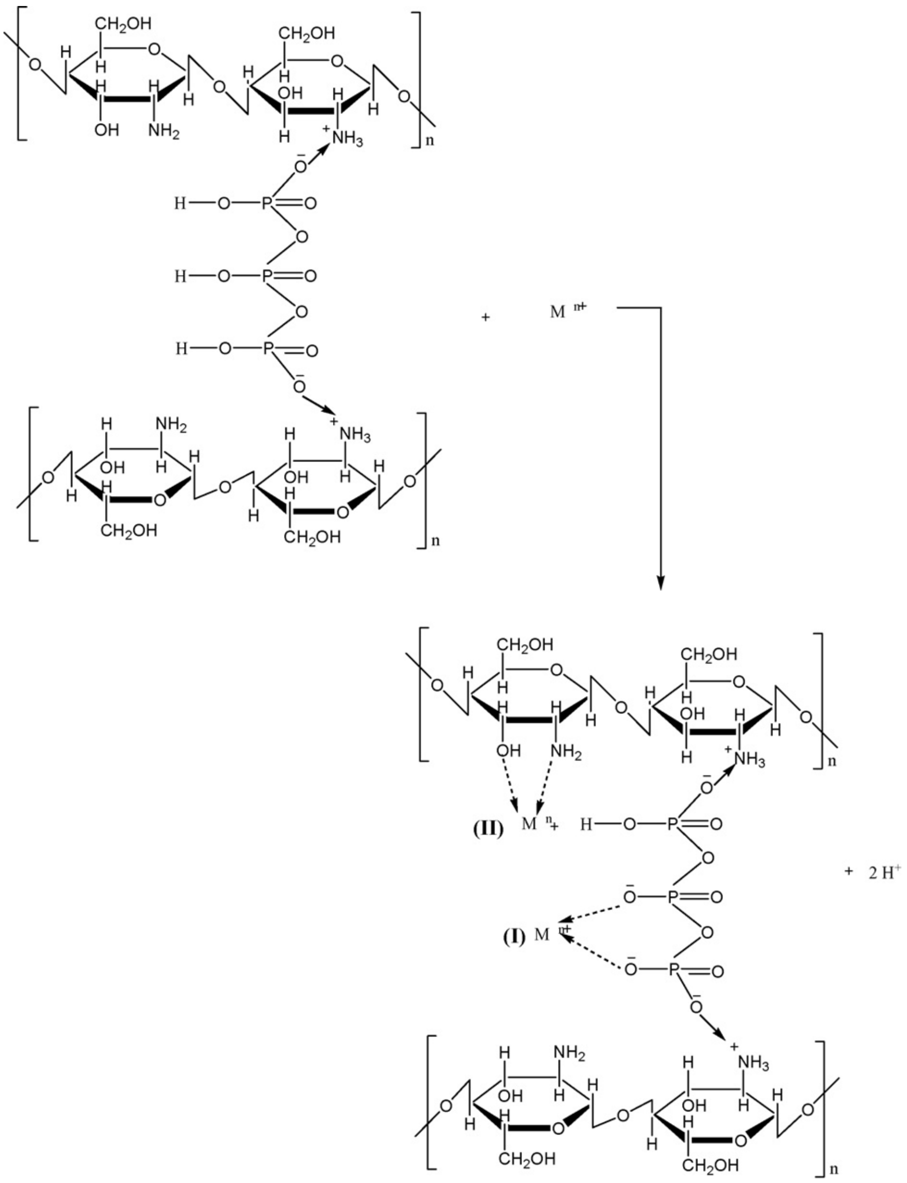

Fig. 7. Schematic presentation of binding of uranium by CTPP beads.

from the Freundlich constant *n* in which case a value of *n* between 1 and 10 indicates the acceptance of the medium as the suitable adsorbent.

3.6. Sorption kinetics

Experiments for studying the adsorption kinetics were carried out at higher agitation speed in order to minimize the effect of bulk diffusion and film diffusion on the adsorption process. It is assumed that at the experimental agitation rate of 400 rpm, intraparticle diffusion or chemical reactions may be the rate limiting step. Both pseudo-first order and pseudo-second order kinetics were applied to analyse the experimentally observed kinetic data [34]. Pseudo-first order kinetic model can be expressed as:

$$\log(q_e - q_t) = \log q_e - \left(\frac{k_1}{2.303}\right) t \qquad (5)$$

where q_e and q_t are the concentration of uranium adsorbed on CTPP beads (mg/g) at equilibrium time, and time t (h) respectively, and k_1 is the pseudo-first order rate constant (h^{-1}) for the adsorption of uranium onto CTPP beads. The model parameters q_e and k_1 can be obtained form the linear plot of $\log(q_e - q_t)$ against time. Pseudo-second order kinetics can be expressed as:

$$\frac{t}{q_t} = \frac{1}{k_2 q_e^2} + \frac{t}{q_e} \qquad (6)$$

where q_e (mg/g) and q_t (mg/g) have the same meaning as earlier and k_2 is the rate constant (g mg^{-1} h^{-1}) of the pseudo-second order kinetic model. The equilibrium adsorption capacity q_e and the second order rate constant k_2 can be obtained from the plot of t/q_t against t. The model parameters and the equilibrium concentration obtained by both the models are given in Table 3. From the results it can be observed that both pseudo-first and pseudo-second order models are matching with the experimental kinetics data. From the better correlation coefficient and the fact that the equilibrium concentration obtained by the pseudo-second order plot (209 mg/g) is more close to the experimental value than that obtained from the pseudo-first order plot (141.5 mg/g), it can be concluded that pseudo-second order model is more relevant to explain the kinetics of adsorption of uranium on CTPP beads.

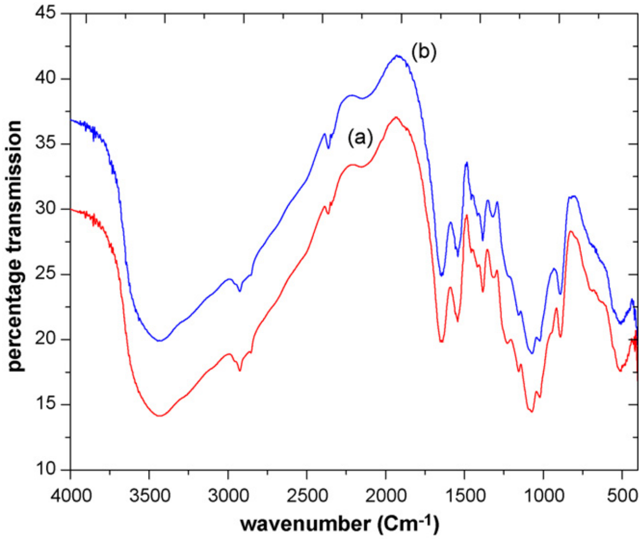

Fig. 8. FTIR spectra of CTPP beads before (a) and after (b) adsorption of uranium.

Adsorption of the metal ions to the active sites of the adsorbent depends on the concentration level of metal ions near the vicinity of the binding sites. Concentration distribution within the beads is controlled by the intraparticle diffusion and in many cases the Fickian diffusion equation is applicable to explain the sorption process [34], which can be expressed as:

$$q_t = k_{id} \times t^{1/2} \qquad (7)$$

where q_t is the adsorption capacity (mg/g) at time t, and k_{id} is the intraparticle diffusion constant (mg g^{-1} h^{-1}). The plot of quantity adsorbed (q_t) at time t as a function of $\sqrt{t}$ gives a straight line, from which the intraparticle diffusion constant, k_{id} can be obtained. The experimental curve (Fig. 6) gives three straight lines with three different slopes (all with $r^2 \geq 0.97$). Thus it is clearly evident that intraparticle diffusion is not applicable to the entire time scale of the adsorption process. The initial straight line, which corresponds to the fast adsorption, could be due to the surface adsorption on the dried beads where intraparticle diffusion has no significant contribution. Similarly the last straight line might be corresponding to the chemical equilibration of uranium in the swollen CTPP beads. Among the three lines, one corresponding to the intermediate time scales has the best statistical fit as per the intraparticle diffusion model. Thus it can be assumed that uranium diffusion inside the beads have significant influence in controlling the kinetics of uranium sorption at intermediate time scales. However it should be noted that this straight line does not pass through the origin which means intraparticle diffusion is not the sole rate determining factor controlling the adsorption of uranium onto CTPP beads. Similar three-stage kinetics was earlier reported for the sorption of humic acid by cross-linked chitosan beads [34].

3.7. *Mechanism of uranium adsorption on CTPP beads*

Two potential binding sites in CTPP beads available for the adsorption of uranium is presented in Fig. 7 [27]. Highly cross-linked beads used for the adsorption studies were prepared at pH = 3, where most of the amine groups are protonated. Ionic cross-linking with tripolyphosphate might have consumed most of these amino groups, thus not available for binding of uranium. Thus the principal functional groups responsible for uranium adsorption by CTPP beads might be the phosphate group. In order to identify the functional groups responsible for the adsorption of uranium onto CTPP beads, FTIR spectra of the CTPP beads were recorded after the adsorption of uranium. Fig. 8 presents the FTIR spectra of the CTPP beads before and after adsorption of uranium. Significant decrease in the peak at 1230 cm^{-1} corresponding to –P═O stretching vibration in the spectrum after adsorption of uranium indicates that phosphate groups are affected due to the adsorption process. Though the peak at 1319 cm^{-1} corresponding to –C–N stretching vibration is slightly shifted, no significant change is observed in the peak position of any other major peaks corresponding to nitrogen and oxygen functional groups. Thus from the spectral characterization of the beads, it is evident that phosphate groups are the major contributor for the adsorption of uranium (binding site I), though it does not preclude some involvement of the amino groups (binding site II) in the adsorption process.

4. Conclusion

CTPP beads were found to have good adsorption capacity for uranium from aqueous solution. Adsorption capacity is found to be more for higher cross-linked CTPP beads than that for the lower cross-linked beads, regardless of the pH of the experimental solution. For beads with higher cross-linking, adsorption capacity is found to depend on the solution pH, and maximum adsorption capacity is observed at pH = 5. Langmuir adsorption isotherm is found to be more suitable to explain the adsorption of uranium onto CTPP beads than Freundlich model. Kinetics of adsorption of uranium by CTPP beads is found to be slow, taking around 3 days to complete the equilibrium, probably due to slow diffusion of the bulky uranium species into the beads. The observed adsorption kinetics data matches with the pseudo-second order model, indicating that the adsorption is dominated by chemisorption. Application of the intraparticle diffusion model gave three straight line portions in the experimental curve, showing the limited utility of this model, in explaining the observed kinetics. From characterization of the beads before and after uranium adsorption using FTIR, it is concluded that phosphate groups are more responsible for the uranium uptake by CTPP beads than the amino groups.

Acknowledgement

The authors are grateful to Dr. D.N. Sharma, Head, Radiation Safety System Division, Bhabha Atomic Research Centre, Mumbai for his keen interest in the progress of the work.

References

[1] D. Brugge, J.L. de Lomos, B. Oldmixon, Exposure pathways and health effects associated with chemical and radiological toxicity of natural uranium, Rev. Environ. Health 20 (2005) 177–193.
[2] USEPA, EPA Integrated Risk Information System (IRIS), Electronic Database, USEPA, Washington, DC, 1996.
[3] S.M. Grashchenko, Naturally occurring radionuclides of uranium and thorium series in non nuclear industrial process, Radiochemistry 47 (2005) 614–618.
[4] A.P. Kryvoruchko, L.Y. Yurlova, I.D. Atamanenko, B.Y. Kornilovich, Ultrafiltration removal of U(VI) from contaminated water, Desalination 162 (2004) 229–239.
[5] X. Shuibo, Z. Chun, Z. Xinghuo, Y. Jing, Z. Xiaojian, W. Jingsong, Removal of uranium(VI) from aqueous solution by adsorption on hametite, J. Environ. Radioact. 100 (2008) 162–166.
[6] S.Y. Lee, E.A. Banditti, Removing uranium from drinking water by metal hydroxide and anion exchange resin, J. Am. Water Works Assoc. 75 (1983) 536–542.
[7] D. Clifford, Z. Zhang, Modifying ion exchange for combined removal of uranium and radium, J. Am. Water Works Assoc. 86 (1994) 214–227.
[8] I.A. Katsoyiannis, H.W. Althoff, H. Bartel, M. Jekel, The effect of groundwater composition on uranium(VI) sorption onto bacteriogenic iron oxides, Water Res. 40 (2006) 3646–3652.
[9] S. Yusan, S. Akyil, Sorption of uranium (VI) from aqueous solution by akaganeite, J. Hazard. Mater. 160 (2008) 388–395.
[10] C. Gok, S. Aytas, Biosorption of uranium (VI) from aqueous solution using calcium alginate beads, J. Hazard. Mater. 168 (2009) 369–375.

[11] T.S. Anirudhan, C.D. Bringle, S. Renjith, Removal of uranium (VI) from aqueous solution and nuclear industry effluents using humic acid immobilized zirconium-pillared clay, J. Environ. Radioact. 101 (2010) 267–276.

[12] D. Chauhan, N. Shankararamakrishnan, Highly enhanced adsorption for decontamination of lead ions from battery wastewaters using chitosan functionalized with xanthate, Bioresour. Technol. 99 (2008) 9021–9024.

[13] X. Liu, Q. Hu, Z. Fang, X. Zhang, B. Zhang, Magnetic chitosan nanocomposite: a useful tool for heavy metal ion removal, Langmuir 25 (2009) 3–8.

[14] E. Guibal, Interaction of metal ions with chitosan based sorbents: a review, Sep. Purif. Technol. 38 (2004) 43–74.

[15] P.A. Miretzky, F. Cirelli, Hg(II) removal from water by chitosan and chitosan derivatives: a review, J. Hazard. Mater. 167 (2009) 10–23.

[16] E. Metwally, S.S. Elkholy, H.A.M. Salem, M.Z. Elsabee, Sorption behavior of ^{60}Co and $^{152+154}$Eu radionuclides on to chitosan derivatives, Carbohydr. Polym. 72 (2009) 622–631.

[17] J. Cao, Y. Tan, Y. Che, H. Xin, Novel complex gel beads composed of hydrolysed poly acrylamide and chitosan: an effective adsorbent for the removal of heavy metal form aqueous solution, Bioresour. Technol. 101 (2010) 2558–2561.

[18] A. Sabarudin, M. Oshima, T. Takayanagi, L. Hakim, K. Oshita, Y.H. Gao, S. Motomizu, Functionalisation of chitosan with 3,4-dihydroxy benzoic acid for the adsorption/collection of uranium in water samples and its determination by inductively coupled plasma mass spectrometry, Anal. Chim. Acta 581 (2007) 214–220.

[19] S. Dutta, P.K. Mohapatra, S.P. Ramnani, S. Sabharwal, A.K. Das, V.K. Manchanda, Use of chitosan derivatives as solid phase extractors for metal ions, Desalination 232 (2008) 234–242.

[20] K. Oshita, M. Oshima, Y. Gao, K.H. Lee, S. Motomizu, Synthesis of novel chitosan resin derivatized with serine moiety for the column collection/concentration of uranium and the determination of uranium by ICP-MS, Anal. Chim. Acta 480 (2003) 239–249.

[21] G. Wang, J. Liu, X. Wang, Z. Xie, N. Deng, Adsorption of uranium(VI) from aqueous solution onto cross-linked chitosan, J. Hazard. Mater. 168 (2009) 1053–1082.

[22] E. Guibal, M.J. Charrier, I. Saucedo, P.L. Cloirec, Enhancement of metal ion sorption performance of chitosan: effect of the structure on the diffusion properties, Langmuir 11 (1995) 591–598.

[23] R.A.A. Muzzarelli, Removal of uranium from solutions and brines by a derivative of chitosan and ascorbic acid, Carbohydr. Polym. 5 (1985) 85–89.

[24] R. Akkaya, U. Ulusoy, Adsorptive features of chitosan entrapped in poly acrylamide hydrogel for Pb^{2+}, $UO_2{}^{2+}$ and Th^{4+}, J. Hazard. Mater. 151 (2008) 380–388.

[25] A.A. Atia, Studies on the interaction of mercury(II) and uranyl(II) with modified chitosan resin, Hydrometallurgy 80 (2005) 13–22.

[26] S.T. Lee, F.L. Mi, Y.J. Shen, S.S. Shyu, Equilibrium and kinetic studies of copper(II) uptake by chitosan-tripolyphosphate chelating resin, Polymer 42 (2001) 1879–1892.

[27] W.S.W. Ngah, S. Fatinathan, Adsorption characterisation of Pb(II) and Cu(II) ions onto chitosan tripolyphosphate beads: kinetic, equilibrium and thermodynamic studies, J. Environ. Manage. 91 (2010) 958–969.

[28] F.L. Mi, S.S. Shyu, S.T. Lee, T.B. Wong, Kinetic study of chitosan-tripolyphosphate complex reaction and acid-resistive properties of the chitosan-tripolyphosphate gel beads prepared by in-liquid curing method, J. Polym. Sci. B 37 (1995) 1551–1564.

[29] A. Suresh, D.K. Pâté, T.G. Srinivasan, P.R. Vasudeva Rao, A new procedure for the spectrophotometric determination of uranium(VI) in the presence of large excess of thorium(IV), Spectrochim. Acta A 58 (2002) 34–347.

[30] S.K. Das, S.G. Rege, A. Mukherjee, A. Ramanujam, R.K. Dhumwad, Direct spectrophotometer method for the determination of microgram quantities of uranium with Br-Padap in aqueous and organic waste streams of PUREX and THOREX process. BARC Report No. 1593, 1991.

[31] E. Guibal, C. Milot, J.M. Tobin, Metal anion sorption by chitosan beads: equilibrium and kinetics studies, Ind. Eng. Chem. Res. 34 (1998) 1463–1554.

[32] L. Maya, Hydrolysis and carbonate complexation of dioxouranium(VI) in the neutral-pH range at 25 °C, Inorg. Chem. 21 (1982) 2895–2898.

[33] B. Kannamba, K.L. Reddy, B.V. Apparao, Removal of Cu(II) from aqueous solutions using chemically modified chitosan, J. Hazard. Mater. 175 (2010) 935–948.

[34] W.S.W. Ngah, M.A.K.M. Hanafiah, S.S. Yong, Adsorption of humic acid from aqueous solution on cross-linked chitosan–epichlorohydrin beads: kinetic and isotherm studies, Colloids Surf. B 65 (2008) 18–24.

This article was downloaded by: [Bhabha Atomic Research Centre]
On: 29 July 2015, At: 22:36
Publisher: Taylor & Francis
Informa Ltd Registered in England and Wales Registered Number: 1072954 Registered office: 5 Howick Place, London, SW1P 1WG

Separation Science and Technology
Publication details, including instructions for authors and subscription information:
http://www.tandfonline.com/loi/lsst20

Adsorption of Pb(II) Ions Using Humic Acid Coated Chitosan-Tripolyphosphate (HA-CTPP) Beads

M. K. Sureshkumar [a], D. Das [b], G. Mary [b] & J. Nuwad [c]

[a] Radiation Safety System Division, Bhabha Atomic Research Centre, Trombay, Mumbai, India

[b] Fuel Reprocessing Division, Bhabha Atomic Research Centre, Trombay, Mumbai, India

[c] Chemistry Division, Bhabha Atomic Research Centre, Trombay, Mumbai, India

Accepted author version posted online: 17 Jan 2013.Published online: 27 Mar 2013.

To cite this article: M. K. Sureshkumar, D. Das, G. Mary & J. Nuwad (2013) Adsorption of Pb(II) Ions Using Humic Acid Coated Chitosan-Tripolyphosphate (HA-CTPP) Beads, Separation Science and Technology, 48:7, 1132-1139, DOI: 10.1080/01496395.2012.724500

To link to this article: http://dx.doi.org/10.1080/01496395.2012.724500

PLEASE SCROLL DOWN FOR ARTICLE

Taylor & Francis makes every effort to ensure the accuracy of all the information (the “Content”) contained in the publications on our platform. However, Taylor & Francis, our agents, and our licensors make no representations or warranties whatsoever as to the accuracy, completeness, or suitability for any purpose of the Content. Any opinions and views expressed in this publication are the opinions and views of the authors, and are not the views of or endorsed by Taylor & Francis. The accuracy of the Content should not be relied upon and should be independently verified with primary sources of information. Taylor and Francis shall not be liable for any losses, actions, claims, proceedings, demands, costs, expenses, damages, and other liabilities whatsoever or howsoever caused arising directly or indirectly in connection with, in relation to or arising out of the use of the Content.

This article may be used for research, teaching, and private study purposes. Any substantial or systematic reproduction, redistribution, reselling, loan, sub-licensing, systematic supply, or distribution in any form to anyone is expressly forbidden. Terms & Conditions of access and use can be found at http://www.tandfonline.com/page/terms-and-conditions

Separation Science and Technology, 48: 1132–1139, 2013
Copyright © Taylor & Francis Group, LLC
ISSN: 0149-6395 print/1520-5754 online
DOI: 10.1080/01496395.2012.724500

Taylor & Francis
Taylor & Francis Group

Adsorption of Pb(II) Ions Using Humic Acid Coated Chitosan-Tripolyphosphate (HA-CTPP) Beads

M. K. Sureshkumar,[1] D. Das,[2] G. Mary,[2] and J. Nuwad[3]
[1]*Radiation Safety System Division, Bhabha Atomic Research Centre, Trombay, Mumbai, India*
[2]*Fuel Reprocessing Division, Bhabha Atomic Research Centre, Trombay, Mumbai, India*
[3]*Chemistry Division, Bhabha Atomic Research Centre, Trombay, Mumbai, India*

A new humic acid (HA) based adsorbent was prepared by coating humic acid on chitosan tripolyphosphate (CTPP) beads. Humic acid-chitosan tripolyphosphate (HA-CTPP) beads thus obtained were characterized using Fourier Transform Infrared Spectroscopy and Scanning Electron Microscopy. Swelling capacity studies of CTPP and HA-CTPP beads conducted in the pH range, pH = 1–10 showed that HA-CTPP beads are more stable against swelling than CTPP beads. Equilibration of HA-CTPP beads in water for different pH showed that leaching of HA from the beads is negligible and the beads are stable for adsorption applications. Adsorption of Pb(II) ions onto HA-CTPP beads were studied as a function of various operational parameters such as initial pH, metal ion concentration, and contact time. The results showed that HA-CTPP beads are suitable for Pb(II) ions adsorption and the kinetics of sorption very well fit into pseudo-second order model. The Langmuir model was found to be more suitable for explaining the observed adsorption data, giving a theoretical maximum adsorption capacity of 223.7 mg/g. HA-CTPP beads could possibly find application in the treatment of waste water contaminated with other toxic and/or heavy metals.

Keywords adsorption; chitosan; humic acid; Pb(II) ions

INTRODUCTION

Humic materials formed by the degradation of biomaterials are one of the biggest pools of carbon on earth (1). Its role in speciation, bioavailability, transport, and sequestration of various organic and inorganic pollutants in aquatic and terrestrial environment is well understood (2). The ability of humic materials to complex with metal ions is primarily attributed to the abundant –COOH and −OH groups present in these macromolecules. The artifact that humic materials can strongly bind heavy metals and radionuclide have been the subject of many investigations, with the aim of developing suitable technology utilizing these materials for treatment of contaminated water (3,4). Humic acid (HA) which is operationally defined as the fraction of the humic materials which is water soluble above $pH > 2$ is the prime candidate in these investigations, principally due to the high abundance of this fraction relative to others. In addition to its pristine form, humic acid in several physico-chemical modifications such as insoluble solid (5), immobilized on silica (6), and as a composite with various polymers (7,8) have been tested for the removal of various metals. Few attempts were also reported on the use of HA as a polymeric macromolecule in the separation of metal ions using polyelectrolyte flocculation (9) and polymer enhanced ultra-filtration (10). Membrane fouling could be a serious bottle-neck in the scaling up of the HA based ultra-filtration process (11,12), whereas the immobilization of HA onto various supports needs multi-step chemical treatment, often resulting in overall poor loading of HA onto the immobilizing medium (13,14). It is also reported that insoluble humic acid (IHA) obtained by heat treatment has significantly lower sorption capacity than pristine HA due to the thermal decomposition of functional groups (15) during the heat treatment. Hence, it is desirable to develop a new immobilization technique for HA on different substrates, without significantly undermining its inherent sorption capacity.

In the present investigation, we have prepared HA coated chitosan beads by dip coating of the wet chitosan beads in HA solution. Pb(II) was selected as a model heavy metal cation for studying the adsorption properties of the newly prepared adsorbent. In this contest, it should be noted that many attempts have already been reported on the use of HA from various origin for removal of Pb(II) from aqueous solution. However, use of HA gel (16) and IHA powder (17) as an adsorbent for Pb(II) required extensive separation of the adsorbent, once the equilibrium is reached. Though Seki et al. (18) studied the adsorption of Pb(II) onto HA immobilized on calcium alginate beads, the sorption kinetics was found to be significantly slow for practical application. In contrast, the humic acid coated chitosan tripolyphosphate (HA-CTPP) beads reported here have faster adsorption kinetics and are easily separable from the liquid phase after equilibration.

Received 9 April 2012; accepted 22 August 2012.

Address correspondence to M. K. Sureshkumar, Radiation Safety System Division, Bhabha Atomic Research Centre, Trombay, Mumbai, India-400085. E-mail: smk@barc.gov.in

EXPERIMENTAL

Materials

Chitosan (medium molecular weight), sodium trypolyphosphate (STPP), ($Na_5P_3O_{10}$), and humic acid (Technical grade) were purchased from Aldrich chemical company, USA. $Pb(NO_3)_2$ (AAS standard) as 1000 mg/l solution in 0.5 M HNO_3 was procured from Merck (India) Limited. All other chemicals used in the experiments were of analytical grade. Deionized water used for all the experiments was obtained from Milli-Q (Millipore Corporation, USA) water purification system.

Preparation of CTPP Beads

Detailed description on the preparation of chitosan tripolyphosphate (CTPP) beads by ionic cross-linking of chitosan and STPP is presented in our previous reports (19,20). Briefly, chitosan (20 g/L) solution prepared in dilute acetic acid (1% v/v) was dropped into tripolyphosphate solution (100 g/l) at moderate stirring of 100 rpm. The beads were prepared at the original pH of the STPP solution (pH = 8.6) in order to obtain beads of lower cross-linking density. The beads were cured for 12 hours, separated by filtration, washed four times with deionized water, and air dried before use in adsorption experiments.

Preparation of HA-CTPP Beads

Dip coating on the wet CTPP beads were employed for the preparation of HA-CTPP beads. Wet CTPP beads, prepared as described in the previous section, were placed into 500 mL of humic acid solution containing 5 g of humic acid. A solution pH = 10 was used for the HA solution to improve the solubility of HA. The beads were stirred in the HA solution for 12 hours, filtered, and washed five times before drying at 50°C in an air oven. Concentration of the unused humic acid in the solution after removal of the beads was estimated using UV-Visible spectroscopy at 400 nm in order to get an estimate of the HA coated onto CTPP beads. From the total weight of the dried HA-CTPP beads and the total HA consumed in the preparation process, it is estimated that the composition of HA in the final dried beads is 43% (w/w).

Characterization of CTPP and HA-CTPP Beads

Surface morphology of the beads was obtained using Scanning Electron Microscope (Model no. AIS 2100, Seron Inc.). FTIR spectra of the powdered CTPP and HA-CTPP beads were recorded on JASCO 4000 FTIR spectrophotometer using KBr pellet method. Swelling studies of the CTPP and HA-CTPP beads were carried out in deionized water for 24 hours by equilibrating the beads at selected pH. After equilibration the beads were separated, excess water was removed using tissue paper, and the final weight was obtained. Swelling capacity of the beads was calculated using the expression:

$$SP = \left[\frac{W_f - W_i}{W_i}\right] \times 100 \tag{1}$$

where W_f is the weight of the beads after equilibration with water for 24 hours and W_i is the original weight of the dried beads.

In order to estimate the stability of HA-CTPP beads in aqueous solution, 100 mg of dried HA-CTPP beads were equilibrated in 100 mL of water after adjusting the initial pH in the range of 1–8 using dilute NaOH or HCl. After 24 hours of equilibration, HA released from the beads to the aqueous medium were measured using UV visible spectroscopy at 400 nm(UNICAM UV500, Thermo electron corporation, USA).

Sorption of Pb(II) on CTPP and HA-CTPP Beads

For batch equilibration studies, experimental solutions containing fixed concentration of Pb(II) and the adsorbent were adjusted to the required pH and equilibrated in a 100 mL Erlenmeyer flask at 250 rpm using a horizontal orbital shaker. Temperature during the adsorption experiments were controlled at 25 +/−0.5°C. All pH adjustments were carried out with 1 M HNO_3/NaOH. After fixed time of equilibration, concentration of the dissolved Pb(II) ions were estimated using ICP-AES (ICP-AES, Model JY 238 Ultrace, Jobin-Yvon, France). The amount of Pb(II), adsorbed onto the bead at time t, was calculated using the expression:

$$q_t = \frac{(c_0 - c_t)}{w} V \tag{2}$$

where q_t (mg/g) is the quantity of Pb(II) adsorbed onto the bead at time t (hrs), C_0 is the initial concentration (mg/L) of Pb(II) used in the experiment, C_t is the measured concentration (mg/L) of Pb(II) presented in the liquid phase after equilibration time t; V is the volume of the solution(L), and w is the mass of the dried beads (g) used in the experiment.

RESULTS AND DISCUSSION

Characterization

Formation of CTPP and HA-CTPP Beads

Cross-linked CTPP beads are formed by the ionic cross-linking between protonated amino groups of chitosan and ionized phosphate groups of tripolyphosphate (20). Cross-linking is essential to bring required mechanical stability to chitosan, though this procedure is expected to decrease its inherent metal sorption capacity, due to partial utilization of the amino groups in the cross-linking process. After drying, CTPP beads were yellowish white in color whereas HA-CTPP beads were uniformly black, clearly indicating complete surface coverage of CTPP beads by HA. In both the cases, dried beads were nearly spherical in shape with average size of 500 micron. A very interesting observation in this study is that the amount of HA incorporated onto CTPP is significantly higher than that reported by other researchers using chitosan derivatives (21,22). This could be ascribed to two reasons. Earlier attempts were made to remove HA from water at environmental concentrations and thus used significantly lower initial HA concentrations in equilibrium studies. At those lower HA concentrations, HA may be present in a different three-dimensional structure than that of high HA concentrations used in the present work, which lead to the significant difference in loading onto the adsorbent. Alternatively, this difference also could be due to the inherent difference in the sorption property of the adsorbent itself. Interestingly, it should be noted that very high sorption capacity for HA (377 mg/g) was reported using another ionic cross-linked chitosan derivative, chitosan-H_2SO_4 beads (23). A widely accepted model structure of HA(1) is presented in Fig. 1. From the structure it can be concluded that at the experimental pH used in the present preparation, due to the ionization of its carboxylic and phenolic functional groups, HA is expected to be present as negatively charged species. Similarly, the phosphate and amino groups of CTPP are also expected to be either neutral or negatively charged. Since both the adsorbent and the adsorbate carry a net negative charge, HA coating onto CTPP beads cannot be assigned to ionic bond formation. Most probably other mechanism such as van der Waals interaction and other electrostatic forces such as hydrogen bonding may be responsible for the deposition of HA onto CTPP beads. A visual observation of the HA-CTPP beads, after smooth cutting, showed dark color penetrating into the beads indicating that HA is not just surface adsorbed alone, but diffuses into the bulk of the CTPP beads. Similar diffusion of HA into the bulk of calcium alginate beads were earlier reported (24) using fluorescence intensity measurements.

SEM Images of the CTPP and HA-CTPP Beads

SEM images of the beads are presented in Fig. 2. The CTPP bead surface is seen to be smooth (Fig. 2a), whereas the presence of HA as a rough coating is clearly visible in case of HA-CTPP bead (Fig. 2b). At higher resolution, the relatively highly porous structure of the HA coated beads is clearly distinguishable form the nearly uniform surface of the CTPP beads (Figs. 2c–2d).

FTIR Spectra of CTPP and HA-CTPP Beads

Though the incorporation of HA into the CTPP beads was visually observable, further characterization of the beads were done using FTIR spectroscopy. Spectra of CTPP and HA-CTPP beads are shown in Fig. 3. The peaks at 1461.8 cm^{-1} which can be assigned to the phenolic groups of the original HA is present in HA-CTPP beads also, showing clear indication of the incorporation of HA onto HA-CTPP beads. No peaks around 1720 cm^{-1} corresponding to C=O stretching of the –COOH groups, typically observed in the spectrum of HA samples, were visible in the spectrum of HA-CTPP specimen, and probably this characteristic peak might have been masked by the broad

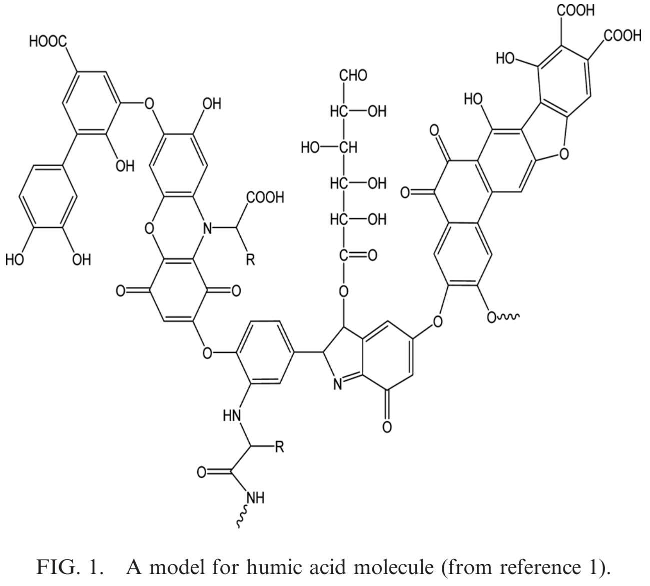

FIG. 1. A model for humic acid molecule (from reference 1).

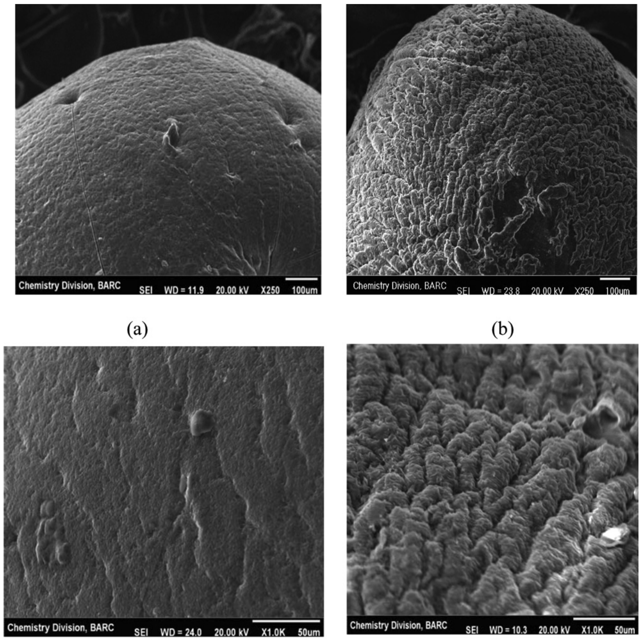

(a) (b)

(c) (d)

FIG. 2. SEM images of CTPP (a) and HA-CTPP (b) bead surface taken at magnification of 250 times; (c) and (d) presents the same surface at 1000 times magnification.

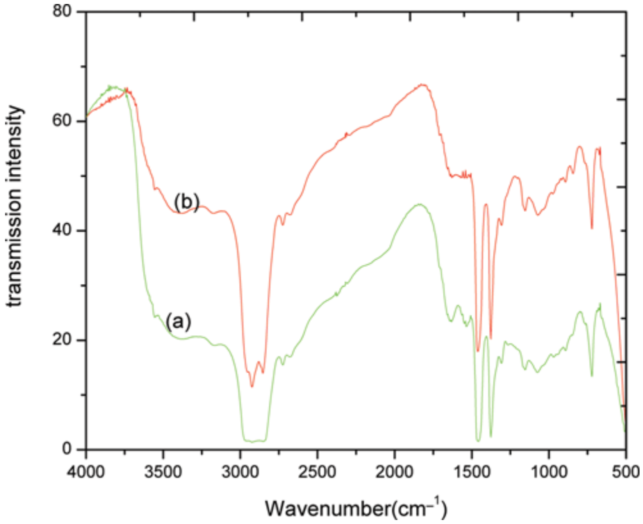

FIG. 3. FTIR spectra of CTPP (a) and HA-CTPP (b) beads. (Color figure available online)

shoulder observed in the wave-number region 1640 cm^{-1}–1840 cm^{-1}. A comparison of the two spectra shows that there is a shift in the position of individual peaks and/or appearance of new peaks due to the incorporation of HA onto CTPP beads. But the differences are not strong enough to assign a specific type of chemical bonding between HA and chitosan molecules.

Swelling Capacities of CTPP and HA-CTPP Beads

Swelling percentage of the two beads as a function of pH is present in Fig. 4. At any given pH, HA-CTPP beads have less swelling compared to CTPP beads. This is due to the complimentary pH dependant solubility properties of humic acid and chitosan. At lower pH, HA is sparingly soluble and thus acts as a protective layer whereas at higher pH, CTPP itself have less solubility. Less swelling of HA-CTPP beads in aqueous solution indicates that the beads can be equilibrated for an extended period of time and thus practically more suitable for the adsorption purposes than CTPP beads.

Stability of HA-CTPP Beads

For practical application of the beads, the stability of the beads in solution is very important. Stability of the HA coating towards aqueous medium as a function of the pH of the equilibrating medium is presented in Fig. 5. If total HA was eluted out of the beads the final HA concentration expected in the mixture is 430 mg/L. In experiments with pH < 3, concentration of HA in the final solution was below the detection limit. As expected, the dissolution of HA from beads increases with increase in pH. However, for all the pH investigated, the dissolution was negligible in the time range of the experiment, indicating that the beads can be utilized for the adsorption applications. Despite the absence of specific chemical bond formation, the stability of the beads is surprising and most likely due to conformational reasons. Difficulties in re-dissolution of air dried humic acid is already reported and it is ascribed to the irreversible conformational changes taking place upon drying of HA (25).

Pb(II)Adsorption Studies

Effect of pH on Adsorption of Pb(II) on to CTPP and HA-CTPP Beads

Adsorption of Pb(II) ions onto CTPP and HA-CTPP beads were investigated as a function of the solution pH using initial metal ion concentration as 200 mg/L and

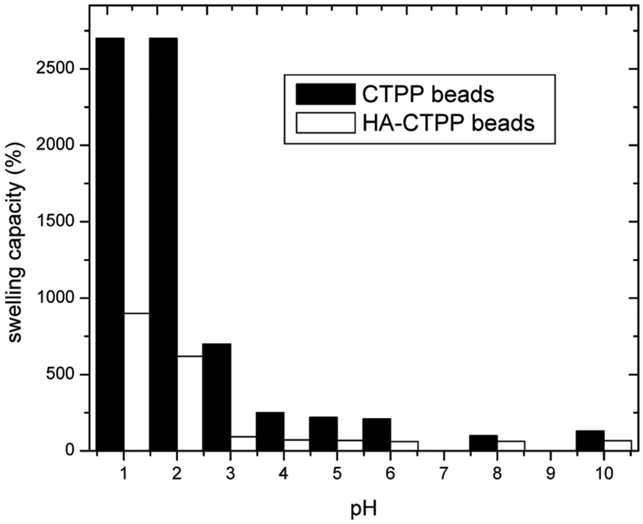

FIG. 4. Swelling capacity of CTPP and HA-CTPP beads as a function of pH; (equilibration time 24 h; T = 25°C).

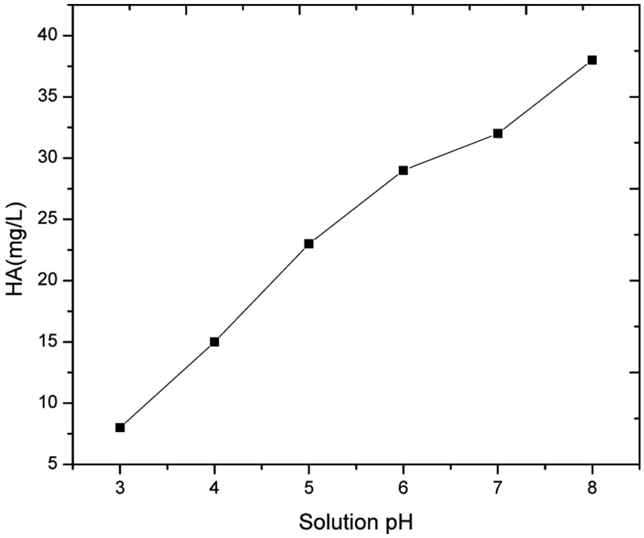

FIG. 5. Leaching of HA from HA-CTPP beads as a function of pH; (equilibration time = 24 hours, volume = 100 mL, T = 25°C).

varying the pH from 1–5. No experiments were conducted for pH higher than five, due to the precipitation of Pb(II) ions from solution. The experimental results (Fig. 6) show that at any given pH, HA-CTPP beads have significantly higher sorption capacity than CTPP beads, which could be assigned to the additional sorption sites provided by the HA. pH dependence on the sorption was different for CTPP and HA-CTPP beads. For CTPP beads, the sorption capacity increased with increase in pH. Similar pH dependence was also reported for sorption of Pb(II) on CTPP beads (26) and the lower sorption capacity at low pH could be due to protonated amino groups which are not available for the binding of positively charged metal ions. In contrast, the sorption capacity of HA-CTPP beads shows a maximum at $\mathrm{pH} = 3$ and thereafter reduced once again. Previous works on metal adsorption onto HA derivatives reported continuous increase in sorption capacity with increase in pH, where it was ascribed to the availability of more ionized anionic functional group at higher pH. One would expect the same behavior in the present case too, where it is evident that HA is primarily responsible for the metal uptake. For both chitosan and HA, the adsorption is found to increase with increase in pH and thus the reduction in Pb(II) adsorption for the HA-CTPP beads at higher pH's cannot be assigned to the electrostatic reasons. One possible explanation is that, due to the reduced swelling of the beads at higher pH, many of the active functional groups of HA are not available for sorption of the metal ions. Cross section of the wet HA-CTPP beads showed that HA is not simply coated on to the surface, but diffused to the bulk of the beads, which could be inaccessible for the bulky Pb(II) ions at higher pH. Higher sorption capacity of HA-CTPP beads in comparison to CTPP beads at all pH showed that the former is a better adsorbent for sorption of Pb(II) ions from aqueous media and thus further investigations were limited to HA-CTPP beads.

Adsorption Kinetics

To understand the effect of contact time on Pb(II) adsorption onto HA-CTPP beads, experiments were conducted with 100 mL of solution having 200 mg/L Pb(II) ions and 100 mg of adsorbent. 100 µL of the sample was analyzed at various intervals to estimate the concentration of dissolved Pb(II) as a function of equilibration time. Figure 7 shows that the adsorption process is rapid, reaching the equilibrium in 4–6 hours. The equilibration time for adsorption of Pb(II) onto HA-CTPP beads are higher than that reported for sorption of Pb(II) onto CTPP beads (26) and HA immobilized on rectorite (27), possibly due to the large size of macro sized beads used in the present investigation. Pseudo-first order, pseudo-second order, and intraparticle diffusion models were applied to analyze the experimentally observed kinetic data (28,29). Among the three tested models, the pseudo-second order model is found to fit the experimental data than other kinetic models. Linear form of the pseudo second order model can be expressed as:

$$\frac{t}{q_t} = \frac{1}{k_2 q_e^2} + \frac{t}{q_e} \tag{3}$$

where q_e (mg/g) and q_t (mg/g) are the quantity of metal ion adsorbed onto the adsorbent at equilibrium and time t,

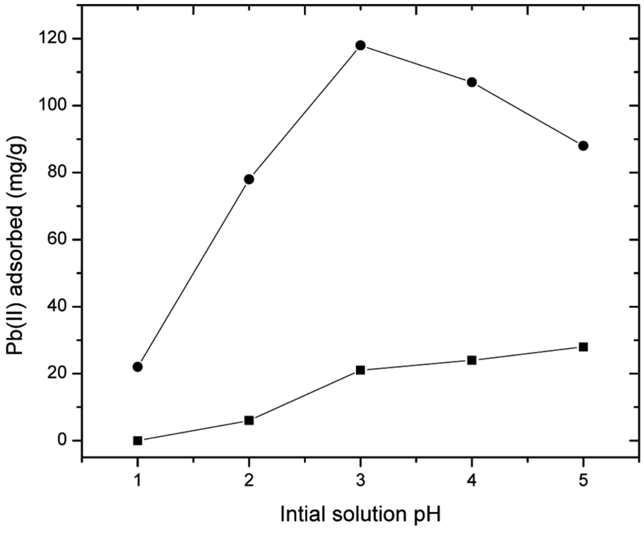

FIG. 6. Effect of pH on adsorption of Pb(II) ions onto CTPP (■) and HA-CTPP (●) beads; (adsorbent = 100 mg, Pb(II) ions = 200 mg/L, volume = 100 mL; T = 25°C).

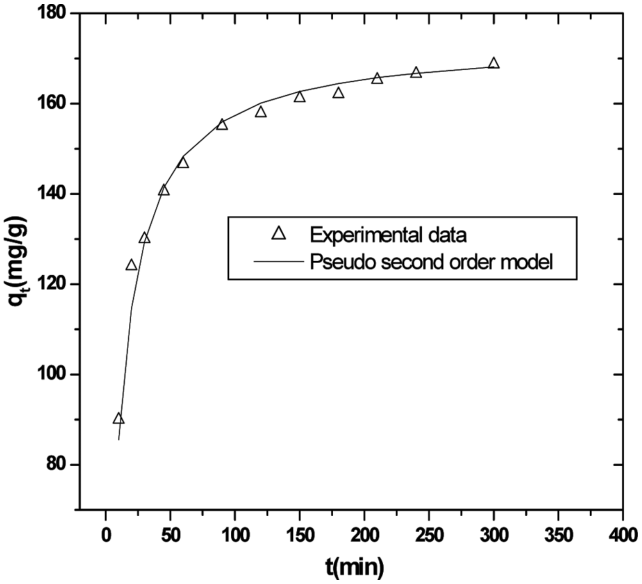

FIG. 7. Effect of contact time of Pb(II) sorption onto HA-CTPP beads; (HA-CTPP = 100 mg, Pb(II) ions = 200 mg/L, volume = 100 mL; T = 25°C).

respectively, and k_2 is the rate constant ($g \cdot mg^{-1} \cdot hour^{-1}$) of the pseudo-second order kinetic model. Very good fit of the observed and experimental data (Fig 7) shows that adsorption of Pb(II) ions onto HA-CTPP beads can very well be described using pseudo-second order kinetic model. The fact that the adsorption depends on the concentration of both the components also indicates that chemical forces such as complex formation are involved in the uptake of Pb(II) ions by the adsorbent.

Effect of Pb(II) Ion Concentration and Adsorption Isotherm

The relation between the adsorbed amount and the equilibrium concentration in the aqueous phase is very important in optimizing the sorption process and understanding the sorption behavior. For investigating the effect of Pb(II) concentration on the adsorption of Pb(II) onto HA-CTPP beads, experiments were conducted with 100 mL solutions having initial Pb(II) concentration varying from 50 mg/L to 800 mg/L and a fixed mass of 100 mg of adsorbent, after adjusting the initial pH = 3 for all experimental solutions. Figure 8 shows the amount of Pb(II) adsorbed at equilibrium verses Pb(II) concentrations remaining in solution at equilibrium. The adsorption curve shows the typical behavior of saturated adsorption, where the entire sorption sites are consumed at higher metal ion concentration and adsorption capacity reaches a limiting value. The steep slope at the initial stage in the adsorption curve is a desirable feature of the sorption system and the results indicate that the HA-CTPP bead is an efficient adsorbent for Pb(II), even at lower concentration of metal ions.

Adsorption data were further analyzed using usually employed isotherm models (30) in order to understand the nature of adsorption of Pb(II) on to the HA-CTPP beads. The simplest adsorption model is the Langmiur isotherm in which it is assumed that the adsorbate form a monolayer on the adsorbent surface and the adsorption energy decreases as the distance from the surface increase, making multilayer adsorption process less favorable. The non- linear form of the Langmuir isotherm can be expressed as:

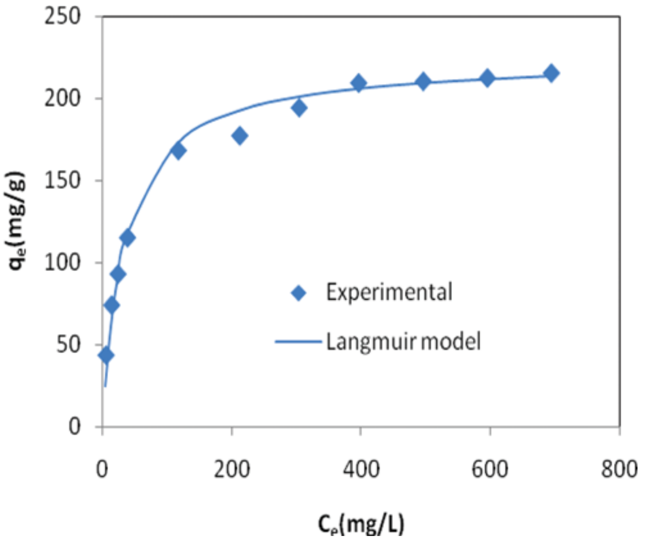

FIG. 8. Effect of Pb(II) ion concentration on adsorption onto HA-CTPP beads. (HA-CTPP = 100 mg, pH = 3, volume = 100 mL; T = 25°C). (Color figure available online)

$$q_e = \frac{bQc_e}{1 + bc_e} \tag{4}$$

where q_e is the amount of metal ion adsorbed at equilibrium (mg/g), c_e is the equilibrium metal ion concentration remaining in solution, Q (mg/g) is the amount of metal ion adsorbed at complete monolayer coverage, and b is the Langmiur constant related to the affinity of the binding site (mL/mg). The monolayer adsorption capacity, Q and the Langmiur constant b can be obtained from the linear plot of $\frac{c_e}{q_e}$ against c_e. Another commonly used adsorption model is the Freundlich isotherm which is an empirical model used to explain the adsorption on heterogeneous surfaces. The Freundlich isotherm can be expressed as:

$$q_e = k_F \times c_e^{1/n} \tag{5}$$

where k_F (mg/g) and n are Freundlich constants related to adsorption capacity and adsorption intensity respectively, and can be obtained from the linear plot of ln q_e against ln c_e. The model parameters obtained by applying both the Langmuir and Freundlich models to the experimental data are given in Table 1. From the better correlation coefficient and the fact that the equilibrium adsorption capacity (Q) obtained from the Langmiur model (223 mg/g) is close to the experimentally observed saturation capacity (215 mg/g), it can be concluded that the monolayer Langmiur adsorption isotherm is more suitable to explain the adsorption of Pb(II) ions onto HA-CTPP beads.

TABLE 1
Model constants and correlation coefficients for adsorption of Pb(II) onto HA-CTPP beads

Isotherm model	Value
Langmiur	
Q (mg/g)	223.7
b (L/mg)	0.029
R^2	0.998
Freundlich	
k_F (mg/g)	40.4
N	3.72
R^2	0.963

TABLE 2
Adsorption of Pb(II) ions onto various humic acid based adsorbents

Adsorbent material	Isotherm	pH	Adsorption capacity	Reference
SiO_2-HA	E	7	34.65	(31)
HA-Rectorite composite	L	5.3	34.96	(27)
HA gel	L	1–4	353.6	(32)
HA gel	E	4	455.5	(33)
IHA	L	4	33.2	(16)
HA-gel	E	5	382.7	(17)
HA-gel/solid HA	E	1.5–5.4	220–262	(34)
HA-CTPP beads	L	3	223	present work

E = experimental sorption capacity; L = Langmuir model.

Reported sorption capacities for humic acid based adsorbents for Pb(II) ions from aqueous media is presented in Table 2. Adsorption capacity of HA-CTPP beads reported here is significantly higher than most other solid or insoluble HA reported in literature. In comparison to HA gel, HA-CTPP beads show slightly lower sorption capacity. As discussed earlier at pH = 3, CTPP beads show nearly 20 percent of the adsorption capacity of HA-CTPP beads. This indicates that the sorption of Pb(II) ions onto HA-CTPP beads can be largely assigned to HA present in the HA-CTPP beads. Taking into account the fact that only less than fifty percentage of HA is present in the HA-CTPP beads, it can be concluded that the metal uptake capacity of HA in HA-CTPP beads is comparable to that of HA gel reported by Coles and Young (33). After completion of equilibrium, solid-liquid separation can be easily achieved by the use of macro-sized HA-CTPP beads instead of HA-gel and HA powder and thus is a significant advantage in designing HA based industrial separation process.

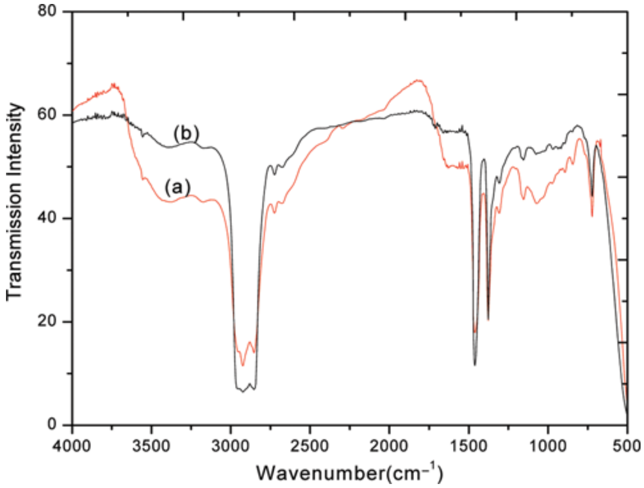

FIG. 9. FTIR spectra of HA-CHTPP (a) and Pb(II) loaded HA-CTPP (b) beads. (Color figure available online)

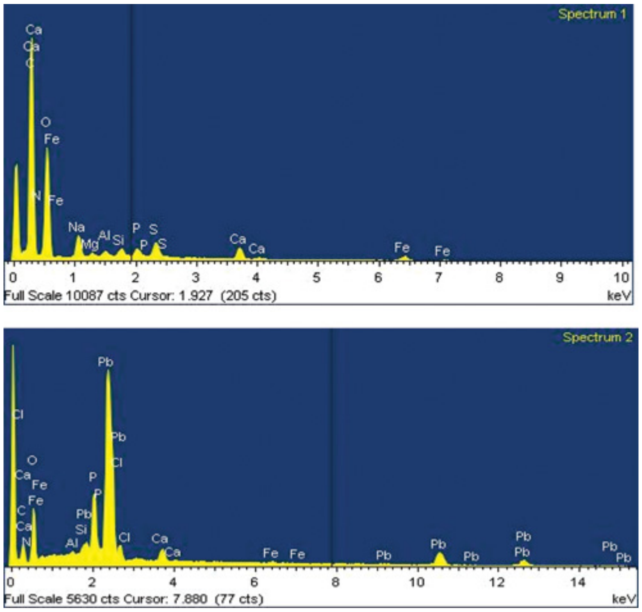

FIG. 10. EDS spectra of HA-CTPP (spectrum1) and Pb(II) loaded HA-CTPP (spectrum 2) beads. (Color figure available online)

Characterization of Pb(II) Loaded HA-CTPP Beads

FTIR spectra of the bare and Pb(II) loaded HA-CTPP beads is present in Fig. 9. A comparison of the two spectra shows that no additional peaks are present in the spectra of Pb(II) loaded material while broad difference can be observed between the two spectra. This indicates that chemical forces are involved in the sorption process though specific functional groups responsible for the uptake cannot be identified using this technique. As explained earlier, metal uptake of HA-CTPP can be largely assigned to HA present in the adsorbent and carboxylic and phenolic groups present in HA could be the probable centers of metal interaction. Comparison of EDS spectra of the bare (spectrum 1) and lead ions loaded HA-CTPP beads (spectrum 2), presented in Fig.10, shows the presence of a significant peak of lead on the latter surface and is a direct evidence for the uptake of Pb(II) ions by HA-CTPP beads.

CONCLUSION

Humic acid coated chitosan tripolyphosphate (HA-CTPP) beads, with high loading of humic acid can easily be prepared by the dip coating of humic acid onto wet chitosan tripolyphosphate beads at alkaline pH. HA-CTPP beads are stable against swelling in aqueous medium in comparison to uncoated CTPP beads. Leaching out of

HA from the HA-CTPP beads is found negligible in the pH range 1–8. HA-CTPP beads has considerably higher sorption capacity for Pb(II) ions than CTPP beads due to the additional adsorption sites provided by humic acid. The kinetics of adsorption of Pb(II) ions onto the HA-CTPP beads follows a pseudo-second order kinetics model and the adsorption data is found to fit into the Langmiur adsorption isotherm. Analysis of adsorption data showed that the HA-CTPP beads is a favorable sorption medium for Pb(II) ions and presumably could be applied for other toxic metal ions also.

ACKNOWLEDGEMENTS

The authors are grateful to Dr. D.N. Sharma, Associate Director, HS&E Group, BARC, Mumbai, for his keen interest in the progress of the work. Sincere thanks to Shri S.K Prasad, Head, RHC Section, RSSD and Dr. R.K Gopalakrishnan for their support during the course of this research project.

REFERENCES

1. Stevenson, F.J. (1994) *Humic Substances, Genesys, Composition, and Structure*, 2nd Ed.; John Wiley and Sons: NewYork.
2. Gabbour, E.A.; Davies, G. (Eds.) (2002) *Humic Substances: Natures most Versatile Materials*; Taylor and Francis, Inc: New York.
3. Yates, L. M.; Von Wandruszka, R. (1999) Decontamination of polluted water by treatment with a crude humic acid blend. *Environ. Sci. Technol.*, 33: 2076.
4. Bogush, A.A.; Voronin, V.G. (2011) Application of a peat-humic agent for treatment of acid mine drainage. *Mine Water Environ.*, 30 (3): 185.
5. Celebi, O.; Kilikli, A.; Erten, H.N. (2009) Sorption of radioactive cesium and barium ions onto solid humic acid. *J Hazard. Mater.*, 168 (2–3): 695.
6. Klavins, M.; Eglıte, L. (2002) Immobilisation of humic substances. *Colloids and Surfaces A: Physicochemical and Engineering Aspects*, 203: 47.
7. Zhang, Y.; Li, Q.; Sun, L.; Tang, R.; Zhai, J. (2010) High efficient removal of mercury from aqueous solution by polyaniline/humic acid nanocomposite. *J. Hazard. Mater.*, 175: 404.
8. Anirudhan, T.S.; Suchithra, P.S. (2010) Heavy metals uptake from aqueous solutions and industrial wastewaters by humic acid-immobilized polymer/bentonite composite: Kinetics and equilibrium modeling. *Chem. Eng. J.*, 156: 146.
9. Hankins, N.P.; Lub, N.; Hilal, N. (2006) Enhanced removal of heavy metal ions bound to humic acid by polyelectrolyte flocculation. *Sep. Sci. Technol.*, 51: 48.
10. Baek, K.; Yang, J.W. (2005) Humic substance enhanced ultrafiltration for the removal of heavy metals. *Sep. Sci. Technol.*, 40 (1–3): 699.
11. Yuan, W.; Zydney, A.L. (2000) Humic acid fouling during ultrafiltration. *Environ. Sci. Technol.*, 34: 5043.
12. Hilal, N.; Al-Abri, M.; Al-Hinai, H.; Somerfield, C. (2008) Combined humic substance and heavy metals agglomeration, and membrane filtration under saline conditions. *Sep. Sci. Technol.*, 43 (6): 1488.
13. Koopal, L.K.; Yang, Y.; Minnaard, A.J.; Theunissen, P.L.M.; Van Riemsdijk, W.H. (1998) Chemical immobilization of humic acid on silica. *Colloid. Surf. A. Physicochem. Eng. Aspects*, 141: 385.
14. Jing, F.; Zong, S., Gui, B. (2008) Coating Fe_3O_4 magnetic nanoparticles with humic acid for high efficient removal of heavy metals in water. *Environ. Sci. Technol.*, 42: 6949.
15. Seki, H.; Suziki, A. (1995) Adsorption of heavy metal ions onto insolubilised humic acid. *J Coll. Inter Sci.*, 171: 490.
16. Havelcova, M.; Mizeraa, J.; Sykorova, I.; Pekar, M. (2009) Sorption of metal ions on lignite and the derived humic substances. *J Hazard. Mater.*, 161: 559.
17. Baker, H., Khalili, F. (2004) Analysis of the removal of lead(II) from aqueous solutions by adsorption onto insolubilized humic acid: Temperature and pH dependence. *Anal. Chim. Acta*, 516: 179.
18. Seki, H.; Suziki, A.; Kashiki, I. (1990) Adsorption of lead(II) ions on immobilized humic acid. *J Coll. Inter Sci.*, 130: 59.
19. Das, D.; Sureshkumar, M.K.; Radhakrishnan, K.; Nuwad, J.; Pillai, C.G.S. (2011) Adsorptive removal of Cr(III) from aqueous solution using,tripolyphosphate cross-linked chitosan beads. *J. Radioanal. Nucl. Chem.*, 289: 275.
20. Sureshkumar, M.K.; Das, D.; Mallia, M.B.; Gupta, P.C. (2010) Adsorption of uranium from aqueous solution using chitosan-tripolyphosphate; (CTPP) beads. *J. Hazard. Mater.*, 184: 65.
21. Wan Ngah, W.S.; Musa, A. (1998) Adsorption of humic acid onto chitin and chitosan. *J. App. Poly. Sci.*, 69: 2305.
22. Sun, X.F.; Wang, S.G.; Liu, X.W.; Gong, W.X.; Bao, N.; Ma, Y. (2008) The effects of pH and ionic strength on fulvic acid uptake by chitosan hydrogel beads. *Colloid. Surf. A. Physicochem. Eng. Aspects*, 324 (1–3): 28.
23. Ngah, W.S.; Fatinathan, S.; Yosop, N.A. (2011) Isotherm and kinetic studies on the adsorption of humic acid onto chitosan-H_2SO_4 beads. *Desalination*, 272: 293–300.
24. Pandey, A.K.; Pandey, S.D.; Misra, V.; Santha Devi (2003) Role of humic acid entrapped calcium alginate beads in removal of heavy metals. *J. Hazard Mater.*, B98: 177.
25. Klucakova, M.; Pekar, M. (2008) Behaviour of partially soluble humic acids in aqueous suspension. *Colloids and Surfaces A: Physicochem. Eng. Aspects*, 318: 106.
26. Wan Ngah, W.S.; Fatinathan, S. (2010) Adsorption characterization of Pb(II) and Cu(II) ions onto chitosan-tripolyphosphate beads: Kinetic, equilibrium, and thermodynamic studies. *J. Environ. Manag.*, 91: 958.
27. Tanga, Y.; Yub, F.; Chen, F.; Chen, C. (2011) Research on adsorption of Pb2+ on to microspheres prepared by rectorite and humic acid. *Adv. Mater. Res.*, 233–235: 1972.
28. Ho, Y.S.; Mckay, G. (1999) Pseudo-second order model for sorption processes Process. *Biochem.*, 34: 451.
29. Azizian, S. (2004) Kinetic models of sorption: A theoretical analysis. *J. Colloid and Interface Sci.*, 276: 47.
30. Senthil Kumar, P.; Ramalingam, S.; Abhinaya, R.V.; Thiruvengadaravi, K.V.; Baskaralingam, P.; Sivanesan, S. (2011) Lead(II) adsorption onto sulphuric acid treated cashew nut shell. *Sep. Sci. Technol.*, 46 (15): 2436.
31. Stathi, P.; Deligiannakis, Y. (2010) Humic acid-inspired hybrid materials as heavy metal absorbents. *J Colloid and Interface Sci.*, 351: 239.
32. Cezıkov, J.; Kozler, J.; Madronova, L.; Novak, J.; Janos, P. (2001) Humic acids from coals of the North-Bohemian coal field. II. Metal-binding capacity under static conditions. *React. Funct. Polym.*, 47: 111.
33. Coles, C.A.; Yong, R.N. (2006) Humic acids preparation, properties and interactions with metals: lead and cadmium. *Eng. Geol.*, 85: 26.
34. Martyniuk, M.; Wieckowska, J. (2003) Adsorption of metal ions on humic acids extracted from brown coals. *Fuel Process. Technol.*, 84: 23.

J Radioanal Nucl Chem (2011) 289:275–285
DOI 10.1007/s10967-011-1074-2

Adsorptive removal of Cr(III) from aqueous solution using tripolyphosphate cross-linked chitosan beads

Debasish Das · M. K. Sureshkumar ·
K. Radhakrishnan · J. Nuwar · C. G. S. Pillai

Received: 24 March 2011 / Published online: 11 April 2011

Abstract Chitosan tripolyphosphate (CTPP) beads were prepared at two different cross-linking densities and adsorption of Cr(III) onto it were studied as a function of different operational parameters such as solution pH, equilibration time and initial Cr(III) ion concentration. Higher cross-linked beads were found to have more adsorption capacity at all the experimental pH employed ($pH = 3–5$), whereas adsorption capacity is found to increase with increase in pH. Adsorption data were analyzed using Langmuir and Freundlich isotherm models. Langmuir model is found be more suitable to explain the experimental results with a monolayer adsorption capacity of 469.5 mg/g. Among the kinetic models used, pseudo-second order kinetic model could best describe the adsorption process. Competition experiments done in presence of Na(I), Mg(II), Ca(II), Al(III) and Fe(III) revealed that, except in the case of Al(III), adsorption of Cr(III) is not significantly affected by the presence of foreign cations. NaCl is found to be a suitable leaching agent for the desorption of adsorbed Cr(III) from CTPP beads. FTIR spectroscopic investigations confirmed that phosphate groups are the principal binding site responsible for the sorption of Cr(III) onto CTPP beads.

Keywords Adsorption · Chitosan · Chromium(III) · Tripolyphosphate

Introduction

Chromium is significantly present in many of the industrial effluents such as leather tanning, electroplating, textile, metal processing, wood preservatives, paint and pigments, dyeing and steel fabrication. Though chromium can exists in numerous oxidation states, Cr(III) and Cr(VI) are the two most stable ones in aqueous media among which the latter is proved to be more toxic to human being and environment [1]. Regardless, the fact that most of the industrial effluents contain chromium in its trivalent oxidation state and its potential to re-oxidize to Cr(VI) in presence of certain oxidants that are commonly found in soil and water environments [2], there has been increasing concern on the release of Cr(III) into the environment. The permissible limit of Cr(III) in drinking water set by World Health Organization (WHO) is 0.05 mg/L [3] and the effluents of the industries should be reduced to a value lower than it. Traditional method for the removal of Cr(III) is to precipitate it as hydroxide, but is found to have serious drawback due to formation of excessive amount of sludge with long settling times [4]. This lead to the search for alternate technologies for Cr(III) removal and sorption on biomaterial is one such suitable method, which attracted significant interest in recent decades, due to their environmentally benign nature, abundance and low-cost [5, 6].

Chitin is the most abundant biopolymer after cellulose, and its partially deacetylated form, chitosan is found to have excellent sorption capacity for various heavy metals including radionuclides [7, 8]. Chitosan is the copolymer composed of 2-amino-2-deoxy-D-glucopyranose units and

D. Das · K. Radhakrishnan
Fuel Reprocessing Division, Bhabha Atomic Research Centre,
Trombay, Mumbai 400085, India

M. K. Sureshkumar (✉)
Radiation Safety System Division, Bhabha Atomic Research
Centre, Trombay, Mumbai 400085, India
e-mail: smk@barc.gov.in

J. Nuwar · C. G. S. Pillai
Chemistry Division, Bhabha Atomic Research Centre, Trombay,
Mumbai 400085, India

the residual 2-acetamido-2-deoxy-D-glucopyranose units and the metal uptake by it is primarily attributed to the amine and hydroxyl groups present in the polymer chain, which can interact with various metallic species through ion exchange and/or chelation mechanism. Most of the available data on the application of chitosan derivatives for chromium removal deals with the hexavalent chromium [9–14]. In addition, the limited number of studies on the use of chitosan, and its physico-chemically and functionally modified derivatives, for adsorption of Cr(III) from aqueous solution resulted in limited success and contrasting results, with an experimentally observed sorption capacity ranging from 6 mg/g [15] to 85.99 mg/g [16]. This warrants additional research on the use of chitosan derivatives for Cr(III) removal from the industrial effluents. In this communication we report highly enhanced adsorption of Cr(III) on chitosan beads cross-linked with tripolyphosphate as the cross-linking agent, where the newly added tripolyphosphate moiety is found to be responsible for the increase in uptake. Chitosan-tripolyphosphate (CTPP) beads were prepared at two different cross-linking densities and the sorption of chromium(III) onto it were studied as a function of solution pH, contact time and initial Cr(III) ion concentration. Competition effect of few common cations on the sorption of chromium(III) was investigated using binary mixtures. Attempts were also made to identify the sorption sites using infrared spectroscopy technique.

Experimental

Materials

Chitosan (medium molecular weight) and sodium tripolyphosphate ($Na_5P_3O_{10}$) were procured from Aldrich chemical company, USA. As per the manufacturer, the product is 85% deacetylated. Cr(III), Al(III), Fe(III), Ca(II), Mg(II) and Na(I) solutions of required concentrations were prepared by diluting AAS standard nitrate solutions (Merck, Germany) with initial concentration of 1,000 mg/L. Higher concentration Cr(III) solutions were prepared by dissolving appropriate quantity of $Cr(NO_3)_3 \cdot 9H_2O$ (Merck, Germany) in deionized water. All other chemicals used in the experiments were of analytical grade (AR) purity. Deionized water used for all the experiments was obtained from Milli-Q (Millipore Corporation, USA) water purification system.

Preparation and characterization of the CTPP beads

Details of the preparation of higher and lower cross-linked CTPP beads by ionotropic gelation between chitosan and sodium tripolyphosphate is described in our previous paper [17]. The formation of cross-linked CTPP beads by the interaction between phosphate groups of tripolyphosphate and amino group of chitosan is schematically represented in Fig. 1. The beads were cured for 12 h, separated by filtration, washed four times with deionized water and air dried before use in adsorption experiments. Dried beads were spherical and slightly yellowish in colour. The surface morphology of the dried beads was imaged using scanning electron microscope (Model no. AIS 2100, Seron Inc.). Atomic composition on the surface of the beads before and after sorption of chromium is analyzed with energy dispersive X-ray spectroscopy (EDS Model INCA E350, OXFORD Instruments INC, UK). FTIR spectra of the powdered beads before and after adsorption of chromium were recorded using JASCO 6000 FTIR spectrometer as KBr pellets.

Batch adsorption studies

Batch adsorption experiments were conducted in 250 mL Erlenmayers flask with 50 mL solution containing predetermined concentration of the metal ions and the adsorbent. Unless otherwise specified 50 mg of the adsorbent were used in each equilibration experiment. pH of the solutions were adjusted by addition of dilute HNO_3/NaOH as required. Equilibration of the experimental mixtures were carried out at fixed temperature of 298 K, using a temperature controlled orbital shaker at 250 rpm, except the case of kinetic investigation in which case 400 rpm were used to minimize the effect of bulk diffusion and film diffusion on the sorption process [18]. 50–100 μL of the sample was analyzed at specific intervals after sufficient dilution to give a final concentration of approximately 2 mg/L. Cr(III) ion concentrations were measured using inductively coupled plasma atomic emission spectrometer (ICP-AES, Model JY 238 Ultrace, Jobin-Yvon, France). The amount of Cr(III) adsorbed onto CTPP beads was calculated by,

$$q_t = \frac{(c_0 - c_t)}{w} V \tag{1}$$

where, q_t (mg/g) is the quantity of Cr(III) adsorbed on CTPP bead at time t (h), C_0 is the initial concentration (mg/L) of Cr(III) used in the experiment, C_t is the measured concentration (mg/L) of Cr(III) presented in the liquid phase after equilibration time t; V is the volume of the solution (L) and w is the mass of the CTPP beads (g).

Competition and desorption experiments

Competition experiments were carried out using binary mixtures having Cr(III) as one component and one of the

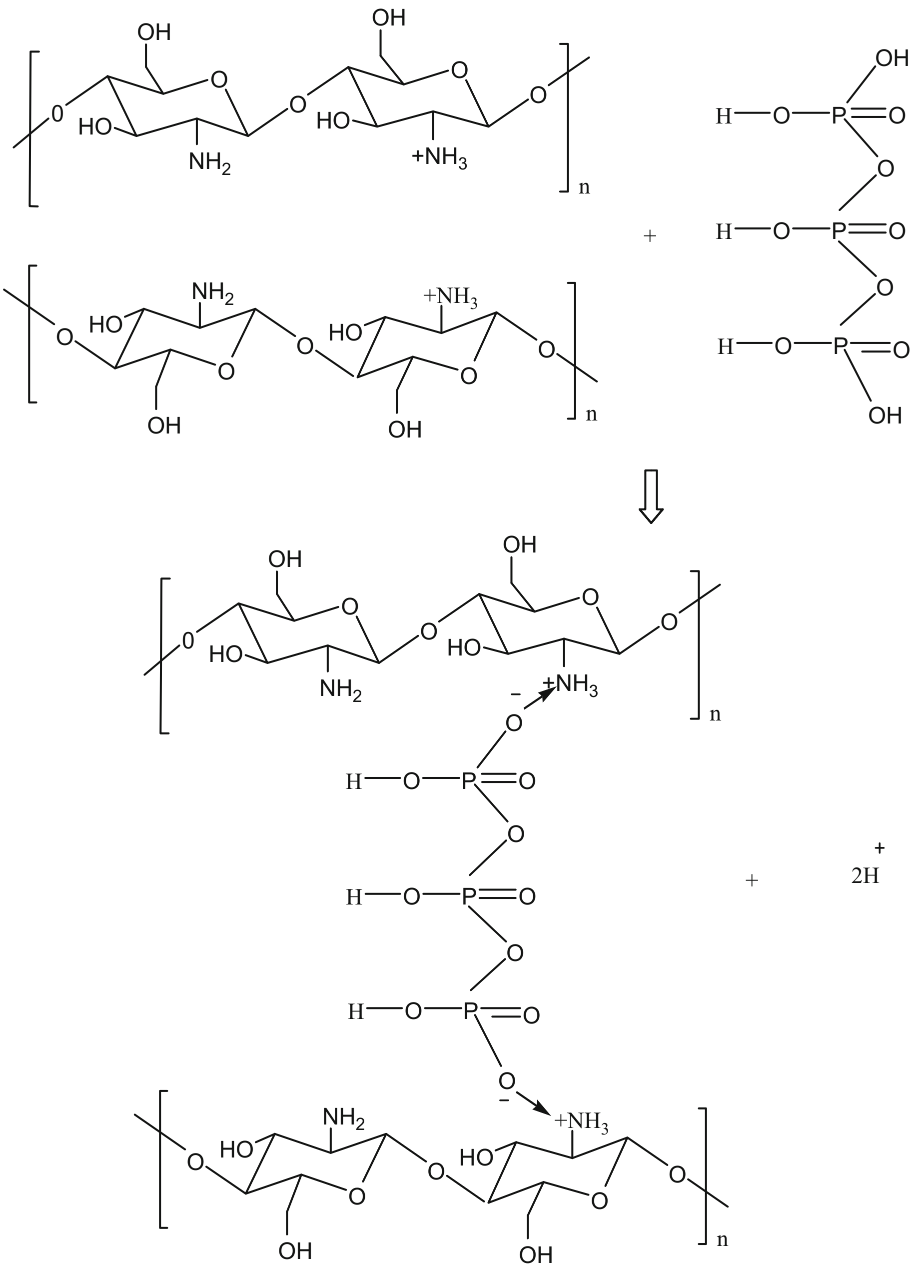

Fig. 1 Schematic representation of cross linking of chitosan with sodium-tripolyphospate

selected cation as the competing ion. Concentration of both the cations were fixed at 100 mg/L. pH of all the experimental mixtures were fixed at 5, except for Al(III) containing mixture, where operational pH = 4 was used due to the hydrolysis of Al(III) at pH above 4. Dissolved concentrations of both the components were analyzed after completing the equilibration for 72 h. For desorption experiments, 400 mg of Cr(III) loaded CTPP beads were prepared under optimum sorption conditions of pH = 5 and equilibration time of 72 h. The Cr(III)-loaded CTPP beads were separated, washed thoroughly with distilled water and air dried. 25 mg of the dried Cr(III) loaded CTPP beads were then equilibrated with 25 mL EDTA or NaCl solutions at three different concentrations i.e. 0.001, 0.01 and 0.1 M and the amount of desorbed Cr(III) ions were determined at specific intervals using ICP-AES. All adsorption and desorption experiments were carried out in duplicates and the average values were taken.

Results and discussion

Characterization of CTPP beads

SEM image of the single bead (Fig. 2a) shows that the bead is spherical in shape with diameter of around 1 mm. The

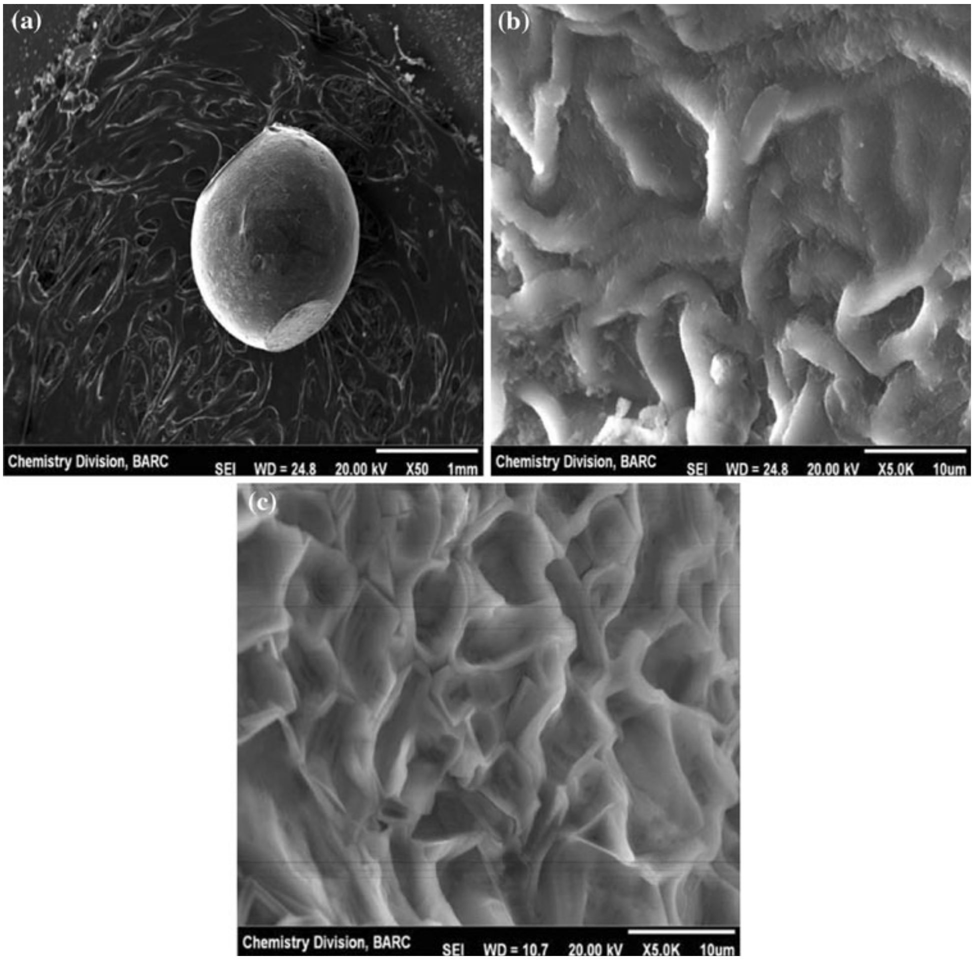

Fig. 2 SEM images of CTPP beads

surface of the original beads (Fig. 2b) is found to be rough and wavy in nature, which is a suitable morphology for an adsorbent to show high adsorption capacity. Due to the adsorption of Cr(III), the CTPP bead surface has undergone significant change in its morphology (Fig. 2c) and clearly visible pores are appeared on the surface. No granular chromium is observed on the surface shows that the sorption is more chemical in nature. The IR spectra of chitosan powder and the CTPP bead are provided in Fig. 3. The main differences in the IR spectra is the additional peak in the CTPP bead spectrum at 1,230 cm^{-1}, which can be assigned to the –P=O stretching vibration indicating the presence of phosphate group in the prepared beads. Peak at 1,694 cm^{-1} corresponding to $-\mathrm{NH}_2$ group and 1,419 cm^{-1} corresponding to –NH deformation vibration of $-\mathrm{NH}_2$ groups, present in the original chitosan spectrum is completely disappeared in the spectrum of CTPP bead, with appearance of a fresh peak at 1,541 cm^{-1} which can be assigned to $-\mathrm{NH}_3{}^+$ [19]. The beads are prepared at pH = 3 where the amino groups are mostly protonated. From the spectral information it can be concluded that the cross-linking is taking place through the ionic interaction between the negatively charged $-\mathrm{P–O}^-$ moieties of the phosphate group and protonated $-\mathrm{NH}_3{}^+$ moieties of the chitosan molecule.

Effect of pH on adsorption

Studies on the effect of pH on Cr(III) adsorption onto CTPP beads were limited to the pH range 3–5. For $\mathrm{pH} < 3$, solubility of the beads were significant and at higher pH ($\mathrm{pH} > 5$) Cr(III) start to precipitate as insoluble $\mathrm{Cr(OH)}_3$ affecting the interpretation of the results. For pH studies, 50 mL of solution containing 200 mg/L of Cr(III) ions were equilibrated with 50 mg of either lower or higher cross-linked CTPP beads. Amount of Cr(III) adsorbed onto CTTP beads in each case were estimated after 24 h of equilibration. The result (Fig. 4) shows that with increase in pH, the amount of Cr(III) adsorbed onto CTPP beads also increases. Speciation data of chromium [20] shows that below pH = 6, chromium(III) is mostly present as positively charged species. With increase in pH, the sorption site on CTPP beads responsible for the metal uptake is increasingly deprotonated, making it favorable for the sorption of positively charged chromium ions. Moreover under identical experimental conditions, beads with higher cross-linking showed higher adsorption capacity for chromium. As inferred from the IR spectra, as a result of cross-linking, phosphate moieties are introduced into the beads at the expense of original amino groups of chitosan which are in-turn used for the ionic cross-linking with tripolyphosphate. If amino groups were the principal functional groups responsible for chromium uptake, for a given pH, lower cross-linked beads should have more sorption capacity in comparison to the higher cross-linked beads. The contrary results indicate that phosphate groups might be the principal site, responsible for Cr(III) uptake. Due to the higher adsorption capacity, beads with higher cross-linking and the optimum pH = 5, were used for further experiments.

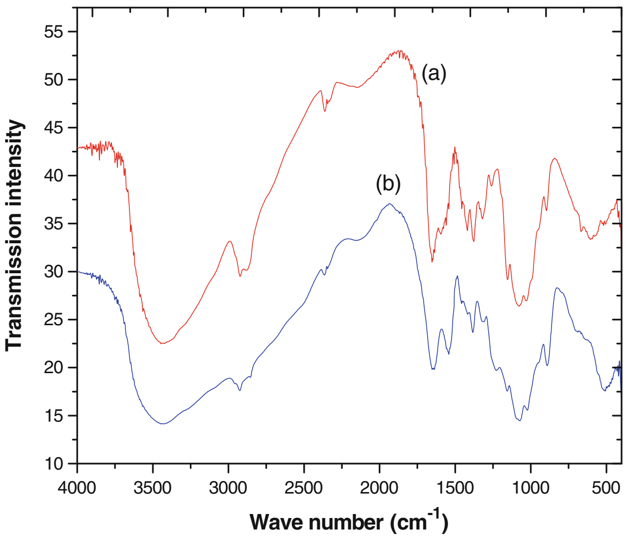

Fig. 3 FTIR spectra of (*a*) chitosan and (*b*) CTPP beads cross-linked at pH = 3

Effect of contact time

To understand the effect of contact time on Cr(III) adsorption onto CTPP beads, experiments were conducted using 100 mL of solution having 200 mg/L Cr(III) and 100 mg of adsorbent. 100 μL of the sample were analyzed at various intervals to estimate the concentration of dissolved Cr(III) as a function of equilibration time. Figure 5 shows that the process is characterized by a rapid adsorption in the initial 4 h of equilibration time, followed by a slow process, leading to equilibrium adsorption in around 3 days. The initial fast sorption might be due to the surface adsorption of Cr(III) on the CTPP beads. During longer stay of the beads in the experimental solution, they become swollen, and the chromium ions are slowly diffused into the bulk of the beads, gradually increasing the adsorption capacity. Other researchers also observed long equilibration time for adsorption of metal ions onto macro-sized CTPP beads [21]. As reported by Ngah [19] it could be possible to reduce the equilibration time using powdered beads instead of the original beads. However for the ease of separation we preferred to use macro-sized beads for the present investigations.

Effect of initial chromium concentration on adsorption

To investigate the effect of initial chromium ion concentration on adsorption, experiments were conducted with 50 mL solutions having initial chromium concentration varying from 10 to 5,000 mg/L and a fixed mass of 50 mg

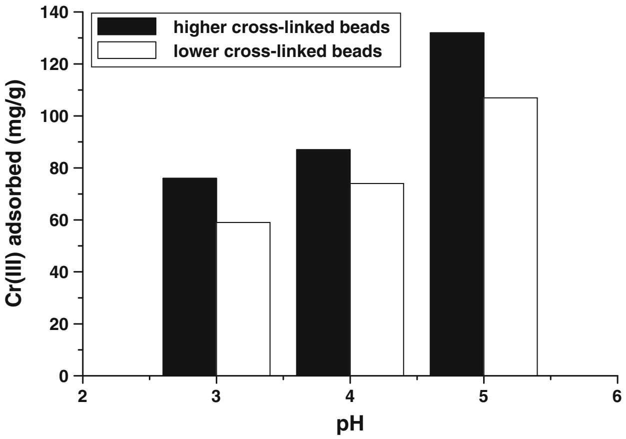

Fig. 4 Effect of pH on the adsorption of Cr(III) on CTPP beads; (volume = 50 mL, Cr(III) = 200 mg/L, CTPP = 50 mg and *T* = 25 °C)

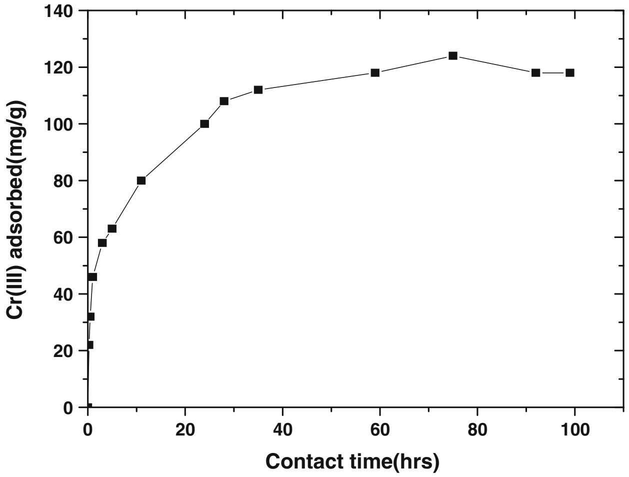

Fig. 5 Effect of contact time on the adsorption of Cr(III) on CTPP beads; (volume = 100 mL, Cr(III) = 200 mg/L, CTPP = 100 mg, pH = 5 and *T* = 25 °C)

of adsorbent. Figure 6 shows the amount of Cr(III) adsorbed onto CTPP beads (mg/g) as a function of initial concentration of Cr(III) ions in solution. As expected, with increase in Cr(III) ion concentration, the adsorption capacity increased and reached a plateau at still higher concentrations. This is the typical behavior of saturated adsorption in which the sorption capacity is limited by the availability of active sites on the adsorbent. The steep slope at initial Cr(III) concentrations is a desirable feature for the sorption system and the results indicate that CTPP bead is an efficient sorbent for Cr(III).

Adsorption isotherm

Adsorption isotherm is fundamental in understanding the type of interaction between the adsorbate and the adsorbent [22, 23]. The Langmuir isotherm, which is the most commonly used isotherm model assumes a monolayer adsorption on to a surface with a finite number of identical sites and is represented as;

$$\frac{c_e}{q_e} = \frac{1}{Qb} + \frac{c_e}{Q} \tag{2}$$

Where, c_e is the equilibrium concentration of metal ions in solution at equilibrium (mg/L), q_e is the amount of Cr(III) ions adsorbed at equilibrium (mg/g), Q is the maximum adsorption capacity of metal ions (mg/g), and b is the Langmuir adsorption equilibrium constant (mL/mg). The Langmuir parameters Q and b can be estimated from the plot of c_e/q_e against c_e (Fig. 7a). The Freundlich isotherm equation, the most important multilayer adsorption isotherm for heterogeneous surfaces, is described as;

$$\log q_e = \log K_F + \frac{1}{n} \log c_e \tag{3}$$

where, c_e is the equilibrium concentration of metal ions (mg/L) in solution, q_e is the amount of metal ions adsorbed (mg/g), K_F is the maximum adsorption capacity of metal ions (mg/g), and n is the adsorption intensity. Freundlich constants, K_F and n, can be determined from a linear plot of $\log q_e$ versus $\log c_e$ (Fig. 7b). The calculated results of the Langmuir and Freundlich isotherm constants are given in Table 1. From the results it can be seen that, the experimental data is best fitted with the Langmuir model and the maximum adsorption capacity (469.5 mg/g) obtained from Langmuir plot is very close to the experimental saturation value (471.0 mg/g). The essential characteristics of the Langmuir isotherm can be expressed in terms of the dimensionless constant, separation factor R_L, which is used to predict if an adsorption system is 'favorable' or 'unfavorable'. The separation factor, R_L is given by,

$$R_L = \frac{1}{1 + bc_0} \tag{4}$$

Where, c_0 is the initial Cr(III) concentration (mg/L) and b is the Langmuir adsorption constant (L/mg). Table 2 lists the calculated results of R_L at different initial Cr(III) ion concentrations. For all the tested Cr(III) concentrations, R_L values are in the range of $0 < R_L < 1$, which indicates that the adsorption of Cr(III) on CTPP beads is a favorable process. The same conclusion can be arrived from the Freundlich constant 'n' in which case a value of n between 1 and 10 indicates the acceptance of the medium as the suitable adsorbent.

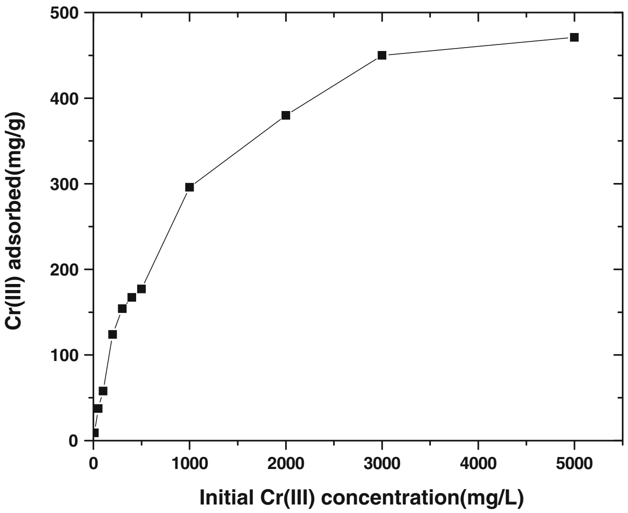

Fig. 6 Effect of initial Cr(III) concentration on adsorption on CTPP beads; (volume = 50 mL, CTPP = 50 mg, pH = 5, and $T = 25$ °C)

Adsorption kinetics

Both pseudo-first order and pseudo-second order kinetic models [24, 25] were applied to analyze the experimentally observed kinetic data. Pseudo-first order kinetic model can be expressed as:

$$\log(q_e - q_t) = \log q_e - \left(\frac{k_1}{2.303}\right)t \tag{5}$$

where, q_e and q_t are the amount of chromium adsorbed on bead (mg/g) at equilibrium and time t (h) respectively, and k_1 is the pseudo-first order rate constant (h^{-1}) for the adsorption of chromium onto CTPP beads. The model parameters q_e and k_1 can be obtained form the linear plot of $\log(q_e - q_t)$ against time (t) (Fig. 8a). Pseudo second order kinetics can be expressed as:

$$\frac{t}{q_t} = \frac{1}{k_2 q_e^2} + \frac{t}{q_e} \tag{6}$$

where, q_e (mg/g) and q_t (mg/g) have the same meaning as earlier and k_2 is the rate constant (g mg^{-1} h^{-1}) of the pseudo-second order kinetic model. The equilibrium

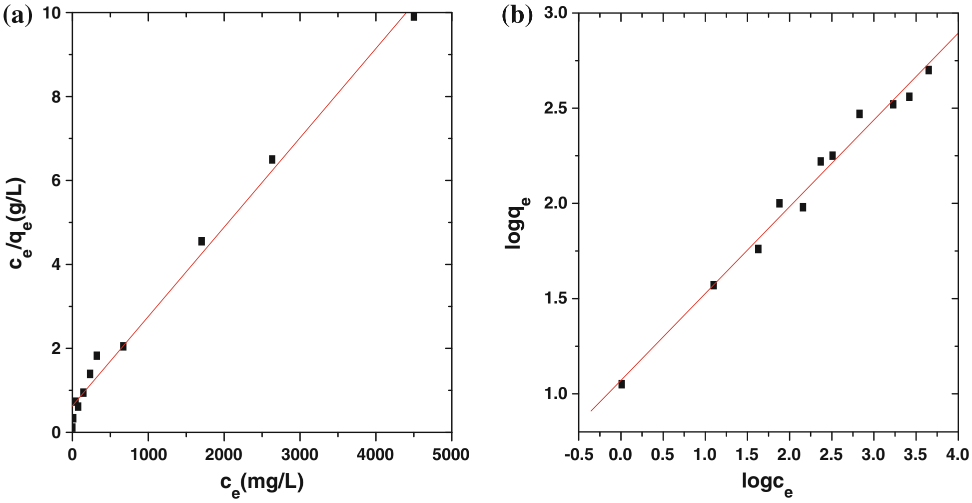

Fig. 7 **a** Langmuir isotherm and **b** Freundlich isotherm plot of adsorption of Cr(III) onto CTPP beads

Table 1 Model constants and correlation coefficients for adsorption of Cr(III) onto CTPP beads

Isotherm model	Value
Langmuir model	
Q (mg/g)	469.5
b (L/mg)	3.4×10^{-3}
R^2	0.9898
Freundlich model	
K_F (mg/g)	12.8
n	2.19
R^2	0.9720

Table 2 R_L values for adsorption of Cr(III) onto CTPP beads

Initial Cr(III) concentration (c_0) (mg/L)	Separation factor (R_L)
10.0	0.967
50.0	0.856
100.0	0.748
200.0	0.597
300.0	0.497
400.0	0.426
500.0	0.372
1000.0	0.229
2000.0	0.129
3000.0	0.090
5000.0	0.056

adsorption capacity q_e and the second order rate constant k_2 can be obtained from the plot of $\frac{t}{q_t}$ against t (Fig. 8b). The model parameters and the equilibrium concentration obtained by both the models are given in Table 3. From the results it can be observed that both pseudo-first and pseudo-second order models are matching with the experimental kinetics data. From the better correlation coefficient and the fact that the equilibrium concentration obtained by the pseudo-second order plot (126.1 mg/g) is more close to the experimental value (124.0 mg/g) than that obtained from the pseudo-first order plot (81.1 mg/g), it can be concluded that pseudo-second order model is more relevant to explain the kinetics of adsorption of Cr(III) on CTPP beads.

Competition of metal ions in binary mixture

Table 4 shows the competitive effect of few selected metal ions on the adsorption of Cr(III) onto CTPP beads. Among the cations studied in competition experiments, Na(I), Mg(II) and Ca(II) have no significant sorption onto CTPP beads and thus does not affect the sorption of Cr(III). Interestingly in Fe(III)/Cr(III) binary system, CTPP beads showed almost equal sorption capacity towards both the metal ions. However adsorption of Fe(III) didn't affect the sorption Cr(III) presumably due to the fact that these metal ions are going to different adsorbing sites of the adsorbent. In presence of Al(III), sorption capacity for Cr(III) is significantly reduced. Al(III) is a small cation, which effectively compete for the same adsorbing sites on the CTPP beads. The results of competition experiments shows that CTPP beads are effective in removing Cr(III) even in presence of other common cations.

Desorption study

Desorption of the loaded adsorbents is essential for the recovery of the metal ions and reuse of the adsorbent. Among the two desorption agents used, NaCl is found to be better than EDTA at all the three concentration studied (Table 5). For NaCl itself, the desorption is found to be

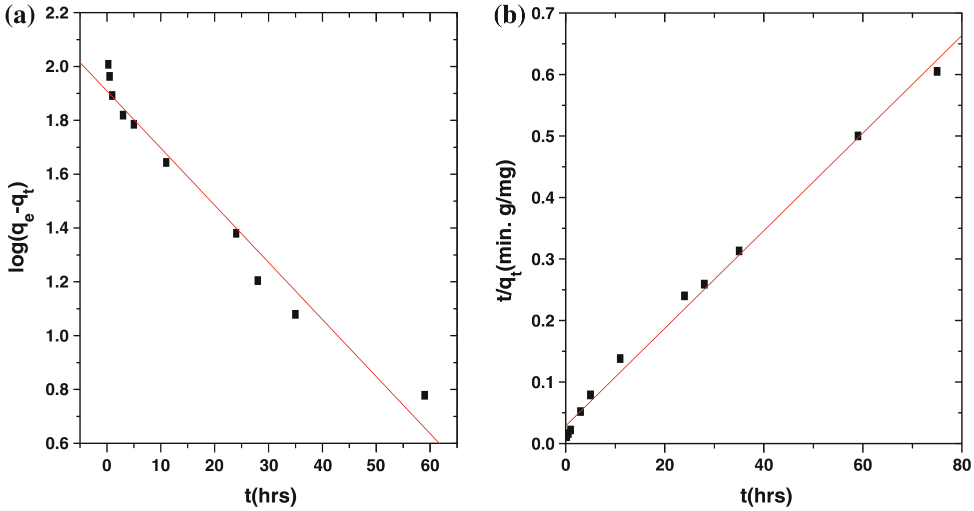

Fig. 8 **a** First and **b** second order kinetic plot of adsorption of Cr(III) onto CTPP beads

Table 3 Kinetics parameters of Cr(III) adsorption onto CTPP beads

Kinetic model						Experimentally observed adsorption capacity (mg/g)
Pseudo-first order			Pseudo-second order			
k_1 (h^{-1})	q_e (mg/g)	R^2	k_2 (g mg^{-1} h^{-1})	q_e (mg/g)	R^2	124.0
0.049	81.1	0.967	21.8×10^{-4}	126.1	0.995	

Table 4 Results of competition experiments

Binary mixture	Metal ions	Initial concentration (ppm)	Final concentration (ppm)	Adsorption capacity (mg/g)
Al(III)–Cr(III)	Al(III)	100	61.2	38. 8
	Cr(III)	100	81.2	18.8
Fe(III)–Cr(III)	Fe(III)	100	42.7	57.3
	Cr(III)	100	39.7	60.3
Ca(II)–Cr(III)	Ca(II)	100	89.5	10.5
	Cr(III)	100	43.1	56.9
Mg(II)–Cr(III)	Mg(II)	100	100.2	–
	Cr(III)	100	53.4	46.6
Na(I)–Cr(III)	Na(I)	100	99.3	–
	Cr(III)	100	47.7	52.3

more efficient at higher concentrations. It is also observed that at higher NaCl concentration, the swelling of the beads are more compared to lower NaCl concentration. Better desorption at higher NaCl concentrations could be attributed to the easy diffusion of the metal ions from the bulk of the beads into the desorbing medium due to its higher swelling. Incidentally it should be noted that the desorption is completed around 72 h, a time scale similar to that required for reaching the adsorption equilibrium, indicating that both desorption and adsorption are slow process probably due to the larger size of the beads used in these investigations.

Characterization of Cr(III) loaded CTPP beads and mechanism of adsorption

EDS analysis of the CTPP beads before and after sorption of Cr(III) (Fig. 9) clearly shows the presence of chromium on the surface of the beads. The residual amino groups of chitosan or the phosphate groups introduced as a result of the cross-linking could be the binding sites for metal ions. FTIR spectra of CTPP beads before and after sorption (Fig. 10) shows that the peak at 1,230 cm^{-1} corresponding to –P=O stretching vibration, originally present in the CTPP beads, is significantly decreased as a result of the

Table 5 Results of desorption studies

Desorption time (h)	Percentage recovery (%)					
	0.001 M EDTA	0.01 M EDTA	0.1 M EDTA	0.001 M NaCl	0.01 M NaCl	0.1 M NaCl
5	1.2	1.6	2.9	1.2	1.4	2.8
14	1.5	2.0	4.9	2.4	3.3	3.9
24	2.4	3.2	6.0	8.4	21.1	32.2
48	4.4	5.0	8.2	20.4	52.0	81.7
72	6.3	7.4	12.5	31.8	97.3	98.7

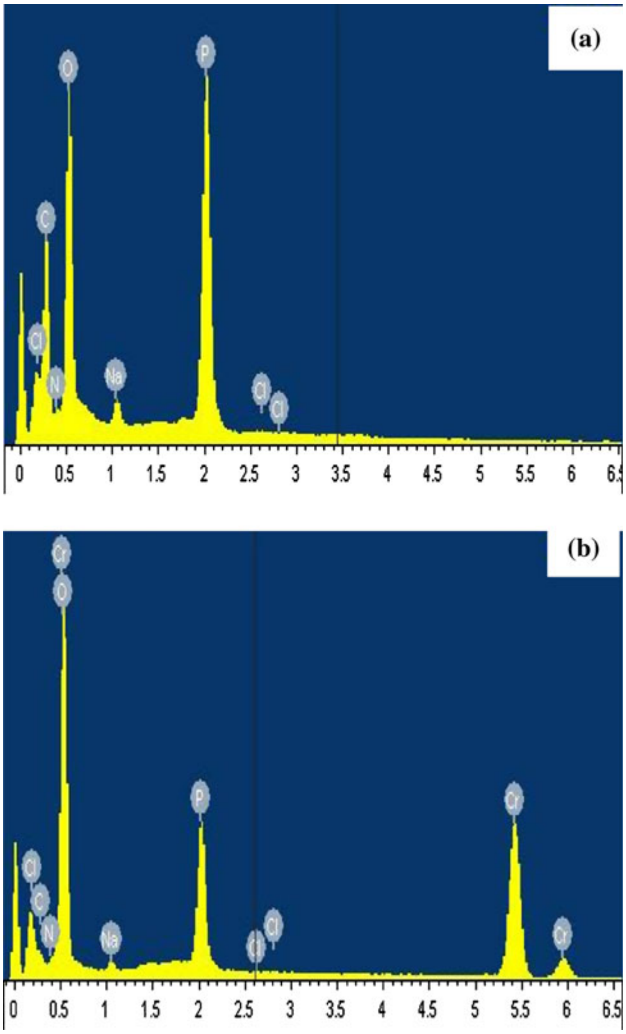

Fig. 9 EDS spectra of CTPP beads **a** before and **b** after adsorption of Cr(III)

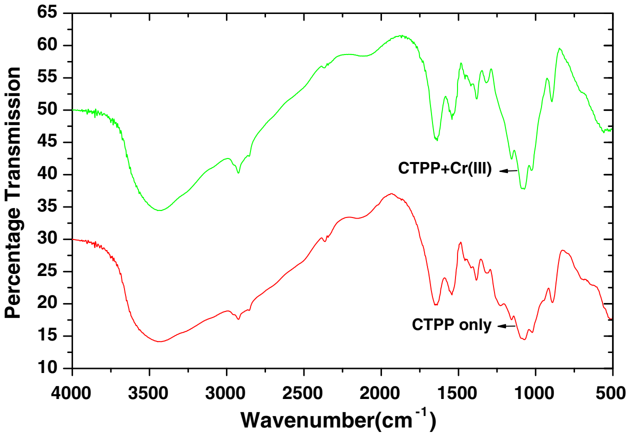

Fig. 10 FTIR spectra of CTPP beads before and after adsorption of Cr(III)

sorption of Cr(III) onto CTPP beads. This indicates that phosphate group is involved in the sorption of Cr(III) onto CTPP beads. No significant change is observed in the peak position of nitrogen and oxygen containing functional groups of the original chitosan moiety signifying their limited role in the sorption process. The fact that higher cross-linked beads have more sorption capacity than the lower cross-linked beads also points to the fact that the density of phosphate groups is decisive in controlling the sorption of Cr(III) on to CTPP beads as depicted in Fig. 11. In an earlier report [26] phosphonic acid functionalized mesoporous adsorbent was reported as good sorbent for Cr(III), were phosphonic acid groups were identified as the adsorption sites using NMR investigations on the Cr(III) loaded adsorbent.

Conclusions

Chitosan tripolyphosphate (CTPP) beads were found to be an efficient adsorbent for Cr(III) in aqueous solutions. Langmuir adsorption model and pseudo-second order kinetics model were found suitable for explaining the experimentally observed adsorption data of Cr(III) onto CTPP beads. Among the different competing cations used along with Cr(III), only Al(III) is found adversely affecting the sorption of Cr(III) onto CTPP beads.

NaCl at different concentrations were found as a suitable leaching agent for the desorption of adsorbed Cr(III). Both

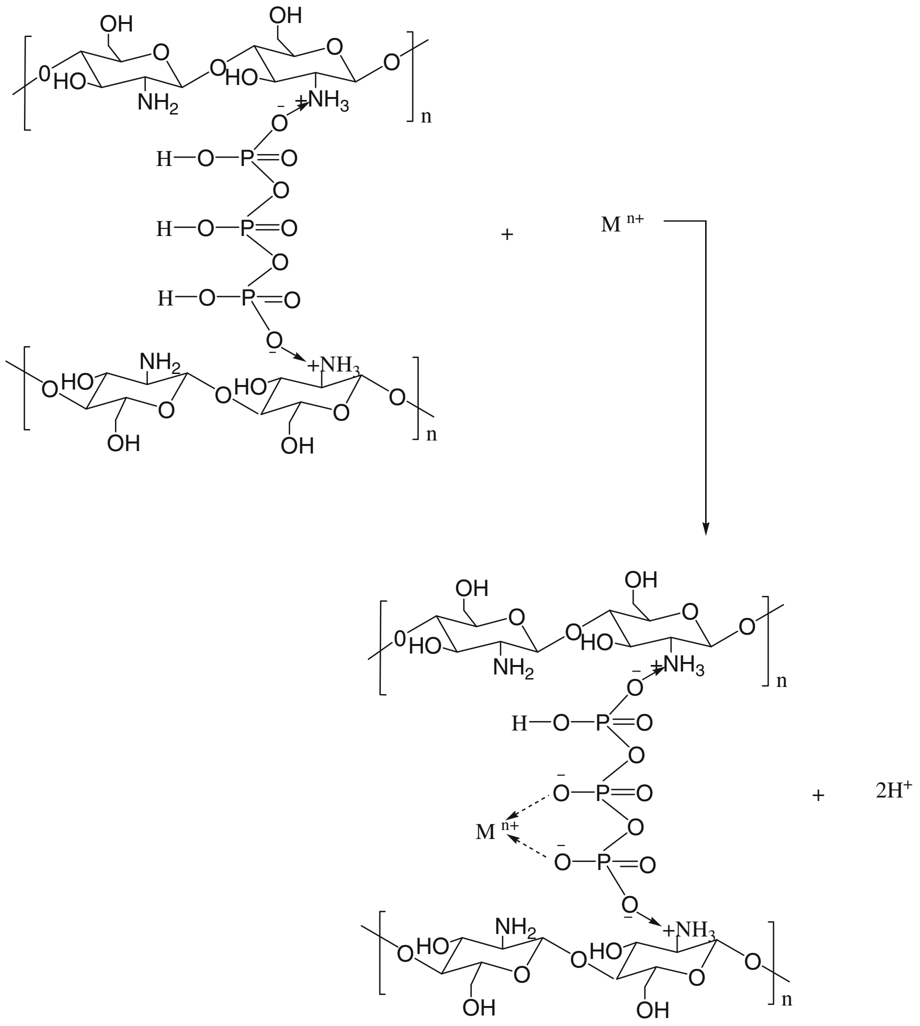

Fig. 11 Schematic presentation of binding of Cr(III) onto CTPP beads

adsorption and desorption were found slow, presumable due to the use of larger sized beads in this study. Structural investigations showed that newly added phosphate groups were the predominant binding sites for sorption of Cr(III) onto CTPP beads.

Acknowledgment The authors are grateful to Dr. D.N. Sharma, Associate Director, Health Safety and Environment group, BARC for constant support for the progress of the work. Sincere thanks to Dr. R.K. Gopalakrishnan for his consent to carry out these studies.

References

1. Nieboer E, Jusys AA (1988) In: Nriagu JO, Nieboer E (eds) Chromium in the natural and human environments. Wiley, New York
2. Sethunathan N, Megharaj M, Smith L, Kamaludeen SPB, Avudainayagam S, Naidu R (2005) Microbial role in the failure of natural attenuation of chromium(VI) in long-term tannery waste contaminated soil. Agric Ecosyst Environ 105:657–661
3. World Health Organization (2008) Guidelines for drinking-water quality, 3rd edn. World Health Organization, Geneva
4. Chakir A, Bessiere J, Kacemi KEL, Marouf B (2002) A comparative study of the removal of trivalent chromium from aqueous solutions by bentonite and expanded perlite. J Hazard Mater 95:29–46
5. Romero-Gonza'lez J, Peralta-Videa JR, Rodri'guez E, Delgado M, Gardea-Torresdey JL (2006) Potential of *Agave lechuguilla* biomass for Cr(III) removal from aqueous solutions: thermodynamic studies. Bioresour Technol 97:178–182
6. Wang LH, Lin CI (2009) Equilibrium study on chromium(III) ion removal by adsorption onto rice hull ash. J Taiwan Inst Chem Eng 40:110–112
7. Miretzky P, Cirelli AF (2009) Hg(II) removal from water by chitosan and chitosan derivatives: a review. J Hazard Mater 167:10–23
8. Laus R, Costa TG, Szpoganicz B, Favere VT (2010) Adsorption and desorption of Cu(II), Cd(II), and Pb(II) ions using chitosan cross-linked with epichlorohydrin—tripolyphosphate as the adsorbent. J Hazard Mater 183:233–241
9. Gandhi MR, Viswanathan N, Meenakshi S (2010) Preparation and application of alumina/chitosan biocomposite. Int J Biol Macromol 47:146–154
10. Chauhan D, Shankararamakrishnan N (2011) Modeling and evaluation on removal of hexavalent chromium from aqueous systems using fixed bed columns. J Hazard Mater 185:55–62

11. Boddu VM, Abburi K, Talbott JL, Smith ED (2003) Removal of hexavalent chromium from waste water using a new composite chitosan biosorbent. Environ Sci Technol 37:4449–4456
12. Huang G, Zhang H, Shi JX, Langrish TAG (2009) Adsorption of chromium(VI) from aqueous solution using cross-linked magnetic chitosan beads. Ind Eng Chem Res 48:2646–2651
13. Zimmerman AC, Mecabo A, Fagundes T, Rodrigues CA (2010) Adsorption of Cr(VI) using Fe-crosslinked chitosan composite (Ch-Fe). J Hazard Mater 179:192–196
14. Elwakeel KZ (2010) Adsorption of Cr(VI) from alkaline aqueous solution using chemically modified magnetic chitosan resins. Desalination 250:105–112
15. Rojas G, Silva J, Flores JA, Rodriguez A, Ly M, Maldonado H (2005) Adsorption of chromium onto cross-linked chitosan. Sep Purif Technol 44:31–36
16. Dantas TNC, Neto AAD, Moura MCPA, Neto ELB, Telemaco EP (2001) Chromium adsorption by chitosan impregnated with microemulsion. Langmuir 17:4256–4260
17. Sureshkumar MK, Das D, Mallia MB, Gupta PC (2010) Adsorption of uranium from aqueous solution using chitosan–tripolyphosphate (CTPP) beads. J Hazard Mater 184:65–72
18. Guibal E, Charrier MJ, Saucedo I, Cloirec PL (1995) Enhancement of metal ion sorption performances of chitosan: effect of the structure on the diffusion properties. Langmuir 11:591–598
19. Nagh WSW, Fatinathan S (2010) Adsorption characterization of Pb(II) and Cu(II) ions onto chitosan tripolyphosphate beads: kinetic, equilibrium and thermodynamic studies. J Environ Manag 91:958–969
20. Fahim NF, Barsoum BN, Eid AE, Khalil MS (2006) Removal of chromium(III) from tannery wastewater using activated carbon from sugar industrial waste. J Hazard Mater 136:303–309
21. Lee ST, Mi FL, Shen YJ, Shyu SS (2001) Equilibrium and kinetic studies of copper(II) uptake by chitosan-tripolyphosphate chelating resin. Polymer 42:1879–1892
22. Pang C, Liu Y, Cao X, Hua R, Wang C, Li C (2010) Adsorptive removal of uranium from aqueous solution using chitosan coated attapulgite. J Radioanal Nucl Chem 286:185–193
23. Zou W, Zhao L, Han R (2011) Adsorption characteristics of uranyl ions by manganese oxide coated sand in batch mode. J Radioanal Nucl Chem 288:239–249
24. Hassan HS, Attallah MF, Yakout SM (2010) Sorption characteristics of an economical sorbent material used for removal of radioisotopes of Cesium and Europium. J Radioanal Nucl Chem 286:17–26
25. Bagherifam S, Lakzian A, Ahmadi ZJ, Rahimi MF, Halajnia A (2010) Uranium removal form aqueous solution by wood powder and wheat straw. J Radioanal Nucl Chem 283:289–296
26. Nam KH, Tavlarides LL (2005) Synthesis of a high-density phosphonic acid functional mesoporous adsorbent: application to chromium(III) removal. Chem Mater 17:1597–1604